Functional characterization of *BCL11B*-a human transcription factor and UBR1-a human protein ubquitin ligase aided by proteomic analysis

I n a u g u r a l d i s s e r t a t i o n
zur
Erlangung des akademischen Grades
doctor rerum naturalium (Dr. rer. nat.)
an der Mathematisch-Naturwissenschaftlichen Fakultät
der
Ernst-Moritz-Arndt-Universität Greifswald

vorgelegt von
Narasimha Kumar Karanam
geboren am 16.07.1979
Nandyal, India

Dekan: Prof. Dr. rer. nat. Klaus Fesser

1. Gutachter: Prof. Dr. rer. nat. Uwe Volker

2. Gutachter: Prof. Dr. rer. nat. Walter Halangk

Tag der Promotion: 22nd November 2010

……..dedicated to my dear parents and wife

Content

1. Abbreviations

2-DE	two-dimensional polyacrylamide gel electrophoresis
ACN	acetonitrile
AP	alkaline phosphatase
APS	ammonium persulphate
BCIP	5-brom-4-chlor-3-indoxylphosphate
BSA	bovine serum albumin
CHX	cycloheximide
Conc.	concentration
CyDye	CyDye DIGE fluorescent dyes
DMF	dimethylformamide
DNA	desoxyribonucleic acid
DTT	Dithiothreitol
E coli	*Escherichia coli*
EDTA	ethylenediaminetetraacetic acid
EGTA	ethylene glycol-bis(-aminoethyl. ether)-N,N-tetraacetic acid
EMBL-EBI	European molecular biology laboratory- European bioinformatics institute
Em	emission
ExPASy	Expert Protein Analysis System
Ex	excitation
Fig.	figure
IAA	indoleacetic acid
IEF	isoelectric focusing
IP	Immunoprecipitation
JBS	Johanson-Blizzard-Syndrome
KO	Knockout
min	Minute
M	Molar
mM	milli molar
NBT	nitro blue tetrazolium, chloride
NCBI	National Center for Biotechnology Information

PANTHER	Protein ANalysis THrough Evolutionary Relationships
PBS	phosphate buffered saline
PMSF	phenylmethylsulphonyl fluoride
PSA	prostate specific antigen
PTM	post-translational modification
PVDF	polyvinylidene difluoride
RNA	ribonucleic acid
rpm	revolution per minute
S. cerevisiae	*Saccharomyces cerevisiae*
SC siRNA	scrambled control siRNA
SDS	sodium dodecyl sulphate
TBS	TRIS-buffered saline
TEMED	N,N,N',N'-tetramethylethylenediamine
TFA	trifluoroacetic acid
TRIS	tris (hydroxymethyl) aminomethane
WT	wildtype

2. Summary

In the post genomic era, novel "Omics" technologies like genomics and proteomics can be used in powerful screening approaches to provide unbiased lists of candidate genes and proteins and thus facilitate a comprehensive analysis of complex diseases such as cancer, which would not have been possible applying traditional genetic and biochemical approaches alone. During my PhD tenure I applied functional genomics screening technologies including proteomics in combination with traditional biochemical and cell biology approaches in two disease oriented projects:

1. Characterization of the role of BCL11b in Human T cell lymphomas (and)
2. Elucidation of the mechanism of pathophysiology of Johanson Blizzard Syndrome using UBR1 knockout mice and JBS patients' lymphoblasts cell lines.

2.1. Characterization of the role of BCL11b in Human T cell lymphomas

The Bcl11b protein belongs to the C_2H_2-family of Krueppel-like zinc finger proteins and thus is a member of the largest family of transcription factors in eukaryotes. It was shown to be important for a variety of functions such as T cell differentiation, normal development of central nervous system and DNA damage response. Malignant T cells undergo apoptotic cell death upon *BCL11B* down-regulation. However, the detailed mechanism of this cell death is not fully understood. Two dimensional difference in-gel electrophoresis (2D-DIGE), mass spectrometry and cell biological experiments were employed to investigate the functional impact of knock down of *BCL11B* in malignant T cell lines such as Jurkat and huT78. To further confirm the findings of these experiments, changes in protein patterns were also recorded after down-regulation of *BCL11B* expression in Jurkat cells over expressing BcL-xL and in Jurkat cells over expressing *BCL11B*. These experiments provide evidence for the involvement of the mitochondrial apoptotic pathway and increased levels of cleavage fragments of known caspase targets such as myosin, spectrin and vimentin were observed after *BCL11B* knockdown. The findings suggest an involvement of ERM proteins, which were up-regulated and phosphorylated upon *BCL11B* down-regulation. Besides ERM proteins, PDCD5, a key regulator of apoptosis, was also found at increased levels upon down regulation of *BCL11B*. Moreover, the levels of several proteins implicated in cell cycle entry, including DUT-N, UCK2, MAT1, CDK6, MCM4 and MCM6 were elevated, which might lead to uncontrolled cell cycle progression, uracil misincorporation and cell death. Interestingly, an inverse regulation pattern, i.e. decreased levels of ERM proteins, DUT-N, UCK2 and PDCD5 was seen upon over expression of *BCL11B* in Jurkat cells.

In summary, proteome analyses revealed several previously unidentified mechanisms which could significantly contribute to the cell death following *BCL11B* knockdown.

2.2.   Elucidation of the mechanism of pathophysiology of Johanson Blizzard Syndrome   using UBR1 knockout mice and JBS patients' lymphoblasts cell lines

Johanson-Blizzard syndrome (JBS; OMIM 243,800), which was first described in 1971, is a rare autosomal recessively inherited genetic disorder with a unique combination of congenital abnormalities. The most constant clinical feature of JBS is the loss of exocrine pancreatic function due to progressive destruction of pancreatic acini. Genome wide linkage analysis identified the disease associated locus in the 15q14-q21 chromosome region and high-throughput sequencing of this region revealed several truncated and some missense mutations in the UBR1 gene. UBR1 gene contains 47 exons and spans over 161 kilobases. The UBR1 protein belongs to the E3 ubiquitin ligase family and is an important component of the N-end rule pathway of ubiquitous protein degradation. It was hypothesized that stabilization of direct and unique substrates of UBR1 could be the main cause of the JBS pathophysiology. So far sequencing of the UBR1 gene is the only available diagnostic procedure. However, sequencing might not always allow precise prediction of residual UBR1 activity. Hence, this study was started to develop a protein based diagnostic assay for the detection of subclinical cases of JBS and to identify signalling pathways contributing to the pathophysiology of this complex disorder using a murine UBR1 knockout model.

2D-DIGE proteome analysis was carried out for a comparative evaluation of lymphoblast samples of 14 patients and 11 controls. Principal component Analysis (PCA) clearly discriminated JBS patients from controls. However, 4 JBS patients differed from the rest and resembled controls more closely. Western-blot analysis revealed residual UBR1 levels in these patients, which were linked to a milder phenotype. Hierarchical clustering of the three groups (controls, patients with residual UBR1 levels and patients without UBR1) showed group-specific characteristic differences in the abundance of differentially regulated proteins. Quantification of a panel of five selected protein spots encompassing Interferon-induced GTP binding protein, HLA class II histocompatibility antigen, Annexin A6, FK506-binding protein 4 and GRP78 permitted discrimination of controls and JBS patients with mild phenotypes. Of note, the molecular chaperones GRP78 (BiP) and FK506BP were consistently altered in level in JBS patients and probably constitute UBR1 dependent substrates. This

suggested JBS as an ER-stress related disease also indicating a possible way of therapeutic intervention.

Comparative proteome analysis of UBR1 knockout and wild type animals after caerulein treatment revealed a significant accumulation of pancreatic proteases such as chymotrypsin B, anionic trypsin and pancreatic elastase in animals lacking UBR1. Furthermore, an up-regulation of ER-stress proteins and inflammation related proteins was observed. Phenotypic characterisation revealed in UBR1 knockout animals significantly increased lipase levels, a significantly increased histological score and significantly increased elastase activity 8h after the onset of pancreatitis. In isolated pancreatic acini of UBR1 knockout animals we found a significant increase in intracellular elastase activation upon supramaximal CCK stimulation, which was associated with a significant rise in the rate of necrosis explaining the more severe phenotype in the UBR1 knock-out animals. A TUNEL assay showed that there was more apoptosis in wild type compared to UBR1 knockout mice.

Another set of experiments was designed to identify physiologically important substrates of UBR1. Inhibition of such substrates might then in turn allow reversion or prevention of the severe form of pancreatitis in UBR1 knockout mice. However, using the trypsin specific and reversible inhibitor S-124 it was shown that impaired trypsin degradation and thereby prolonged activation of this protease did not critically influence the phenotype. Calcium analysis after physiological stimulation revealed an increase of pathological Ca^{2+} signalling events, i.e. significant decrease of spike number and significant increase of spike duration. Of the candidates potentially influencing Ca^{2+} signalling RGS4 turned out to be of particular importance. Pre-incubation of pancreatic acini of UBR1 knockout animals with a specific RGS4 inhibitor (CCG-4986, 10 μM) normalized Ca^{2+} patterns, did not affect trypsin activity itself but prevented Ca^{2+}-triggered premature trypsin activation and thus acinar disintegration.

In summary, using lymphoblasts samples of JBS patients we were able to deduce a protein panel which could be developed as a possible diagnostic tool for confirmation of JBS syndrome. Furthermore, using UBR1 knockout mice in an experimental model we were able to elucidate the vital function of UBR1 and its direct substrate RGS4 in the defense against pathologic pancreatic damage thereby manifesting JBS as an inflammatory disorder due to an inadequate UBR1 mediated defense.

3. Introduction

3.1. Medical research and available technologies

There are numerous types of diseases reported so far and medical research and scientists focus on discovering new biomarkers and drug targets to detect disease early for better outcome by a personalized medical intervention. Many disorders including cancer arise due to gene mutations, translocations, deletions and duplications along with loss of protein function or over expression of important transcriptional regulators or tumour suppressors or oncogenes etc.

There are several technologies available to discover biomarkers and drug targets. Though they were proven to be successful, these techniques are time taking, cumbersome and moreover focussed on limited number of proteins or genes. With the advent of new technologies like proteomics and genomics it is easy to fish large number of candidates out of complex data or networks. The emergence of novel "Omics" technologies allows researchers to facilitate the comprehensive analysis of total protein or gene level changes during disease states and to characterise significantly altered genes or differentially expressed proteins. The heterogeneity of both, patient populations and various disease states may best be modelled through multiplexed biomarkers (Liotta et al 2003), which can be observed not only in the present study. During my PhD tenure I applied functional genomics screening technologies including proteomics in combination with traditional biochemical and cell biology approaches in two disease oriented projects.

1) Characterization of the role of BCL11b in Human T cell lymphomas

2) Elucidation of the mechanism of pathophysiology of Johanson Blizzard Syndrome (JBS) using UBR1 knockout mice and JBS patients' lymphoblasts cell lines.

A brief introduction about the history and development of "Proteomics" will be given as these techniques were mainly used to study the role of BCL11b in T cell lymphomas and UBR1 in the pathogenesis of JBS. Later in the course of the study candidate proteins were investigated by biochemical and cell biology techniques.

3.2. Technical introduction: Proteomics

The word "Proteome" was first coined by Prof. Marc Wilkins in 1994 (Wilkins et al 1996), while he was working as a PhD student. He used the word "proteome" as a blend of "protein" and "genome". Later on the word "proteomics" was coined in 1997 (James 1997) describing the study of the whole proteome. Proteome can be defined as "the complete profile

of proteins expressed in a given tissue, cell, or biological system at a given time and under specified condition".

The DNA structure was already discovered by Watson and Crick in 1953 which was a great achievement in the history of science and led science to the world of "Genomics" which is the study of all genetic information and material possessed by an organism. The development of DNA sequencing methodology in 1970 by Maxam Gilbert and in 1975 by Fredrick Sanger started the race of sequencing genomes. To understand and study the complete physiology of an organism it is essential to know the entire sequence of genetic material possessed by it. In this mission, the Human Genome project was initiated in 1990 by the International Human Genome Sequencing Consortium and Celera Genomics. According to the Human Genome Organization, the size of the human genome was estimated with about 3200 Mbp, but only two percent of the human genome codes for genes while the rest of its function is yet to be discovered. The first overall view of the human genome was published in February 2001 (Lander et al 2001, Venter et al 2001). Later on, successful sequencing projects led to the development of "reverse" approaches such as focusing more on phenotype than genotype. After the genome sequencing gene annotation received prime importance as these gene products are the real functional units of all biological events *in vivo* and those can be dealt with by proteomics technologies. Although studies of differential mRNA expression are informative, they do not always correlate with protein concentrations (Anderson and Seilhamer 1997, Gygi et al 1999b). Moreover, a small number of human genes can give rise to large numbers of proteins in the human total proteome due to splice variants (Black 2003), processing of mRNA(Schaub and Keller 2002) and posttranslational modification (Han and Martinage 1992). These biological complexities can be unravelled by proteomics approaches which help to understand molecular mechanisms and to integrate signals in cellular systems (Ahram and Emmert-Buck 2003). Genetic material of an organism is mostly static over time, it is not varying with environmental conditions and there are techniques like PCR to amplify the DNA. These characteristics of genomics make the study easy and attractive, while the proteome of an organism is very dynamic over time, age and state dependent and it is site specific and no techniques are available for protein amplification which makes the proteomics study challenging and difficult. Proteomic studies enable us not only to identify the protein but also to sequence, localize and do functional analysis with the aid of wide array of techniques possible. In the recent past, a whole collection of protoemcis approaches, advanced tools and techniques allow investigation of even complex proteomes including the expression level, isoforms and post translational modifications and their relation to protein activity. The

journey of proteomics in terms of technology and tools development is quite interesting and fruitful so far with regard to establishing "proteomics" as a separate and successful emerging field of modern science (Fig. 1).
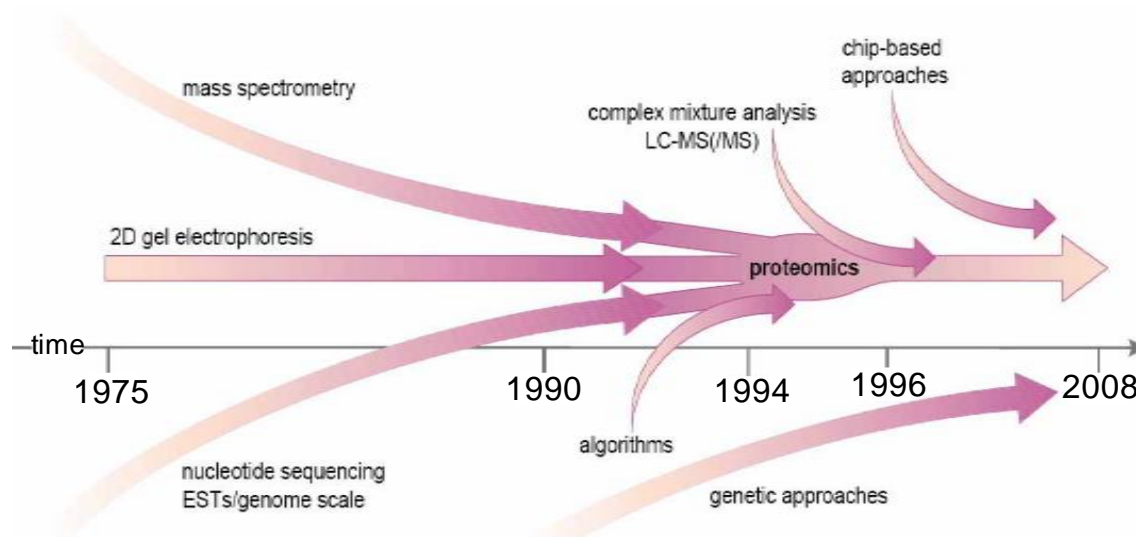
Fig. 1: Time line indicating development and convergence of different technologies and resources into proteomics field. (Patterson and Aebersold 2003)

In the basic workflow of proteomics there are three important steps:

1) Sample preparation or extraction - The success of proteomics studies depends on well defined samples and their clean and reproducible preparation.

2) Separation of protein mixtures by electrophoresis and/ or chromatography - High resolution pre-separation is required for complex samples.

3) Analysis of resolved proteins by mass spectrometry - This is the critical step to characterize the protein. There is a massive development in mass spectrometry in the recent past to increase the sensitivity of machines to as low as femto mole levels.

3.2.1. Separation techniques:

Mainly there are two types of separation techniques routinely used. One is the gel based technique and the other is chromatography based. These two techniques have their advantages and disadvantages and are moreover complementary to each other.

Gel based separation:

This is used as a gold standard of separation in proteomics. Proteomics has its roots in analytical biochemical techniques used for protein separation. Before the 2D-PAGE era

proteins were usually separated based on their molecular weight which is called one dimensional electrophoresis (1D PAGE) separation. In two dimensional electrophoresis (2D-PAGE) proteins are separated by virtue of their pI values in the first dimension called isoelectric focussing (IEF), later on proteins are separated based on their molecular weights in the second dimension. First high resolution protein separations were achieved by two-dimensional gel electrophoresis by P.H. O'Farrel and J. Klose in 1975 (Klose 1975, O´Farrell 1975). In the original 2-DE, first dimension pH gradients in polyacrylamide tube gels were achieved by using carrier ampholytes. However, due to the lack of reproducibility and a computerized image analysis platform, this first generation of 2D systems was not widely used. In 1982 an alternative method to prepare immobilized pH gradients was developed (Bjellquist et al 1993, Bjellqvist et al 1982) and much improved second generation IPG strips were developed in the late 80s. The new 2-DE methods use immobilized pH gradient gels for IEF and in combination with other developments these modifications provided much better resolution and reproducibility and paved the way for computer based analysis of the result (Gorg et al 1988a, Gorg et al 1988b, Gorg et al 1988c). Immobilized pH gradient (IPG) based 2-DE separations have more advantages than ampholyte based 2-DE such as high protein loading (Bjellquist et al 1993) and samples can be applied during rehydration of the precast IPG strips (Rabilloud et al 1994). Hence nowaday's 2D-PAGE is a more routinely used technique for separation of complex mixtures and 2D databases are also available in the public domain where one can access reference maps of different organisms. For visualization of the spots on 2D coomassie blue, colloidal coomassie and silver nitrate staining procedures are routinely used. Coomassie staining is very much compatible with mass spectrometric analysis, whereas silver nitrate staining is not due to the use of formaldehyde in staining procedure (Richert et al 2004). Thus, alternative silver staining procedures were developed for mass spec compatibility (Gharahdaghi et al 1999, Switzer et al 1979, Yan et al 2000).

Other sensitive detection techniques which are developed are based on fluorescence detection (Patton 2000), either of purely organic probes like SYPRO Orange and SYPRO Red (Steinberg et al 1996a, Steinberg et al 1996b) or of ruthenium or europium complexes like SYPRO® Ruby, SYPRO Rose and ruthenium II Tris (bathophenanthroline disulfate) (RuBPS) complex) (Steinberg et al 2000). Organic probes show a sensitivity slightly better than colloidal coomassie blue, while ruthenium complexes have sensitivity slightly inferior to that of silver staining but a much improved compatibility with MS (Berggren et al 2000, Rabilloud et al 2001). Though there are several fluorescent dyes for sensitive detection, quantification of spots is quite challenging due to inter gel running variations. To overcome

this problem, the 2D-DIGE (Differential Gel Electrophoresis) technique was developed, where three different samples can be labeled with different CyDyes and run on the same gel (Marouga et al 2005). By exciting at three different wavelengths using e.g. a Typhoon scanner (GE Healthcare), one can get three different images from one gel.

Apart from total protein staining procedures, there are special staining procedures to stain specifically the phosphoproteome by Pro-Q® Diamond staining (Schulenberg et al 2003, Schulenberg et al 2004) and glycoproteome by Pro Q emerald staining (Steinberg et al 2001). These are most useful when used in conjunction with SYPRO® Ruby staining (Ge et al 2004, Steinberg et al 2003).

The 2D-DIGE technique for differential proteome analysis and Pro-Q® Diamond staining for phosphoproteome analysis were used in the present study. 2-DE has a great advantage of visualizing also many post-translational modifications and isoforms of proteins. However, 2-DE has some disadvantages as well. Very low abundant, highly hydrophobic and highly acidic and basic proteins cannot be resolved by 2-DE technique (Zuo et al 2001).

Gel free/ chromatographic separation:

Chromatographic techniques separate molecules based on differences in their structure and/or composition. They involves passing a mixture dissolved in a "mobile phase" through a "stationary phase", which separates the analyte to be measured from other molecules in the mixture and allows it to be isolated depending on the interaction forces. Chromatographic separations can be carried out using a variety of supports, including immobilized silica on glass plates (thin layer chromatography), volatile gases (gas chromatography), paper (paper chromatography), and liquids which may incorporate hydrophilic, insoluble molecules (liquid chromatography). For the separation of the peptide mixtures for mass spectrometry analysis in this study reverse phased liquid chromatography technique was used. The name "reversed phase" has a historical background. In the 1970s most liquid chromatography was done on non-modified silica or alumina with a hydrophilic surface chemistry and a stronger affinity for polar compounds - hence it was considered "normal". The introduction of alkyl chains bonded covalently to the support surface reversed the elution order (Molnar and Horvath 1976) such that polar compounds are eluted first while non-polar compounds are retained - hence "reversed phase". The separation resolution is proportional to the length of the column. One of the main advantages of the LC based separations is to use very low amount of protein mixture for analysis. Though we can separate low abundant proteins and high hydrophobic

proteins by chromatography we cannot get the information about post translational modifications and isoforms of proteins which are counted as disadvantages.

Because of advantages and disadvantages of both gel based and gel free chromatographic separations, these two techniques are complementary to each other in the separation of complex mixtures.

Gel free quantitation methods:

With the progression of the technology development, apart from 2D gel based quantitation now it is also possible to quantitate proteins in gel free approaches as well, moreover we can do quantitative analysis using very low amounts of protein mixture. There are different methods available for gel free quantification like ICAT (Isotope-coded affinity tags) (Gygi et al 1999a), iTRAQ (isobaric tag for relative and absolute quantitation) (Zieske 2006) mass spectrometric based label free quantitation (Asara et al 2008, Bantscheff et al 2007) and SILAC (Stable isotope labelling with amino acids in cell culture) (Ong et al 2002, Ong and Mann 2006), pulsed SILAC (Schwanhausser et al 2009) and TMT (Tandem mass tags) (Thompson et al 2003).

3.2.2. Mass spectrometry:

While the separation of hundreds of proteins using 2-D gels and chromatography techniques was welcomed, and changes in protein abundance between samples could be quantitated, frustration also grew with the lack of useful and sensitive tools to identify proteins of interest. This coincided with the development of mass spectrometry ionization techniques for peptides, allowing protein identification and characterisation on a large scale. The two basic ionization methods development Matrix-Assisted Laser Desorption/Ionization (MALDI) (Karas and Hillenkamp 1988), Karas M, Anal chem 1988) and electro spray ionization (ESI) (Fenn et al 1989) in analytical chemistry have revolutionized mass spectrometric based protein identification in proteomics. These developments in mass spectrometry techniques shifted the classical activity centered biology approach to a sequence centered biology approach (Aebersold 2003).

There are 4 important components in mass spectrometers.

1) Ion source- which produces ions

2) Mass analyzer- which sorts ions

3) Detector- which detects ions

4) Signal processor- which converts the data into a form of mass spectrum

There are different types of ion sources available. Here we used two different ion sources which can be used for non gaseous compounds like peptides. One is ESI and the second one is MALDI. These ion sources are coupled with mass analyzers. MALDI is commonly coupled with a time of flight (TOF) analyzer and ESI with ion traps or quadrupole analyzers.

MALDI: MALDI MS, a form of laser desorption MS, was developed in 1985 by Franz Hillenkamp and Michael Karas in Germany (Karas and Hillenkamp 1988, Karas M, Anal chem 1988) and independently by Koichi Tanaka and coworkers at Shimadzu Corp., Kyoto, Japan. In MALDI, sample molecules are laser-desorbed from a solid or liquid matrix containing a highly UV-absorbing substance (Fig. 2).
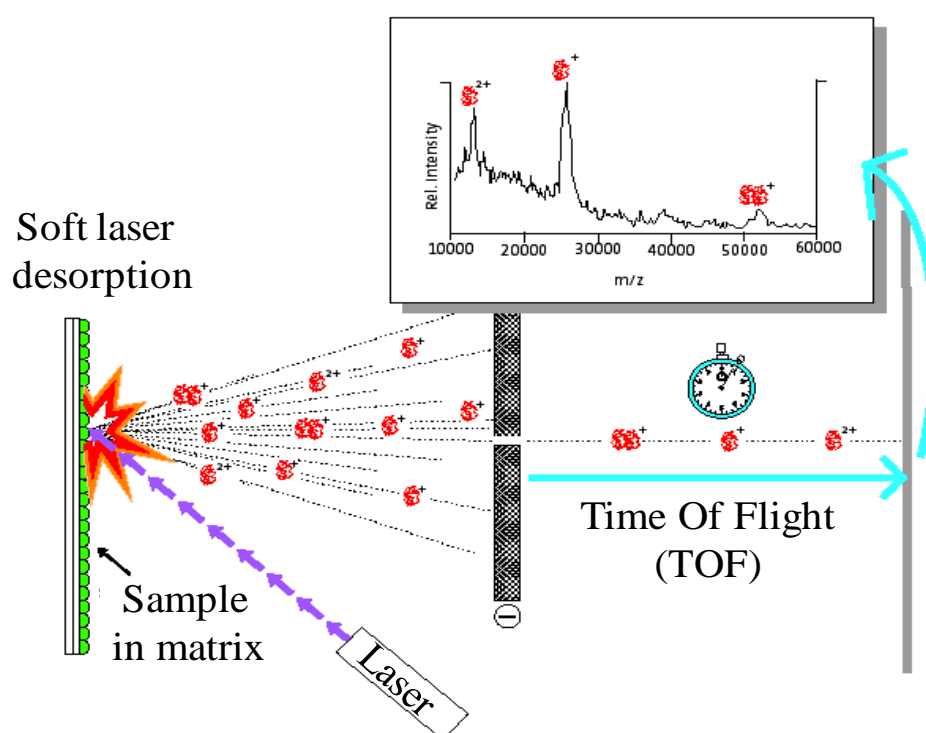
Fig. 2: Matrix Assisted Laser Desorption Ionization (MALDI). A pulsed laser on matrix-analyte mixtures results in vaporization of the matrix and acceleration of the ions. The ions entering the flight tube are separated according to their m/z ratio and recorded by recorder. (Courtesy www.bioalgorithms.info)

Electro Spray Ionisation: In ESI MS, highly charged droplets dispersed from a capillary in an electric field are evaporated, and the resulting ions are drawn into an MS inlet (Fig. 3). The technique was first conceived in the 1960s by Malcolm Dole of Northwestern

University, Evanston, but it was put into practice in the early 1980s by the molecular beam researcher John B. Fenn (Fenn et al 1989) of Yale University.

For their development of soft desorption ionisation methods for mass spectrometric analyses of biological macromolecules Koichi Tanaka and John B.Fenn were awarded the Nobel Prize in Chemistry in 2002.
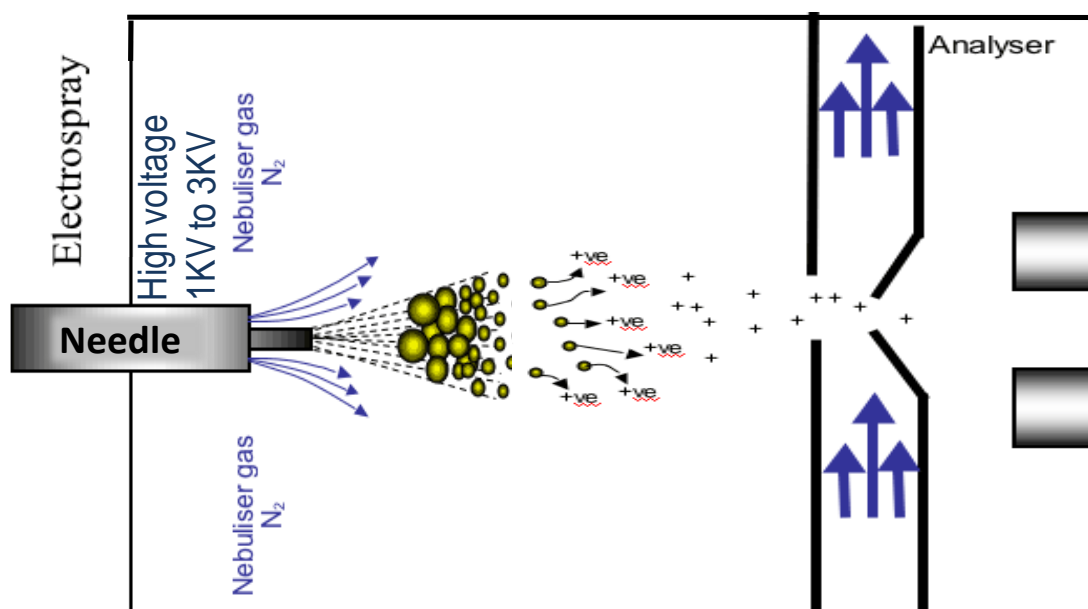
Fig. 3: Electro Spray Ionisation MS (ESI MS). A sample is pumped through the needle held at high voltage to produce fine spray of charged droplets, which are then directed to inlet of a mass analyzer (modified from UCL institute of child health).

3.2.3. Identification of proteins:

The accelerated ions produced by the ion source travel through mass analyzers (TOF, Ion trap) of mass spectrometer and fly towards the detector according to their mass to charge ratio (m/z). The detector will collect the ions and the signal processor generates the proportional electrical signal which is recorded as a function of m/z by the recorder and is finally converted to a mass spectrum. The mass spectrum generated by MALDI/ESI provides masses of the analyzed peptides. Then the protein identification is carried out by peptide mapping or a peptide mass finger printing method. In this method, the match of a list of experimental peptide masses with the calculated list of all peptide masses of each entry in a database (e.g., a comprehensive protein database) identifies the protein. Five groups almost coincidentally developed computer tools for the identification of proteins by peptide mapping (Henzel et al 1993, James et al 1994, Mann et al 1993, Yates et al 1993). In the other method protein

identification was based on sequence information generated from selected peptides in a tandem mass spectrometer. Since the information contained in collision-induced dissociation spectra (CID) is not readily convertible into a full, unambiguous peptide sequence, the CID spectra are scanned against comprehensive protein sequence databases using one of a number of different algorithms of which Sequest is the prototypical tool (Eng et al 1994).

3.3. BCL11b role in T lymphomas

Kruppel like transcription factors (Kaczynski et al 2003), such as Ikaros family of proteins and the lung Kruppel like transcription factor, are essential for lymphoid development (Georgopoulos 2002) and T cell homeostasis (Buckley et al 2001). By database analysis, Satterwhite et al. (Satterwhite et al 2001) identified a human homolog of BCL11a, designated BCL11b. The deduced 823-amino acid *BCL11B* protein is 61% identical to BCL11A overall but 95% identical in the zinc finger domains. It is also 86% identical to mouse Ctip2. Northern blot analysis detected expression of *BCL11B* in malignant T-cell lines derived from patients with adult T-cell leukemia/lymphoma but not in any malignant B-cell lines examined. Sequence analysis revealed that human *BCL11B* gene is located on chromosome 14Q32.1 (Satterwhite et al 2001) and mouse *BCL11B* which was termed Rit1 is located on chromosome 12 (Wakabayashi et al 2003a).
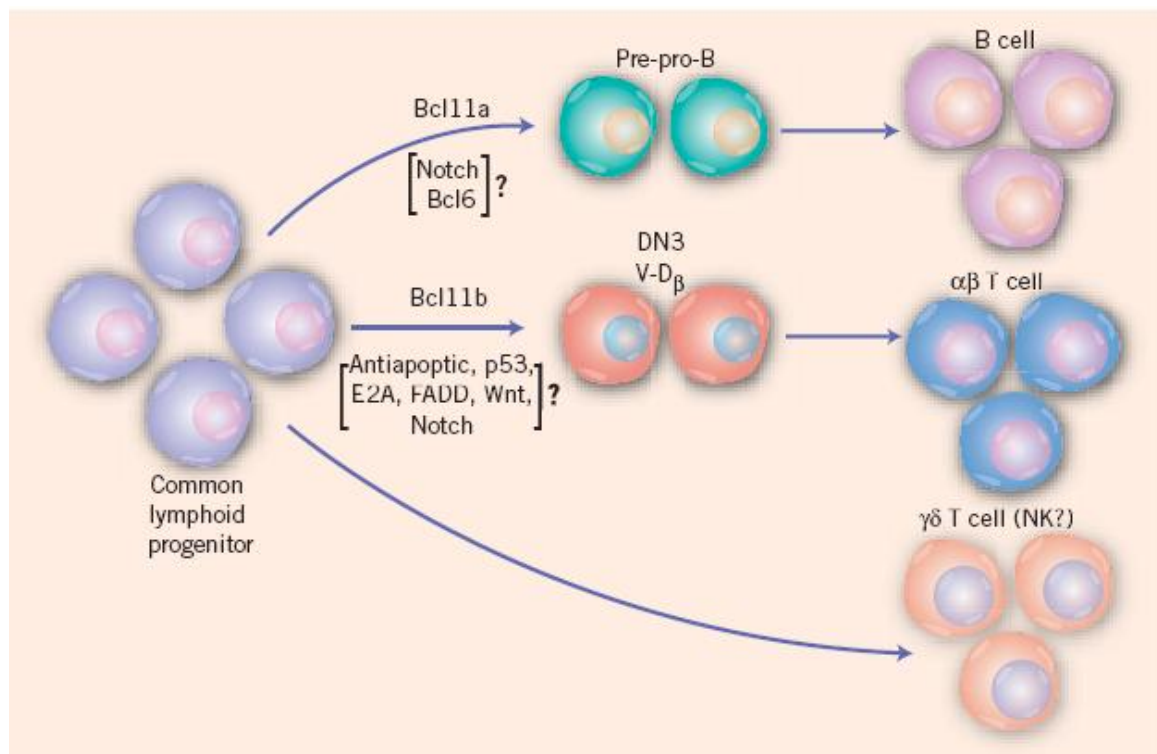
Fig. 4: Schematic diagram showing the role of Bcl11a and Bcl11b in lymphoid development. Bcl11a is a transcription factor required in the development of B cells, where as its close paralog Bcl11b is required in the αβ T cell development (Durum 2003).

The Bcl11b protein (B-cell chronic leukemia/lymphoma 11b), initially described as chicken ovalbumin upstream promoter transcription factor (COUP-TF)-interacting protein 2 (CTIP2) (Avram et al 2000b) and radiation induced tumor suppressor gene 1 (RIT1) (Shinbo et al 1999) is involved in a variety of biological processes. They range from the regulation of T-cell differentiation (Fig. 4) (Wakabayashi et al 2003b) and normal development of central nervous system (CNS) during embryogenesis (Arlotta et al 2005, Leid et al 2004) to DNA damage response (Kamimura et al 2007a) and the maintenance of latent human immunodeficiency virus (HIV) infections (Marban et al 2007). However, as shown recently, its role is not restricted to the central nervous and immune system. The data published within the last two years implicated the essential requirement for *BCL11B* in developing skin (Golonzhka et al 2007), where it regulates keratinocyte proliferation and the late differentiation phases determining the process of skin morphogenesis (Golonzhka et al 2009a). Furthermore, normal tooth development was significantly impaired in *BCL11B*-deficient mice which was accompanied by the decreased expression of ameloblast marker genes and transcription factors driving odontogenesis (Golonzhka et al 2009b).

Structurally, Bcl11b belongs to the C_2H_2-family of Krueppel-like zinc finger proteins and thus is a member of the largest family of transcription factors in eukaryotes. Amino acids on the surface of an alpha-helix contact a GC rich target sequence in the major groove and confer direct DNA-binding (Avram et al 2002, Wolfe et al 2000). Additionally, Bcl11b possesses transcriptional regulatory domains. Among the interaction partners identified so far are COUP-TF (Avram et al 2000a), NuRD (nucleosome remodelling and histone deacetylation complex) (Cismasiu et al 2005) and the ubiquitous transcription factor Sp1 (Marban et al 2005). It was shown that as a consequence of recruiting both histone deacetylases (HDAC1 and HDAC2, resp. SIRT1) (Cismasiu et al 2005, Senawong et al 2003) and a histone methyltransferase SUV39H1, Bcl11b induces heterochromatin formation and thus acts as a potent transcriptional repressor (Marban et al 2007). In contrast Bcl11b interaction with p300 coactivator on the upstream site 1 (US1) of the IL-2 promoter results in transcriptional activation and subsequently increased IL-2 expression after T-cell activation (Cismasiu et al 2006). However, although interaction partners and the direct binding sequence have been described only few direct target genes of Bcl11b are known. The *P57KIP2* gene, e.g., a cyclin-dependent kinase inhibitor, is repressed by Bcl11b (Topark-Ngarm et al 2006).

Apart from *P57* and *IL-2* genes, the cancer Osaka thyroid oncogene (Cot) has been recently identified as a direct transcriptional target of *BCL11B*. As a consequence, Cot expression was induced and its kinase activity enhanced the phosphorylation of IkappaB kinase which led to increased translocation of NF-kappaB to the nucleus and activation of its target genes (Cismasiu et al 2009). Recently, Bcl11b was shown to bind the p21 promoter and in cooperation with SUV39H1 methyltransferase silenced the transcription of p21. This epigenetical silencing of p21 *via* the cooperative action of Bcl11b and SUV39H1 contributed indirectly to HIV latency in macrophages (Cherrier et al 2009).

The biological function of Bcl11b *in vivo* is still a matter of debate. In humans overexpression of Bcl11b mRNA has been linked to lymphoproliferative disorders like the T-cell acute lymphoblastic leukemia, T-ALL (Nagel et al 2003, Przybylski et al 2005) and an acute form of adult T-cell leukemia/lymphoma (Oshiro et al 2006). Moreover, *BCL11B* upregulation correlated with the low differentiation status in head and neck squamous cell carcinoma. Interestingly, the Bcl11b protein co-localized with cancer stem cell marker BMI-1 (Ganguli-Indra et al 2009).

Conversely, in the mouse models of T-cell leukemia the *BCL11B* locus is frequently homozygously deleted or mutated and the expression of the gene is impaired (Wakabayashi et al 2003a). The loss of only one allele was identified as a factor predisposing to lymphoma development in p53 (+/-) mice which suggested that *BCL11B* is haploinsufficient suppressor for thymoma development in this genetic background and that deletion of one gene copy promotes for tumor growth (Kamimura et al 2007b). The mutated variants of murine *BCL11B* isolated from chemically induced T cell lymphomas in turn were able to enhance proliferation of hematopoietic progenitor cell line *in vitro* (Karlsson et al 2007). In conclusion, the contradictory results provided by animal models and human diseases intensify the dispute on the tumor suppressor or oncogenic properties of *BCL11B*.

Malignant T-cell lines undergo apoptosis, when Bcl11b-expression is inhibited, which makes Bcl11b a potential therapeutic target in T cell derived tumours (Grabarczyk et al 2007). Apoptosis is executed by simultaneous activation of receptor mediated and intrinsic apoptotic pathways and accompanied by a decrease in Bcl-xL and an increase in Trail expression. This is in line with the apoptotic phenotype of Bcl11b$^{-/-}$ thymocytes that express lower levels of Bcl-xL and additionally Bcl-2 (Wakabayashi et al 2003b). Moreover, a recent report by Kamimura et al. (Kamimura et al 2007a) revealed that loss of Bcl11b leads to impaired response to DNA-damage and lack of cell cycle checkpoint activation accompanied by replication stress and cell death. These data stress the antiapoptotic function of Bcl11b but

also implicate its role in maintaining genome stability which might contribute to the malignant transformation.

Here I used proteomics based 2D-DIGE approach to investigate the role of BCL11b in human T cell lymphoma cell lines i.e. Jurkat and huT by down regulating BCL11b using sequence specific siRNA. Furthermore the same approach was used to explore the specific effects of Bcl11b in *BCL11B* over expressing Jurkat cells.

3.4.   Johanson Blizzard Syndrome

Johanson-Blizzard syndrome (JBS; OMIM 243,800) was first described in 1971 by Johanson and Blizzard, hence named after them (Johanson and Blizzard 1971). JBS is a rare autosomal recessively inherited genetic disorder with a unique combination of congenital abnormalities. The most constant clinical feature of JBS is the loss of exocrine pancreatic function due to progressive destruction of pancreatic acini. Other less constant symptoms comprise hypoplasia or aplasia of the nasal wings and a number of variable abnormalities present in a high proportion of patients, including short stature (>80%); tooth abnormalities (mainly oligodontia >80%); sensorineural hearing loss (80%); mental retardation (77%); scalp defects (76%); hypothyroidism (40%); imperforate anus (39%); and genitourinary malformations (38%) (Fig. 5) (Gershoni-Baruch et al 1990, Hurst and Baraitser 1989, Rudnik-Schoneborn et al 1991, Vanlieferinghen et al 2001, Zenker et al 2006).

Fig. 5: Pictures showing the typical characteristics of Johanson-Blizzard Syndrome A) nasal wing aplasia B) nasal alae hypoplasia together with tooth abnormalities C) imperforate anus and D) scalp defects. (Taken from Alkhouri et al 2008, Zenker et al 2006).

Mental retardation is typically moderate to severe in JBS patients; however normal intelligence can also occur (Moeschler and Lubinsky 1985, Rudnik-Schoneborn et al 1991). Since the first case reported in 1971, more than 65 cases were reported till date (Zenker et al 2006). Recently there are some case reports of JBS patients with severe liver fibrosis, cardiomyopathy (Al-Dosari et al 2008, Elting et al 2008). In several cases of JBS, diabetes was reported, mostly in older children suggesting a progressive course of pancreatic disease (Steinbach and Hintz 2000, Trellis and Clouse 1991). In accordance with this notion, recently a JBS case was reported without any pancreatic damage at the time of premature birth (Al-Dosari et al 2008). Autopsy findings at different ages showed clearly the loss of acini in the pancreas (Daentl et al 1979, Moeschler et al 1987, Vanlieferinghen et al 2003, Vanlieferinghen et al 2001). The incidence rate of JBS was estimated at around 1 per 250,000 based on a study on imperforate anus in a European population which occurs in approximately 40% of JBS patients (Cuschieri 2002).

To identify the disease associated locus, genome wide linkage analysis was done by Zenker M et al. in 12 JBS affected families (Zenker et al 2005). Using a panel of microsatellite markers with average distance of 10cM a homozygous region was identified in 15q chromosome. Further refined studies with additional microsatellite markers shortened the homozygous region to 7.5cM interval of chromosome 15q14-q21 region. By high throughput sequencing of this region, mutations in the UBR1 gene were revealed.
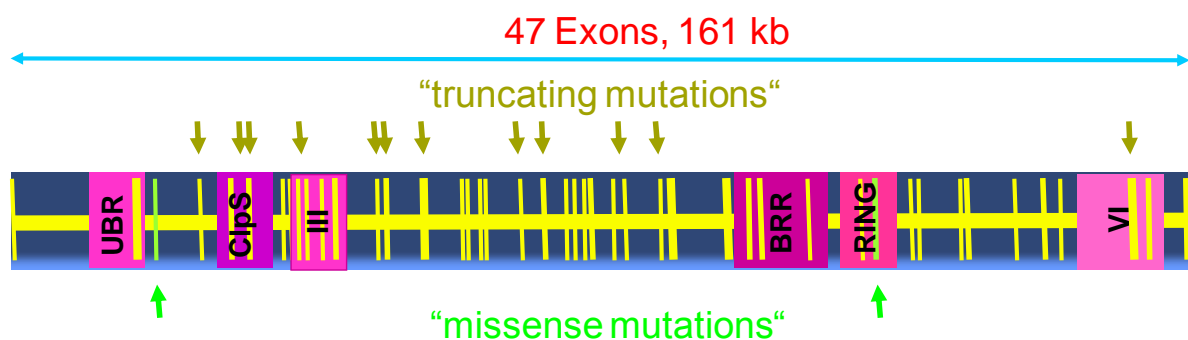
Fig. 6: UBR1 gene- mutation analysis. The UBR1 gene has 47 exons and spans over 161 kb. Mutation analysis revealed truncating mutations, which are shown in yellow coloured bars as well as missense mutations, which are shown with green coloured arrow heads (Modified from Zenker et al 2005)

3.4.1. UBR1 protein

UBR1 is a large gene, which spans over 161 kilobases and contains 47 exons. There are more truncated mutations reported than missense mutations which lead to functional attenuation and in most cases as well to loss of expression (Fig. 6). Sequence analysis of the UBR1 gene for mutations is the only and latest marker available for JBS syndrome confirmation and it was successfully tested recently by other groups (Alkhouri et al 2008). UBR1 belongs to the E3 ubiqutin ligase family and is an important component of the N-end-rule pathway for ubiquitous protein degradation (Fig. 7). UBR1 is a large protein with a relative molecular weight of 225kDa with several distinct functional domains. It has two substrate binding sites that recognize distinct amino termini 1) a type-1 site that recognizes basic residues such as arginine and 2) a type-2 site that binds to bulky hydrophobic residues such as leucine. Although the exact positions of these sites within the UBR1 polypeptide are yet to be discovered, both sites have been extensively characterized through competition studies using dipeptides (Gonda et al 1989, Reiss et al 1988). Dipeptides can competitively inhibit UBR1, provided that the peptide and the substrate shared the same type of N-terminal residue (Turner et al 2000). $UBR1^{-/-}$ mice are viable and fertile but characterized by significant loss of weight due to the abnormalities in fat metabolism (Kwon et al 2001). However, UBR1 knockout mice showed a mosaic fashion of N-end-rule pathway activity by exhibiting apparently no activity in skeletal muscle and normal activity levels in fibroblasts. This might be due to the fact that the mammalian N-end-rule pathway is mediated by more than one E3 ubiquitin ligase (N recognin) unlike in yeast where UBR1 serves as the only E3 ubiquitin ligase of the N-end-rule pathway. Supporting this hypothesis it was found that $UBR1^{-/-}$ and $UBR2^{-/-}$ double knockout mice were embryonical lethal. It was also shown that UBR1 together with NTAN1 was involved in learning and memory (Balogh et al 2002).
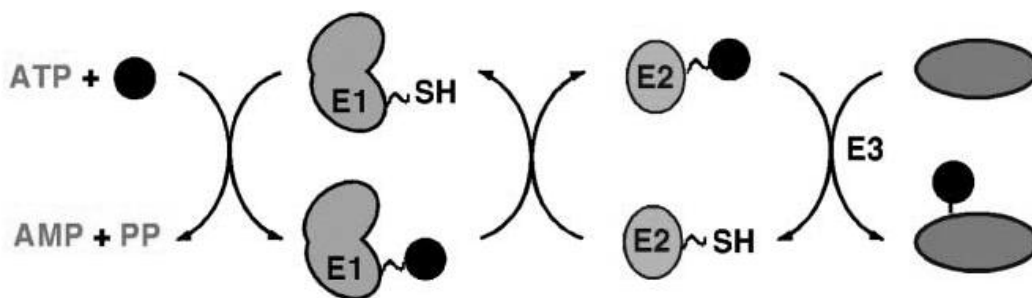
Fig. 7: Ubiquitination cascade. Ubiquitination of protein involves the action of 3 enzymes E1 (Ubiquitin activating enzyme), E2 (Ubiquitin conjugating enzyme) and E3 (Ubiquitin ligase) with the expense of ATP molecule at the activation step.

3.4.2. N-end rule pathway of degradation

Damaged, unwanted and abnormal proteins are characterized by short *in vivo* half-live in cells. There are a number of regulatory mechanisms involved in the process of removing these unstable proteins. These unstable proteins contain signals for degradation called degrons. One of the essential components of degradation signal is the N-degron, which is defined as a destabilizing N-terminal residue of a protein (Bachmair et al 1986). The set of destabilizing N-terminal amino acids in a given cell type yields a rule called N-end rule. The N-end-rule pathway is a ubiquitin-dependent proteolytic system and is present in all organisms that have been examined from mammals to fungi and bacteria, though comprising distinct variants dependent on the organism (Varshavsky 1996). The hierarchical structure of N-end-rule pathway is shown in the following figure (Fig. 8).
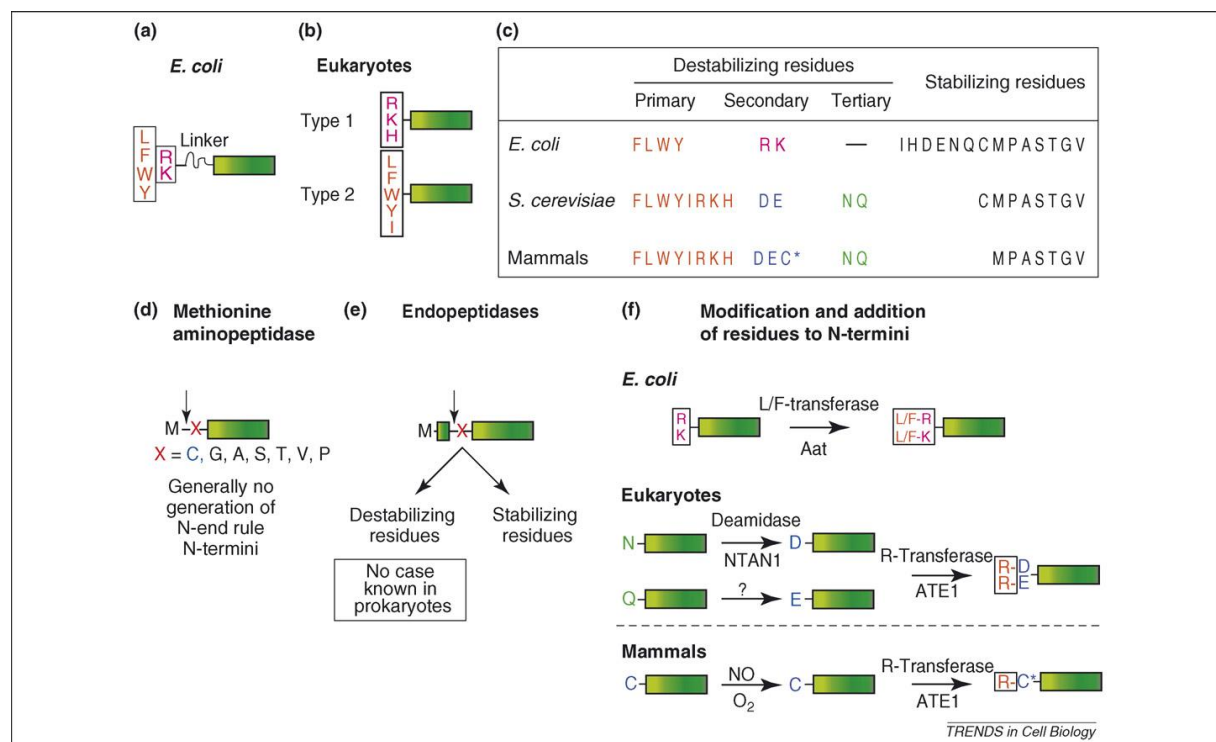
Fig. 8: The N-end rule: code and generation of N-degrons. (a–c) Comparison of the N-end rule determinants in different model organisms. (a,c) In *E. coli*, large hydrophobic (Leu, Phe, Trp, Tyr) and basic residues (Arg, Lys) represent primary and secondary destabilizing residues, and both contribute to the N-degron code. In addition the N-end-rule substrate harbors a flexible linker that separates the N-terminal degradation signal from the substrate moiety which is required for transfer to and degradation by the ClpA/ClpP protease. (b,c) In eukaryotes, basic residues (Arg, Lys, His) and large hydrophobic residues (Leu, Phe, Trp, Tyr, Ile) function

independently as type 1 and type 2 primary destabilizing residues. (c) Table summarizing the characteristics of individual amino acids according to the present N-end rule. C* indicates an oxidized Cys residue. (d) Newly synthesized proteins harbor a stabilizing N-terminal Met and do not function as N-end rule substrates. Methionine aminopeptidases can remove Met from the N-terminus if the adjacent residue has a small side chain, generating proteins that still harbor stabilizing N-terminal residues with the exception of Cys, which can act as a secondary destabilizing residue in mammals. (e) Endoproteolytic cleavage events generate protein fragments with novel N-termini including both, stabilizing and destabilizing residues. (f) Enzymatic cascades convert tertiary and secondary destabilizing residues into primary ones. Tertiary destabilizing residues (e.g. Asn) can be converted by N-terminal amidases (NTAN1) into secondary destabilizing residues. Secondary residues function through their ATE1-mediated conjunction to Arg in eukaryotes or through the Aat-mediated attachment of Leu/Phe in bacteria. Oxidized Cys (C*), generated in the presence of nitric oxide or oxygen, acts as a secondary destabilizing residue in mammalian cells and is converted into primary destabilizing Arg via R-transferase. Note: amino acids are represented in the figure using the IUPAC one-letter code. Red, primary destabilizing residues; purple, prokaryotic secondary destabilizing residues; blue, eukaryotic secondary destabilizing residues; green, tertiary destabilizing residues; black: stabilizing residues (Mogk et al 2007).

Ubiquitin mediates proteolysis of regulatory proteins such as transcription factors and signal transduction proteins and hereby functions as an important regulatory mechanism of different cellular mechanisms such as cell growth, division, differentiation and programmed cell death. Hence, the study of substrates of N-end-rule pathway is important to reveal different cellular regulatory mechanisms. So far there are few direct N-end-rule pathway substrates known and are listed in the table given below (Table 2).

Table 2: List of known N-end-rule pathway substrates.

Protein Name	Source or Species	References
c-Fos	HeLa cells	(Sasaki et al 2006)
CUP9	*S.cerevisiae*	(Byrd et al 1998)
GPA1 encoded Gα	*S.cerevisiae*	(Madura and Varshavsky 1994, Schauber et al 1998)
RNA polymerase	Sindbis virus	(de Groot et al 1991)
HIV type-1 integrase	HIV	(Mulder and Muesing 2000)
Bacterial protein p60	*Listeria monocytogenes*	(Sijts et al 1997)
RGS4, RGS5 and RGS16	Mouse/ Human	(Davydov and Varshavsky 2000, Lee et al 2005)
Encephalomyocarditis (EMC) virus 3C protease	EMC virus	(Lawson et al 1999)
Cohesin	*S.cerevisiae*	(Rao et al 2001)

RIN4	*Arabidopsis*	(Takemoto and Jones 2005)
Putriscine aminotransferase (PATase)	*E.coli*	(Ninnis et al 2009)
Mgt1 alkyl guanine transferase	*S.cerevisiae*	(Hwang et al 2009)
c-IPA1	Mouse	(Wickliffe et al 2008)

However, the physiological function and purpose of the degradation of these substrates is yet not clearly understood. Here we used a proteomics approach to search for new N-end-rule pathway substrates i.e direct UBR1 substrates and tried to study their biological relevance employing the UBR1 knock-out animals. We focused on UBR1 dependent changes in a model of experimental pancreatitis where severity in UBR1 knockout and wild type mice is different (Zenker et al 2005). Besides UBR1 knockout mice experiments, we used JBS patient's lymphoblast samples to explore differences between patients and controls and tried to distinguish between these groups based on their proteome profiles. As pancreatic exocrine insufficiency is the most constant feature of JBS and all other symptoms can be mild or absent and as pancreatic exocrine insufficiency can also be caused by a number of different pancreatic diseases such as cystic fibrosis [OMIM 602421], Shwachman-Diamond-syndrome [OMIM 260400], Beckwith-Wiedemann-syndrome [OMIM 130,650], Pearson-Marrow-syndrome [OMIM 557,000], hereditary and idiopathic chronic pancreatitis or simply chronic pancreatitis [reviewed in (Lerch et al 2006), (Weiss et al 2006)], hence we aimed to develop a non-invasive diagnostic test to detect subclinical cases of JBS using proteomic approach. Moreover, such frequent diseases as inflammatory bowel disease, celiac disease and several infectious diseases affecting the small bowel are also associated with pancreatic exocrine insufficiency suggesting that a simple non-invasive test might be of great diagnostic value.

4. Materials and Methods

4.1. Materials

4.1.1. Chemicals

Name	Source
β-mercaptoethanol	Roth
β-glycerolphosphate	Sigma
ammonium bicarbonate (NH_4HCO_3)	Sigma
ammonium cloride (NH_4Cl)	Roth
ammonium sulphate (($NH_4)_2SO_4$)	Merck
acetic acid	Roth or Sigma
acetonitrile (ACN)	Merck
acetylated-Lysine Polyclonal antibody	CellSignalling
agarose	Invitrogen
silver nitrate ($AgNO_3$)	AppliChem
alkaline phosphatase-conjugated AffinPure goat anti rabbit IgG (H+L)	Jackson Immuno Research
ammonium persulphate (APS)	GE HealthCare
aureon BSA	Aurion
bis/acrylamide 40 %	AppliChem
bovine serum albumin (BSA)	Sigma
bromophenol blue	Sigma
5-brom-4-chlor-3-indoxylphosphat (BCIP)	Roth
Bradford reagent	Bio-Rad
calcium cloride ($CaCl_{2)}$	Sigma
calcium cloride dihydrate ($CaCl_2$ $2H_2O$)	Sigma
caerulein	Sigma
CHAPS	Sigma
cocktail (protease inhibitors)	Calbiochem
coomassie brilliant blue G-250	Merck
CyDye DIGE flours	GE HealthCare
DeStreak	GE HealthCare
o-dianisidin	Sigma
diethylether	Roth
dimethylformamide (DMF)	Roth or Sigma
dithiothreitol (DTT)	GE HealthCare
dimethyl sulfoxide (DMSO)	Roth
dihexyloxacarbocyanine iodide [$DiOC_6$]	Molecular probes
drystrip cover fluid	GE HealthCare
eosin	Sigma

Name	Source
ethanol	Merck
ethylenediaminetetraacetic acid (EDTA)	Merck
formaldehyde 37 %	Sigma
gelatine	Roth
glucose	Sigma
glycerol 87 %	GE HealthCare
glycine	Roth
guanidine-HCl	Boehringer
hematoxylin	Sigma
4-(2-hydroxyethyl)-1-piperazineethanesulfonic acid (HEPES)	Sigma
hexacetryltrimethyl ammonium bromide	Roth
hydroden peroxide (H_2O_2) (30%)	Sigma
indoleacetic acid (IAA)	Sigma
IPG buffer 6-11	GE HealthCare
IPG Strip	GE HealthCare
isopropanol	Merck
potassium chloride (KCl)	Merck
$KHCO_3$	Sigma
potassium dihydrogen phosphate (KH_2PO_4)	Roth
K_2HPO_4 (H_2O frei)	Sigma
KOH	Roth
L-lysine	Sigma
methanol	Merck
magnesium chloride hexahydrate ($MgCl_2.6H_2O$)	Roth
sodium carbonate (Na_2CO_3)	Merck
sodium fumerate	Sigma
sodium glutamate	Sigma
sodium pyruvate	Sigma
di-sodium hydrogen phosphate (Na_2HPO_4)	Sigma
sodium thiosulfate pentahydrate ($Na_2S_2O_3 .5 H_2O$)	Merck
sodium orthovanadate (Na_3VO_4)	Sigma
sodium chloride (NaCl)	Roth
sodium hydroxide (NaOH)	Roth
sodium dihydrogen phosphate (NaH_2PO_4)	Sigma
nitro blue tetrazolium, chloride (NBT)	Roth
nonfat dry milk	Roth
n-protein A sepharose 4 fast flow	GE HealthCare
pelikan Ink 4001	Pelikan

Name	Source
Pen Strep	GIPCO
Pharmalytes 3-10 and Pharmalytes 8-10.5	GE HealthCare
phenylmethylsulphonyl fluoride (PMSF)	Roth
phosphoric acid	Roth
ponceau S	Serva
propidiumiodide (PI)	Roth
sodium dodecyl sulphate (SDS)	Roth
sodium pyrophosphate	Sigma
TEMED	GE HealthCare
thiourea	Sigma
trifluoroacetic acid (TFA)	Merck
tris(hydroxymethyl)amino methane	Merck
Triton X-100	Sigma
Trizol	Invitrogen
trypsin	Promega
Tween-20	Sigma
vectaMount	VectorLaboratories Inc.
urea	Merck
water (MS grade)	JT Baker
xylol	Roth

4.1.2. Enzymes and Substrates

Name	Source
Collagenase	Serva
Elastase	Sigma
Enterokinase	Sigma
Myoloperoxidase	Sigma
Trypsin	Sigma
Trypsinogen	Sigma
R110-Ile-Pro-Arg	Invitrogen
R110-Ala$_4$	Invitrogen

4.1.3. Animals

Animal strain	Supliers
C57BL/6 Mäuse	Charles River
UBR1 knockout mice (C57BL6/129 background)	Courtesy by Prof. Dr. A.Varshavsky, USA

4.1.4. Antibodies

Antibodies	Supliers
Primary antibodies:	
Anti-BCL11b antibody, polyclonal rabbit	Bethyl
Anti-phospho ERM antibody, polyclonal rabbit	Cell Signaling
Anti-total ERM antibody, polyclonal rabbit	Cell Signaling
Anti-GAPDH antibody, polyclonal rabbit	Santa Cruz Biotechnology
Anti-DUT-N antibody, polyclonal rabbit	Abcam
Anti-PDCD5 antibody, polyclonal, rabbit	Abcam
Anti-MNAT1 antibody, polyclonal, rabbit	Santa Cruz Biotechnology
Anti-UCK2 antibody, ployclonal, chicken	Abcam
Anti-RGS4 antibody,polyclonal rabbit	Abcam
Anti-UBR1 antibody, monoclonal, mouse	Abnova
Secondary antibodies:	
Anti mouse IgG HRP-linked antibody	Dianova
Anti mouse IgG HRP-linked antibody	Dianova
Anti rabbit IgG HRP-linked antibody	Dianova
Anti rabbit IgG ALP-linked antibody	Dianova
Anti chicken IgG HRP-linked antibody	Dianova

4.1.5. Instruments

Name	Source
BioRad-protein plus Dodeca Cell	Bio-Rad
Cellculture hood US Autoflow	AntAir
Centrifuge	Eppendorf
CO_2-Incubator	Heraus
Epson Expression 1680 pro scanner	Epson
Fluorometer	BMG Labtech
Heating cum shaking blocks	Eppendorf
IEF device, Multiphor II	GE HealthCare
Microscope	Olympus
Mini-PROTEAN 3 Dodeca cell	Bio-Rad
nanodrop ND-1000 spectrophotometer	Peqlab
Nucleofection Device II	Amaxa
pH Meter	SCHOTT Instruments
Semi-dry blotter	GE HealthCare or Bio-Rad
Sonicator	Bandelin Sonopuls
Spectrophotometer (Ultrospec 2100 pro)	GE HealthCare
Typhoon 9400 scanner	GE HealthCare
Ettan Spot Handling Workstation	GE HealthCare
4700- or 4800-Proteomics-Analyzer	Applied Biosystems

Name	Source
MDLC nano-HPLC	GE Healthcare
API QStar Pulsar	Applied Biosystems
Vortex mixer	Scientific Industries Inc.,
Waterbath	GFL
7-Tesla Finnigan LTQ-FT mass spectrometer	Thermo Electron

4.1.6. Kits

Name	Source
Amyl-Kit	Roch Hitachi
Annexin-V-FITC	BD Pharmingen
Annexin-V-APC	BD Pharmingen
CBA Kit (mouse inflammation Kit)	Bectorn Dickinson
DAP Immunhistochemie KIT	Vector Laboratories
ECL-Reagent	Thermo Scientific
Lip-Kit	Roch Hitachi
Nucleofection Kit V	Amaxa
PageRuler, prestained protein marker	Fermentas
Pro-Q® diamond	Molecular probes
SYPRO® Ruby	Bio-Rad
Cell death detection kit, TMR red	Roche

4.1.7. Cell culture material

Cell lines/ Reagents	Supliers
Jurkat human T cell leukemia	DSMZ
huT78 human T cell lymphoma	ATCC
Lymphoblasts cell lines (JBS patients/controls)	University of Erlangen (Prof. Dr. Med. M. Zenker)
100x penicillin/streptomycin	PAA Laboratories
10x Trypsin soyabean inhibitor	PAA Laboratories
FBS	Invitrogen
FCS	Invitrogen
Glucose solution 40% sterile	Braun
HEPES 1M sterile	PAN Biotech
OptiMEM	Invitrogen
RPMI-1640	Invitrogen
Sodium pyruvate 100 mM sterile	Invitrogen
Sodium bicarbonate	Sigma
Plasmocin	Amaxa

Table 1: Lymphoblasts cell lines details:

Chracteristics of Johanson-Blizzard-Syndrome patients

Patient No.	Gender	Mutation	Suspected mutation effect	Suspected Phenotype
P1	Male	Q587X homozygote	No protein	Complete phenotype moderate MR
P2	Male	H136R IVS20+2T>C	Presumed loss of function No protein	Complete phenotype mild MR
P3	Male	Y286X R665X	No protein No protein	Complete phenotype mild to moderate MR
P4	Male	IVS9-13A>G homozygote	Normal splicing at low level possible	Complete phenotype mild MR
P5	Female	IVS4-13G>A homozygote	Normal low splicing	Complete phenotype mild MR
P6	Male	E765del R1242G	No protein Possible residual function	Partial phenotype, normal cognitive function
P7	Female	IVS35-1G>C c.4939delG	No protein No protein	Complete phenotype mild MR
P8	Female	A563D homozygote	Possible residual function	Partial phenotype, normal cognitive function
P9	Female	A563D homozygote	Possible residual function	Partial phenotype, normal cognitive function
P10	Female	IVS1+5G>C V660del	Normal splicing at low level possible Possible residual function	Partial phenotype, normal cognitive function
P11	Female	IVS26+5G>A homozygote	Normal splicing at low level possible	Complete phenotype mild MR
P12	Male	c.3694delC S1427F	No protein Possible residual function	Partial phenotype, normal cognitive function
P13	Female	A563D delExon33	Possible residual function No protein	Partial phenotype, normal cognitive function
P14	Male	c.2546insA IVS16+14C>G	No protein Normal splicing at low level possible	Partial phenotype, normal cognitive function

Chracteristics of controls

Control No.	Gender
K1	Female
K2	Female
K3	Female
K4	Female
K5	Male
K6	Male
K8	Female
K9	Female
K10	Male
K11	Female

4.1.8. Softwares

Software	Supliers
Office (Word, Exel) 2007	Microsoft
GraphPad Prism V5	Graphpad software Inc.,
Sigma Plot V11	Systat Software Inc.,
Soft MaxPro	BMG Labtech
Delta2D	Decodon GmbH
GeneSpring	Agilent Technologies
Cell explorer	BioSciTec GmbH

4.2. Methods

4.2.1. Cell culture

Jurkat human T-cell leukemia (DSMZ, Braunschweig, Germany) and HuT78 human T-cell lymphoma cell lines (ATCC, Manassas, VA, USA) were cultured in Rosewell Park Memorial Institute (RPMI) 1640 medium (Invitrogen, Paisley,UK), supplemented with 1 mM sodium pyruvate, 1x non-essential amino acids (Invitrogen), 10% fetal calf serum (FCS) (Invitrogen) and 5 mg/ml Plasmocin (Amaxa, Cologne, Germany) and maintained in a humidified incubator at 37°C and 5% CO_2. All experiments were performed using cells in the exponential phase of growth.

JBS patients' lymphoblasts cell lines were procured in Martin Zenker´s lab, University of Erlangen (see Table 1 for details). The study was approved by the University Erlangen-Nuremberg Institutional Review Boards. A total of 14 Johansson Blizzard Syndrome (JBS) patients' and 11 controls' cell lines were obtained from University of Erlangen and were grown in Rosewell Park Memorial Institute medium (RPMI) 1640 medium (Invitrogen, Paisley, UK) supplemented with 1mM sodium pyruvate, 1x non-essential amino acids (Invitrogen), 20% fetal calf serum (FCS) (Invitrogen) and 5 mg/ml Plasmocin (Amaxa, Cologne, Germany) and maintained in a humidified incubator at 37°C and 5% CO2. All experiments were performed using cells in the exponential phase of growth.

4.2.2. Cell stocks preparation

For making the JBS patients lymphoblasts cell stocks, approximately 1 million of cells were taken, harvested by centrifugation and resuspended in 2 ml of RPMI media containing

20% FCS, 10% DMSO and 6% glucose (Sigma). The cell suspension was dispensed into cryo-vials placed in a cryo-freezing container filled with isopropanol and stored at -70°C for 24 h and then stored in liquid nitrogen. To revive cells from stocks, the cryo-vial from liquid nitrogen was allowed to thaw at 37°C and diluted with culture medium. The cells were spin down by centrifugation (1000 g, 4°C for 4 min), and supernatant was discarded. The cells were then resuspended in appropriate medium and seeded into culture bottles.

4.2.3. siRNA and cell transfections

BCL11B-specific (*BCL11B*-674) stealth siRNAs and the corresponding non-silencing control (SC) RNA duplexes were designed and synthesized by Invitrogen.

The following sequences of siRNAs were used:

BCL11B specific siRNA-674: CCAAGCAGGAGAACAUUGCAGGUAA

Non-silencing control (SC) siRNA: CCAAAGGACGAGAGCAGGUUCAUAA

Five micrograms of each siRNA were used for each transfection. Cells were transfected with an Amaxa Nucleofection Device II (Amaxa), using the Amaxa nucleofection Kit V or T-cell nucleofection kit according to the manufacturer's instructions.

The *BCL-xL* coding sequence was amplified and ligated into *Xho*I and *Hind*III sites of the pIRES2-EGFP vector (BD Clontech, Heidelberg, Germany) using T4-DNA Ligase (Promega, Madison, WI, USA). Primers for amplification of BCL-xL coding sequence (restriction sites are underlined):

BCLxLcds-F: CCG<u>CTCGAGG</u>CAGATTGCAGATCTGAGGCA

BCLxLcds-R: CCC<u>AAGCTT</u>CAGTGGACTCTGAATCTC

For stable transfection, Jurkat and HuT78 cells were transfected and selected in the presence of 1 mg/ml geneticin (Invitrogen).

4.2.4. Determination of apoptosis: Annexin V binding assay

Phosphatidylserine is an anionic phospholipids located in the inner leaflet to the plasma membrane (PM) of living cells. During apoptosis PS residues are translocated to the external leaflet of the PM through complex mechanisms, involving at least in part the increase in scrablase activity (Fadeel et al 1999)Fadeel et al. 1999, Farsch et al. 2000). *In vivo*, those residues are recognized by the PS receptor (OSR) on macrophages that phagocyte apoptotic cells through the fixation of annexin-V conjugated to several fluorochromes. The use of annexin-V in combination with propidium iodide (PI) allows one to discriminate early from

late apoptotic/necrotic lymphocytes. Single positive cells (annexin-V$^+$, PI$^-$) are early apoptotic lymphocytes in which apoptotic bodies are just formed, where as double positive cells (annexin-V$^+$, PI$^+$) are late apoptotic/necrotic lymphocytes in which necrosis is started.

Cells were transfected with *BCL11B* siRNA, and Annexin-V/PI binding assays were performed at 24 h, 48 h and 72 h after siRNA nucleofection using the BD Clontech ApoAlert Annexin-V-FITC or Annexin-V-APC (BD Pharmingen) kits according to the manufacturer's instructions. The percent of apoptotic cells was quantified by FACS analysis as described in Grabarczyk, P et al, (Grabarczyk et al 2007).

4.2.5. Cytofluorometric analysis of mitochondrial transmembrane potential ($\Delta\psi_m$):

An early drop in mitochondrial membrane potential occurs during the intrinsic pathway of apoptosis which occurs through mitochondria (Petit et al 1995). Thus, the analysis of the mitochondrial transmembrane potential (ψ_m) is the direct and best method to establish the mitochondrial pathway of apoptosis. Variations in ψ_m can be analyzed following uptake of the cationic lipophilic dye DiOC$_6$ by apoptotic cells. The accumulation of the cationic lipophilic fluorochrome 3,3′-dihexyloxacarbocyanine iodide (DiOC$_6$) in the mitochondrial matrix is directly proportional to mitochondrial potential ($\Delta\psi_m$). DiOC$_6$ diffuses through the plasma membrane enters cytoplasm and finally accumulates inside the mitochondrial matrix. DiOC$_6$ accumulation is driven by the ψ_m and thus any significant loss of this potential is evidenced by a decrease in DiOC$_6$ staining. $\Delta\psi_m$ was determined at 3 different time points i.e 24 h, 48 h, 72 h after cell transfection in Jurkat and HuT cells. Cells were incubated with 50 nM DiOC$_6$ (Molecular Probes; distributed by Mobitec, Göttingen, Germany) at 37°C for 30 min (Sonnemann et al 2004). After washing, at least 10,000 cells were analysed using a Becton Dickinson (Heidelberg, Germany) FACS calibur and CellQuest and WinMDI2.8 software (Becton Dickinson, Heidelberg, Germany). Data were gated to exclude debris.

4.2.6. Cell lysate preparation

Cells were harvested when the confluency of the cells is not high and centrifuged at 100 g. The pellet was washed 2 times with 1x PBS to remove the media and debris. After washes the cell pellet was resuspended in desired buffer for the experiment [for 2D-DIGE experiments- 2D rehydration buffer (8 M Urea, 2 M Thiourea, 2% CHAPS) and for western blots-RIPA buffer (50 mM Tris-HCl pH 7.5, 150 mM NaCl, 1% NP-40 and 0.1% SDS, 0.5% sodium-deoxycholate) and completely lysed by sonication i.e. 3 times for 5 seconds each with

9 cycles at 50 % of energy (Bandelin Electronics, Berlin, Germany). After removal of cell debris by centrifugation (20,000 g for 20 min at 4°C), the protein concentration of the crude protein extracts was determined according to the Bradford method.

4.2.7. Bradford's method of protein estimation:

A BSA-standard stock solution (0.1 µg/µl) was serially diluted for preparation of a standard curve as described in the following table.

Amount (µg)	0	1	2	4	6	8	10	12
0.1 µg/µl BSA (µl)	0	10	20	40	60	80	100	120
H_2O (µl)	800	790	780	760	740	720	700	680

Then, 200 µl of Bradford reagent was added into each tube, thoroughly mixed by vortexing and incubated for 5 min at room temperature in dark. The absorbance was measured at 595 nm using a spectrophotometer.

For the protein measurement of samples, the extract was diluted 1 to 10 and then 10 µl of the diluted sample was used for the protein assay. The protein concentrations of the samples were calculated with the aid of the standard curve.

The samples were first tested by silver staining method for quality control by using minimum quantity of sample. Once it is affirmed that sample preparation is good by not observing any degradation of high molecular weight proteins, these samples were used for 2D-DIGE and 1D SDS-PAGE followed by western blot.

4.2.8. 1D SDS-PAGE:

The charge to mass ratio varies for each protein (in its native or partially denatured form). Hence, SDS-PAGE uses an anionic detergent (SDS) to denature proteins. Upon denaturation the protein molecules become largely linearized. One SDS molecule binds to 2 amino acids. Due to this, the charge to mass ratio of all the denatured proteins in the mixture becomes constant. These protein molecules move in the gel matrix (towards the anode) on the basis of their molecular weights only and are separated accordingly. The gel matrix is formed of polyacrylamide using 1.5 M Tris-HCl pH 8.8, 12.5% acrylamide/bisacrylamide [37.5:1], 0.4% SDS, 0.05% APS, 0.0025% TEMED. The polyacrylamide chains are cross linked by N, N-methylene bisacrylamide monomers. Polymerisation is initiated by ammonium persulfate

(radical source) and catalysed by TEMED (a free radical donor and acceptor). Samples were taken in equal amounts and boiled together with 2x SDS-PAGE sample buffer containing 125mM Tris-HCl pH 8.8, 4% SDS, 30% Glycerine, 10% β- mercaptoethanol and 0.01% bromophenol blue for 5 min and loaded in wells. These gels are usually run at constant current in 1x running buffer (25 mM Tris, 192 mM glycine, 0.4% SDS) and gel run was stopped once the dye front reached the bottom and processed for western blot transfer.

4.2.9. Fluorescent dye labelling for DIGE

Prior to the two-dimensional protein gel electrophoresis (2-DE), protein extracts were labeled with fluorescent CyDyes according to the manufacturer's instructions (GE Healthcare, Freiburg, Germany). CyDye stock solution of 1 mM was prepared by addition of a defined volume of high quality DMF and vortexed vigorously for 30 seconds and then centrifuged for 30 seconds at 15000 g. The CyDye stock solution was stored at -20°C in a freezer or directly used to prepare a working solution by mixing one volume of CyDye with 1.5 volumes of DMF.

The pH of the protein extracts was adjusted to pH 8.5 with 50 mM NaOH and final protein concentrations were recalculated. 50 µg of each sample was labeled with 400 pmol of CyDye on ice in the dark for 30 min. The labelling reaction was stopped by adding an equivalent (CyDye solution) volume of 10 mM lysine and kept for 10 min on ice in the dark again. The samples were now ready for performing 2-DE or were stored at - 70°C for up to three months in the dark. The fluorescent properties of Cy2, Cy3 and Cy5 can be adversely affected by exposure to light, so it is highly recommended that the exposure to light sources is kept as minimum as possible. The details of the samples amount taken and processing are described below.

BCL11B siRNA transfected samples: 100 µg of each protein extract was labeled with 800 pmol of Cy5 and Cy3 dyes in case of Jurkat, HuT, Jurkat *BCL-xL* over expressing cells transfected with *BCL11B* siRNA and SC and BCL11b over expressing and non-over expressing cells. Furthermore, 100 µg of each sample was mixed and labeled with 800 pmol of Cy2 dye, generating a pooled standard of all proteins present in the crude protein extracts. Labelling of 200 µg of protein extract from each experimental condition allowed the separation of four replicates by 2-DE.

JBS Lymphoblasts samples: For JBS lymphoblasts samples, only 50 µg of each patients sample was labeled with 400 pmol of Cy5 and Cy3 dyes and 400 µg of controls pooled

sample was labeled with 3200 pmol of Cy5 and Cy3 samples. A standard pool was made by taking all 14 individual patient samples and controls pooled sample in equal concentrations. This standard pool was labeled with Cy2 dye. Labelling of 100 µg of patient sample and 400 µg of control pooled samples permitted two technical replicates for each patient's sample (1 Cy3, 1 Cy5) and 8 technical replicates for controls pooled sample (4 Cy3, 4 Cy5) in total.

4.2.10. Rehydration

Usually 2D-DIGE gels were loaded with 50 µg of each Cy2-labeled pooled standard, Cy5 and Cy3-labeled samples. Mixed CyDye-labeled protein extract (150 µg) was added to a desired volume of rehydration solution containing 8 M urea, 2 M thiourea, 2% (w/v) CHAPS, 28 mM DTT, 1·3% (v/v) Pharmalytes, pH 3–10, and trace amount of bromophenol blue. Immobilized pH gradient (IPG) strips (GE Healthcare) with a pH range from 4 to 7 were rehydrated in the protein-containing solution for 24 h under low-viscosity paraffin oil. For 24 cm long IPG dry strips, 450 µl of 2-D rehydration solution containing various concentrations of protein sample was used. This rehydration process allows all proteins in the buffer to attach to the gel surface of the IPG strip by capillary action and this can be visualized with the aid of blue colour by the attribute of bromophenol blue in the buffer.

4.2.11. IEF (Iso Eletric Focusing)

Subsequently, the IPG strips were washed with distilled water and subjected to isoelectric focusing by keeping a paper wick wetted with 15 mM DTT in water at the cathode end with the following voltage/time profile keeping constant current at 2 mA and constant power at 5 W. DTT, which is a strong reducing agent, was added to ensure reduced condition of proteins during 1st dimension.

IPG strip pH 4-7, 24 cm:

step	V	Vh	time (h:min)
1	500	1	0:01
2	3500	3000	1:30
3	3500	57000	16:20
total		60001	17:51

4.2.12.2D SDS-PAGE second dimension

After 1st dimension IEF, IPG strips were incubated consecutively for 15 min each in equilibration solutions A and B [Solution A: 50 mM Tris/HCl, pH 8·8, 6 M urea, 30% (v/v) glycerol, 4% (w/v) SDS, 10 mg DTT ml^{-1}; Solution B: as solution A, but 25 mg iodoacetamide ml^{-1} instead of DTT]. By this equilibration process, all proteins on the strips will be reduced and alkylated at their free −SH group containing cystein residues to remove the disulfide bridges. After equilibration IEF strips are subjected to 2nd dimension SDS-PAGE separation by use of continuous gels of pH 8.8 as resolving gels (1.5 M Tris-HCl pH 8.8, 12.5% acrylamide/bisacrylamide [37.5:1], 0.4% SDS, 0.05% APS, 0.0025% TEMED). Strips were sealed with 0.5% agarose in 1x SDS-PAGE running buffer solution (25 mM Tris, 192 mM glycine, 0.4% SDS). In the second dimension, proteins were separated according to their molecular weights on 12·5% acrylamide gels run in a Dodecan Electrophoresis System (Bio-Rad) at 2 W per gel over night.

4.2.13.DIGE scanning

After 2nd dimension separation, gels were cleaned with distilled water and each gel was scanned with separate laser excitation for each of the three CyDyes with a Typhoon 9400 scanner (GE Healthcare, Munich). The three different laser excitations used are listed below.

(1) channel Cy2: 520 BP 40 / Blue2 (488 nm).

(2) channel Cy3: 580 BP 30 / Green (532 nm).

(3) channel Cy5: 670 BP 30 / Red (633 nm).

The photo multiplier tube (PMT) voltage for each channel was adjusted such that the intensities in all three channels are almost equal, which is a prerequisite for later analysis. This PMT voltage adjustment was done using the Image Quant software, where we can see the intensity of a spot in all three channels. After scanning, gels were soaked in fixing solution containing ethanol (50%), acetic acid (12%) to remove excess SDS on gels and subsequently washed with distilled water and stained with appropriate volume of colloidal coomassie brilliant blue (coomassie brilliant blue G-250- 0.08%, $(NH_4)_2SO_4$-8%, phosphoric acid- 0.8%, methanol- 20%) for visualization of proteins. After overnight incubation in staining solution, gels were washed with 20% methanol to remove excess dye colour on gel.

4.2.14. Silver staining method of proteins visualization

To validate the quality of the sample preparation prior to do 2D-DIGE or Western blotting experiments samples an aliquot of the sample (75 μg) was separated by 2D-PAGE and stained with a silver staining method. Prior to the staining gels were soaked in fixing solution containing ethanol (50%), acetic acid (12%) and formaldehyde (0.05%) for a minimum of 1 h. Then, the gels were washed with 50% ethanol to remove excess acetic acid and sensitized in 0.02 % $Na_2S_2O_3$ solution for 1 min. Longer exposure time leads to more intense background staining. Immediately after sensitization gels were washed thoroughly for 20 sec with distilled water twice. Then, the gels were incubated for 20 min in silver nitrate solution containing 0.2% of $AgNO_3$ and 0.0375% of formaldehyde. Gels were washed twice for 20 sec with distilled water and developed in solution containing 0.025% formaldehyde, 0.005% $Na_2S_2O_3$ and 6% Na_2CO_3 till all proteins on gel are visualized without much background signals. The developing reaction was stopped with 1% glycine solution and gels were kept in the same for 30 min before they were washed with distilled water and scanned.

4.2.15. Image analysis

One 2D-DIGE gel scanning gave 3 different images corresponding to the 3 CyDyes used in the labelling reaction. All gel images obtained were cropped in Image Quant v5.2 (Molecular Dynamics) by selecting almost the same area of interest and then imported into Delta2D version 2.4 (Decodon GmbH, Greifswald, Germany) for further analysis. In Delta2D, the images were organized into different groups' i.e. internal standard group (Cy2) and sample groups (Cy3, Cy5). All internal standard images were matched with a selected internal standard image which was chosen as the master image. This Cy2 channel images matching allows matching other channel images also by usage of the implicit mode of matching. Once all the internal standard images were matched well a fused gel image was created by union fusion of all images in the project. Subsequently, spot detection was performed for the fusion gel and spots were edited finely to remove unwanted spot detection. The spot map of the fusion gel was then transferred to all gel images. Spots were labeled on fusion gel image with IDs. After background subtraction absolute spot volumes were calculated with the Delta2D software and exported to the GeneSpring software version 7.3 (Agilent Technologies) for statistical analysis.

4.2.16. GeneSpring analysis

The text file containing absolute volumes of all spots with IDs was imported into GeneSpring and the data were divided into groups and experiments as in Delta2D. All data were transformed and normalized applying the following procedure:

i) All spot volume values below 0.01 were raised to 0.01 (data transformation) in order to prevent later on artificially high ratios that originate from spots with very low volumes.

ii) All spots values in each image were normalized to the median spot value of the image to remove intergel differences in the spot intensities (median normalization).

iii) Spots in the same position in the same gel were normalized to the corresponding spot of the internal image standard Cy2-channel (internal standard normalization).

iv) Spots derived from treated cells and patients were divided by the corresponding control (ratio normalization).

Protein levels were considered to be changed when the following two criteria were fulfilled: (i) changes in the level of the protein had to be statistically significant, as defined in a statistical group comparison of the values of the selected conditions with a parametric test (Welch t test, P value cut-off 0·05), as defined in the GeneSpring software package; and (ii) the change in level had to exceed a factor of 1.5.

PCA analysis and class prediction analysis of JBS lymphoblasts

PCA analysis and class prediction analysis of JBS lymphoblasts was done using Gene spring software version 7.3.1 (Agilent Technologies, Waldbronn, Germany). For PCA analysis a one way ANOVA test was done using all spots volumes data keeping a p value of 0.01 as filter. A total of 350 spots passed this one way ANOVA test and out of these 350 spots, the 20 spots having the highest predictive strength values were selected using Golub's method (Golub T R, Science 1999) and used by a support vector machine to predict different classes (i.e. Controls, Patients with UBR1 signal and Patients without UBR1 signal).

To distinguish between controls and patients with UBR1 signal a one way ANOVA test was done like above but keeping a p value as low as 0.001 as filter. Only 12 spots passed this filter value and out of this 12, the top 5 with high predictive strength were selected using the same Golub's method mentioned above, to predict controls and patients with residual UBR1 signal. For this 5 spots ROC curves were drawn using Graph Pad prism software version 5

(GraphPad software Inc., CA, USA) and these individual ROC curves drawn together using MS-Excel.

4.2.17. Assessment of protein phosphorylation by staining with Pro-Q® diamond staining

Pro-Q® Diamond phosphoprotein staining (Molecular probes, Oregon, USA) is very useful for analyzing the phosphorylation state of the entire proteome, because it selectively stains phosphoproteins in polyacrylamide gels. This proprietary fluorescent stain allows direct, in-gel detection of phosphate groups attached to tyrosine, serine, or threonine residues, without the need for antibodies or radioisotopes. 150 µg of each scrambled control and siRNA samples were subjeted to isoelectric focusing on 24 cm, 4 to 7 pH range immobilized pH gradient (IPG) strips (GE Healthcare), followed by second dimension separation as described above. After second dimension gels were fixed in ethanol (50%) acetic acid (12%) solution overnight to ensure all SDS is removed and washed with distilled water for 4 times, 15 min each. Then, the gels were incubated in Pro-Q® Diamond phospho protein staining solution for 2 h in dark with gentle agitation. After staining, gels were destained using propylene glycol (20%), 1M sodium acetate pH4 (5%) for 3 times, 30 minute each. This step is crucial to reduce the background and nonspecific signals. Prior to the scanning gels were washed with distilled water for two times, 10 min each. Then, the gels were scanned using a Molecular imager FX (Biorad, Munich, Germany) at the ex/em wavelength of 532/555 nm.

4.2.18. SYPRO® Ruby staining

The Pro-Q® Diamond phosphoprotein gel staining is most useful when used in conjunction with SYPRO® Ruby (Biorad) protein gel staining. The SYPRO® Ruby dye is a total-protein stain that is quantitative over three orders of magnitude. Determining the ratio of Pro-Q® Diamond dye to SYPRO® Ruby dye signal intensities for each band or spot thus provides a measure of the phosphorylation level normalized to the total amount of protein. Using both stains in combination, it is possible to distinguish a lightly phosphorylated, high-abundance protein from a heavily phosphorylated, low-abundance protein. After Pro-Q® Diamond phospho staining the same gels were washed with distilled water for 1 h with 3 changes and fixed in 40% ethanol and 10 % acetic acid for 1h and again washed with water 3 times, 10 minutes each. Then, the gels were stained with SYPRO® Ruby (Biorad) stain for

overnight. Finally, the gels were washed with water prior to scanning using a Molecular imager FX at the ex/em wavelength of 450/610 nm.

The images of the Pro-Q® Diamond and SYPRO® Ruby stains, which reflect protein phosphorylation and total protein level, respectively, were matched using version 3.4 of the Delta2D software (Decodon GmbH) as described above. The phosphorylation signal was considered specific and significant when the signal in the Pro-Q® Diamond stained image was stronger than that of the SYPRO® Ruby stained image.

4.2.19. Protein identification

MALDI TOF-TOF measurement: Differentially expressed and statistically significant spots were manually excised from preparative Colloidal CBB-stained 2-D gels, digested by trypsin, and resulting peptides were spotted onto a MALDI-target using an Ettan Spot Handling Workstation (Amersham Biosciences), according to the standard protocol as described by Eymann et al,. (Eymann et al 2004). The MALDI TOF-TOF measurement of spotted peptide solutions was carried out using a 4800 MALDI TOF/TOF Analyzer (4800 MALDI TOF-TOF Analyzer, Applied Biosystems, Foster City, CA, USA). MS analysis was performed with the following settings: 10 sub-spectra with 100 shots per sub-spectrum were accumulated using a random search pattern, a mass range of m/z 804 to 4000. An internal calibration was automatically performed as a one or two point calibration for self-digested trypsin fragments at m/z 1045.5 and m/z 2211.1. MS/MS analysis was performed for the 5 most intensive peaks of the MS spectrum. For one main spectrum, 20 sub spectra with 125 shots per sub spectrum were accumulated using a random search pattern. An internal calibration was automatically performed as one-point calibration if the mono-isotopic arginine $(M+H)^+$ m/z at 175.119 or lysine $(M+H)^+$ m/z at 147.107 reached a signal-to-noise (S/N) ratio of at least 20. The peak lists were created using the GPS Explorer software (Applied Biosystems) with the following settings: mass range from 60 Da to a mass that was 20 Da lower than the precursor mass; peak density of 10 peaks per 200 Da; minimal area of 100 and maximal 100 peaks per precursor; minimal S/N ratio of 7. Database searches employed *Homo sapiens* specific databases (SwissProt Version 51.5, IPI human Version 3.23 and 3.26 respectively) and *Mus musculus* specific databases (SwissProt Version 54.6) using the Mascot search engine (Ver. 2.0) (Matrix Science Ltd, London, UK). The identification of a protein spot was considered significant if the Mowse score exceeded a value of 60, which corresponds to a *p* value of 0·05.

ESI-MS/MS measurement: 2D Gel spots of interest were excised and in gel digested using sequence grade trypsin (Promega) over night. Peptides were extracted using 50% acetonitrile containing 1% acetic acid in water bath sonicator. The MS analysis of the peptide mixture extracted from gel was carried out using a Finnigan LTQ/Orbitrap (Thermo Electron, Bremen, Germany) coupled to nano Acquity UPLC system (Waters Inc, USA). Chromatographic separation of peptide mixture was done using 100µm X 100mm Nano acquity UPLC column thermostatt at 35°C. Followed by 2 min wash using solution A (2% acetonitrile,0.1% aceticacid) peptides were eluted using a 50min linear gradient to 60% solution B (90% acetonitrile, 0.1% acetic acid) with a flow rate of 1µl/min. Data acquisition and reduction was performed with Xcalibur version 2.0 (Thermo Electron, San Jose, CA, USA). Protein identification search was done on a Sequest cluster (Thermo Electron, San Jose, CA, USA) with Swissprot human database version 51.5. Protein score above 60 with 2 unique peptides was the criteria for true identification.

4.2.20. Western blotting

Western blots were performed after proteins separation by 1D SDS-PAGE (Chapter 4.2.8) or 2D SDS-PAGE (Chapter 4.2.12). Immobilized pH gradient (IPG) strips of pH range 4-7 ,7 cm were rehydrated with 50 µg of protein and 11cm pH 4-7 range IPG strips were rehydrated with 125 µg of protein containing rehydration buffer (8 M urea, 2 M thiourea, 2% (w/v) CHAPS, 28 mM DTT, 1.3% (v/v) Pharmalytes, pH 3-10, and bromphenol blue) for over night and subjected to isoelectric focussing with the following voltage/time profile keeping constant current at 2 mA and constant power at 5 W:

IPG strip pH 4-7, 7 cm:

step	V	Vh	time (h:min)
1	200	1	0:01
2	3500	2800	1:30
3	3500	5200	1:30
total		8001	3:01

IPG strip pH 4-7, 11 cm:

step	V	Vh	time (h:min)
1	300	1	0:01
2	3500	2900	1:30
3	3500	9100	1:30
total		12001	3:01

A)
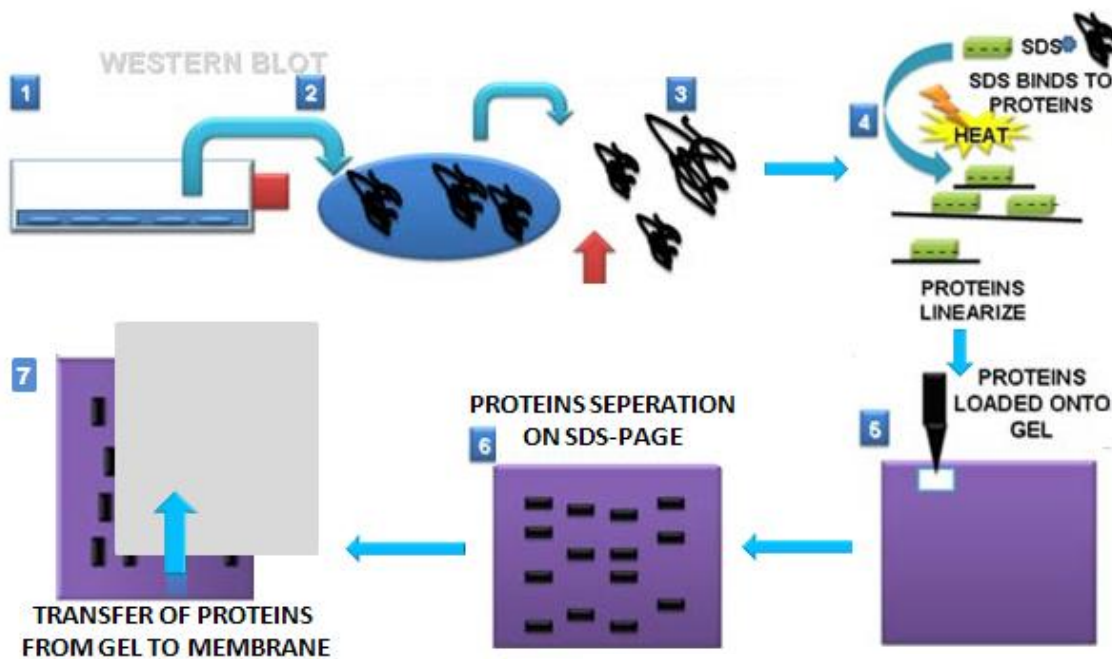
(Modified from molecularstation.com)

B)
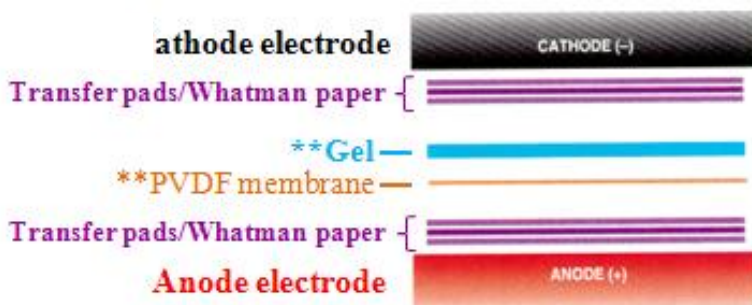
Fig. 9: A) Work flow describing steps from cell culture to Western blotting. Cells were grown in appropriate medium (1) and harvested at their exponential growth phase (2). These cells were lysed and protein extraction was done using sonication (3). These proteins were loaded on SDS-PAGE gels (4, 5) where they were separated according to their molecular weights (6). Then, the separated proteins were blotted onto a PVDF membrane using a semidry transfer apparatus. **B) The set-up of proteins transfer from gel to PVDF membrane.** Pre-equilibrated PVDF membrane was kept at positive end (Anode) and gel was kept at negative end (Cathode) as

the negatively charged proteins move towards positive end under electric field. Both gel and membranes were sandwiched by set of biorad transfer pads or Whatman paper.

2D separation was performed in the pH range of 4-7 using two different lengths of IPG strips. 7cm strips were used for separation of 50 µg, whereas 11cm strips were used for separation of 125 µg of protein. After 2nd dimension and normal 1D SDS-PAGE separation, proteins were blotted onto a pre equilibrated Immobilon PVDF membrane (Millipore, Schwalbach, Germany) using a semidry western transfer apparatus (GE Healthcare). For pre-equilibration the PVDF membrane was soaked in 100% high purity methanol solution for 15 sec to open the pores on the membrane to capture the proteins which were going to be transferred. Then, the membrane was immediately washed with distilled water for a couple of minutes and equilibrated with chilled transfer buffer for 10 min. Biorad transfer pads or Whatman papers were taken in the same size of the gel and soaked in chilled transfer buffer (25 mM Tris, 200 mM Glycine, 20% Methanol, pH 8.5). As it is shown in the Fig. 9B the gel was placed at the cathode end and the membrane was placed at anode end and both of these are sandwiched by Biorad transfer pads or Whatman papers, which aid in transfer by conducting the current through. Transfer process was carried out for 90 min using 1.5mA per cm^2 of membrane area. To test whether proteins are transferred or not blot was stained with ink stain. Ink stain can be prepared by adding 1% acetic acid and 0.1% pelikan ink in PBS/T solution (150 mM NaCl, 2.7 mM KCl, 10 mM Na_2HPO_4, 1.8 mM KH_2PO_4, pH 7.4 containing 0.1% Tween-20). After scanning the membranes, the stain was removed by washing vigorously in PBS/T for three times, 5 min each. Then, the membrane was incubated in blocking solution containing 5% non-fat dry milk powder (Carl Roth GmbH, Karlsruhe, Germany) in TBS/T solution (20 mM Tris, 138 mM NaCl, pH 7.6 containing 0.1% Tween-20) for at least 1 h. This blocking step is useful to cover the non-protein area to avoid any non specific binding of antibodies onto the membrane. After blocking the membrane was washed with TBS/T solution three times, 5 min each before the membrane was incubated with primary antibody, which was diluted according to manufacturer's suggestion i.e. BCL11b (1:5000) (Bethyl, Montgomery, TX, USA), phospho ERM (1:1000), total ERM (1:1000) (Cell signaling, Danvers, MA, USA), DUT-N (1:1000) (Abcam, Cambridge, UK), PDCD5 (1:1000) (Abcam, Cambridge, UK), MNAT1 (1:1000) (Santacruz Biotechnology, Santa Cruz, CA, USA), UCK2 (1:2000) (Abcam, Cambridge, UK), UBR1 (1:500) (Abnova GmbH, Heidelberg, Germany), RGS4 (1:500) (Abcam, Cambridge, UK) and GAPDH (1:1000) (Santacruz Biotechnology, Santa Cruz, CA, USA) in TBS/T for overnight at 4^oC. The dilution

used for different antibodies is given in the table of materials also. After overnight incubation with primary antibodies the membrane was washed in TBS/T solution for three times, 5 min each. The membrane was incubated with an anti-rabbit or anti-mouse or anti-chicken secondary antibody (Dianova GmbH, Hamburg, Germany) solution in TBS/T according to primary antibody source for 1h at room temperature. Afterwards, the blot was washed three times for 5 min each with TBS/T buffer. In case of Alkaline Phosphatase (AP) conjugated secondary antibodies, the detection reaction was carried out in NBT/BCIP (Carl Roth GmbH, Karlsruhe, Germany) solution after the blot was equilibrated with AP buffer (100 mM Tris, 100 mM NaCl, 5 mM $MgCl_2$. $6H_2O$ pH 9.5) for 5 min. After the developing reaction was stopped by washing the blot with distilled water and then the blot was dried at room temperature. Finally, the blot was scanned using an Epson Expression 1680 Pro scanner for further analysis. In case of Horse Radish Peroxidase (HRP) conjugated secondary antibodies, the detection reaction was carried out in super signal west femtomaximum sensitivity substrate solution (Pierce, Rockford, IL, USA) for 5 min, excess substrate solution was removed with soft tissue and the membrane was scanned using a Lumi-Imager instrument (Roche GmbH, Mannheim, Germany). Signal intensities were quantified using Imagequant software version 5.2 (GE Healthcare) and protein specific intensities were corrected for the corresponding GAPDH signal intensity.

4.2.21. DNA isolation

Jurkat, HuT78 and Jurkat *BCL-xL* over-expressing cells transfected with *BCL11B* siRNA and scramble control siRNA were harvested after 48 h of transfection. These cells were centrifuged and washed with cold 1x PBS twice. After washing the cell pellet was used for DNA isolation. DNA isolation was done using a DNeasy blood and tissue kit (Qiagen, Hilden, Germany) according to manufacturer's instructions for cultured cells. DNA concentration was measured using nanodrop ND-1000 spectrophotometer (Peq lab, Biotechnics, GmbH).

4.2.22. Uracil N-Glycosylase (UNG) assay

Uracil N-Glycosylase is normally used in RT-PCR purification steps to remove any dUTP containing DNA plasmids. Here we used UNG to see whether DNA samples from Jurkat and HuT cells contain dUTP. The UNG enzyme digests dUTP containing DNA and forms apurinic and apyrimidinic (AP) sites, where nucleotide had been excised. These AP

sites containing DNA can be degraded by NaOH reaction. Extracted DNA samples of siRNA and scrambled control transfected Jurkat, Hut and Jurkat *BCL-xL* cells were taken in equal amounts (1 µg) and incubated with 2×10^{-3} U/ml UNG enzyme (Roche Diagnostics, USA) at 37°C in 10x PCR buffer (Roche Diagnostics, USA), containing 15 mM $MgCl_2$ for 1 h. After 1 h, 60 mM NaOH was added to allow cleavage of AP sites and reaction mixtures were incubated at 85°C for 10 min. Products were detected by the standard ethidium-bromide staining after agarose gel electrophoresis on 0.75% (w/w) agarose gels.

4.2.23. Agarose gel electrophoresis

The separation of DNA or RNA molecules on agarose gels can be achieved by moving negatively charged nucleic acid molecules through an agarose matrix in an electric field (electrophoresis). Shorter molecules move faster and migrate further than longer ones. Agarose gels were prepared by solubilizing the agarose powder in 1x TAE buffer (40 mM Tris-acetate, pH 8.3, 1 mM EDTA, pH 8.0) and boiling in a microwave oven. Agarose melted in TAE was allowed to cool down to 60°C and the ethidium bromide (10 mg/ml dd H_2O) was added to a final concentration of 0.5 µg/ml. Then, the mixture was poured into a gel platform fixed on flat surface without any air bubbles. An appropriate comb was inserted to load samples onto gel. The DNA samples were prepared in 5x DNA loading buffer (0.2 mM EDTA, pH 8.0, 25 % (w/v) sacharose, 0.25 % (w/v) bromophenol blue) to fetch 1x final concentration and loaded onto the gel. The electrophoresis was performed in TAE buffer with constant current (80 mA) supply until the tracking dye reached 10 mm above the end of gel. The separated DNA was visualized under UV light by the virtue of ethidium bromide in gel and molecular weight of the unknown bands compared with known marker, which was loaded together with samples.

4.2.24. Animal experiments

For animal studies, we used a previously constructed strain of UBR1^{-/-} mice with a C57BL6/129 mixed background (Kwon et al 2001). Wild-type littermates served as controls. All animal studies were approved by the Animal Use and Care Committee of the University of Greifswald and University of Erlangen.

4.2.25. Induction of acute pancreatitis using Caerulein

Pancreatitis was induced in 6- to 8-week-old UBR1$^{-/-}$ mice and wild-type littermates weighing 20–24 g. After fasting for 18 h, mice were given *ad libitum* access to water; the secretagogue caerulein (Pharmacia Biotech AB) was administered using seven intraperitoneal injections of 50 μg per kg of body weight at hourly intervals to elicit secretagogue induced pancreatitis. As controls, mice injected with isotonic saline solution were used. After eight hours, blood samples were collected under ether anaesthesia, then the pancreas and lung organs were rapidly removed by dissection. The fat was trimmed off and washed in 1x PBS to remove any blood contamination, and portions of pancreas and lung were either fixed in 5% formaldehyde and later on embedded in paraffin according to the standard protocol. The main part of pancreas and lung was snap frozen in liquid N_2 and stored at -80°C until further analyses.

4.2.26. Measurement of enzyme levels in serum

4.2.26.1. Measurement of amylase levels in serum

In acute pancreatitis generally amylase levels in blood increases to 4-6 magnitudes of normal levels within 12 h and 8 h in humans and mice, respectively. Later on amylase levels decrease. Blood was collected by aortic puncture during sacrificing of mice. Serum was prepared from blood clots by centrifugation using standard procedures and stored at -20°C. Serum α-amylase activity levels were measured with a Dynatech MR 5000 Elisa reader machine (EPS method, Kruse-Jarres et al., J Clin Chem Clin Biochem 1989) using the ethylidine protected 4,6-ethylidene-(G_7)-1-4-nitrophenyl-(G_1)-alpha-D-maltoheptaoside (Roche Diagnostics, Mannheim, Germany), as substrate and in accordance with the manufacturer's protocol.

4.2.26.2. Measurement of lipase levels in serum

Lipases are glycoproteins with a molecular weight of 47 kDa. They are defined as triglyceride hydrolases, which catalyze fatty acids by the cleavage of triglycerides, followed by the formation of monoglycerides. Lipase levels increases within 4-6 h in acute pancreatitis conditions. Blood was collected by aortic puncture during sacrificing of mice. Serum was prepared from blood clot and centrifugation using standard procedures and stored at -20°C. Serum lipase levels were measured using 1,2-O-Dilauryl-rac-glycero-3-glutaric acid- (6-methylresorufin)-ester (DGGR assay) as substrate which releases glutaric acid spontaneously

upon cleavage and produce red colour in alkaline solution, which is measured photometrically by the Dynatech MR 5000 Elisa reader in accordance with manufacturer's protocol (Roche Diagnostics, Mannheim, Germany)

4.2.27. Measurement of myeloperoxidase (MPO) activity in lung and pancreas homogenates

The 150 kDa MPO enzyme belongs to peroxidase family and is linked to inflammation and cardiovascular diseases. This enzyme is most abundantly present in neutrophil granulocytes. Generally raised levels of inflammatory mediators like cytokines and MPO are observed during acute pancreatitis. Part of the pancreas or lung was taken and homogenized in dounce S-glass homogenizer (B.Braun-Melsungen AG, Melsungen, Germany) with 5 to 6 strokes using 500 μl of homogenization buffer (20 mM KH_2PO_4, pH 7.4). A small aliquot (100 μl) of this homogenate was taken aside for protein estimation and protein was extracted by ultrasonication using 60% of energy 9 cycles for 10 sec, repeated twice. Then, the homogenate for protein preparation (100 μl) and remaining (400 μl) were centrifuged at 10,000 g for 15 min at 4^oC. The supernatant of the sonicated sample was taken for protein estimation. The supernatant of remaining homogenate was aspirated by vacuum pump and the pellet was resuspended well in 500 ml of freshly prepared extraction buffer containing KH_2PO_4 (50 mM) pH 6, EDTA (5 mM), SBTI (5 mM), PMSF (100 μM) and hexacetyl trimethyl ammonium bromide (0.5%) and snap frozen in liquid nitrogen. The solution was thawed at 37^oC and again snap frozen. This freezing and thawing steps were repeated for four times and at the end the samples were ultrasonicated as described above. Then, the samples were centrifuged at 10,000 g for 15 min and supernatants were collected in fresh tubes and used for MPO activity measurement. MPO activity was measured using 0.53 mM O-dianisidine and 0.15 mM H_2O_2 as substrates in measuring buffer (50 mM KH_2PO_4, pH 6). The increase in colour of chromogenic product was monitored at A_{460} at room temperature, using a Dynatech MR 5000 Elisa reader. The results are expressed as units of MPO activity derived from standard curve, with 1 unit corresponding to oxidation of 1 μmol H_2O_2 per min per mg of pancreatic or lung protein.

4.2.28. Detection of protease activity in pancreatic homogenates

Generally protease activity levels are elevated upon pancreatic damage, which are secreted by pancreas. Among the proteases trypsin, chymotrypsin and elastase are most commonly observed and effective in indulging pancreatic tissue damage. Trypsin preferentially cuts at arginine (R) and lysine (K), elastase at alanine (A) and chymotrypsin at tryptophan (W), phenylalanine (F) and tyrosine (Y). Pancreas tissue samples were homogenized with a Dounce-S glass homogenizer (B.Braun-Melsungen AG, Melsungen, Germany) in ice-cold 0.1 M Tris-HCl (pH 8.0) containing 5 mM $CaCl_2$. Homogenised samples were centrifuged at 10,000 g for 15 min at 4°C. Protein concentrations were determined using a standard Bradford assay. In the pancreatic homogenates from UBR1$^{-/-}$ or wild-type controls, spontaneous elastase activity as well as enterokinase activated (0.005 U ml^{-1}, 60 min at 37°C) elastase activity with unstimulated pancreas or after supramaximal caerulein stimulation over 8 h, was measured using the specific fluorogenic substrate (CBZ-Ile-Pro-Arg)$_2$-R110 (Molecular probes, Eugene, OR) (final concentration 10µM in 0.1 M Tris-HCl, 5mM Ca Cl_2 pH 8.0). Enterokinase is a serine protease enzyme, which activates inactive pro-protease form to active protease form, so that we can observe all active and inactive protease content which are eventually turned into the active form. Besides trypsin activity spontaneous elastase activity as well as enterokinase-activated (0.001 U ml^{-1}, 60 min at 37°C) elastase activity was also measured using (CBZ-Ala-Ala-Ala-Ala)$_2$-R110 (Molecular probes, Eugene, OR), a specific fluorogenic substrate (final concentration 30µM in 0.1 M Tris-HCl, 5mM Ca Cl_2 pH 8.0). Rates of substrate hydrolysis in arbitrary fluorescence units per min was calculated and measured enzymatic activities were calibrated against the activity of bovine trypsinogen or bovine elastase activated with enterokinase (0.001 U ml^{-1}, 60 min at 37°C) as standards and expressed as U mg^{-1} protein.

4.2.29. Histopathology

Formalin fixed pancreas and lung specimens were embedded in paraffin according to standard protocols. The 5 µm paraffin sections were sliced and mounted on glass slides. The sections were incubated at 37°C overnight, to dehydrate completely. Then these sections were deparaffinised using xylene (20 min) and later on hydrated with a series of decreasing ethanol concentration solutions (94%, 70%, and 50% each 5 min) and finally washed in 1x PBS (5 min). The slides were immersed in hematoxylin for 3 min and flushed with running tap water

for 5 min. After rinsing with distilled H_2O slides were placed in eosin for 1 min and then dehydrated with increasing alcohol concentration solutions (50%, 70% and 94%, 5min each step). After dehydration slides were dried in air and mounted with vector shield mounting media and cover slip on top of it. The histopathology pictures of pancreas and lung were taken using microscope (Olympus) with different magnifications.

4.2.30. Terminal deoxynucleotidyl transferase–mediated dUTP nick end labeling (TUNEL) assay

One of the main characteristic features of apoptotic cells is randomly cleaved DNA in the nuclei. There are many assays like ISNT (InSitu Nick Translation) assay and TUNEL (Terminal deoxynucleotidyl transferase–mediated dUTP nick end labelling) assay which work on the principle that DNA strand breaks occur during apoptosis. The TUNEL assay is more sensitive than the ISNT assay (Gorczyca et al 1993) since higher rate of dUTP incorporation can be observed with Terminal deoxynucleotidyl transferase (Tdt) which is used in TUNEL assay compared to DNA polymerase which is used in ISNT assay. Terminal deoxynucleotidyl transferase (Tdt) catalyzes the labelling of the free 3'-OH ends with tetramethylrhodamine dUTP (TMR-dUTP), which are then analyzed by fluorescent dUTP containing cells.

Antigen retrieval and detection:

In this assay 5 μm pancreas paraffin sections were first deparaffinised in xylene solution for 20 min and hydrated by dipping in series of decreasing concentrations of ethanol solutions (94%, 70%, and 50% each 5 min) and finally washed in 1x PBS. Meanwhile adequate 10 mM citrate buffer, pH 6.0 was boiled in a pressure cooker on a heating plate. After washing sections were kept in boiling 10mM citrate buffer on a pressure cooker for 5 min. Then, the sections were immediately cooled down by rinsing with tap water and then finally kept in 1X PBS solution. Sections were dried in air for some time and incubated with aura-BSA solution for 2 h for blocking. This step helps in reducing the background signal. After blocking sections were washed with 1x PBS solution for 3 times. Then, the sections were incubated with the TUNEL reaction mixture of the *In Situ* Cell Death Detection Kit, TMR red (Roche) containing tetramethyl-rhodamine dUTP (TMR-dUTP) and terminal deoxynucleotidyl transferase (Tdt) enzyme for 1h at 37^0 C. Once reaction time was over the sections were washed with 1x PBS solution for 3 times. The sections were counterstained with DAPI to stain all nuclei which aid in counting percentage of apoptotic cells. Then, the sections were mounted with vector shield mounting media for fluorescence by keeping the

cover slip on top of it. The pictures of UBR1 KO and WT groups, per group minimum 4 mice, were taken using fluorescent microscopy (Olympus). Calculation of the number of apoptotic cells per 100 DAPI-positive nuclei was done using the "Cell explorer" software (BioSciTec GmbH). Calculated percentage of apoptotic cells per group was expressed as mean ±S.D.

4.2.31. Acinar cell preparation and in-vivo elastase activity measurment

Animals were starved over night before sacrificing them. After starvation animal was sacrificed and pancreas was dissected out and kept in one of the small beaker containing 6ml of collagenase solution (50 µl of 2 µg/100 µl in 12 ml of DMEM high glucose media, HEPES 100 mM and BSA 5%). Oxygen (O_2) was flown through this buffer well just before the experiment to ensure the tissue and acinar cells won't be devoid of oxygen supply. Pancreas was minced into very small pieces using scissors and incubated for 15 min at 37°C in shaking water bath. After 15 min the fat tissue was decanted and fresh 6 ml of collagenase solution was added and again minced into very small pieces and incubated for 15 min at 37°C in shaking water bath. After 15 min of incubation the solution was transferred into 50 falcon tube. This solution was gently aspirated for three to four times with the tips cut at their edges so that acinar cells won't get stressed. This has to be repeated 5 times with descending order of wide at the tip end. Then the cell suspension was passed through a net cloth into 15 ml falcon tube. Later on the solution containing falcon tube was centrifuged and the supernatant was decanted. Fresh DMEM media with 100 mM HEPES and 5% BSA were added to the cell pellet and re-suspended. The filtering step was repeated twice as described above. After final washing cells were re-suspended in fresh DMEM media and incubated for 30 min at 37°C and subjected to further measurements of protease activity.

After an equilibration for 30 min secretagogue CCK-8 (Sigma) was added at either supramaximal concentration (10^{-6} M) or left untreated (control) for up to 60 min and incubated at 37°C in a water bath. For *in vivo* elastase activity and necrosis measurements, 1ml of acini solution was taken from each condition (i.e. UBR1 KO CCK, UBR1 WT CCK, UBR1 KO control and UBR1 WT control) at 4 different regular time point with 20 minutes duration (i.e. 0, 20, 40, 60 min) and then washed and resuspended in 1x measuring buffer (40 ml of 5x measuring buffer and 160 ml of distilled water) containing propidium iodide (PI) and the synthetic fluorescent elastase substrate (CBZ-Ala-Ala-Ala-Ala) $_2$-R110 (30 µM/L).

Measuring buffer 5x (pH 7.4):

Component	Final concentration	volume per 1 liter
DMEM	1%	50 ml
BSA	1%	50 g
HEPES	24,5 mM	29,17 g
NaCl	96 mM	28,05 g
KCl	6 mM	2,236 g
$MgCl_2$ $6H_2O$	1 mM	1,015 g
$CaCl_2$ $2H_2O$	0,5 mM	0,368 g
NaH_2PO_4 H_2O	2,5 mM	1,725 g
Glucose	11,5 mM	10,35 g
Na-Fumarate	5 mM	4,000 g
Na-Pyruvate	5 mM	4,225 g
Na- Glutamate	5 mM	2,750 g

To quantify substrate cleavage, acini together with substrate and PI were transferred to 96-well microtiter plates and the $\Delta F/\Delta T$ ratio was determined by cytofluorometry (Molecular devices, Spectra Max Gemini) over 60 min at 32°C. Necrosis rate was also determined cytoflourometrically after completely disrupting the cells at the end of the experiment using 3% Triton X-100.

4.2.32. Histological scoring

Histological scoring was done according to Niederau et al (Niederau et al 1985). After HE staining 5 images of each pancreatic section were used for histological scoring. The scoring was done based on the extent of the alterations in 1) necrosis, 2) vacuolization and 3) inflammation of pancreas upon caerulein treatment in UBR1 knockout and control mice. The histological grading of necrosis and vacuolization refers to the approximate percentage of cells involved as listed below and the grading of the inflammatory alterations refers to a scale ranging from 0 as minimal to 4 as maximal alterations.

Histological score	Percentage of cells involved (%)
0	0-5
1	5-15
2	15-35
3	35-50
4	>50

4.2.33. Measurment of cytokines by CBA kit

The Cytometric Bead Array (CBA) from BD Pharmingen is a flow cytometric based assay for the detection of human or mice cytokines from cell supernatants or serum samples. The kit uses a set of beads that have been coated with cytokine specific antibodies which serves as a capture surface for cytokines. Each cytokine specific set of beads is assigned a discrete fluorescence intensity that can be resolved on the FL-3 channel of a flow cytometer. The beads are incubated with the sample of interest, washed, and then incubated with a second cytokine antibody that is PE labeled. In this manner, a bead that is positive for a cytokine will stain both PE and FL-3 positive, while beads that are specific for cytokines that are not present will stain only FL-3 positive. A mixture of the capture beads and PE labeled secondary antibodies allow for the detection of multiple cytokines/proteins from a single, small sample volume. 25 µl of UBR1 knockout mice and control mice serum samples from all time points after pancreatitis induction were taken for cytokines measurement and processed them according to the manufacturer's instructions and results were analyzed using BD FACS array bio analyzer machine.

4.2.34. Simultaneous Calcium signal and protease activity measurements

Calcium signal measurement was done using freshly prepared acinar cells (protocol described in 1.4.31). For simultaneous Ca^{+2} signal and protease activity measurements acini were loaded for 30 min with acetoxymethyl ester of the Ca^{+2} sensitive dye fura-2 (2 µM/L) (Molecular Probes, Eugene, OR) together with either rhodamine coupled trpsin substrate or elastase substrate. The Ca^{+2} signals (fura-2 ratio; Ex1 340 nm/Ex2 380 nm, Em 510 nm) and the rhodamine-110 flourescence signals (Ex 485nm, Em 530nm) were recorded in identical regions of interest 5 µM in diameter. For quantitative measurements more than 400 cells per experiment were evaluated.

4.2.35. *In vivo* trypsin activity measurements using trypsin specific inhibitor S-124

The highly specific, reversible and cell-permeant trypsin inhibitor Na-(2-naphthylsulfonyl)-3- amidinophenylalanine-carboxymethylpiperazide (S-124) was kindly provided by Dr. Walter Halangk (Magdeburg, Germany). The specificity, kinetics and reversible nature of inhibition of S-124 was very well shown by Halangk et al (Halangk et al 2002). Pancreatic acinar cell preparation from UBR1 KO and WT mice was done as described earlier (section 4.2.31). After equilibration for 30 min at 37°C, acini of UBR1 KO and WT

mice were devided into four portions and one portion was kept aside, which was untreated by any chemicals (Control). From the three portions of acini left two of them were pre-incubated with S-124 (10 µM/L) for 30 min prior to the incubation with the cholecystokinin analog caerulein (Bachem, Heidelberg, Germany) at supramaximal concentration (10 nM/L) for up to 60 min in all 3 portions. Reversible trypsin inhibitor S-124 was washed away from one portion out of two S-124 pre-incubated portions just prior to the trypsin activity measurement and in one more portion of acini S-124 was maintained through out the measurement at 10 µM/L concentration. For *in vivo* measurement of trypsin activity 1ml of acini solution was taken from each condition (i.e. for both UBR1 KO and WT groups- control, caerulein, S124 without wash prior measurment+caerulein and S-124 with wash prior measurment+caerulein) at 4 different regular time points with 20 min duration (i.e. 0, 20, 40, 60 min) and then washed and resuspended in measuring buffer containing the synthetic fluorescent trypsin substrate (CBZ-Iso-Pro-Arg)$_2$-R110 (30 µM/L). To quantify substrate cleavage, acini together with substrate were transferred to 96-well microtiter plates and the $\Delta F/\Delta T$ ratio was determined by cytofluorometry (Molecular devices, Spectra Max Gemini) over 60 min at 32°C.

4.2.36. *In vivo* trypsin activity measurements using RGS4 specific inhibitor CCG-4986

CCG-4986 was found to be a specific inhibitor of RGS4 using an *in vitro* high-throughput flow cytometry protein interaction assay, despite its close similarity with RGS8 (Roman et al 2007). The effect of RGS4 on trypsin activity alone was tested using commercially available purified trypsin (Sigma Chemical Co., Missouri, USA). The ability of *in vivo* inhibition of RGS4 was determined using freshly isolated pancreatic acini. Pancreatic acinar cell preparation from UBR1 KO mice was done as described earlier (section 4.2.31). Isolated acini were equilibrated in fresh DMEM medium and devided into three portions. One portion of acini was kept aside to be used as control, where as other two portions of acini were treated with supramaximal (10 nM) concentration of CCK-8 analog caerulein. One of the caerulein treated portion was pre-equilibrated with 10 µM of RGS4 inhibitor CCG-4986 prior to caerulein treatment. For in-vivo measurement of trypsin activity 1ml of acini solution was taken from each condition (i.e. for both UBR1 KO and WT groups- control, caerulein and CCG-4986+caerulein) at 4 different regular time points with 20 minutes duration (i.e. 0, 20, 40, 60 min) and then washed and resuspended in measuring buffer containing the synthetic fluorescent trypsin substrate (CBZ-Iso-Pro-Arg)$_2$-R110 (30 µM/L). To quantify substrate cleavage, acini together with substrate were transferred to 96-well microtiter plates and the

$\Delta F/\Delta T$ ratio was determined by cytofluorometry (Molecular devices, Spectra Max Gemini) over 60 min at 32°C.

4.2.37. Data presentation and statistical analysis

Data in graphs are expressed as mean ±S.D. Statistical comparison of groups was done using Mann-Whitney rank-sum test, followed by Student's t-test for independent samples using SigmaPlot version 11 (Systat Software, Inc., IL, USA) and Graphpad Prism version 5 (Graphpad software Inc, CA, USA) which were also used for data presentation. We used at least four mice in each experiment. Differences were considered significant at a level of $p < 0.05$ and were denoted by asterisks.

5. Results

5.1. Proteome and functional analysis of BCL11b induced cell death in human T cells

5.1.1. Induction of apoptosis by knockdown of *BCL11B* in Jurkat and huT78 cells but not Jurkat *BCL-xL*

It has previously been reported that Bcl11b is important for cell survival and that reduction of its level leads to apoptosis.(Grabarczyk et al 2007) Apoptosis due to reduction of Bcl11b levels can be prevented by stable transfection with and over-expression of *BCL-xL*. Initially, we monitored the level of apoptosis triggered by transfection with a *BCL11B* specific siRNA with the aid of an Annexin-V fluorescein isothiocyanate binding assay. Quantification of the proportion of apoptotic cells by FACS analysis revealed time dependent increases of apoptosis in Jurkat and huT78 cells from 10.1% and 9.3% at day 1 through 32% and 33% at day 2 and 68.5% and 55% at day 3 after transfection with *BCL11B* specific siRNA, respectively (Fig. 10A). However, in Jurkat *BCL-xL* cells, in which the anti-apoptotic *BCL-xL* protein was continuously over-expressed, the transfection with *BCL11B* siRNA did not trigger enhanced apoptosis (Fig. 10A). Based on these data, a proteomic analysis of cells treated with siRNA for 48 h was done, because the siRNA treatment already triggered clear effects but the majority of cells had not committed to apoptosis (Fig. 10B). The level of apoptosis triggered by transfection with scrambled control RNA was in the range of 4 to 7 % and thus in the range observed for transfection with *BCL11B* siRNA in Jurkat *BCL-xL* cells. Western blot analysis was used to verify that siRNA treatment indeed triggered the expected reductions in Bcl11b levels in all three cell lines. Fig. 10C demonstrates that the levels of Bcl11b had already significantly decreased to similar degrees (approximately 20% residual level) in Jurkat, huT78 as well as Jurkat *BCLxL* cells 48 h after the transfection with *BCL11B* specific siRNA compared to the transfection in scrambled control RNA. Transfections with scrambled control RNA did not trigger any change in Bcl11b level compared to mock or non transfected cells (Fig. 10C). On the other hand levels of Bcl11b could be significantly increased by transient overexpression of *BCL11B*. (Fig. 10C).
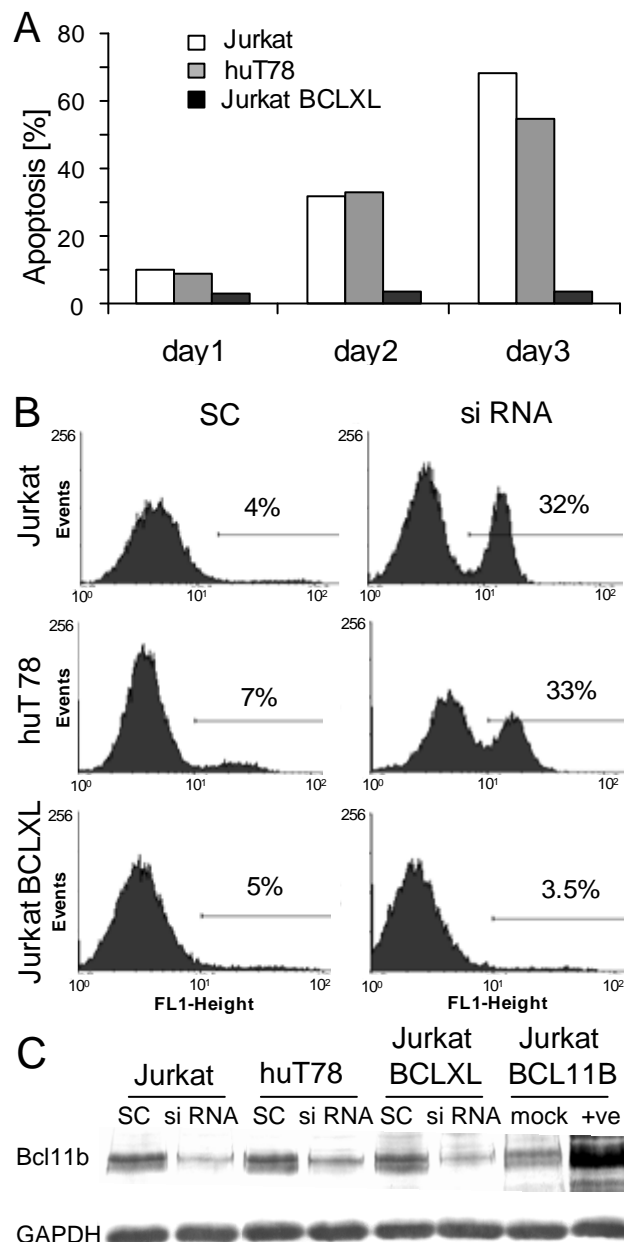
Fig. 10: Influence of *BCL11B* suppression on apoptosis. A) Time resolved analysis of apoptosis induced by siRNA mediated knockdown of *BCL11B*. Apoptosis was determined by measuring Annexin-V fluorescein isothiocyanate binding by FACS analysis in Jurkat (white bars), huT78 (grey bars) and Jurkat *BCL-xL* (Black bars) cells at days 1 through 3 after transfection with *BCL11B* specific siRNA. B) Annexin-V binding at day 2 after transfection with scrambled control RNA (SC) or siRNA specific for *BCL11B*. Aliquots of these cells were also used for the proteomic analysis of the effects of *BCL11B* knockdown. Percentages of apoptotic cells are indicated by numbers above the bars. C) Western blot analysis of Bcl11b. Levels of Bcl11b were monitored using polyclonal Bcl11b antibodies in Jurkat, huT78 and Jurkat *BCL-xL* cell lines. Cells were harvested 48 h after transfection with scrambled control RNA (SC) or *BCL11B* specific siRNA and after mock transfection (mock) or transfection with a vector triggering overexpression of *BCL11B* (Jurkat *BCL11B* +ve). 50 µg of crude protein extract was loaded per lane and after separation by SDS-PAGE levels of Bcl11b were determined by

Western blotting as described in materials and methods. Equal loading was verified by using a GAPDH antibody.

5.1.2. Analysis of the effects of the reduction of Bcl11b levels on the protein pattern of Jurkat and huT78 cells - *BCL11B* knockdown predominantly triggers increases of protein levels

The impact of suppression of *BCL11B* by a specific siRNA was analyzed in a gel-based approach by 2D-DIGE to facilitate precise quantification of the changes in the proteome. In order to focus the analysis onto effects that are consistently observed, proteomics experiments were performed for protein extracts originating from two independent siRNA treatments of huT78 cells. Furthermore, we included the Jurkat human T cell leukemia cell line in the proteomic analysis to focus attention onto changes conserved in different cell lines. The variations in the protein pattern upon treatment with scrambled control RNA were minimal for both cell lines, indicating consistency of the 2D-DIGE analysis. The representative 2D pattern of Jurkat cells that is illustrated in Fig. 11 indicates that reduction of the level of Bcl11b did not change the protein pattern in general but rather caused specific effects in both cell types. Jurkat and huT78 cells displayed a similar magnitude of response with more proteins being induced than suppressed (Fig. 11 and 12).

Of the 1639 protein spots consistently monitored in hut78 cells, 208 and 141 displayed statistically significant differences in the two experiments performed for the huT78 cells. In Jurkat cells 1881 protein spots were quantified and 203 of those changed in level following siRNA mediated knockdown of *BCL11B*. In order to focus on general effects and to minimize the number of false positives we concentrated the subsequent detailed analyses on the 78 protein spots displaying increased and 25 proteins spots displaying reduced intensities in the three experiments of both cell lines.
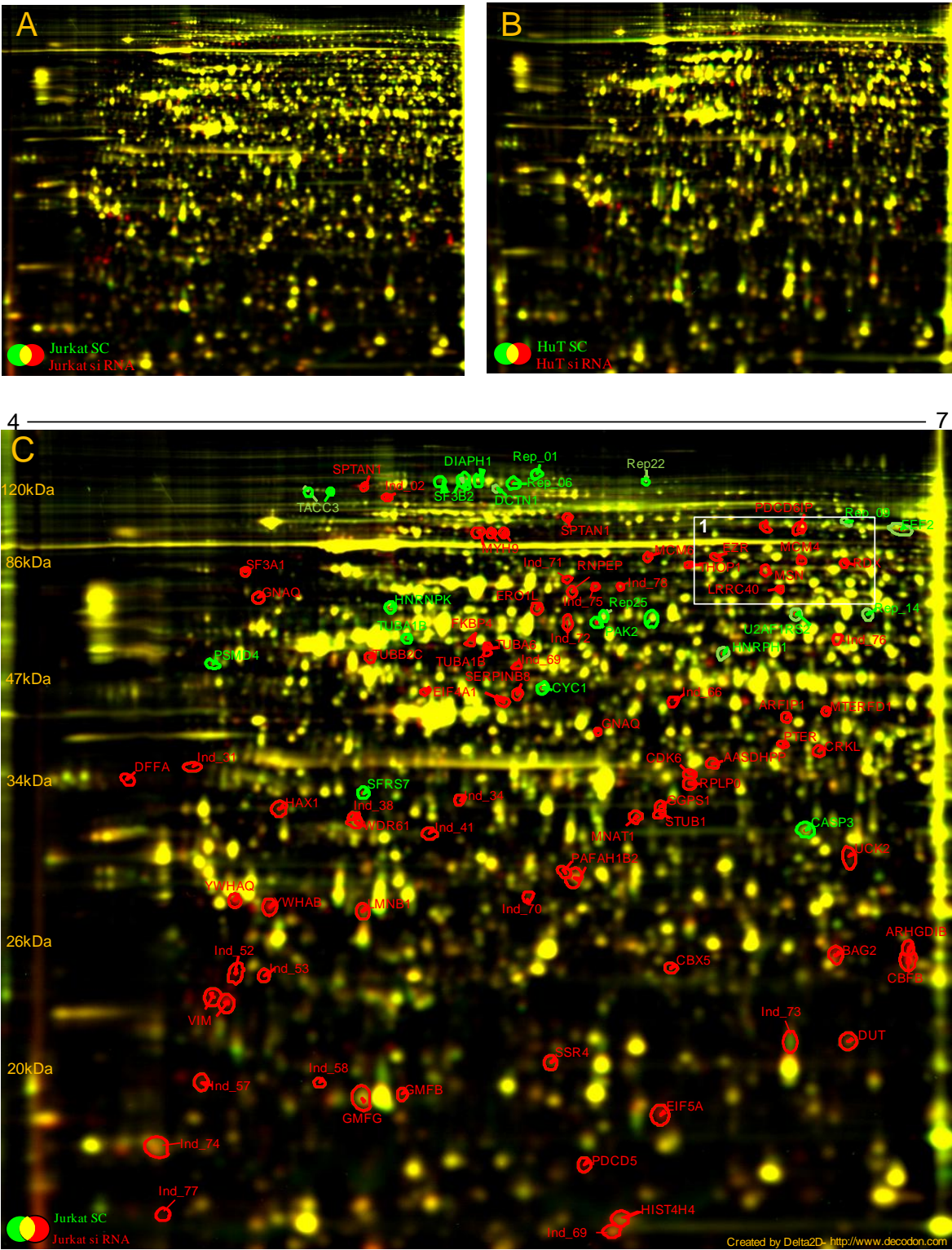
Fig. 11: 2D-DIGE analysis of the influence of *BCL11B* suppression on the proteome of Jurkat cells.

Jurkat cells were transfected with scrambled control RNA (SC) or siRNA specific for *BCL11B* for 48 h, crude protein extracts were prepared and the protein patterns were subsequently analyzed by 2D-DIGE. Images of protein extracts of sc and siRNA treated cells were warped and superimposed onto each other using the Delta-2D software package. Protein spots from the controls cells (SC –treated) are displayed in green and those from the *BCL11B* knockdown cells (siRNA-treated) are indicated in red. Representative 2D-DIGE images of HuT (A) and Jurkat (B) cells. C) Jurkat 2D-DIGE image- Spots appearing in yellow do not show any difference in intensity between sc and siRNA treated cells, whereas red and green spots reflect increased and reduced levels upon *BCL11B* siRNA knockdown, respectively. Proteins displaying changes in intensity related to *BCL11B* siRNA knockdown are labeled. Red labels mark proteins that are present in higher levels after knockdown of *BCL11B* and green labels identify protein spots significantly reduced in level upon *BCL11B* knockdown. The white square marks the region containing ERM proteins (Square 1 – see also Fig. 18). D) Illustration of DIGE experiment scheme in Jurkat and HuT cells.

The reproducibility was checked using the differentially expressed proteins as the reference in a box plot using the Genespring software, which showed a good reproducibility among the 3 different DIGE experiments i.e. one experiment in Jurkat cells and two independent experiments in HuT cells (Fig. 12A). The number of proteins that were commonly regulated was shown in a pie diagram and the number proteins that were differentially expressed in each 2D-DIGE experiment were shown in brackets on the top of each circle which indicates each experiment. From these numbers of proteins we mainly focused on the proteins which were regulated by BCL11b in all 3 DIGE experiments (indicated by bold letters at the center) with the criteria that fold change must be 1.5 in at least one experiment and 1.3 in the other 2 experiments (Fig. 12B).
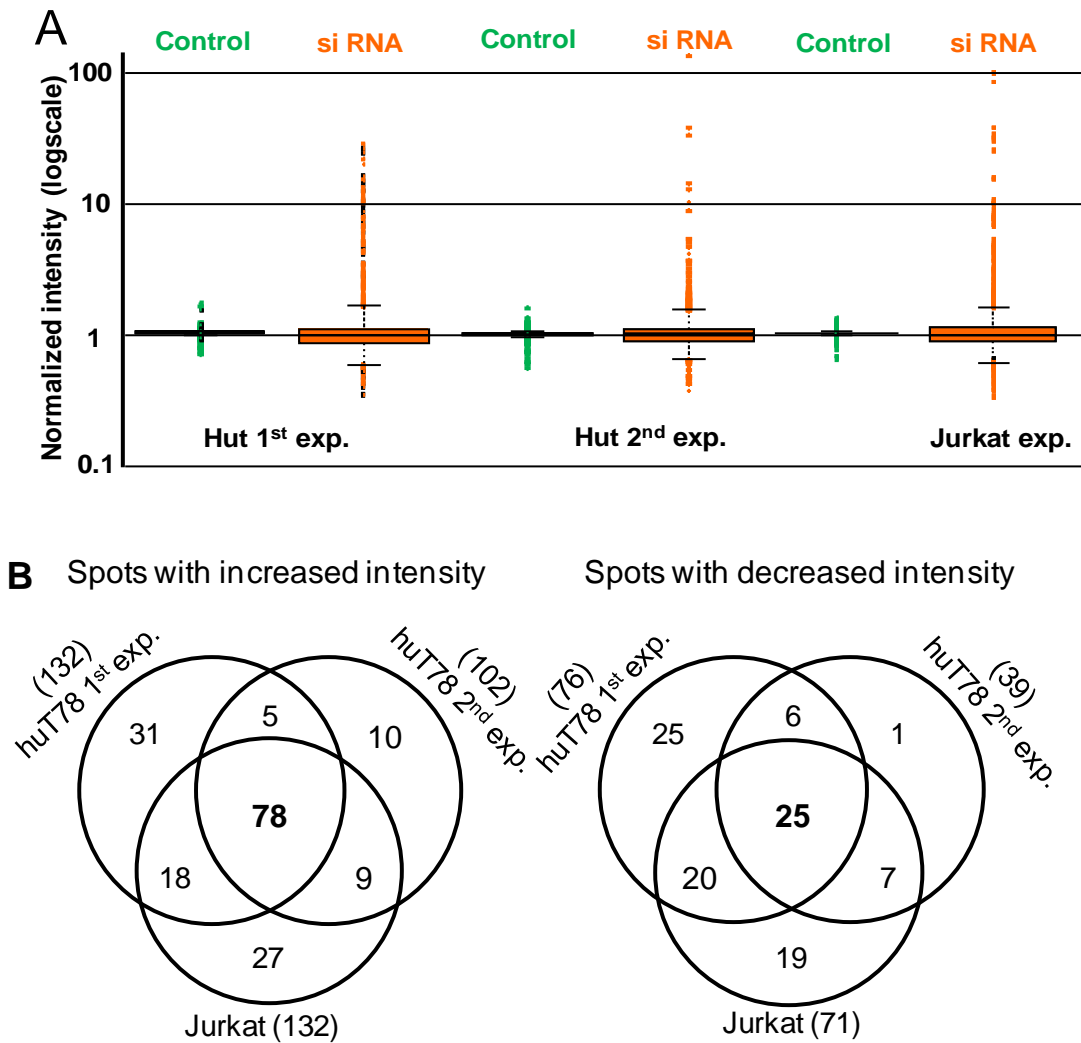
Fig. 12: Quantitative analysis of impact of *BCL11B* knockdown on the proteome pattern of HuT78 and Jurkat cells. A) Box-plot displaying the reproducibility of the quantification and the proportion of differentially expressed proteins (fold change > 1.5, *p*-value < 0.05) of the three proteomics experiments (huT78 1st, huT78 2nd and Jurkat). Cy2-normalized intensities were divided by the median of the values of the respective scrambled control samples. Orange colour boxes indicate the variation of the 2nd and 3rd quartile of protein spot ratios and thus the low technical variation of the measurements. Dots above and below the horizontal lines indicate spots fulfilling the criteria for differential regulation. B) Venn-diagram summarizing protein spots with significantly different levels after 48 h of suppression of *BCL11B* vs. samples treated with scrambled control RNA. The numbers in parenthesis indicate the total numbers of affected spots observed in the respective experiment. The numbers in the outer sections indicate spots only observed in one experiment and the numbers in the intersections indicate spots observed in two or three of the three different experiments (huT78 1st, huT78 2nd and Jurkat). For the intersections of several experiments, protein spots were considered as present at significantly different levels, when *p*-values < 0.05 were observed in all experiments and a greater than 1.5 fold change in at least one experiment and greater than 1.3 fold change in the other two experiments were verified (indicated in bold).

5.1.3. Identification of Bcl11b regulated proteins by mass spectrometry

Proteins displaying consistent changes in levels upon *BCL11B* knockdown in both Jurkat and huT78 cell lines were selected for identification by mass spectrometry. Of those 103 protein spots, 78 were identified by a combined approach relying primarily on MALDI-MS/MS, which was partially supported by LC-ESI-MS/MS. These identifications revealed changes in 63 distinct proteins. The detailed data of the identifications are summarized in Table 3 and the protein names of identified spots are indicated in Fig. 11B, which displays a representative overlay of 2D-DIGE images.

Table 3: Identification of proteins which are consistently regulated in all 3 experiments (i.e. huT78 1st ,2nd and Jurkat experiments)

Label[a]	Identification	Protein ID[b]	MW [c] (kDa)	pI[d]	Fold change huT78-1[e]	Fold change huT78-2[f]	Fold change Jurkat [g]	p-value huT78-1	p-value huT78-2	p-value Jurkat	Protein Score[h]	Peptide count[i]	SC[j] (%)
rep_02	splicing factor 3B subunit 2	SF3B2	100.2	5.37	1.44	1.36	1.5	0	0.001	0.001	111	17	26
rep_03	splicing factor 3B subunit 2	SF3B2	100.2	5.37	1.48	1.5	1.7	0.004	0.001	0.005	105	17	24
rep_04	splicing factor 3B subunit 2	SF3B2	100.2	5.37	1.45	1.45	1.5	0	0	0.002	79.4	18	27
rep_05	Protein diaphanous homolog 1	DIAPH1	140.4	5.06	1.4	1.39	1.7	0	0.046	0.002	68.9	23	22
rep_07	Isoform p135 of Dynactin-1	DCTN1	127.4	5.09	1.3	1.3	1.6	0.006	0.002	0.002	196	30	36
rep_08	Transforming acidic coiled-coil-containing protein 3	TACC3	90.36	4.69	1.51	1.5	1.5	0	0.003	0.005	96.3	21	35
rep_10	Elongation factor 2	EEF2	95.21	6.82	1.79	1.3	1.7	0	0.001	0.001	389	33	48
rep_11	Heterogeneous nuclear ribonucleoprotein K	HNRNPK	47.56	5.28	1.64	1.48	1.7	0	0	0.001	326	26	57
rep_12	Serine/threonine-protein kinase PAK 2	PAK2	58.08	5.76	1.42	1.3	1.7	0	0.002	0.001	495	26	56
rep_13	U2 (RNU2) small nuclear RNA auxiliary factor 2 isoform b(H) [k]	U2AF1RS2	53.73	9.59	1.35	1.5	1.9	0	0.001	0	437	15	45
rep_15	Serine/threonine-protein kinase PAK 2	PAK2	58.08	5.76	1.62	1.3	1.6	0.001	0.034	0.002	257	20	51
rep_16	Tubulin alpha-ubiquitous chain	TUBA1B	50.15	4.7	1.57	1.5	1.6	0	0	0.001	200	17	51
rep_17	Heterogeneous nuclear ribonucleoprotein H1	HNRPH1	49.23	6.25	1.42	1.37	1.7	0	0	0.001	582	19	61
rep_18	Proteasome (Prosome, macropain) 26S subunit, non-ATPase, 4	PSMD4	41.08	4.43	1.36	1.36	1.6	0.014	0.005	0.001	350	14	46
rep_19	Ubiquinol-cytochrome-c reductase complex core protein I, mitochondrial precursor	CYC1	52.65	6.32	1.34	1.7	1.6	0	0.001	0.001	649	26	65
rep_20	Isoform 1 of Splicing factor, arginine/serine-rich 7 [k]	SFRS7	27.37	12.3	1.32	1.38	1.5	0	0	0.001	429	15	44
rep_21	Caspase-3 precursor	CASP3	31.61	6.51	1.58	1.34	1.5	0	0.002	0.001	296	20	70

Label[a]	Identification	Protein ID[b]	MW[c] (kDa)	pI[d]	Fold change huT78-1[e]	huT78-2[f]	Jurkat[g]	p-value huT78-1	huT78-2	Jurkat	Protein Score[h]	Peptide count[i]	SC[j] (%)
rep_23	Transforming acidic coiled-coil-containing protein 3	TACC3	90.36	4.69	1.78	1.5	1.4	0	0.003	0.001	160	20	27
rep_24	Isoform 2 of Protein kinase C and casein kinase substrate in neurons protein 2	PACSIN2	51.35	5.04	1.5	1.6	1.4	0	0.002	0.001	140	15	34
Ind_01	Isoform 1 of Spectrin alpha chain, brain	SPTAN1	284.5	5.01	6.23	3.9	6.6	0	0.034	0.001	172	46	20
Ind_03	Isoform 1 of Spectrin alpha chain, brain	SPTAN1	284.5	5.01	5.64	2.3	2.1	0	0.003	0.001	164	32	13
Ind_04	PDCD6IP protein	PDCD6IP	96.82	6.46	2	1.8	2.3	0	0.001	0.001	663	44	53
Ind_05	PDCD6IP protein	PDCD6IP	96.82	6.46	1.6	1.4	1.5	0.003	0	0.001	199	25	36
Ind_06	Myosin-9(H)	MYH9	226.4	5.29	11.46	3.5	11.1	0	0.001	0.001	661	45	26
Ind_07	Myosin-9(H)	MYH9	226.4	5.29	5.1	2.6	5.3	0	0.001	0.001	436	33	19
Ind_08	Myosin-9(H)	MYH9	226.4	5.29	3	2.2	4.6	0	0.001	0.001	558	38	24
Ind_09	Villin 2 (Ezrin)[k]	EZR	69.41	6.17	1.4	1.3	2.2	0.024	0.025	0.004	133	18	30
Ind_10	DNA replication licensing factor MCM6	MCM6	92.89	5.09	2.7	1.4	1.7	0	0.047	0.001	243	27	41
Ind_11	DNA replication licensing factor MCM4	MCM4	96.56	6.71	4.13	3.7	5.1	0	0.001	0.001	239	30	46
Ind_12	Radixin	RDX	68.56	6.3	1.6	1.7	1.7	0	0.001	0.001	332	28	43
Ind_13	Thimet oligopeptidase	THOP1	78.71	5.93	1.6	1.4	2.2	0	0.021	0.001	117	18	32
Ind_14	Leucine-rich repeat-containing protein 40[k]	LRRC40	68.25	6.37	1.4	1.3	1.6	0	0.049	0.001	326	29	60
Ind_15	Aminopeptidase B[k]	RNPEP	73.5	6.02	2.33	2.6	1.5	0	0.012	0.004	417	27	45
Ind_16	ERO1-like protein alpha precursor	ERO1L	54.39	5.41	1.5	1.3	2	0	0	0.003	573	24	61
Ind_17	Moesin	MSN	67.64	6.09	1.99	1.8	1.6	0	0.002	0.003	464	35	65
Ind_18	FK506-binding protein 4	FKBP4	51.67	5.11	2.72	1.5	1.8	0	1	0.002	270	22	56
Ind_19	Tubulin alpha-6 chain	TUBA6	49.9	4.73	5.16	3.6	1.7	0	0.002	0	102	17	50
Ind_20	Tubulin alpha-6 chain[k]	TUBA6	49.9	4.73	19.12	8.9	8.5	0	0.001	0.001	478	16	51

Label[a]	Identification	Protein ID[b]	MW[c] (kDa)	pI[d]	Fold change			p-value			Protein Score[h]	Peptide count[i]	SC[j] (%)
					huT78-1[e]	huT78-2[f]	Jurkat[g]	huT78-1	huT78-2	Jurkat			
Ind_21	Tubulin beta-2 chain	TUBB2C	49.67	4.52	4	2.9	3	0	0.001	0	496	27	68
Ind_22	Serpin B8	SERPINB8	42.79	5.26	1.5	1.7	1.7	0.006	0.001	0.001	613	22	53
Ind_23	Eukaryotic initiation factor 4A-I	EIF4A1	46.15	5.12	2.25	1.3	2.8	0	0.001	0.001	380	20	61
Ind_24	Eukaryotic initiation factor 4A-I	EIF4A1	37.91	6.69	1.5	1.5	1.7	0	0.004	0.001	544	25	73
Ind_25	Isoform 2 of mTERF domain-containing protein 1, mitochondrial precursor	MTERFD1	38.6	6.52	1.3	1.4	1.6	0.001	0.012	0.001	91.2	15	42
Ind_26	Isoform A of Arfaptin-1	ARFIP1	32.72	4.51	2.3	2	2.6	0	0.001	0.001	463	18	60
Ind_27	Guanine nucleotide binding protein	GNAQ	42.14	5.37	4.3	2	2.6	0	0.007	0.001	124	13	42
Ind_28	Phosphotriesterase-related protein	PTER	39.02	6.51	1.3	1.6	2.3	0.007	0.001	0.001	517	16	60
Ind_29	Crk-like protein	CRKL	33.78	6.73	1.38	1.7	1.7	0	0.001	0	643	20	61
Ind_30	L-aminoadipate-semialdehyde dehydrogenase-phosphopantetheinyl transferase	AASDHPPT	35.78	6.79	2	2	1.9	0	0.001	0.001	215	14	44
Ind_32	Cell division protein kinase 6	CDK6	36.94	6.43	8.5	3.6	2.5	0	0.001	0	88.6	10	42
Ind_33	60S acidic ribosomal protein P0	RPLP0	34.27	5.77	8.5	10	9	0	0	0.001	637	17	60
Ind_35	Geranylgeranyl pyrophosphate synthetase	GGPS1	34.87	6.06	2.3	2.9	1.6	0	0.004	0.01	222	13	46
Ind_36	HS1 binding protein[k]	HAX1	28.49	4.56	1.7	1.5	1.8	0	0.032	0.001	164	11	39
Ind_37	Isoform 1 of STIP1 homology and U box-containing protein 1	STUB1	34.86	5.68	4	2.9	9.9	0	0.004	0.004	101	18	54
Ind_39	CDK-activating kinase assembly factor MAT1	MNAT1	35.82	5.96	4.6	2.3	1.7	0.0492	0.014	0.008	234	16	69
Ind_40	WD repeat protein 61	WDR61	33.58	5.12	1.36	1.3	1.6	0	0.047	0.001	189	14	63
Ind_42	Isoform 1 of Uridine-cytidine kinase 2[k]	UCK2	29.3	6.68	1.8	1.7	2.5	0	0.002	0.001	350	13	58
Ind_43	Platelet-activating factor acetylhydrolase IB subunit beta	PAFAH1B2	25.57	5.8	1.63	2	1.5	0	0.001	0.001	221	6	29

Label[a]	Identification	Protein ID[b]	MW[c] (kDa)	pI[d]	Fold change			p-value			Protein Score[h]	Peptide count[i]	SC[j] (%)
					huT78-1[e]	huT78-2[f]	Jurkat	huT78-1	huT78-2	Jurkat			
Ind_44	Platelet-activating factor acetylhydrolase IB subunit beta	PAFAH1B2	25.57	5.8	1.6	2	1.6	0	0.001	0.001	257	7	39
Ind_45	14-3-3 protein theta	YWHAQ	17.05	5.42	2.96	1.9	3.9	0	0.004	0.001	452	20	68
Ind_46	Tyrosine 3-monooxygenase/ tryptophan 5-monooxygenase activation protein, beta polypeptide	YWHAB	28.08	4.47	10.6	10.7	17.1	0	0.001	0	324	16	75
	Isoform Short of 14-3-3 protein beta/alpha[k]	YWHAB	27.85	4.47									
Ind_47	LMNB1 protein	LMNB1	44.64	4.7	2.3	1.6	2.1	0	0.013	0.001	336	22	51
Ind_48	Rho GDP-dissociation inhibitor 2[k]	ARHGDIB	22.86	4.84	2.22	4	104.7	0	0.001	0.001	203	8	52
Ind_49	Core-binding factor subunit beta	CBFB	21.51	6.55	13.73	4	8.6	0	0.001	0.001	376	16	70
Ind_50	BAG family molecular chaperone regulator 2	BAG2	23.77	6.68	6.3	1.9	4.9	0	0.012	0	406	17	72
Ind_51	Chromobox protein homolog 5	CBX5	22.22	5.57	1.5	1.7	1.6	0	0.001	0.001	120	6	47
Ind_54	Vimentin	VIM	53.52	4.77	5.3	2.6	8.4	0	0.002	0.001	331	23	41
Ind_55	Vimentin	VIM	53.52	4.77	7.8	7.5	11.1	0	0.001	0.001	376	19	29
Ind_56	Isoform DUT-N of Deoxyuridine 5'-triphosphate nucleotidohydrolase, mitochondrial precursor	DUT	17.75	6.53	1.54	1.47	1.5	0	0.002	0.001	375	13	84
Ind_59	Glia maturation factor gamma[k]	GMFG	16.8	4.9	1.52	1.48	1.5	0	0.001	0.006	93.2	9	61
Ind_60	GMFB protein	GMFB	18.11	4.94	1.6	1.3	2	0	0.014	0.001	216	10	68
Ind_61	Eukaryotic translation initiation factor 5A-1	EIF5A	16.7	4.86	8.9	4.6	5.7	0	0.001	0.001	316	11	78
Ind_62	Programmed cell death protein 5	PDCD5	14.15	5.84	4.4	2.3	10.2	0	0.004	0	117	6	39
Ind_63	Tubulin beta-2 chain	TUBB2C	49.67	4.52	4	2	1.7	0	0.001	0.001	554	30	75
Ind_64	Splicing factor 3 subunit 1	SF3A1	88.89	4.88	11.2	128.5	15.7	0	0.001	0.001	115	23	34

Label[a]	Identification	Protein ID[b]	MW[c] (kDa)	pI[d]	Fold change			p-value			Protein Score[h]	Peptide count[i]	SC[j] (%)
					huT78-1[e]	huT78-2[f]	Jurkat[g]	huT78-1	huT78-2	Jurkat			
Ind_65	Hypothetical protein SSR4 (Fragment)	SSR4	20.21	5.62	1.3	1.7	1.5	0.001	0.032	0.002	179	6	30
Ind_67	Isoform DFF35 of DNA fragmentation factor subunit alpha (Fragment)[k]	DFFA	29.41	4.22	1.9	1.7	1.8	0.002	0.026	0.001	573	17	62
Ind_68	Histone H4	HIST4H4	11.24	11.9	7.7	1.44	1.4	0	0.041	0	364	13	62
Ind_76	Tubulin alpha-ubiquitous chain[k]	TUBA1B	50.15	4.7	1.6	1.3	1.3	0	0	0.005	417	20	51

[a] Label: Spot identification number; [b] Protein ID: SwissProt Entry name;

[c] MW: Molecular weight calculated from amino acid sequence (in kDa)

[d] pI: isoelectric point calculated from amino acid sequence,

[e] huT78-1: huT78 1st DIGE experiment,

[f] huT 78-2: huT78 2nd DIGE experiment

[g] Jurkat: Jurkat DIGE experiment,

[I] Peptide count: number of matched peptides

[h] Protein score: significance of protein identification,

[j] SC (%): Sequence coverage in percentage

[k] identifications: Isoforms of the protein observed

5.1.4. Global protein degradation upon *BCL11B* knockdown

The quantitative analysis of the 2D-DIGE data revealed that *BCL11B* knockdown resulted mostly in increased protein levels with reductions of protein levels contributing to less than 25%. Among the proteins displaying reduced levels we also found caspase 3 precursors. Since *BCL11B* suppression has previously been shown to trigger increased apoptosis we wanted to explore if we can validate apoptosis on the proteomic level. Here, we could exploit the advantage of gel-based proteomics approaches that assignment occurs at the protein level and thus protein species including post-translationally modified or partially degraded products could be distinguished.

A closer inspection of the distribution of spots displaying differential regulation revealed an overrepresentation of protein spots with increased intensity in the low molecular weight region already providing a first hint for potential protein degradation. Therefore, for the differentially regulated protein spots identified by mass spectrometry, predicted molecular mass and observed migration distance were plotted. Those proteins displaying clear deviation from the expected linear relationship constituted candidates that represented degradation products (longer migration distance than predicted). The summary of this analysis, which is displayed in Fig. 13A, revealed significant accumulation of protein fragments for isoform-1 of spectrin alpha chain, myosin-9, vimentin, and LMNB1 protein. For myosin-9, vimentin and isoform-1 of spectrin alpha chain these data were supported by more detailed analyses. Potential fragments of all three proteins displayed pronounced increases in intensity in Jurkat and huT78 cells treated with *BCL11B*-specific siRNA (Fig. 13B) and thus, these proteins were subjected to detailed analysis by LC-MS/MS, in which significant proportions of the total protein coding region should be covered by identified peptides. In accordance with the hypothesis for all five spots characterized in detail, the majority of peptides were allocated to either the N-terminal or C-terminal parts of the proteins. For spectrin fragments corresponding to the N- (12 peptides) and C-terminus (28 peptides) were found. In case of vimentin one spot contained the C-terminus only (10 peptides), whereas the other probably consisted of two fragments representing both the C- and N-terminal part (17 peptides) of the full length protein. The C-terminal part of myosin was covered by 25 peptides (Fig. 13C). For myosin the analysis with the phosphoprotein specific stain Diamond-Pro Q® additionally indicated increased phosphorylation of the C-terminal protein-fragments following knockdown of *BCL11B*, which was not seen in the cells treated with the scrambled control RNA (Fig. 13B).

C
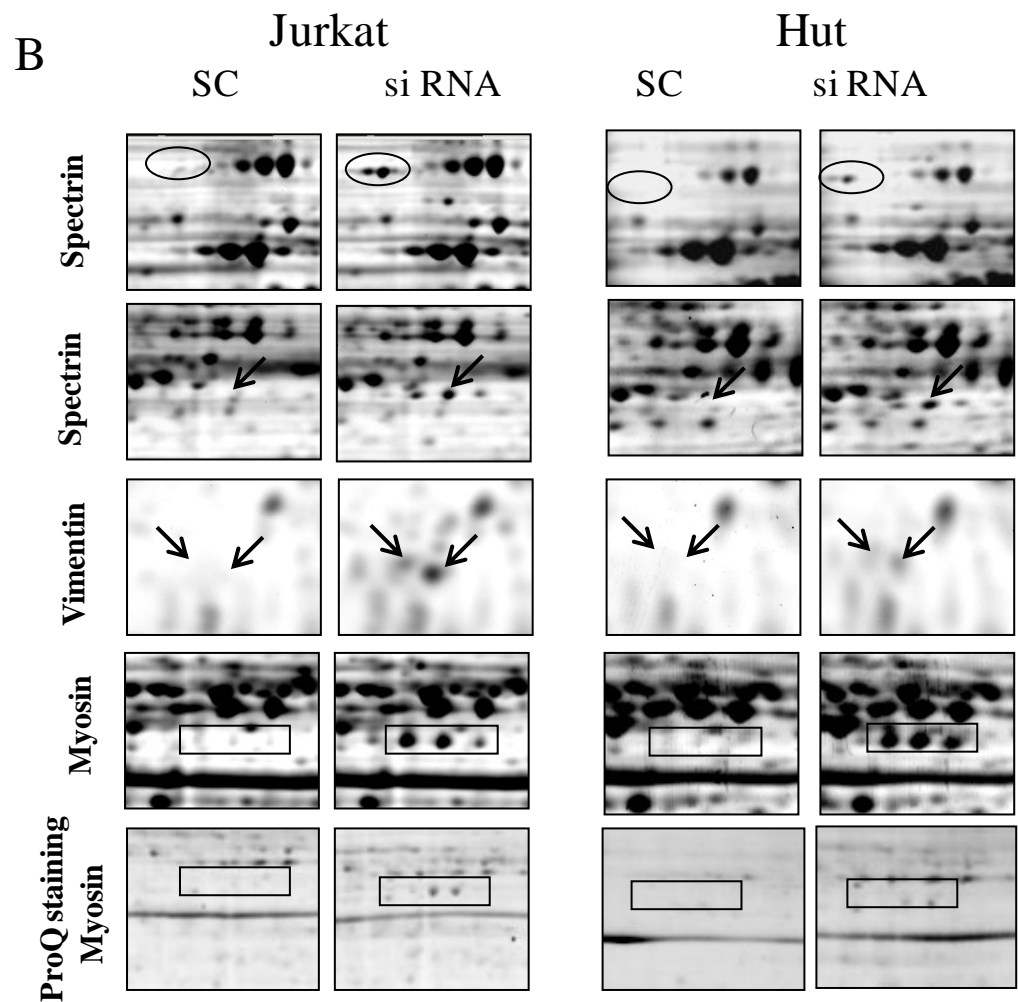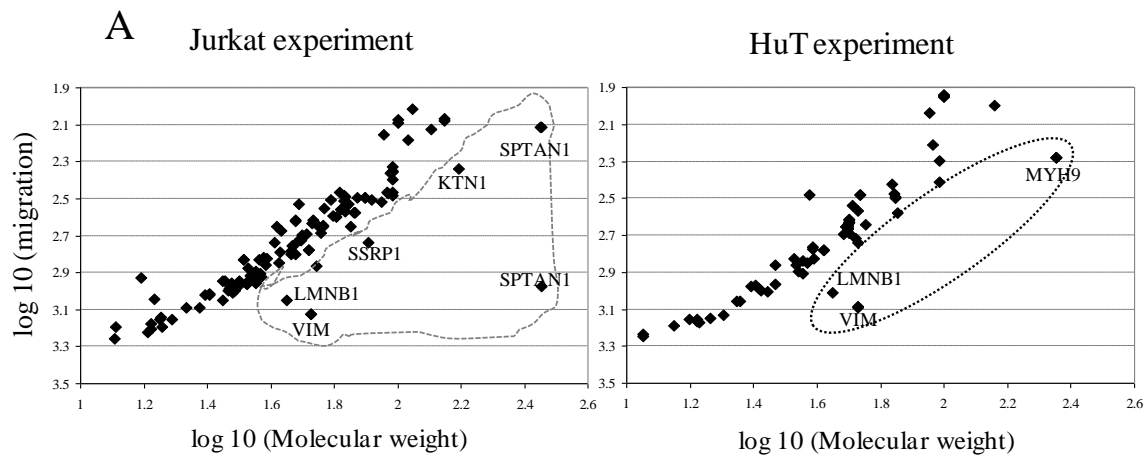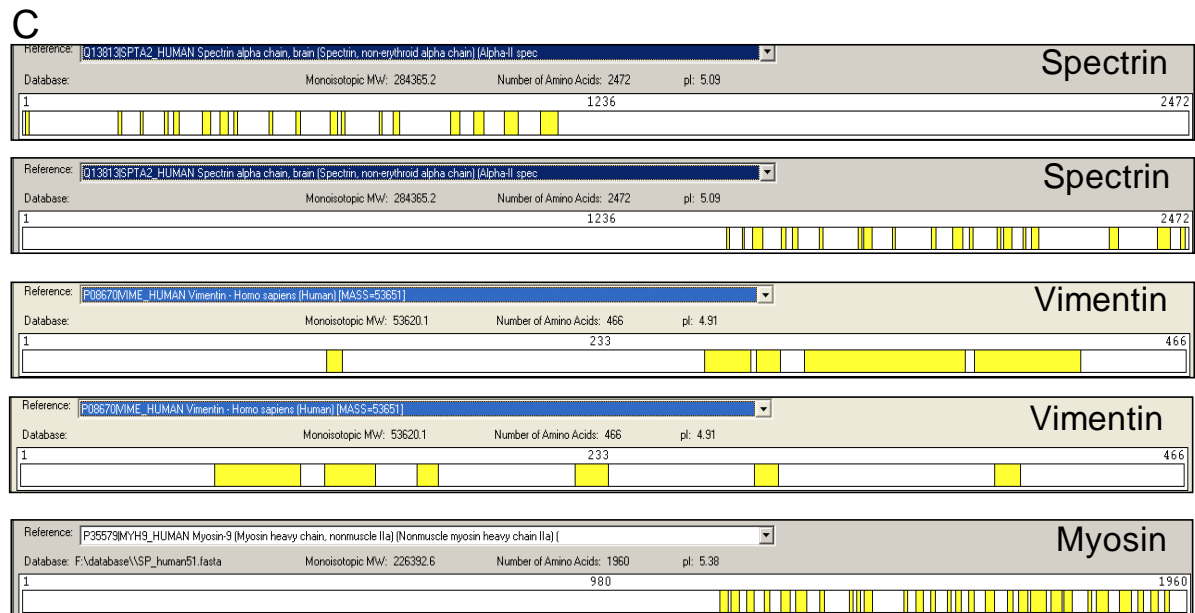
Fig. 13: Analysis of *BCL11B* knockdown on global protein degradation. Logarithms of predicted molecular masses of proteins identified as differentially regulated after suppression of *BCL11B* were plotted against the logarithms of observed migration distance in the second dimension of the 2-DE for Jurkat cells and huT78 cells (A). Proteins deviating from the assumed correlation and thus indicating degradation are encircled and labeled with their protein names. B) Display of enlarged section of the respective 2-DE images of Jurkat and huT78 cells displaying protein spots of degradation products of spectrin, vimentin and myosin-9. For myosin-9 the protein staining by 2D-DIGE was complemented by a phosphoprotein specific staining with Pro Q® Diamond, which preferentially stains proteins containing either phosphorylated serine or threonine. Proteins of interest are marked with arrow heads and boxes. C) Detailed mass spectrometric characterization of the truncated forms of spectrin, containing the N-terminal and C-terminal parts of the protein, respectively, vimentin and myosin-9. Protein spots selected for detailed analysis by LC-MS/MS are marked with arrow heads in the enlarged sections of part B.

5.1.5. Pro Q® diamond staining/ Phosphoproteome analysis

Apart from quantitation of total protein levels changes the phosphoproteome are important as phosphorylation and dephosphorylation of proteins are important mechanism to regulate the proteins functions. Hence phosphospecific Pro Q® diamond staining was used to estimate the differences in phosphoproteomes of Jurkat, HuT scrambled control and siRNA treated cells. Subsequently, the same gels were stained with SYPRO® Ruby staining, which detects the total protein. These Pro Q® diamond and SYPRO® Ruby stained gel images were superimposed for comparative analysis to investigate the phosphospecific signals. Image analysis revealed that a minor portion of total proteome is phosphorylated and more over there were minor differences observed in phosphoproteomes level of scrambled control and

siRNA treated Jurkat as well as HuT cell lysates. It was interesting to observe that some of the conserved differentially expressed proteins from Jurkat and HuT siRNA 2D-DIGE experiments were showing differences in their phosphorylation levels as well. Among them were truncated forms of Myosin as well as Ezrin, Radixin and Moesin (ERM). However, we limited our efforts of identification to those proteins which displayed significant differences in the phosphorylation pattern following treatment with Bcl11b specific siRNA and did not identify all proteins phosphorylated.

5.1.6. Influence of reduction of *BCL11B* levels on protein phosphorylation in Jurkat cells

Images of Pro Q® diamond stained gels of protein extracts of Jurkat cells treated with scrambled control RNA (Fig. 14A.1) or Bcl11B siRNA (Fig. 14A.2) and the corresponding total protein patterns obtained by SYPRO® Ruby staining (scrambled control Fig. 14B.1, siRNA Fig. 14 B.2) and an overlay picture showing a differential display of the phosphoprotein pattern fo controls and siRNA treated cells are exemplarily shown in Fig. 14. By overlaying the Pro Q® diamond stained gels with SYPRO® Ruby stained gels it was found that the level of phosphorylation of ERM (Ezrin, Radixin, Moesin) proteins increased in siRNA treated cells compared to SC treated cells (Fig. 14).
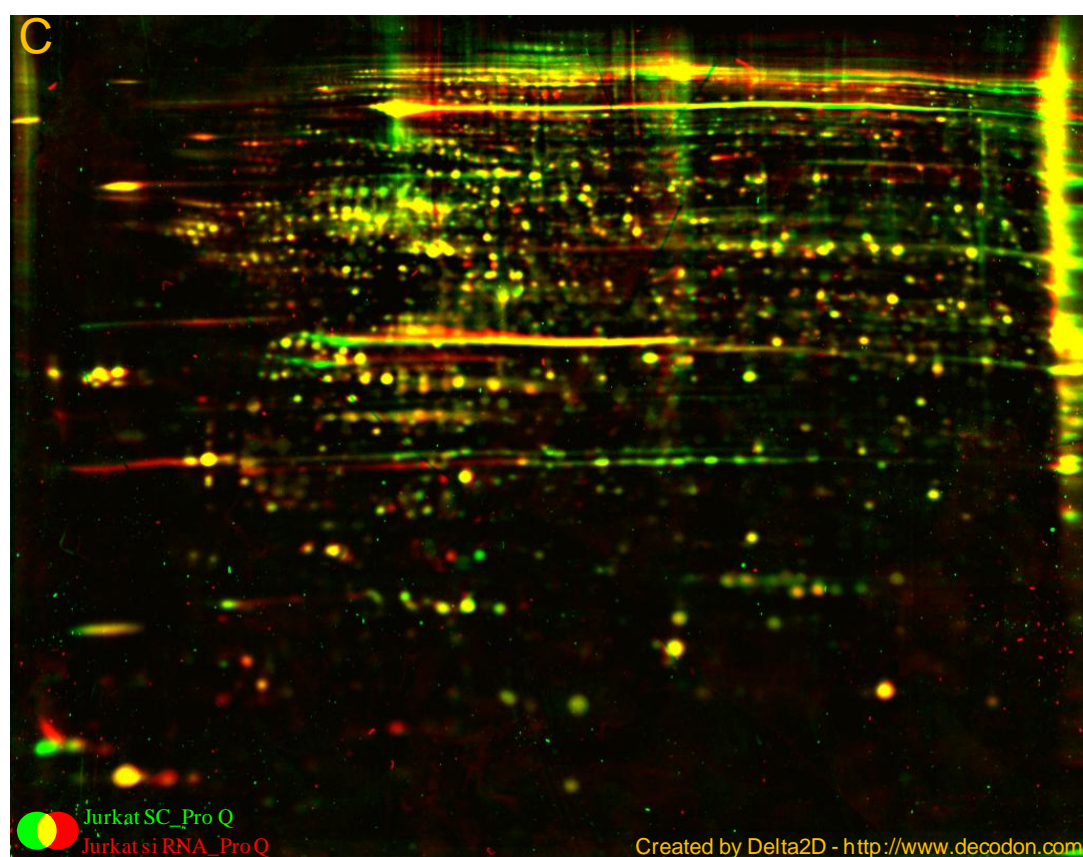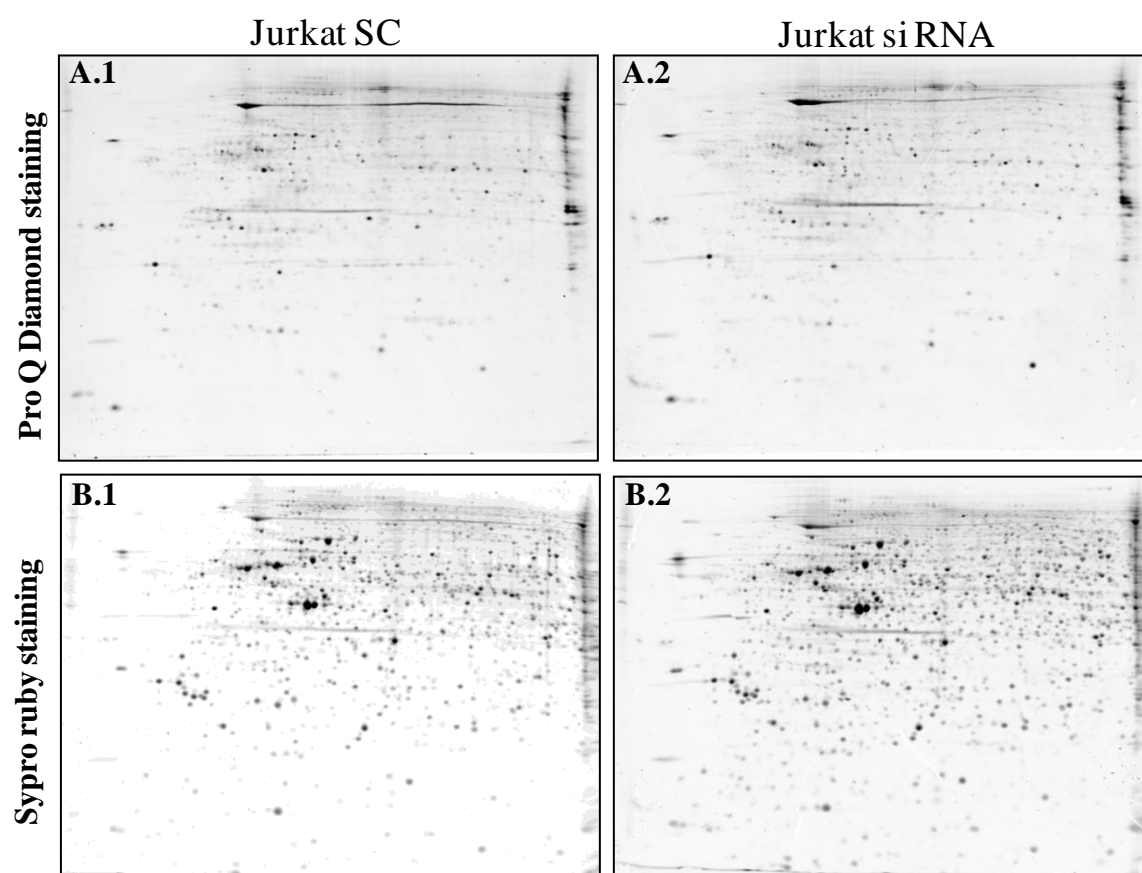
Fig. 14: Phospho proteome analysis by Pro Q® diamond staining in Jurkat cells. A) 2D images of Jurkat scrambled control and Bcl11b siRNA treated cells protein extracts stained with Pro Q® diamond (A.1&A.2) and SYPRO® Ruby (B.1&B.2) C) Overlapping image of Pro Q® diamond stained 2D gels of Jurkat scrambled control and siRNA treated cells which were represented by green and red colours, respectively. Yellow spots indicate no change in the intensity levels between SC and siRNA treated cells, where as red spots indicate increased and green spots indicate decreased phosphorylation levels in control upon *BCL11B* downregulation.

5.1.7. Influence of reduction of *BCL11B* levels on protein phosphorylation in HuT cells

The same analysis was performed for the differential analysis of the phosphoproteome in HuT cells treated with scrambled controls and *BCL11B* siRNA. Pro Q® diamond and SYPRO® Ruby stained gels of the corresponding HuT cell extracts and an overlay picture showing protein phosphorylation in HuT cells are shown in Fig. 15. Treatment of HuT cells with *BCL11B* siRNA also influenced the phosphoproteome. In case of HuT cells we also observed increased phosphostain intensities of ERM (Ezrin, Radixin, Moesin) proteins in *BCL11B* siRNA treated cells compared to SC treated cells (Fig. 15).
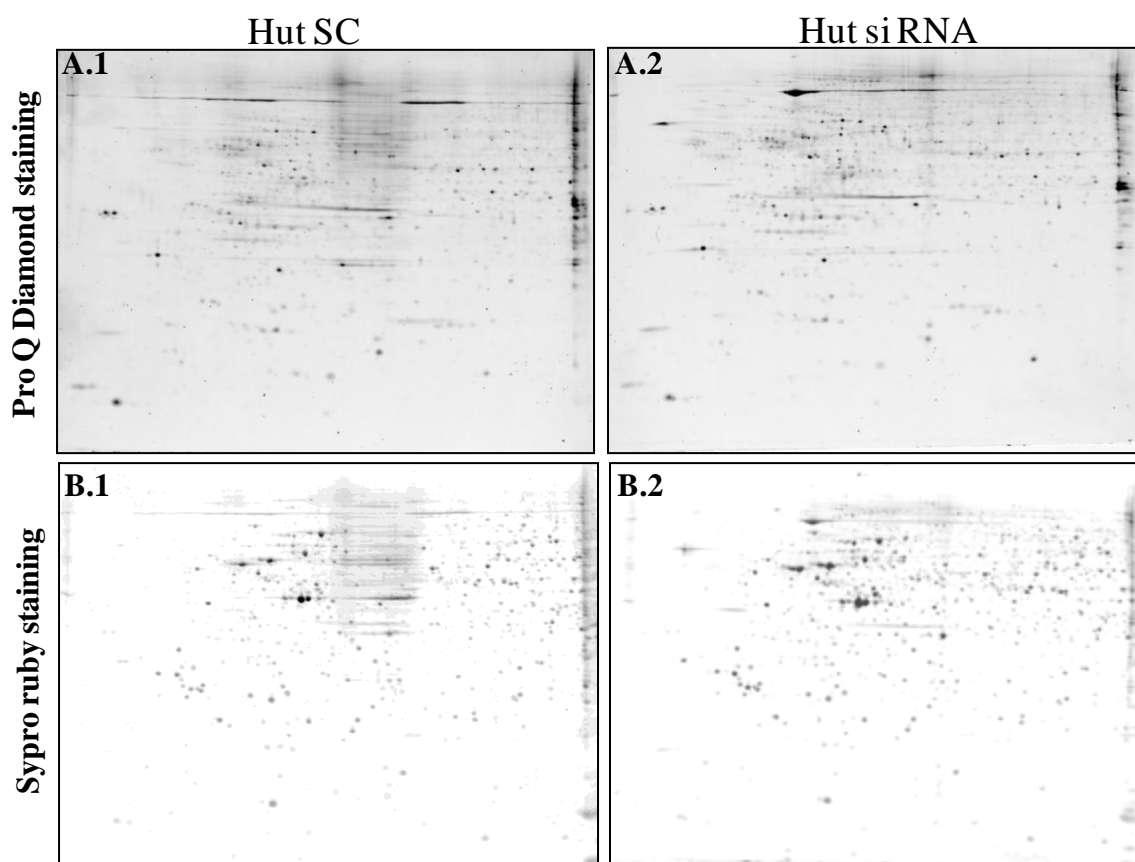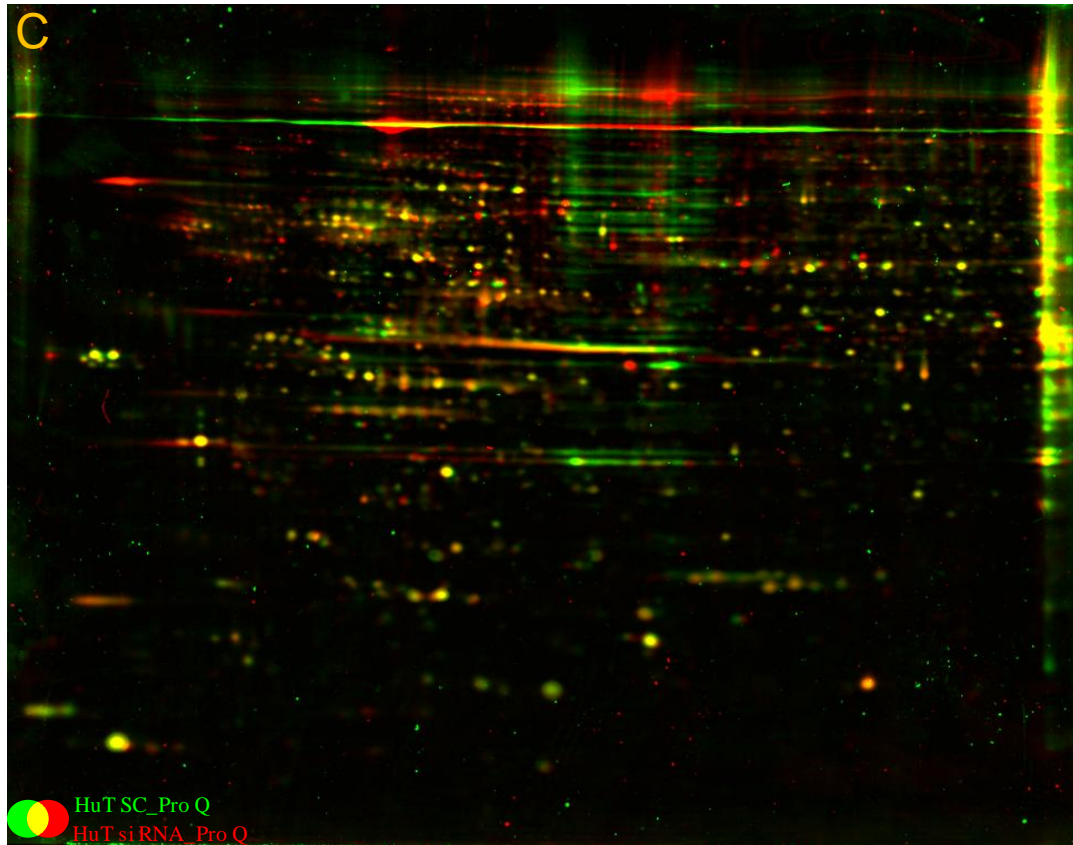
Fig. 15: Phospho proteome analysis by Pro Q® diamond staining in Jurkat cells. A) 2D gel images of protein extracts of HuT scrambled control and siRNA treated cells stained with Pro Q® diamond (A.1&A.2) and SYPRO® Ruby (B.1&B.2) C) Overlapping image of Pro Q® diamond stained 2D gels of HuT scrambled control and siRNA treated cells which were represented by green and red colours, respectively. Yellow spots indicate no change in the intensity levels between SC and siRNA treated cells, where as red spots indicate increased and green spots indicate decreased intensity at their phosphorylation levels upon BCL11b downregulation.

5.1.8. Analysis of the effect of reductions of *BCL11B* levels in Jurkat *BCL-xL* cells

To analyze the upstream events of *BCL11B* induced apoptosis the Jurkat *BCL-xL* cell line was chosen where the upstream events of induction of apoptotic cell death occur but not the cell death itself. One more advantage of this system is that we should be able to separate primary effects induced by reduction of *BCL11B* levels and secondary effects induced by apoptosis. Jurkat cells transfected with *BCL-xL* specific sequences overexpression of *BCL-xL*, which is an anti-apoptotic protein and hampers the apoptotic process at the mitochondrial level, occurs. A 2D-DIGE experiment was performed to quantify the differentially expressed proteins by collecting a total of 4 technical replicates for each sample (2 Cy3, 2 Cy5 values for SC and *BCL11B* siRNA treated samples). Only a minor portion of the proteome was

observed to be affected upon Bcl11b downregulation in *BCL-xL* overexpressing cells, unlike in Jurkat and HuT cells. Altogether there were 1519 spots quantified and among them the intensities of 19 proteins were increased and 9 proteins were decreased after the statistical analysis employing cutoff levels of a minimum 1.5 fold change and p-value less than 0.05. An overlay image in which spots displaying different intensities were labeled with numbers prefixing "Ind" for increased and "Rep" for decreased intensities after *BCL11B* siRNA induction (Fig. 16). Out of the 28 differentially altered protein spots 23 were successfully identified by MALDI-MS/MS and the details of the identifications of these protein spots are given in Table 4.
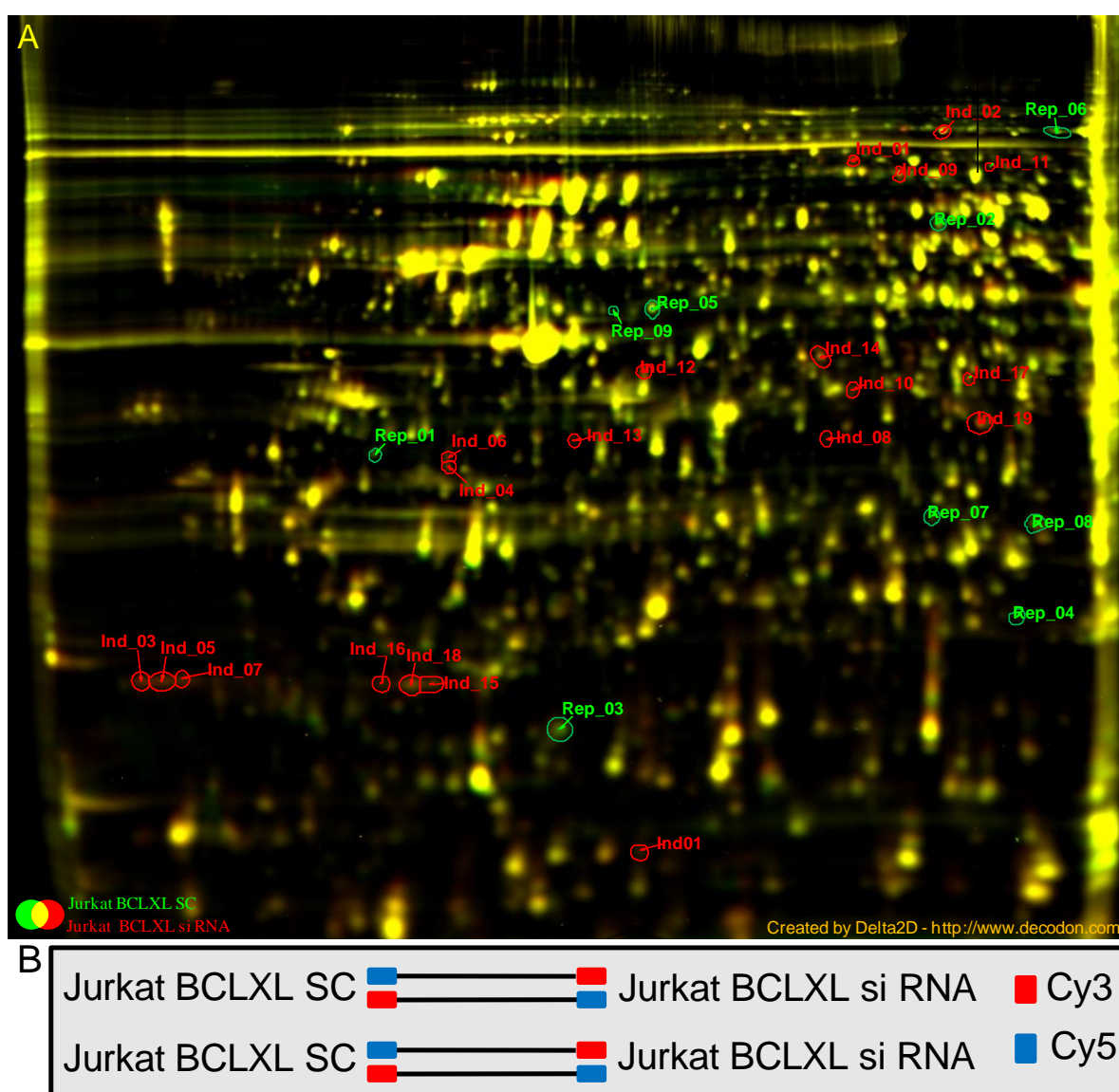
Fig. 16: 2D-DIGE analysis of influence of *BCL11B* suppression on the proteome of Jurkat cells over expressing *BCL-xL*. A) Overlay of representative 2D-DIGE images showing differentially expressed proteins in

Jurkat cells overexpressing *BCL-xL* upon *BCL11b* knockdown. 2D-DIGE images of Jurkat cells overexpressing *BCL-xL* treated and treated either with a scrambled control (SC) or *BCL11B* siRNA are represented by green and red colours, respectively. Yellow spots indicate no change in intensities between SC and siRNA treated cells, where as red spots indicate increased intensity and green spots indicate decreased intensity. The differentially expressed spots which follow the criteria of minimum fold change 1.5 and a p-value below 0.05 were labeled with numbers prefixing "Ind" for increased and "Rep" for decreased intensities upon *BCL11B* downregulation in *BCL-xL* overexpressing cells. B) Scheme of the sample combination in the DIGE experiment

Table 4: Identification of differentially expressed proteins in Jurkat BcL-xL over expressing cells upon *BCL11B* down regulation

Lable[a]	Identification	Protein ID[b]	Fold change	p-value	MW[c]	pI[d]	Protein score[e]	Peptide count[f]
Ind_01	Ezrin	EZR	2.7	0.001	69.64	5.94	164	17
Ind_02	PDCD6IP protein	PDCD6IP	2.2	0.000	96.76	6.13	333	35
Ind_03	Not identified		2.0	0.574	0.00			
Ind_04	WD repeat protein 61	WDR61	2.0	0.006	33.56	5.16	100	8
Ind_05	Not identified		2.0	0.533	0.00			
Ind_06	Not identified		1.8	0.022	0.00			
Ind_07	Not identified		1.8	0.591	0.00			
Ind_08	Isoform 2 of Inorganic pyrophosphatase 2, mitochondrial precursor	PPA2	1.7	0.056	39.61	6.47	182	16
Ind_09	Moesin	MSN	1.7	0.002	67.78	6.08	312	17
Ind_10	L-aminoadipate-semialdehyde dehydrogenase-phosphopantetheinyl transferase	AASDHPPT	1.7	0.004	35.75	6.35	154	13
Ind_11	Radixin	RDX	1.7	0.000	68.52	6.03	187	13
Ind_12	Ubiquitin-binding protein homolog	UBFD1	1.7	0.050	33.36	5.55	75.7	11
Ind_13	Isoform ASF-1 of Splicing factor, arginine/serine-rich 1	SFRS1	1.6	0.004	27.73	10.4	166	17
Ind_14	Macrophage capping protein	CAPG	1.6	0.000	38.49	5.88	220	12
Ind_15	Prostaglandin E synthase 3	PTGES3	1.6	0.009	18.69	4.35	68.4	7
Ind_16	CDNA: FLJ21190 fis, clone CAS12333	DCTPP1	1.5	0.010	18.67	4.93	68.3	6
Ind_17	not identified		1.5	0.000	0.00			
Ind_18	c-Myc-responsive protein Rcl	RCL	1.5	0.024	19.10	4.97	203	9
Ind_19	Splicing factor U2AF 35 kDa subunit	U2AF1	1.5	0.000	27.85	9.09	76.3	11

Lable[a]	Identification	Protein ID.[b]	Fold change	p-value	MW[c]	pI[d]	Protein score[e]	Peptide count[f]
Rep_01	EEF1D protein	EEF1D	1.5	0.001	28.54	4.81	180	12
Rep_02	U2 (RNU2) small nuclear RNA auxiliary factor 2 isoform b	U2AF1RS2	1.5	0.000	53.69	9.25	57	4
Rep_03	Hypothetical protein LOC51237	MGC29506	1.6	0.003	20.68	5.37	111	7
Rep_04	Isoform 1 of Zinc finger protein 250	ZNF250	1.6	0.001	63.43	8.65	41.5	6
Rep_05	Ubiquinol-cytochrome-c reductase complex core protein 1, mitochondrial precursor	CYC1	1.6	0.000	52.61	5.94	366	22
Rep_06	Elongation factor 2	EEF2	1.7	0.023	95.28	6.41	155	9
Rep_07	Isoform p27-L of 26S proteasome non-ATPase regulatory subunit 9	PSMD9	1.7	0.000	24.64	6.46	95.2	11
Rep_08	Isoform p27-L of 26S proteasome non-ATPase regulatory subunit 9	PSMD9	1.7	0.012	24.64	6.46	175	10
Rep_09	Ubiquinol-cytochrome-c reductase complex core protein 1, mitochondrial precursor	CYC1	3.9	0.060	52.61	5.94	162	11

[a]Label: Spot identification number; [b]Protein ID: IPI database accession number;
[c]MW: Molecular weight calculated from amino acid sequence (in kDa);
[d]pI: isoelectric point calculated from amino acid sequence;

[e]Peptide count: number of matched peptides; [f]Protein score: significance of protein identification

5.1.9. Analysis of differentially expressed proteins in Jurkat *BCL11B* overexpressing cells

To further verify the specificity of the effects observed, Jurkat cells were transfected with *BCL11B* sequence to overexpress the Bcl11b protein constitutively. To investigate if the overexpression of Bcl11b could induce almost opposite effects compared to downregulation in Jurkat cells, a 2D-DIGE experiment was performed to analyze the differentially expressed proteins between Jurkat control cells and Jurkat Bcl11b overexpressing cells. In agreement with our hypothesis not all but some of the effects which were observed in the Bcl11b down regulation system were found to be regulated in exactly the reversed fashion in the BC11b overexpression system. These conserved changes might point to direct targets or effects of BCL11b as these proteins were found to be altered or affected in both the overexpression and downregulation systems. In total 1802 spots were quantified in this 2D-DIGE experiment and among them the intensities of 28 protein spots were increased whereas 21 protein spots were decreased employing cutoffs of a minimum of a 1.5 fold change and a p-value less than 0.05. These differentially altered protein spots are highlighted on a representative 2D-DIGE image (Fig. 17). Out of the 49 spots which were altered upon *BCL11B* overexpression 48 spots were identified successfully by MALDI-MS/MS mass spectrometry and the details of the idnetifications are given in Table 5.
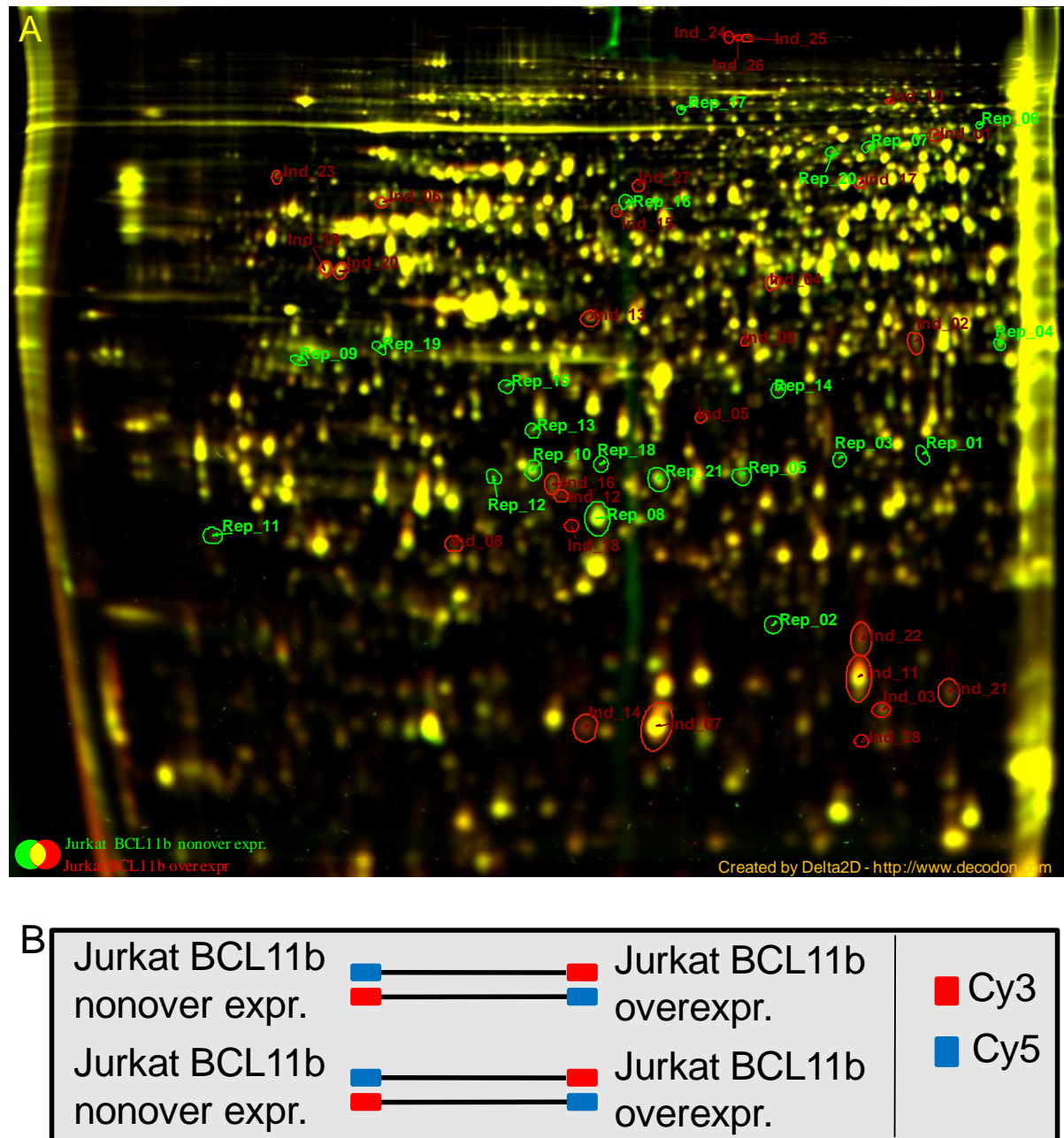
Fig. 17: 2D-DIGE analysis of influence of *BCL11B* over expression on the proteome of Jurkat cells.
A) Overlay of representative 2D-DIGE images showing differentially expressed proteins in Jurkat cells upon overexpression of *BCL11B*. 2D-DIGE images of Jurkat cells not overexpressing Bcl11b and overexpressing Bcl11b which were represented by green and red colors, respectively. Yellow spots indicate no change in the intensities between non-overexpressing and overexpressing cells, where as red spots and green spots indicate increased and decreased intensities respectively upon Bcl11b overexpression. The differentially expressed spots which follow the criteria of minimum fold change 1.5 and p value below 0.05 were labeled with numbers prefixing "Ind" for increased and "Rep" for decreased intensities upon Bcl11b overexpression. B) Scheme of the separation strategy of the DIGE experiment.

Table 5: Identification of differentially expressed proteins in Jurkat upon *BCL11B* overexpression

Lable[a]	Identification	Protein ID.[b]	Fold change	p-value	MW[c]	pI[d]	Protein score[e]	Peptide count[f]
Ind_01	Diacylglycerol kinase alpha	P23743	1.5	0.01	82.6	6.28	463	28
Ind_02	UDP-glucose 4-epimerase	Q14376	1.5	0.00	38.3	6.26	507	20
Ind_03	Low molecular weight phosphotyrosine protein phosphatase	P24666	1.5	0.02	18.0	6.3	348	9
Ind_04	Synaptic vesicle membrane protein VAT-1 homolog	Q99536	1.5	0.04	41.9	5.88	494	21
Ind_05	Sulfatase-modifying factor 2 precursor	Q8NBJ7	1.5	0.01	33.8	7.79	156	18
Ind_06	Rab GDP dissociation inhibitor alpha	P31150	1.5	0.03	50.6	5	714	35
Ind_07	Stathmin	P16949	1.5	0.00	17.3	5.76	188	8
Ind_08	Cathepsin B precursor	P07858	1.6	0.00	37.8	5.88	189	12
Ind_09	Farnesyl pyrophosphate synthetase	P14324	1.6	0.00	40.5	5.06	93.3	7
Ind_10	2-oxoglutarate dehydrogenase E1 component, mitochondrial precursor	Q02218	1.6	0.00	115.9	6.4	591	47
Ind_11	Cofilin-1	P23528	1.6	0.00	18.5	8.22	291	12
Ind_12	Actin, cytoplasmic 1	P60709	1.6	0.02	41.7	5.29	339	18
Ind_13	Adenosine deaminase	P00813	1.6	0.00	40.7	5.63	371	20
Ind_14	Stathmin	P16949	1.6	0.00	17.3	5.76	260	13
Ind_15	G1 to S phase transition protein 1 homolog	P15170	1.6	0.00	55.7	5.45	219	19
Ind_16	Chloride intracellular channel protein 4	Q9Y696	1.6	0.00	28.8	5.45	398	24
Ind_17	Dihydropyrimidinase-related protein 2	Q16555	1.7	0.00	62.3	5.95	679	34
Ind_18	Vacuolar protein sorting-associated protein 37B	Q9H9H4	1.7	0.03	31.3	6.78	230	12
Ind_19	Gamma-enolase	P09104	1.7	0.00	47.2	4.91	498	31
Ind_20	Gamma-enolase	P09104	1.7	0.00	47.2	4.91	606	32

Lable[a]	Identification	Protein ID.[b]	Fold change	p-value	MW[c]	pI[d]	Protein score[e]	Peptide count[f]
Ind_21	Destrin	P60981	1.7	0.00	18.5	8.06	365	12
Ind_22	Cofilin-1	P23528	1.8	0.00	18.5	8.22	282	13
Ind_23	Signal transducing adapter molecule 1	Q92783	1.8	0.00	59.1	4.7	543	20
Ind_24	Myosin-11	P35749	2.2	0.04	227.2	5.42	67.2	27
Ind_25	Myosin-9	P35579	2.4	0.00	226.4	5.5	66.6	29
Ind_26	Myosin-9	P35579	2.5	0.04	226.4	5.5	66.6	29
Ind_27	Coronin-1B	Q9BR76	4.9	0.00	54.2	5.61	231	15
Ind_28	Peptidyl-prolyl cis-trans isomerase A	P62937	5.0	0.02	18.0	7.68	193	12
Rep_01	Uridine-cytidine kinase 2	Q9BZX2	3.1	0.00	29.3	6.23	513	18
Rep_02	Not identified		2.1	0.00	0.0			
Rep_03	Uridine-cytidine kinase 2	Q9BZX2	2.0	0.00	29.3	6.23	672	23
Rep_04	Heterogeneous nuclear ribonucleoprotein H3	P31942	1.9	0.00	36.9	6.37	414	23
Rep_05	Proteasome activator complex subunit 1	Q06323	1.9	0.00	28.7	5.78	248	17
Rep_06	Not identified		1.9	0.04	0.0			
Rep_07	Moesin	P26038	1.8	0.00	67.8	6.08	334	18
Rep_08	NADH dehydrogenase [ubiquinone] iron-sulfur protein 3, mitochondrial precursor	O75489	1.8	0.00	30.2	6.99	208	18
Rep_09	Nucleophosmin	P06748	1.8	0.03	32.6	4.64	181	13
Rep_10	Proteasome activator complex subunit 2	Q9UL46	1.7	0.00	27.3	5.44	603	20
Rep_11	Membrane-associated progesterone receptor component 1	O00264	1.7	0.01	21.7	4.56	137	9
Rep_12	Cathepsin D precursor	P07339	1.7	0.04	44.5	6.1	353	17
Rep_13	N-terminal acetyltransferase complex ARD1 subunit homolog A	P41227	1.6	0.00	26.4	5.41	352	15
Rep_14	Protein CDV3 homolog	Q9UKY7	1.6	0.00	27.3	6.06	481	11

Lable[a]	Identification	Protein ID.[b]	Fold change	p-value	MW[c]	pI[d]	Protein score[e]	Peptide count[f]
Rep_15	Heme oxygenase 2	P30519	1.6	0.00	36.0	5.31	402	23
Rep_16	Nucleosome assembly protein 1-like 1	P55209	1.6	0.02	45.3	4.36	273	10
Rep_17	Heat shock 70 kDa protein 4L	O95757	1.6	0.02	94.4	5.63	433	38
Rep_18	Synaptosomal-associated protein 29	O95721	1.6	0.02	29.0	5.56	295	16
Rep_19	Heat shock cognate 71 kDa protein	P11142	1.6	0.00	70.9	5.37	167	17
Rep_20	N6-adenosine-methyltransferase 70 kDa subunit	Q86U44	1.6	0.00	64.4	5.98	214	15
Rep_21	Proteasome activator complex subunit 1	Q06323	1.5	0.00	28.7	5.78	413	22

[a]Label: Spot identification number;
[b]Protein ID: SwissProt Entry name;
[c]MW: Molecular weight calculated from amino acid sequence (in kDa);
[d]pI: isoelectric point calculated from amino acid sequence;
[e]Peptide count: number of matched peptides;
[f]Protein score: significance of protein identification

5.1.10. ERM-proteins (Ezrin, Radixin, Moesin) are overexpressed and hyperphosphorylated upon *BCL11B* knockdown

The detailed inspection of the differential proteome analysis using the DIGE-technology already revealed increased levels of ERM-proteins after *BCL11B* knockdown (Fig. 18A). Since phosphorylation of ERM proteins in their C-terminal parts has previously been shown to occur in the course of TNF alpha induced activation of PKC and p38 in the non-mitochondrial pathway of apoptosis (Koss et al 2006), we wanted to ascertain if the increased levels of ERM proteins observed in our study were also paralleled by increased phosphorylation. In a first step protein phosphorylation was analyzed by staining 2-DE separated protein extracts with Diamond-ProQ®, which preferentially stains proteins phosphorylated at either serine or threonine. This Diamond-Pro Q® staining revealed increased levels of phosphorylation of ERM proteins following transfection of both Jurkat and huT78 cells with siRNA specific for *BCL11B* compared to the scrambled control RNA (Fig. 18B). This first hint of increased levels and phosphorylation of ERM proteins was than substantiated by Western blotting. As expected, ERM proteins displayed two bands in the Western blot analysis. Employing antibodies directed against the phosphorylated forms of ERM-proteins increased levels of phosphorylation of ERM proteins were observed in Jurkat and huT78 cells as well as in Jurkat *BCL-xL* cells (Fig. 18C). Phosphorylation probably also triggered conformational changes in ERM proteins that resisted treatment with SDS resulting in changes of migration of ERM proteins after transfection with siRNA specific for *BCL11B*. Western blot analysis with an antibody directed against total ERM proteins supported the observation of the DIGE analysis that ERM proteins were increased in total level following *BCL11B* knock down (Fig. 18C). However, increases in levels of ERM proteins were less pronounced than the changes in their phosphorylation status.
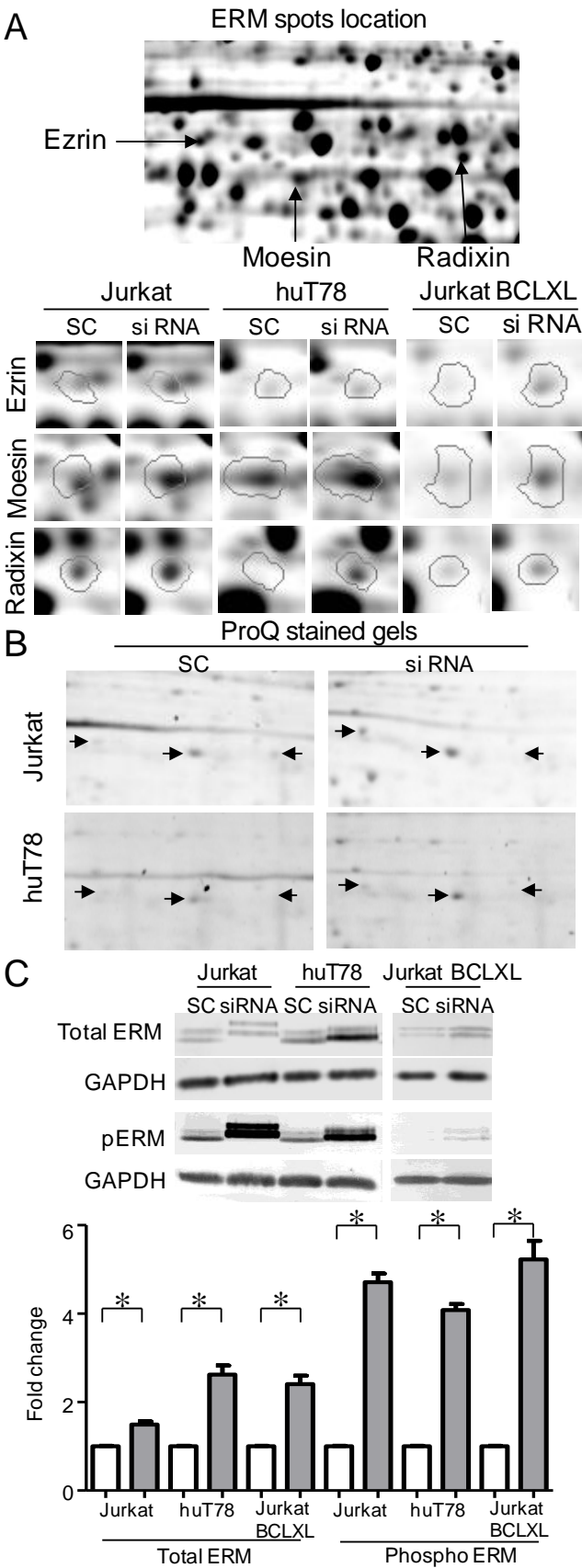
Fig. 18: Detailed proteomic analysis of ERM-proteins (Ezrin, Radixin and Moesin). For ERM proteins the changes in levels observed by the 2D-DIGE analysis were verified by phosphoprotein specific staining with Pro-

Q® Diamond and Western blotting employing antibodies that allow measurement of the total level of ezrin, radixin, and moesin or phosphorylated forms of the three proteins. A) Representative section of a 2D-DIGE image containing ERM proteins (see also box 1 in Fig. 11). Sections of 2D-DIGE gel images demonstrating increases of ERM protein levels in huT78, Jurkat and JurkatBcl-xL cells at 48 h following transfection with *BCL11B*-specific siRNA. B) Sections of Pro-Q Diamond stained gels illustrating increases in phosphorylation of ERM protein levels in huT78 and Jurkat at 48 h following transfection with *BCL11B*-specific siRNA. C) Analysis of ERM-phosphorylation and total ERM level by Western blotting. After separation by SDS-PAGE and transfer to membranes protein extracts were probed with primary antibodies directed against total ERM, phosphorylated ERM proteins and GAPDH. Subsequent to probing with secondary antibodies and visualization of signals, the intensity of the signals was quantified by correcting intensity values for the GAPDH signal detected in the same sample. Intensities of both bands seen for ERM proteins were combined. For calculation of the quantitative effect of Bcl11B suppression the level of the signals in the samples treated with SC-RNA was set to one. Western blot analysis was performed in huT78, Jurkat and JurkatBcl-xL cells at 48 h following transfection with *BCL11B*-specific siRNA. * $p < 0.05$.

5.1.11. *BCL11B* knockdown reduces the mitochondrial membrane potential

We determined the accumulation of the cationic lipophilic fluorochrome 3, 3′-dihexyloxacarbocyanine iodide [DiOC6] in the mitochondrial matrix, which is directly proportional to the mitochondrial membrane potential, to assess the effects of *BCL11B* suppression onto the mitochondrial apoptosis pathway. In both Jurkat as well as huT78 cells the suppression of *BCL11B* triggered significant loss of membrane potential in a time dependent fashion (Fig. 19). Treatment with the scrambled control RNA did not trigger such an effect. In Jurkat BCLxL cells, over-expressing the anti-apoptotic protein BCL-xL, the suppression of *BCL11B* did not affect the DiOC6 accumulation (Fig. 19) and thus induction of the mitochondrial branch of apoptosis.
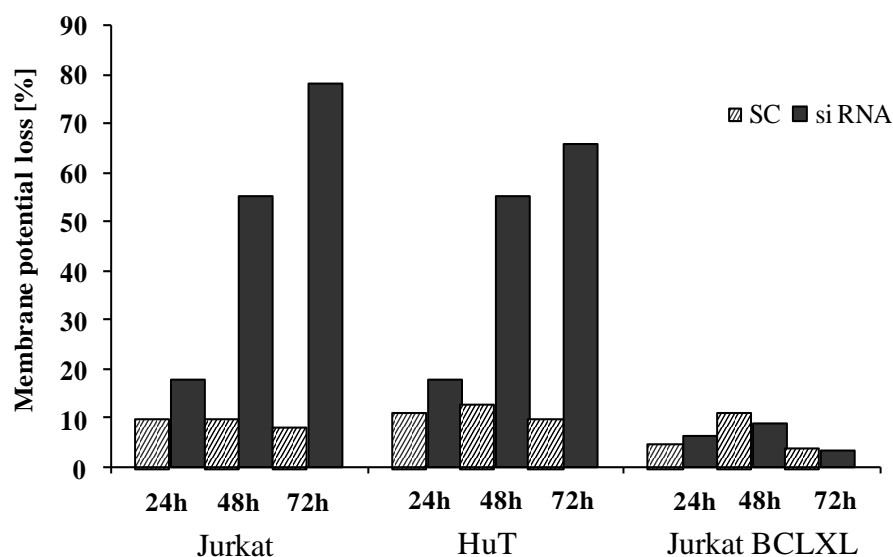
Fig. 19: Measurment of membrane potential. Loss of mitochondrial membrane potential was measured by determining the decrease in the accumulation of the cationic lipophilic fluorochrome 3,3′-dihexyloxacarbocyanine iodide [$DiOC_6$] in the mitochondrial matrix, which is directly proportional to mitochondrial potential. The level of accumulated $DiOC_6$ was measured in Jurkat and huT78 at the beginning of the experiment or 24 to 72 h after transfection with scrambled control RNA or siRNA specific for *BCL11B*. The difference between the $DiOC_6$ accumulated at the respective time point compared to the level of untreated control cells at time point 0 is displayed (which is directly proportional to the loss of membrane potential).

5.1.12. BCL11b knock down results in up regulation of dUTPase enzyme and uracil misincrporation in DNA

BCL11b was implicated in the remedy of DNA replication stress and maintenance of genomics integrity (Kamimura et al 2007a). From our results it was observed that BCL11b knockdown results in higher proliferation stress in Jurkat and HuT cells and dUTPase, CDK6 and UCK 2 enzymes were up regulated, which are implicated in cell cycle progression and DNA replication processes.

The dUTPase enzyme converts dUTP to dUMP during replication process ensuring DNA replication efficiency without uracil misincorporation. The 2D gel insets shown in Fig. 20B demonstrate the up regulation of dUTPase in Jurkat, HuT and Jurkat BCLXL cells following *BCL11B* knockdown. This was confirmed by Western blotting using a polyclonal antibody against DUT-N (abcam) of the dUTPase (Fig. 20B). In this high replication stress scenario in Jurkat and HuT cells uracil misincorporation into DNA was analyzed using a Uracil-DNA Glycosylase (UNG) assay which eliminates uracil from DNA molecules to prevent mutagenesis. For this analysis we excracted DNA from Jurkat HuT and Jurkat *BCL-*

xL cells treated either with scrambled control or siRNA directed against *BCL11B,* treated equal amounts of DNA with UNG and separated the DNAs by gel electrophoresis. DNA degradation was observed in Jurkat, HuT and Jurkat *BCL-xL* cells treated with *BCL11B* siRNA but not in cells treated with scrambled control RNA (Fig. 20C). Degradation of DNA in Jurkat *BCL-xL* cells treated with *BCL11B* siRNA indicates this is an upstream event of apoptosis (Fig. 20C).
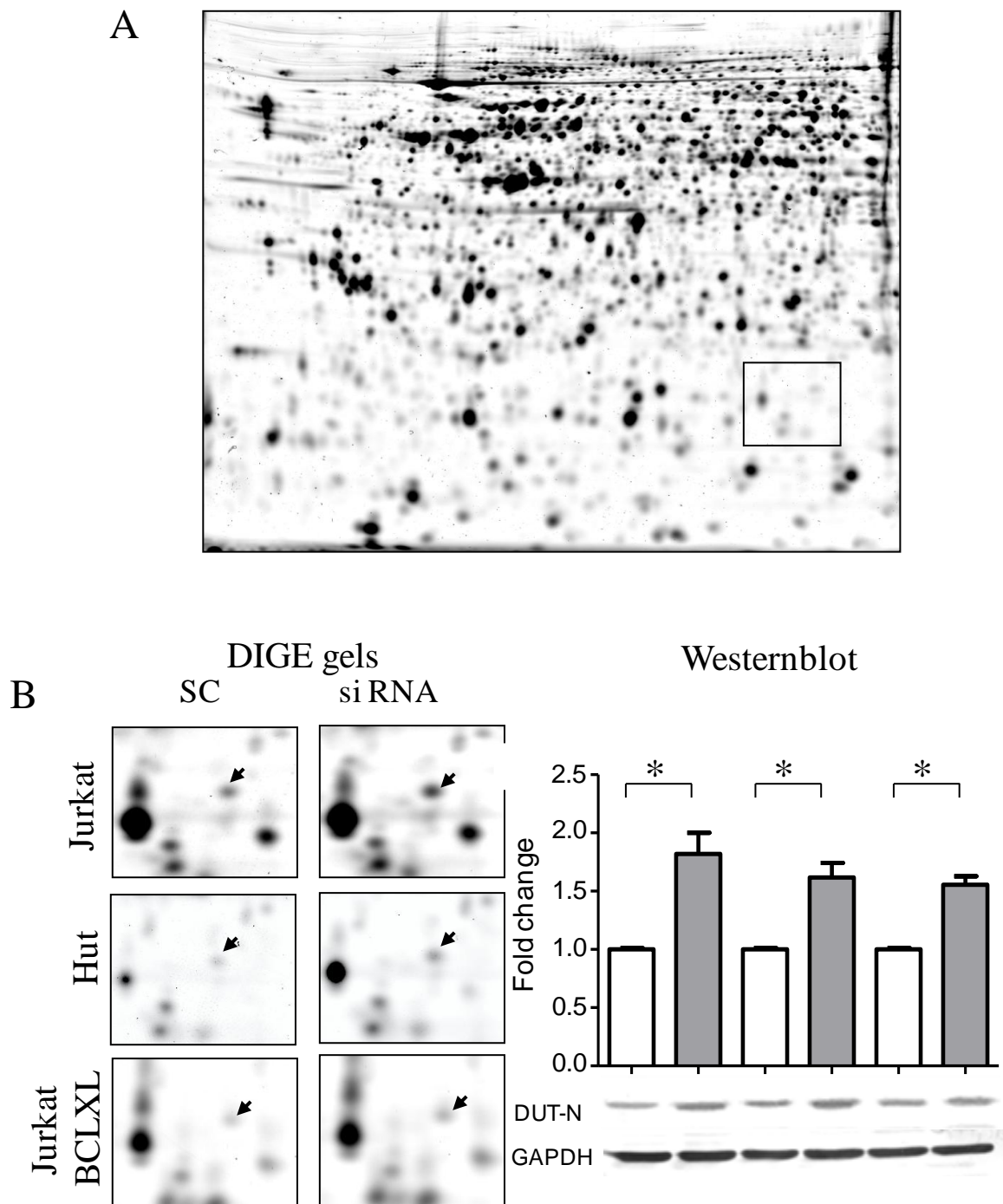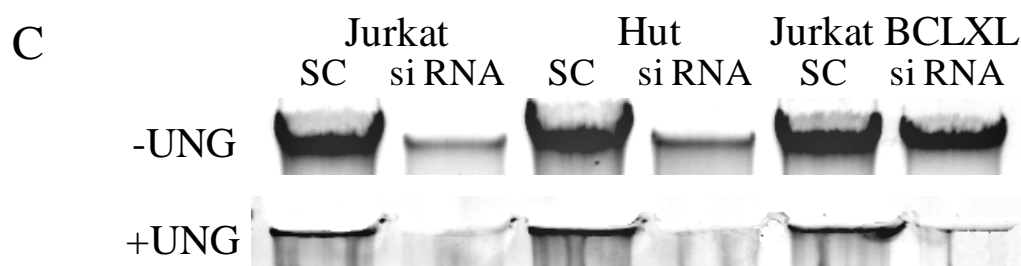
Fig. 20: Analysis of levels of dUTPase and uracil-misincorporation into DNA. A) 2D image of Jurkat cells showing the region of interest containing dUTPase protein spot. B) Assessment of dUTPase protein levels by 2D-DIGE and Western blot analysis. Enlarged sections of images of the DIGE analyses (left panel) and the Western blot analyses (right panel), which was performed with an antibody directed against dUTPase, are displayed. Arrowheads mark dUTPase and sc and siRNA represent protein extracts derived from cells treated with scrambled control RNA or siRNA specific for *BCL11B*. C) Analyses of DNA-degradation. DNA was isolated from Jurkat, huT78 and Jurkat Bcl-xLcell lines that had been transfected with scRNA or *BCL11B* - specific siRNA for 48 h. Equal amounts of non-treated control DNAs (-UNG) or DNA which had been treated with Uracil N-Glycosylase (+UNG) were separated by agarose gel electrophoresis and residual DNA-levels were visualized by staining with ethidium bromide.

5.1.13. Validation of other target proteins by Western blot analysis

BCL11B has also previously been implicated in adjusting the level of replication stress and maintenance of genome integrity.(Kamimura et al 2007a) Inspection of the list of regulated genes revealed increased levels of CDK6, UCK2 and dUTPase (Table 3), which are implicated in cell cycle progression, DNA replication and maintenance of DNA integrity. Increased levels of UCK2 following *BCL11B* knockdown were supported by Western blot analysis employing UCK2 specific antibodies, which again revealed increased intensities of UCK2 protein in Jurkat, huT78 and Jurkat *BCLxL* cells when these cells were transfected with *BCL11B*-specific siRNA but not with scrambled control RNA (Fig. 21).

Looking for other proteins for which changes in levels might be related to apoptosis we decided to also verify the alterations discovered in the proteome analysis for programmed cell death 5 protein (PDCD5) and ménage a trios-1 protein (MAT1). PDCD5 has been identified as an enhancer or key regulator of apoptotic programmed cell death driven by deprivation of growth factor in the human premyeloid cell line TF-1 (Liu et al 1999). MAT1 in turn is part of the CDK-activating kinase complex, which plays an essential role in cell cycle control. Western blot analysis confirmed for both proteins the increased intensity levels in Jurkat and huT78 cells that were already noticed in the proteomic screen (Fig. 21). Levels of both proteins also increased in Jurkat *BCL-xL* cells also following Bcl11b suppression.
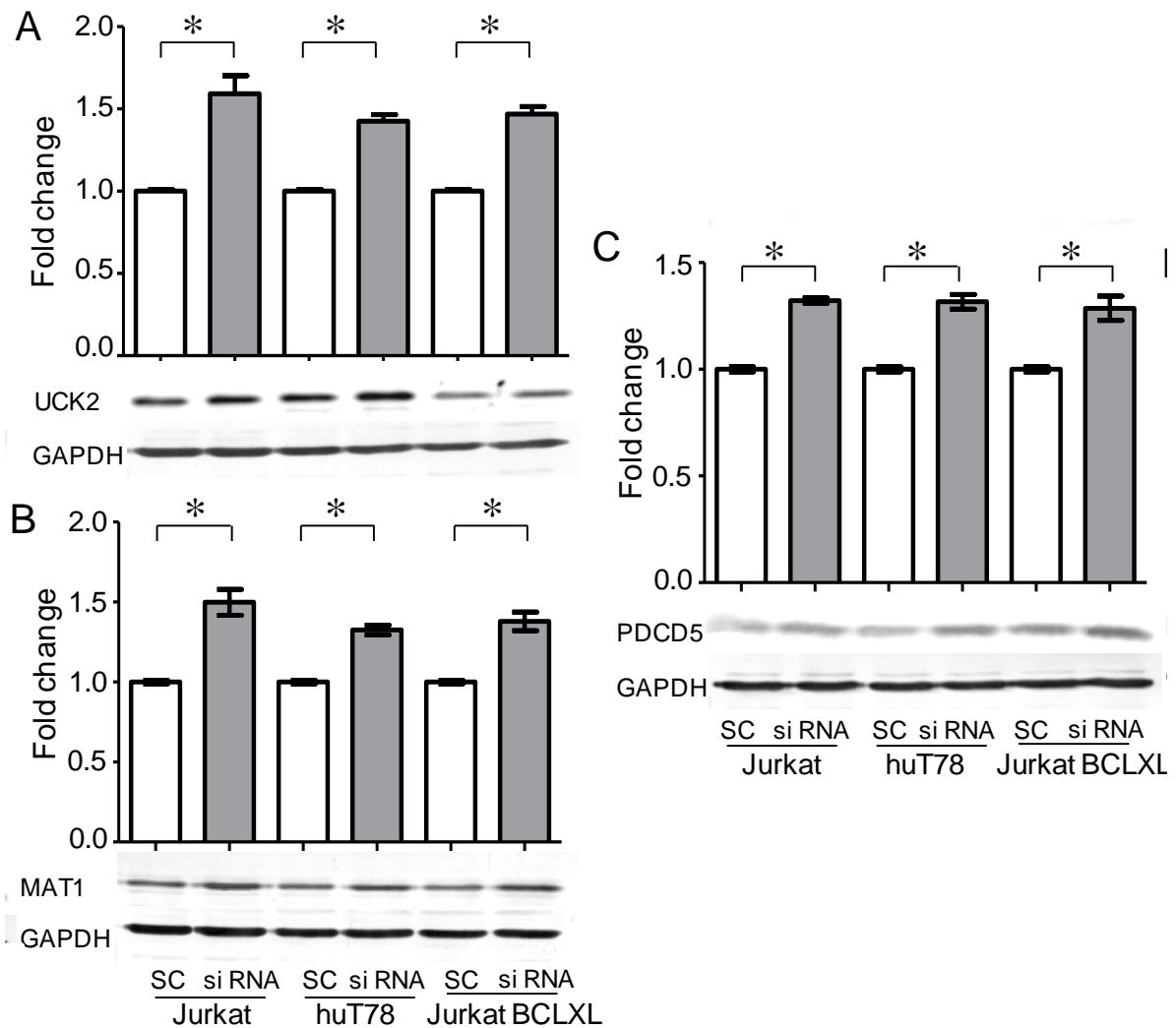
Fig. 21: Levels of proteins shown to be influenced by knock-down of *BCL11B* in the 2D-DIGE experiments were analyzed by Western blotting in Jurkat, huT78 and Jurkat *BCL-xL* cells. Representative images of the immunoblots and the quantification of the signal intensities by correcting corresponding GAPDH signal from three independent biological experiments are displayed. white bars -samples treated with scrambled control RNA; grey bars-samples treated with siRNA specific for *BCL11B*. A) UCK2, B) MAT1 and C) PDCD5. * p < 0.05

5.1.14. Validation of regulated proteins in *BCL11B* overexpression cells

In order to verify the proteomic findings from the *BCL11B* overexpression system the above proteins were also tested by Western blot analysis of crude protein extracts of Jurkat *BCL11B* overexpressing cells. Increasing the level of Bcl11b in Jurkat cells by stable over-expression had the opposite effect of reducing total levels. Similarly to the ERM proteins, dUTPase, UCK2, MNAT1 as well as PDCD5 were reduced in levels following stable overexpression of *BCL11B* in Jurkat cells (Fig. 22), reinforcing the role of Bcl11b in

controlling the levels of these proteins. Also phosphorylation of ERM proteins was reduced in this *BCL11B* overexpression system (Fig. 22).
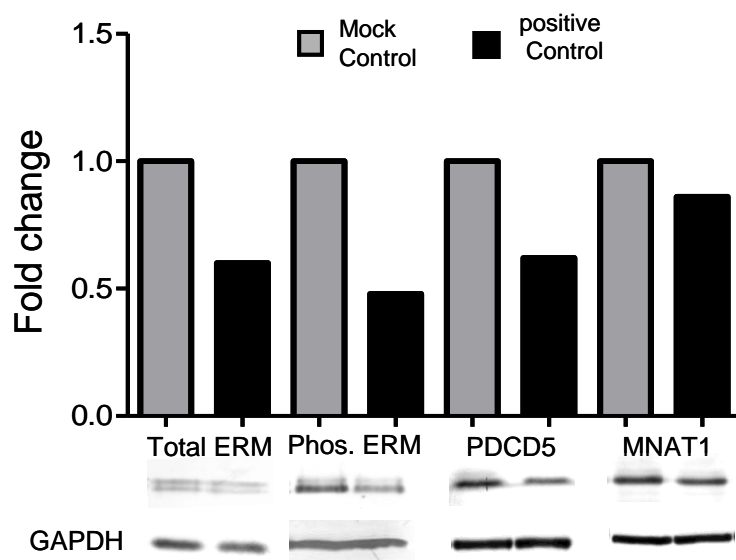
Fig. 22 Validation of regulated proteins in BCL11b overexpressing cells by Western blot analysis using specific antibodies against total ERM, phospho ERM, PDCD5 and MNAT1 proteins. Negative regulation was observed in BCL11b overexpressing cells compared to BCL11b knockdown cells implying that these are BCL11b specific effects.

5.2. Elucidation of the mechanism of pathophysiology of Johanson Blizzard Syndrome (JBS) using UBR1 knockout mice and JBS patients' lymphoblasts cell lines.

5.2.1. Development of a protein based assay to detect subclinical Johanson-Blizzard-Symdrome

5.2.1.1. Proteome analysis of JBS patients lymphoblasts

Johanson-Blizzard syndrome (JBS) patients bear mutations in UBR1 gene. Most of the mutation cause premature truncation of the protein and some of them are missense mutations which eventually result in the complete or partial loss of function and most of the times in expression as well. To analyze the differences in the proteome among controls and patients a 2D-DIGE experiment was carried out as indicated in Fig. 23. In total 12 controls and 14 patients were available for these studies. The details of the mutational analysis of the patients and controls are given in the materials section. To avoid interindividual differences in controls all controls were pooled. However, each patient sample was treated as an independent

biological replicate and a total of 14 individual samples were considered for the DIGE experiment. It was taken care that by dye swap one Cy3 and one Cy5 value was obtained to allow for a total of 2 technical replicate values for each patient sample and 4 Cy3 and 4 Cy5 values to give a total of 8 technical replicate values for the control pool.
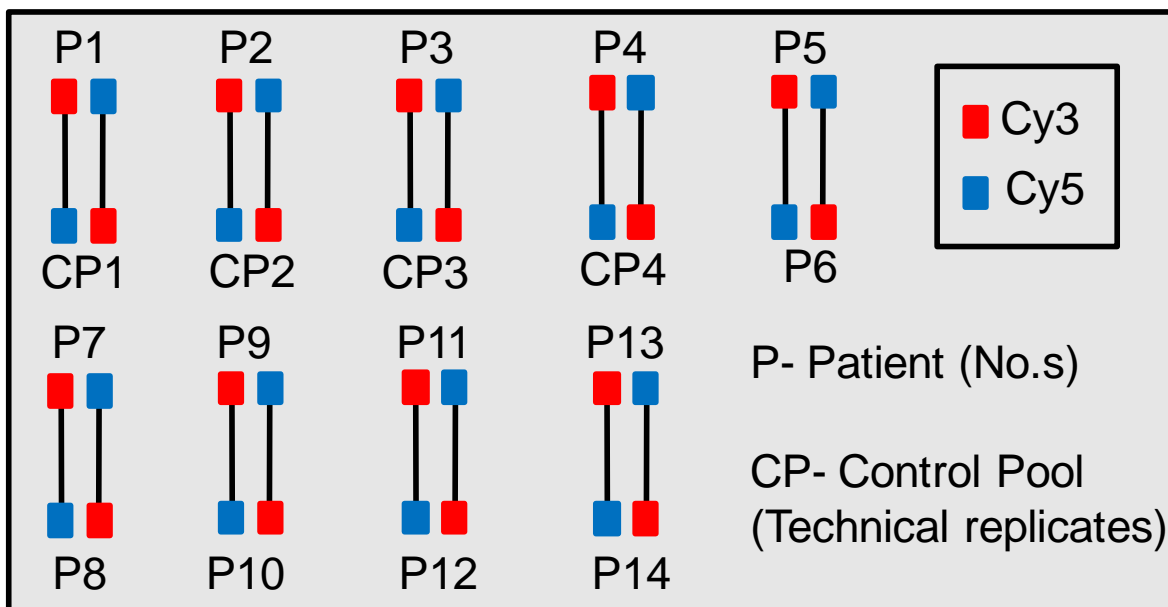
Fig. 23: Scheme of JBS patients' lymphoblast samples 2D-DIGE experiment. Dye swap was planned such that for each patient sample one Cy3 and one Cy5 value were generated to give 2 technical replicate values and for the control pool sample 4 Cy3- and 4 Cy5-labeled samples were processed to give 8 technical replicate values in the experiment.

5.2.1.2. Analysis of differentially expressed proteins by 2D-DIGE in JBS patients lymphoblast

The 2D-DIGE experiment was performed as shown in the DIGE experiment scheme to identify proteins that are present at different levels in control lymphoblast samples and JBS patients' lymphoblast samples. 2D image analysis allowed quantification of a total of 1295 spots using the Delta 2D software and statistical analysis was performed using the gene spring software as given in the method section. Spots which displayed in both groups a minimum fold difference in intensity of 1.5 and a p-value below 0.05 were labeled with numbers prefixing "Ind" for induced and "Rep" for repressed spots. In total 24 protein spots intensities were increased and 42 protein spots were reduced as illustrated by the representative 2D-DIGE image (Fig. 24). The identification of the proteins displaying differential intensities was done using MALDI TOF-TOF according to the protocol given in method section and the identified proteins are listed in Table 6.
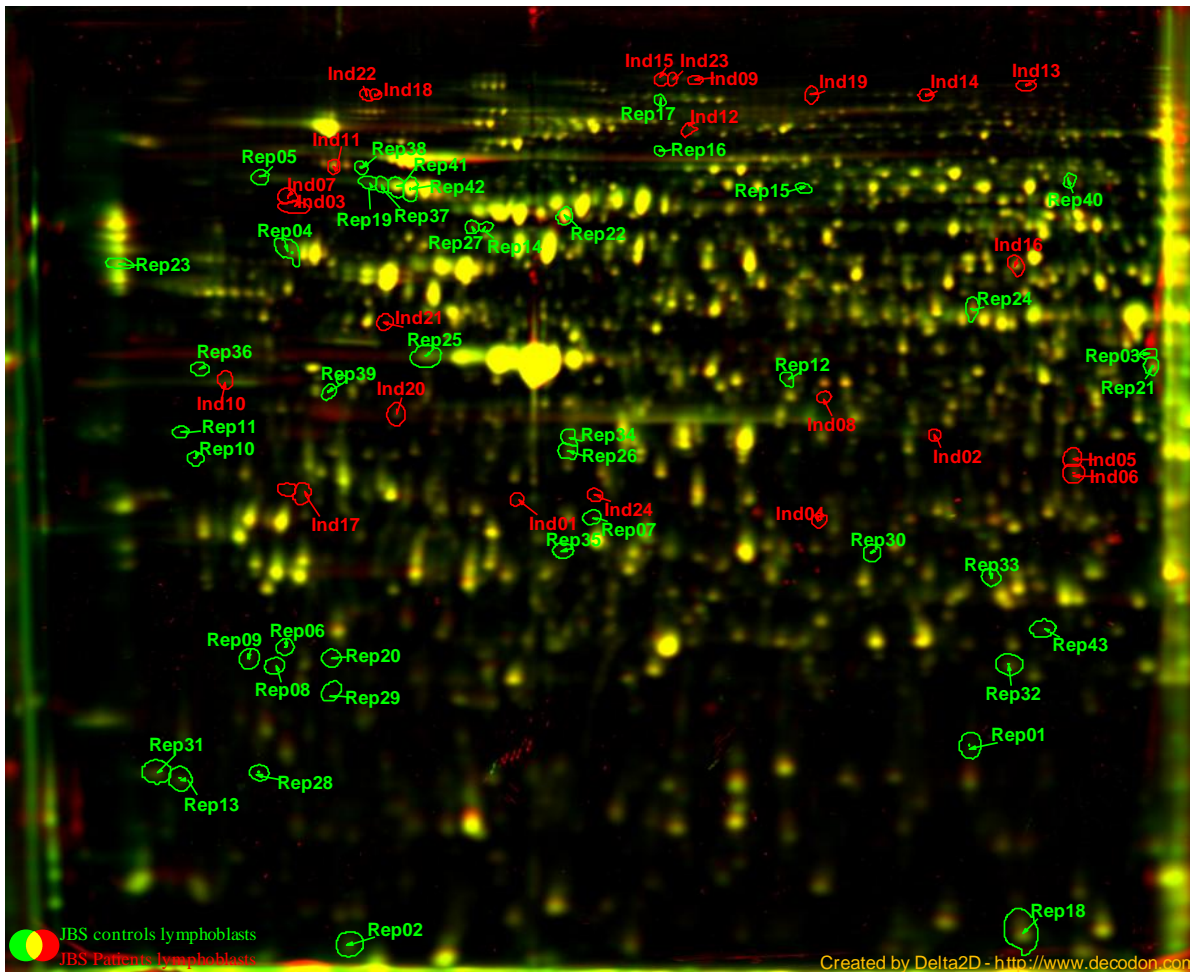
Fig. 24: Representative 2D-DIGE images showing differentially expressed proteins in JBS patients´ lymphoblast cells compared to the controls pooled lymphoblast cells. Overlapping 2D-DIGE images of the controls pooled lymphoblast cells and the JBS patients' lymphoblast cells were represented by green and red colours, respectively. A total of 1295 spots were quantified with the aid of Delat2D image analysis. The differentially expressed spots which follow the criteria of minimum fold change 1.5 and p value below 0.05 were labeled with numbers prefixing "Ind" for increased and "Rep" for decreased intensity of spots. Out of 1295 spots the intensity of 42 spots was decreased whereas 24 spots were increased in their intensity.

5.2.1.3. Principle component analysis (PCA) and cluster analysis

To provide a global impression of the information in the dataset and to assess the differences between the individual data sets from JBS patients and controls we used principal component analysis (PCA) and subsequently clustering. The proteome patterns were evaluated by means of PCA. Altogether, 36.3 % of the total variance of the proteomic data, which were acquired from 14 patients and 11 controls in two biological and three technical replicates, was covered by the two most prominent principal components. PC2 captured the values, which differentiated the phenotypic response of UBR1 mutations. PCA analysis showed that the majority (10 out of 14) of JBS patients behaved similar with regard to the

protein expression pattern on 2-DE. However, P2, P3, P8 and P9 clustered around the controls. This prompted us to look for the differences in UBR1 protein levels in these patients as the most obvious influencing factor changing protein patterns and explaining the individual patient's phenotype (Fig. 25)
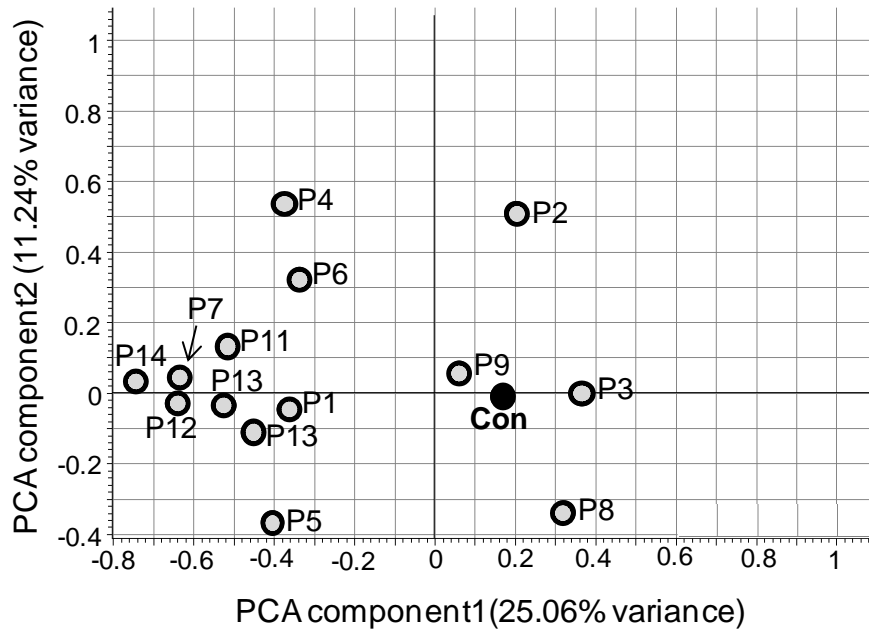
Fig. 25: Principal component analysis (PCA) of the protein patterns of patients with a defect in UBR1 and control samples. The PCA analysis is based on the Cy2-normalized intensities of all 1295 spots detected on the fused gel image. The influence of the 2 most important principal components is displayed. Patients are shown as grey colored filled circles and marked with their respective ID, whereas the pooled control sample is indicated by the black filled circle marked in bold as "Con".

Table 6: Identification of differentially expressed proteins in lymphoblasts cell lines of JBS patients compared to controls

Lable[a]	Identification	Protein ID.[b]	Fold change	p-value	MW[c]	pI[d]	Protein score[e]	Peptide count[f]
Ind01	Actin, cytoplasmic 2	P63261	1.8	0.05	41.8	5.31	319	14
Ind02	Probable O-sialoglycoprotein endopeptidase	Q9NPF4	2.2	0.04	36.4	5.94	261	15
Ind03	Plastin-2	P13796	40.8	0.03	70.2	5.2	308	25
Ind04	Not identified		4.1	0.02				
Ind05	S-formylglutathione hydrolase	P10768	1.6	0.02	31.4	6.54	223	12
Ind06	S-formylglutathione hydrolase	P10768	2.1	0.01	31.4	6.54	627	19
Ind07	Not identified		8.7	0.01				
Ind08	Not identified		2.1	0.01				
Ind09	Not identified		62.5	0.01				
Ind10	Protein SET	Q01105	1.7	0.00	33.5	4.23	209	12
Ind11	Hematopoietic lineage cell-specific protein	P14317	1.7	0.00	54.0	4.74	420	20
Ind12	Not identified		1.6	0.00				
Ind13	Not identified		1.7	0.00				
Ind14	Not identified		1.7	0.00				
Ind15	Talin-1	Q9Y490	1.5	0.00	269.6	5.77	102	26
Ind16	Inosine-5'-monophosphate dehydrogenase 2	P12268	1.6	0.00	55.8	6.44	706	25
Ind17	HLA class II histocompatibility antigen, DQ(5) alpha chain precursor	P01907	1.8	0.00	28.0	5	270	7
Ind18	Golgin subfamily A member 2	Q08379	1.5	0.00	111.6	4.97	129	20
Ind19	Not identified		1.6	0.00				
Ind20	Poly(ADP-ribose) glycohydrolase ARH3	Q9NX46	1.5	0.00	38.9	4.95	412	23
Ind21	Gamma-enolase	P09104	1.6	0.00	47.2	4.91	577	21
Ind22	Not identified		1.6	0.00				

Lable[a]	Identification	Protein ID.[b]	Fold change	p-value	MW[c]	pI[d]	Protein score[e]	Peptide count[f]
Ind23	Early endosome antigen 1	Q15075	1.6	0.00	162.4	5.53	79.8	25
Ind24	N-terminal acetyltransferase complex ARD1 subunit homolog A	P41227	1.7	0.00	26.4	5.41	271	14
Rep01	Not identified		1.9	0.01				
Rep02	Not identified		1.6	0.00				
Rep03	Not identified		1.8	0.00				
Rep04	Protein disulfide-isomerase precursor	P07237	1.6	0.00	57.1	4.76	550	26
Rep05	Not identified		1.8	0.00				
Rep06	Not identified		1.6	0.00				
Rep07	Actin, cytoplasmic 2	P63261	1.5	0.00	41.8	5.31	175	11
Rep08	Not identified		1.5	0.00				
Rep09	Not identified		1.5	0.00				
Rep10	L-lactate dehydrogenase A chain	P00338	2.0	0.00	36.7	8.44	143	14
Rep11	Not identified		1.8	0.00				
Rep12	Not identified		1.5	0.00				
Rep13	Nucleophosmin	P06748	1.5	0.00	32.6	4.64	145	5
Rep14	Not identified		1.8	0.00				
Rep15	Moesin	P26038	1.5	0.00	67.8	6.08	89.4	15
Rep16	Myosin-9	P35579	1.8	0.00	226.4	5.5	157	22
Rep17	Talin-1	Q9Y490	1.7	0.00	269.6	5.77	491	40
Rep18	Actin, cytoplasmic 2	P63261	1.7	0.00	41.8	5.31	575	15
Rep19	78 kDa glucose-regulated protein precursor	P11021	1.8	0.00	72.3	5.07	750	24
Rep20	Not identified		1.6	0.00				
Rep21	Not identified		2.3	0.00				
Rep22	Plastin-2	P13796	1.6	0.00	70.2	5.2	555	40
Rep23	Tubulin alpha-1B chain	P68363	1.7	0.00	50.1	4.94	777	21
Rep24	Not identified		2.0	0.00				

Lable[a]	Identification	Protein ID.[b]	Fold change	p-value	MW[c]	pI[d]	Protein score[e]	Peptide count[f]
Rep25	Actin, cytoplasmic 2	P63261	1.5	0.00	41.8	5.31	660	24
Rep26	Not identified		1.5	0.00				
Rep27	Not identified		2.5	0.00				
Rep28	Actin, cytoplasmic 2	P63261	2.4	0.00	41.8	5.31	123	5
Rep29	Not identified		1.6	0.00				
Rep30	Ig lambda chain C regions	P01842	2.4	0.00	11.2	6.92	123	5
Rep31	Nucleophosmin	P06748	2.2	0.00	32.6	4.64	150	8
Rep32	Peroxiredoxin-1	Q06830	1.7	0.00	22.1	8.27	488	16
Rep33	Phosphoglycerate mutase 1	P18669	1.8	0.00	28.8	6.67	479	16
Rep34	F-actin-capping protein subunit alpha-1	P52907	1.7	0.00	32.9	5.45	312	13
Rep35	Prohibitin	P35232	1.6	0.00	29.8	5.57	413	18
Rep36	Not identified		2.2	0.00				
Rep37	78 kDa glucose-regulated protein precursor	P11021	2.1	0.00	72.3	5.07	974	32
Rep38	Hematopoietic lineage cell-specific protein	P14317	2.2	0.00	54.0	4.74	562	22
Rep39	Actin, cytoplasmic 2	P63261	2.3	0.00	41.8	5.31	563	16
Rep40	Not identified		2.8	0.00				
Rep41	78 kDa glucose-regulated protein precursor	P11021	2.0	0.00	72.3	5.07	1030	41
Rep42	78 kDa glucose-regulated protein precursor	P11021	1.6	0.00	72.3	5.07	1070	39
Rep43	Not identified		1.5	0.00				

[a]Label: Spot identification number; [b]Protein ID: SwissProt Entry name;
[c]MW: Molecular weight calculated from amino acid sequence (in kDa);
[d]pI: isoelectric point calculated from amino acid sequence;
[e]Peptide count: number of matched peptides;
[f]Protein score: significance of protein identification

5.2.1.4. Quantification of UBR1 by western blot

All patients' samples and controls samples were tested for UBR1 levels by Western blot analysis. 50 µg of all these samples were separately separated by 1D SDS-PAGE and blotted on a PVDF membrane as indicated in methods. This blot was analyzed for UBR1 levels using a UBR1 specific monoclonal antibody and equal loading was checked by using a GAPDH specific polyclonal antibody. The quantification was done by subtracting the background value and the value of the pooled control sample in the blot was set to 100%. Values of the patients and controls samples were quantified referring to the control pool value. Three Western blot experiments were carried out to calculate the standard error of mean for each sample value. The graphical presentation of these data (Fig. 26) showed that the patients with the numbers 2, 3, 8 and 9 were displaying considerably more residual UBR1 levels compared to the other patients, which is in agreement with the gene tree cluster analysis or principle component analysis, where these particular samples clustered apart from the group of remaining patients which express very low levels or no UBR1 (Fig. 26).
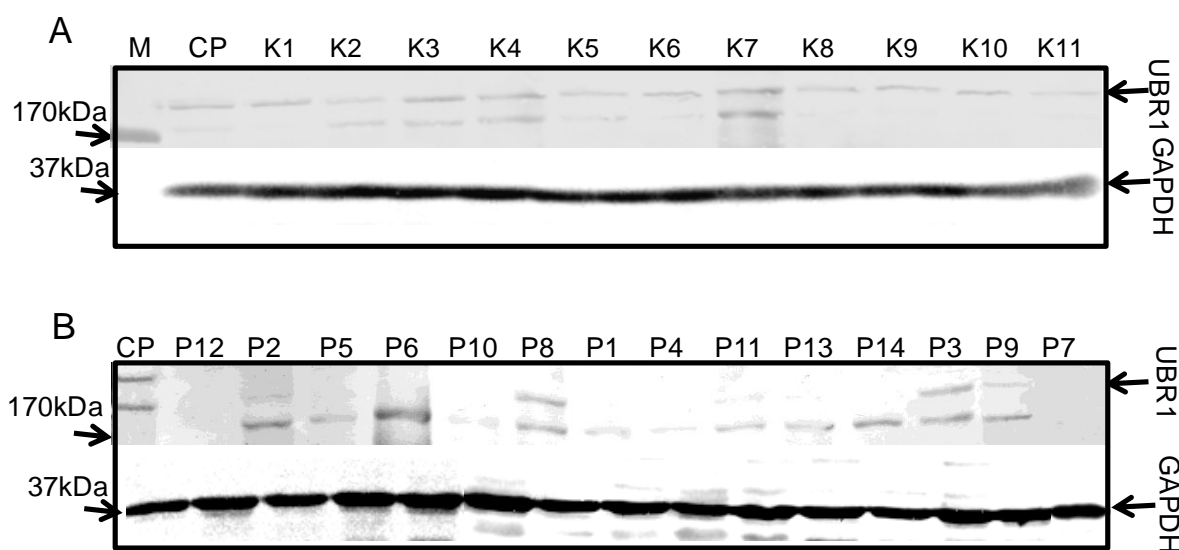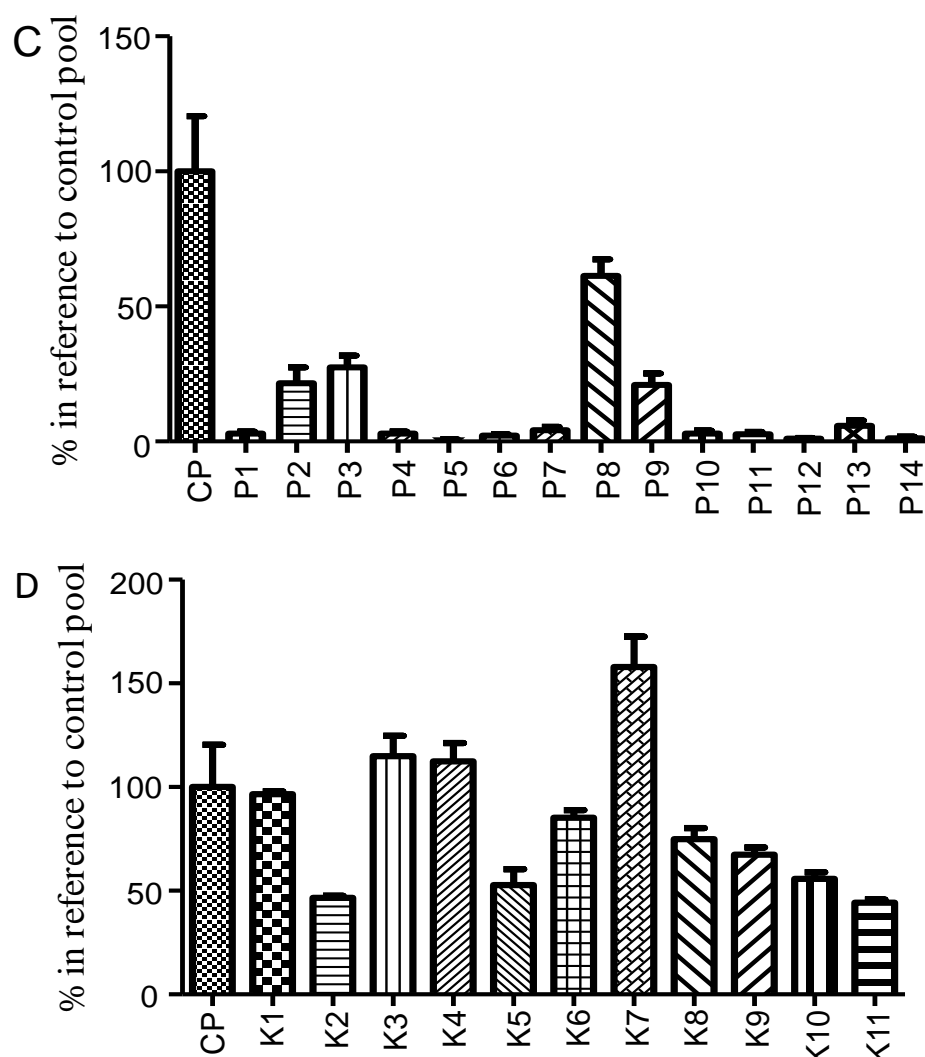
Fig. 26: Western blot analysis of levels of UBR1 in controls (A) and patients (B). Protein aliquots of lymphoblast samples from controls and patients were separated by SDS-PAGE and after blotting onto a PVDF membrane levels of UBR1 were assessed with the aid of a UBR1 specific monoclonal antibody (Abnova). GAPDH levels were determined in parallel as a loading control in order to facilitate quantitative comparisons of UBR1 levels. A and B) Western blot data of patients and controls, respectively. C and D) Bar graphs showing relative expression of UBR1 in patients and controls compared to the signal of the control pool. Error bars indicate the mean standard error of three different western blot experiments with the same samples.

5.2.1.5. Hierarchical clustering of JBS patients and controls

Based on the expression profiles of 20 spots with the lowest p-value derived from the Golubs' algorithm we performed hierarchical clustering of JBS patients and controls. Tree clustering was done using Pearson correlation and condition tree clustering was done using Spearman correlation for similarity measurement. Controls, patients with residual UBR1 expression and those lacking UBR1 activity were clearly discriminated (Fig. 27). This

suggested again that residual UBR1 expression, which was not expected from the genotype analysis, influenced the phenotype. Sample P2, P3, P8 and P9 showed partially characteristics of JBS which could be missed if the patient would have been seen in a non-specialized center. However, pancreatic exocrine insufficiency was a consistent symptom also in these patients. Mere genotype analysis would have suggested a complete loss of the UBR1 protein pointing out the weakness in predicting expression based on sequencing information alone. As UBR1 confers an enzymatic activity which is very difficult to measure (Tasaki et al 2005) we aimed to identify a protein panel as a surrogate marker of UBR1 activity to diagnose mild forms of JBS.
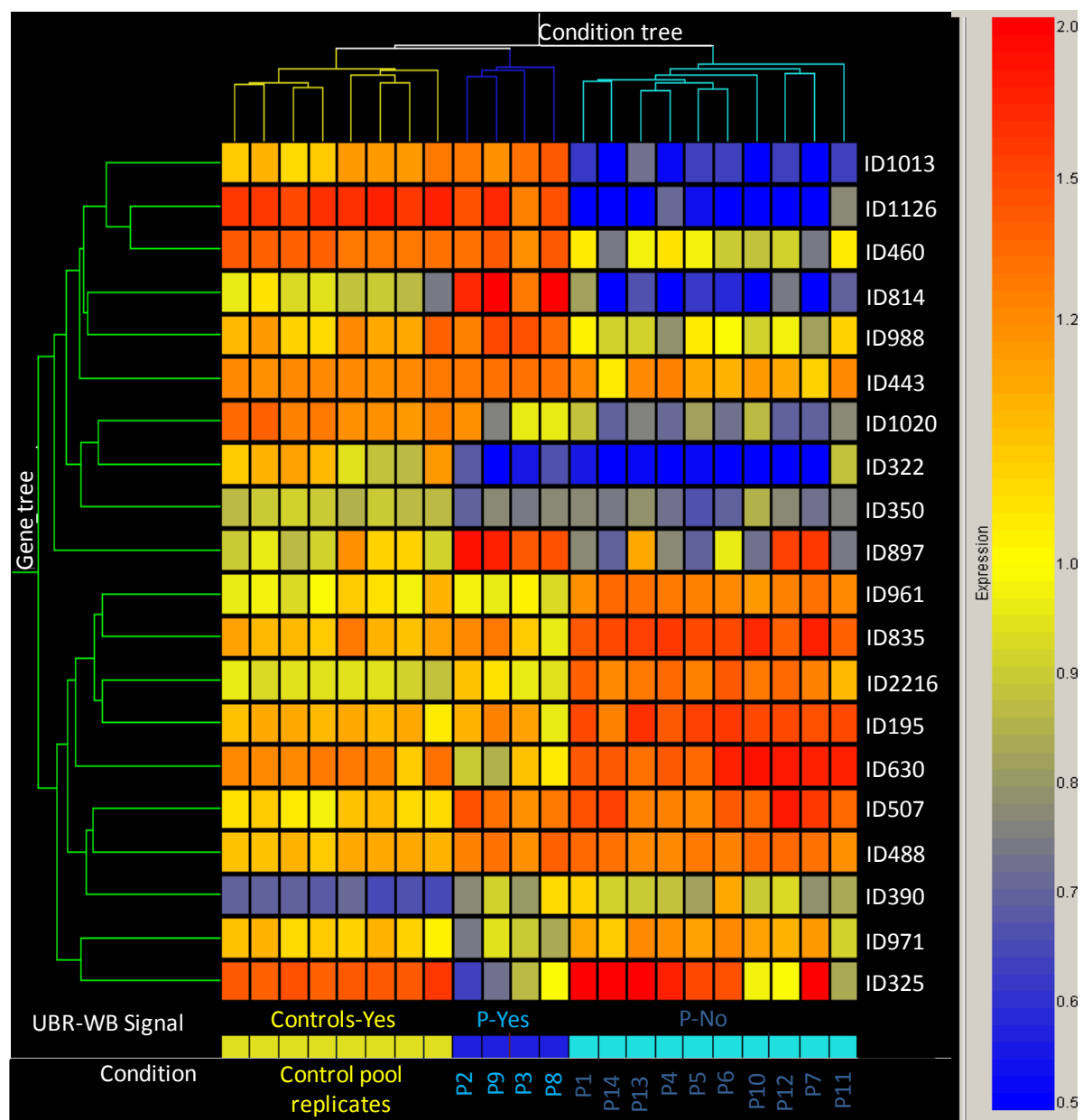
Fig. 27: Hierarchical clustering of patients and controls based on expression profiles of the 20 spots displaying the lowest p-value derived from Golubs' algorithm. Tree clustering was done using Pearson

correlation and condition tree clustering was done using Spearman correlation for similarity measurement. Controls, patients with residual UBR1 activity and those lacking any UBR1 activity are clearly discriminated.

20 spots which were used to distinguish between JBS and controls using hierarchical clustering are labeled on the fusion gel of the combined images given below (Fig. 28)
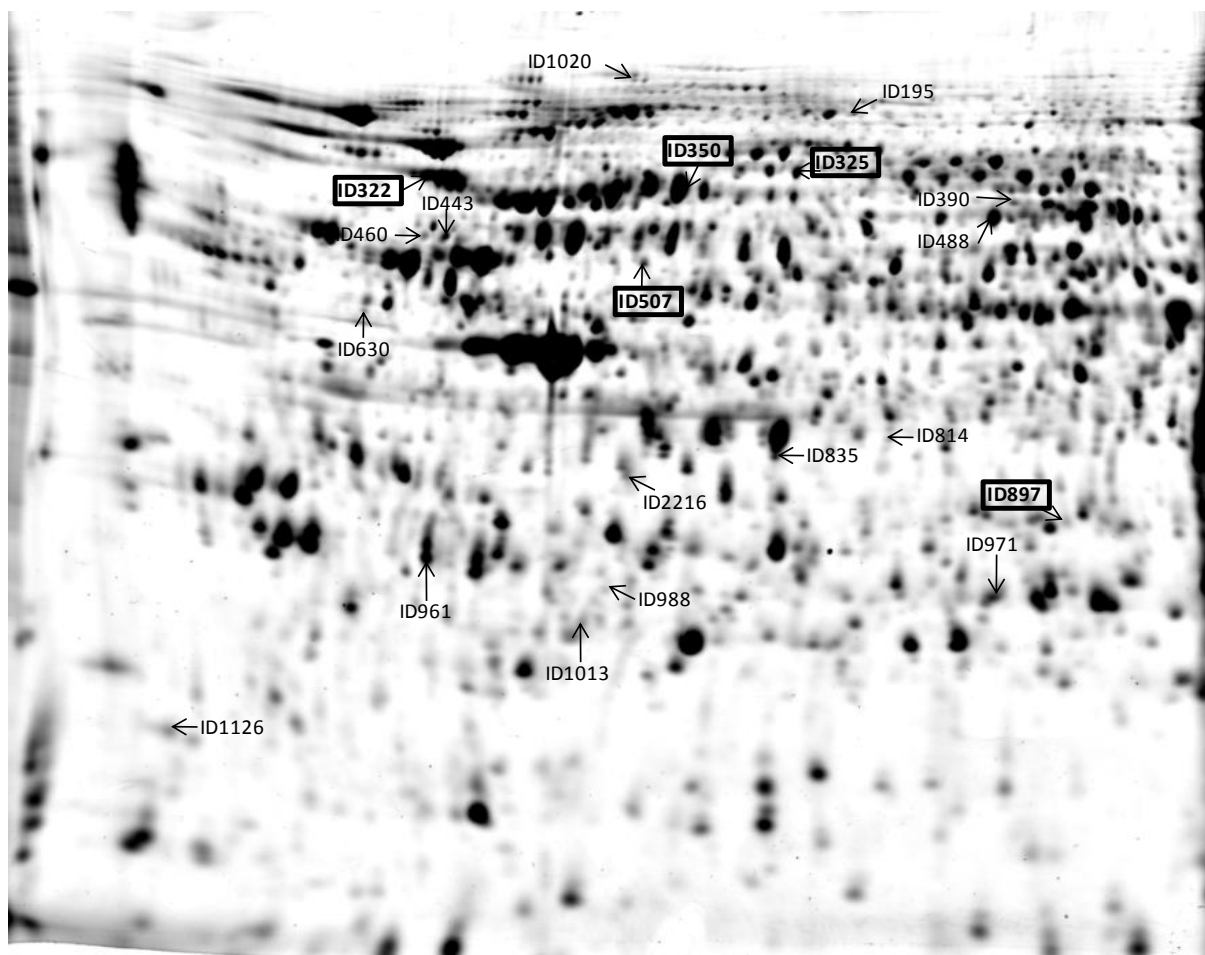
Fig. 28: Representative 2D image of a total lymphoblast protein extract. Crude protein extracts were prepared as indicated in the materials and methods section, separated by 2-DE after labeling with fluorescent dyes and visualized with the aid of a Typhoon imager. In total 1295 spots were reproducibly detected in the fused image of all patients and controls and thus used for the identification of changes in the lymphoblast protein pattern associated with mutations inUBR1. The 20 spots which were used to distinguish controls, patients with mild UBR1 expression and patients with no UBR1 expression were labeled with their ID numbers. The 5 spots which were used to distinguish controls and patients with mild UBR1 expression were also in the above list and they are marked in bold with rectangles.

Hierarchical clustering for 5 proteins, namely Interferon-induced GTP binding protein (ID325), HLA class II histocompatibility antigen (ID897), Annexin A6 (ID350), FK506-binding protein 4 (ID507) and GRP78 (ID322) discriminated mild JBS patients from controls with a predictive strength of 1 (Fig. 29). The protein panel was derived by using a class

prediction optimization from a protein signature displaying differential expression levels between controls and patients with mild UBR1 expression (ANOVA, p<0.01). Tree clustering was again done using Pearson correlation and condition tree clustering was performed using Spearman correlation for similarity measurement.
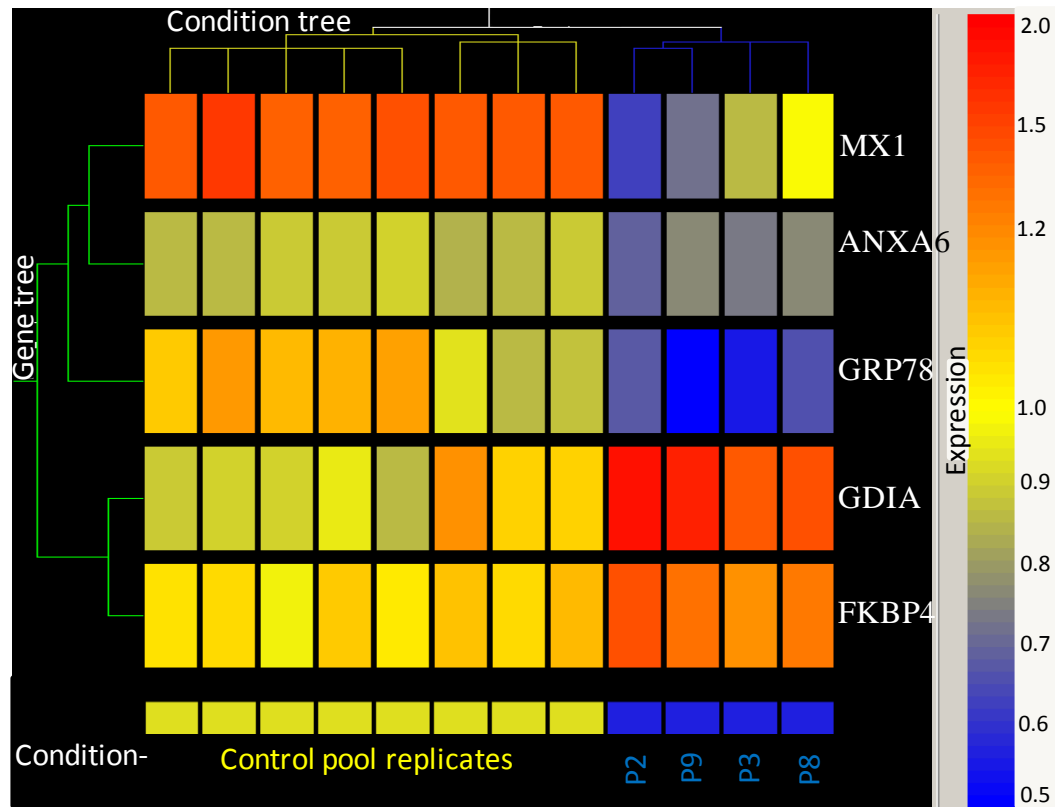
Fig. 29: Discrimination of controls and those patients displaying residual UBR1 activity with the aid of a 5 spot protein panel. The protein panel was derived by class prediction optimization from a protein signature displaying differential expression levels between controls and patients with mild UBR1 expression (ANOVA, p < 0.01). Tree clustering was done using Pearson correlation and condition tree clustering was done using Spearman correlation for similarity measurement.

ROC analysis of the 5 spots showed a predictive strength of 1 with a 95% CI of 0.0066 (Fig. 30). Therefore, the proteins identified might be suitable surrogate markers to determine UBR1 activity in an easily accessible full blood sample of patients with exocrine insufficiency of unknown cause and/or suspected JBS. However, this assumption warrants further testing in a prospective case series determining sensitivity, specificity, PPV and NPV.
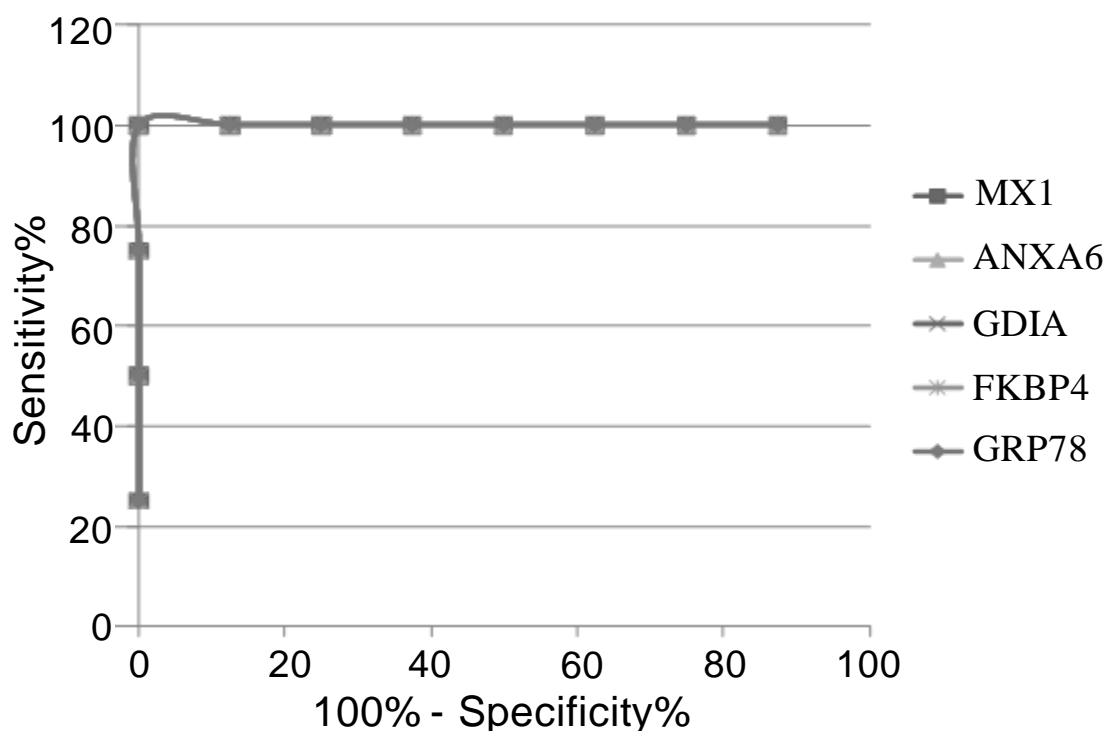
Fig. 30: ROC curves showing the predictive strengths of 5 spots to distinguish controls and patients with UBR1 expression. The receiver operator characteristic (ROC) curve is displayed for Cy2 normalized spot volumes of the top 5 predictive spots determined by Golubs' method to predict control and patients with UBR1 expression groups. The area under ROC curve for all curves was 1 (95% CI=0.0066) for all spots.

5.2.2. Characterization of mechanisms of pancreatic insufficiency in a murine model

5.2.2.1. Comparative analysis of protein patterns of the pancreas of wild type and UBR1 KO mice without or with pancreatitis

To study the pancreatitis induced changes in the protein pattern of the pancrease in UBR1 knockout and UBR1 wild type mice, animals were taken and divided into two groups as shown in the experimental flow diagram (Fig. 31). Each group consisted of 3 UBR1 wild type and 3 UBR1 knockout mice. Pancreatitis was induced by injecting caerulein (50mg/kg). Saline injection served as control. For each wild type and UBR1 knockout animal crude protein extracts were separated by 2-DE after labeling either with the Cy3-dye or Cy5-dye resulting in two technical replicate values for each animal which also allowed the correction of dye-specific effects because all samples were separated after labeling with both dyes employed in the study. Additionally, a mixture of aliquots of all samples was labeled with Cy2 which was used as an internal standard. A total of 1170 spots were quantified by 2D-

DIGE experiment with the aid of the Delta 2D image analysis software. Spots with a minimum fold change of 1.5 in level and a p-value less than 0.05 between two conditions were considered as present at significantly different levels.
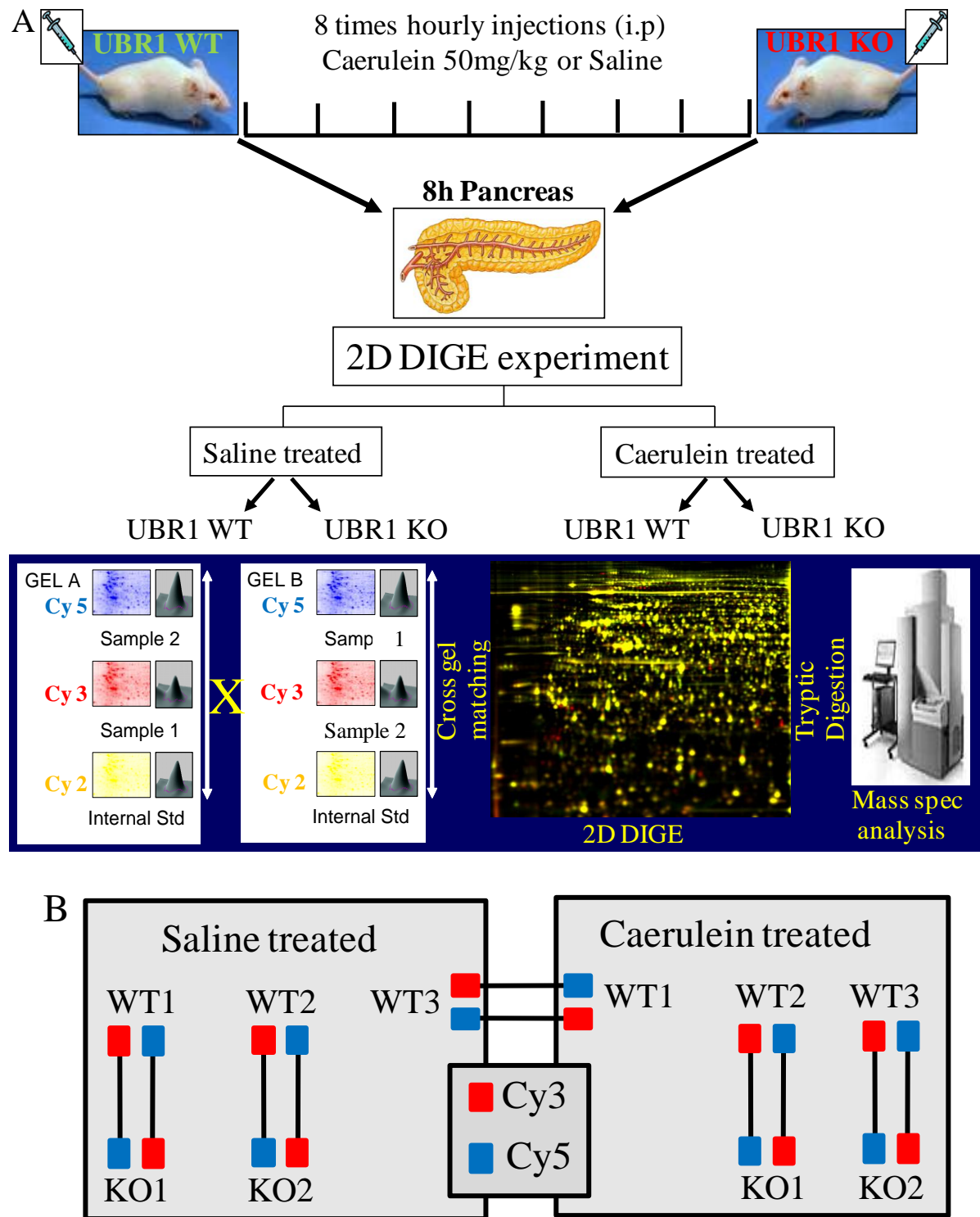
Fig. 31: Experimental design. A) Experimental workflow of 2D-DIGE of pancreatitis induced pancreas of UBR1 WT and UBR1 KO mice, including induction of pancreatitis in both mice types with caerulein, CyDye

labelling strategy, analysis and identification of differentially expressed proteins by MALDI ToF-ToF mass spectrometric analysis. B) 2D-DIGE CyDye labelling scheme of the experiment.

In caerulein treated mice 73 proteins were present at lower levels whereas 95 proteins were present at higher levels in UBR1 wild type compared to knockout mice. These proteins were labeled with numbers prefixing "C" indicating caerulein treatment condition and "Ind" for the spots which intensities were increased and "Rep" for the spots which intensities were decreased (Fig. 32).

Proteins displaying different levels in caerulein treated UBR1 WT vs. KO mice were excised from separately run preparative gels and identified by MALDI ToF-ToF mass spectrometry as described in the methods section. The list of the identified proteins is presented in Table 7.
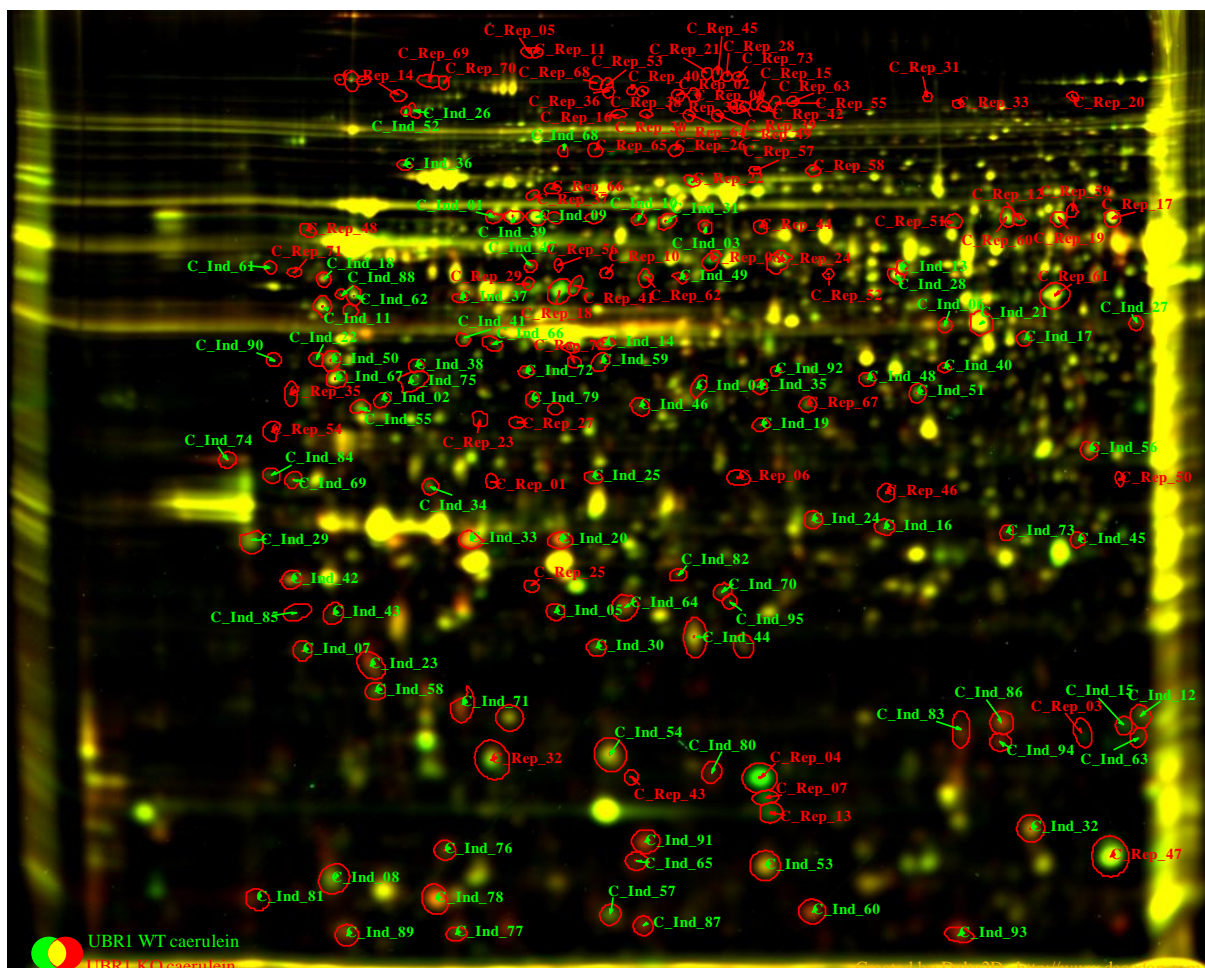
Fig. 32: Representative overlay display of 2D-DIGE images showing differentially expressed proteins in caerulein induced pancreas of UBR1 wild type mice compared to caerulein induced pancreas of UBR1 knockout mice. Color coded overlay of 2D-DIGE images of the caerulein treated pancreas of UBR1 wild type mice and the caerulein treated pancreas of UBR1 knockout mice. Yellow spots indicate no change in intensity

between the WT and UBR1 knockout mice where as red spots indicate higher levels and green spots lower levels in caerulein induced pancreas of UBR1 knockout mice. Changes in spots displaying differing intensity were considered significant when the following criteria were fulfilled: minimum fold change in intensity of 1.5 and p value below 0.05. Such spots were labeled with numbers prefixing "C" indicating caerulein treatment condition and "Ind" for induced and "Rep" for repressed spot intensities.

Table 7: Identification of differentially expressed proteins between UBR1 knockout and wild type mice treated with caerulein

Lable[a]	Identification	Protein ID[b]	N-Term. sequence[g]	Fold change	p-value	MW[c]	pI[d]	Protein score[e]	Peptide count[f]
C_Ind_01	78 kDa glucose-regulated protein precursor	P20029	**EEEDKKED**	1.5	0.05	72.4	5.07	643	31
C_Ind_02	Protein disulfide-isomerase precursor	P09103	**DALEEEDN**	1.5	0.05	57.1	4.79	191	23
C_Ind_03	78 kDa glucose-regulated protein precursor	P20029	**EEEDKKED**	1.5	0.03	72.4	5.07	469	25
C_Ind_04	Tubulin beta-5 chain	P99024	**REIVHIQAG**	1.6	0.04	49.6	4.78	70.4	14
C_Ind_05	Adenylate kinase isoenzyme 1	Q9R0Y5	**EEKLKKAK**	1.6	0.02	21.5	5.67	289	16
C_Ind_06	Elongation factor 2	P58252	VNFTVDQIR	1.6	0.01	95.3	6.41	223	14
C_Ind_07	78 kDa glucose-regulated protein precursor	P20029	**EEEDKKED**	1.6	0.03	72.4	5.07	123	8
C_Ind_08	Chymotrypsinogen B precursor	Q9CR35	**CGVPAIQPV**	1.6	0.00	27.8	4.91	105	1
C_Ind_09	78 kDa glucose-regulated protein precursor	P20029	**EEEDKKED**	1.6	0.00	72.4	5.07	707	31
C_Ind_10	Serum albumin precursor	P07724	**RGVFRREA**	1.6	0.03	68.6	5.75	168	19
C_Ind_11	Protein disulfide-isomerase precursor	P09103	**DALEEEDN**	1.6	0.04	57.1	4.79	226	21
C_Ind_12	Pancreatic alpha-amylase precursor	P00688	**QYDPH TSD**	1.6	0.04	57.4	7.18	196	5
C_Ind_13	Serum albumin precursor	P07724	**RGVFRREA**	1.6	0.02	68.6	5.75	492	31
C_Ind_14	Keratin, type I cytoskeletal 19	P19001	TSYSYRQTS	1.6	0.01	44.5	5.28	66	10
C_Ind_15	Pancreatic alpha-amylase precursor	P00688	**QYDPH TSD**	1.6	0.00	57.4	7.18	200	11
C_Ind_16	Keratin, type II cytoskeletal 8	P11679	SIRVTQKSY	1.6	0.02	54.5	5.7	136	17
C_Ind_17	Protein disulfide-isomerase A6 precursor	Q922R8	**LYSSSDDVI**	1.6	0.00	48.1	5	305	20
C_Ind_18	Protein disulfide-isomerase precursor	P09103	**DALEEEDN**	1.6	0.02	57.1	4.79	229	23
C_Ind_19	Not identified			1.6	0.03				

Lable[a]	Identification	Protein ID[b]	N-Term. sequence[g]	Fold change	p-value	MW[c]	pI[d]	Protein score[e]	Peptide count[f]
C_Ind_20	Chymotrypsinogen B precursor	Q9CR35	**CGVPAIQP**	1.6	0.03	27.8	4.91	227	5
C_Ind_21	Adenosylhomocysteinase	P50247	SDKLPYKV	1.6	0.01	47.7	6.08	334	23
C_Ind_22	Protein disulfide-isomerase precursor	P09103	**DALEEEDN**	1.6	0.00	57.1	4.79	76.2	9
C_Ind_23	Eukaryotic translation initiation factor 5A-1	P63242	ADDLDFET	1.6	0.02	16.8	5.08	189	11
C_Ind_24	Pancreatic alpha-amylase precursor	P00688	**QYDPH TSD**	1.6	0.01	57.4	7.18	251	9
C_Ind_25	Actin, cytoplasmic 1	P60710	**DDDIAALV**	1.7	0.03	41.7	5.29	333	15
	Leukocyte elastase inhibitor A	Q9D154	**EQLSSANT**	1.7	0.03	42.5	5.85	95.8	13
C_Ind_26	Hypoxia up-regulated protein 1 precursor	Q9JKR6	**LAVMSVDL**	1.7	0.04	111.1	5.12	204	30
C_Ind_27	Elongation factor 2	P58252	VNFTVDQI	1.7	0.04	95.3	6.41	223	17
C_Ind_28	Serum albumin precursor	P07724	**RGVFRRE**	1.7	0.05	68.6	5.75	535	27
C_Ind_29	Not identified			1.7	0.00				
C_Ind_30	Not identified			1.7	0.03				
C_Ind_31	Serum albumin precursor	P07724	**RGVFRREA**	1.7	0.01	68.6	5.75	607	36
C_Ind_32	Pancreatic alpha-amylase precursor	P00688	**QYDPH TSD**	1.7	0.02	57.4	7.18	102	
C_Ind_33	Chymotrypsinogen B precursor	Q9CR35	**CGVPAIQPV**	1.7	0.00	27.8	4.91	225	5
C_Ind_34	Toll-interacting protein	Q9QZ06	ATTVSTQRG	1.7	0.03	30.3	5.04	114	7
C_Ind_35	Elongation factor 2	P58252	VNFTVDQIR	1.7	0.05	95.3	6.41	223	20
C_Ind_36	Endoplasmin precursor	P08113	**DDEVDVDG**	1.7	0.02	92.4	4.74	268	29
C_Ind_37	26S protease regulatory subunit 6B	P54775	**EEIGILVEK**	1.7	0.00	47.3	5.18	150	17
C_Ind_38	Not identified			1.7	0.05				
C_Ind_39	Not identified			1.7	0.03				
C_Ind_40	GDP-L-fucose synthetase	P23591	GEPHGSMR	1.7	0.05	35.9	6.26	158	12
C_Ind_41	78 kDa glucose-regulated protein precursor	P20029	**EEEDKKED**	1.7	0.03	72.4	5.07	375	20

Lable[a]	Identification	Protein ID[b]	N-Term. sequence[g]	Fold change	p-value	MW[c]	pI[d]	Protein score[e]	Peptide count[f]
C_Ind_42	Translationally-controlled tumor protein	P63028	**IIYRDLISH**	1.7	0.03	19.5		295	
C_Ind_43	Not identified			1.7	0.04				
C_Ind_44	78 kDa glucose-regulated protein precursor	P20029	**EEEDKKED**	1.8	0.01	72.4	5.07	517	19
C_Ind_45	Pancreatic alpha-amylase precursor	P00688	**QYDPH TSD**	1.8	0.03	57.4	7.18	96	1
C_Ind_46	Not identified			1.8	0.03				
C_Ind_47	Heat shock cognate 71 kDa protein	P63017	SKGPAVGID	1.8	0.00	70.8	5.37	396	14
C_Ind_48	Elongation factor 2	P58252	VNFTVDQIR	1.8	0.01	95.3	6.41	317	21
C_Ind_49	Not identified			1.8	0.05				
C_Ind_50	Protein disulfide-isomerase precursor	P09103	**DALEEEDN**	1.8	0.00	57.1	4.79	205	19
C_Ind_51	Pancreatic lipase-related protein 1 precursor	Q5BKQ4	**KEVCYDNL**	1.8	0.00	52.7	5.92	142	15
C_Ind_52	Hypoxia up-regulated protein 1 precursor	Q9JKR6	**LAVMSVDL**	1.8	0.04	111.1	5.12	153	26
C_Ind_53	40S ribosomal protein S12	P63323	AEEGIAAGG	1.8	0.05	14.5	6.82	102	7
C_Ind_54	Endoplasmic reticulum resident protein ERp27 precursor	Q9D8U3	**DVEEATDG**	1.8	0.05	30.7	4.89	206	12
C_Ind_55	Protein disulfide-isomerase precursor	P09103	**DALEEEDN**	1.8	0.02	57.1	4.79	203	23
C_Ind_56	Pancreatic alpha-amylase precursor	P00688	**QYDPH TSD**	1.9	0.00	57.4	7.18	246	13
C_Ind_57	Endoplasmic reticulum resident protein ERp27 precursor	Q9D8U3	**DVEEATDG**	1.9	0.00	30.7	4.89	172	9
C_Ind_58	Protein disulfide-isomerase precursor	P09103	**DALEEEDN**	1.9	0.05	57.1	4.79	96.7	9
C_Ind_59	Not identified			1.9	0.01				
C_Ind_60	Anionic trypsin-2 precursor	P07146	**FPVDDDDK**	1.9	0.00	26.2	4.4	171	6
C_Ind_61	Endoplasmin precursor	P08113	**DDEVDVDG**	1.9	0.00	92.4	4.74	121	16
C_Ind_62	Protein disulfide-isomerase precursor	P09103	**DALEEEDN**	2.0	0.05	57.1	4.79	184	21

Lable[a]	Identification	Protein ID[b]	N-Term. sequence[g]	Fold change	p-value	MW[c]	pI[d]	Protein score[e]	Peptide count[f]
C_Ind_63	Pancreatic alpha-amylase precursor	P00688	**QYDPH TSD**	2.0	0.00	57.4	7.18	179	7
C_Ind_64	Pancreatic alpha-amylase precursor	P00688	**QYDPH TSD**	2.0	0.02	57.4	7.18	152	9
C_Ind_65	Not identified			2.1	0.05				
C_Ind_66	78 kDa glucose-regulated protein precursor	P20029	**EEEDKKED**	2.1	0.00	72.4	5.07	313	19
C_Ind_67	Protein disulfide-isomerase precursor	P09103	**DALEEEDN**	2.1	0.03	57.1	4.79	203	21
C_Ind_68	Not identified			2.1	0.00				
C_Ind_69	78 kDa glucose-regulated protein precursor	P20029	**EEEDKKED**	2.1	0.00	72.4	5.07	191	17
C_Ind_70	Proteasome subunit beta type-4 precursor	P99026	**TQNPMVTG**	2.1	0.02	29.1	5.47	244	9
C_Ind_71	Eukaryotic translation initiation factor 5A-1	P63242	**ADDLDFETG**	2.2	0.00	16.8	5.08	86.5	8
C_Ind_72	Protein disulfide-isomerase precursor	P09103	**DALEEEDN**	2.2	0.04	57.1	4.79	95.8	15
C_Ind_73	Serum albumin precursor	P07724	**RGVFRREA**	2.2	0.05	68.6	5.75	97.7	18
C_Ind_74	Anionic trypsin-2 precursor	P07146	**FPVDDDDK**	2.3	0.00	26.2	4.4	105	4
C_Ind_75	Protein disulfide-isomerase precursor	P09103	**DALEEEDN**	2.3	0.02	57.1	4.79	244	23
C_Ind_76	Chymotrypsinogen B precursor	Q9CR35	**CGVPAIQP**	2.3	0.05	27.8	4.91	158	5
C_Ind_77	Chymotrypsinogen B precursor	Q9CR35	**CGVPAIQP**	2.4	0.01	27.8	4.91	199	3
C_Ind_78	Chymotrypsinogen B precursor	Q9CR35	**CGVPAIQP**	2.4	0.00	27.8	4.91	95.6	5
C_Ind_79	Serpin I2 precursor	Q9JK88	**SRATDQKI**	2.5	0.03	45.7	5.83	95.6	12
C_Ind_80	Not identified			2.5	0.02				
C_Ind_81	Not identified			2.6	0.02				
C_Ind_82	Not identified			2.6	0.04				
C_Ind_83	Not identified			2.6	0.00				

Lable[a]	Identification	Protein ID[b]	N-Term. sequence[g]	Fold change	p-value	MW[c]	pI[d]	Protein score[e]	Peptide count[f]
C_Ind_84	78 kDa glucose-regulated protein precursor	P20029	**EEEDKKED**	2.6	0.00	72.4	5.07	296	19
C_Ind_85	Not identified			2.8	0.03				
C_Ind_86	Pancreatic alpha-amylase precursor	P00688	**QYDPHTSD**	2.9	0.00	57.4		117	
C_Ind_87	Anionic trypsin-2 precursor	P07146	**FPVDDDDK**	3.0	0.00	26.2		178	
C_Ind_88	Protein disulfide-isomerase precursor	P09103	**DALEEEDN**	3.3	0.05	57.1	4.79	188	18
C_Ind_89	Chymotrypsinogen B precursor	Q9CR35	**CGVPAIQPV**	3.3	0.00	27.8		181	
C_Ind_90	Bile salt-activated lipase precursor	Q64285	AKLGAVYT	3.6	0.00	65.8		244	
C_Ind_91	40S ribosomal protein S12	P63323	AEEGIAAG	3.8	0.00	14.5		159	
C_Ind_92	Serum albumin precursor	P07724	**RGVFRREA**	4.2	0.04	68.6	5.75	294	21
C_Ind_93	Not identified			4.5	0.04				
C_Ind_94	Not identified			4.5	0.00				
C_Ind_95	Actin, cytoplasmic 1	P60710	**DDDIAALV**	4.8	0.02	41.7	5.29	308	15
C_Rep_01	Not identified			10.8	0.05				
C_Rep_02	Not identified			4.7	0.05				
C_Rep_03	Not identified			3.9	0.02				
C_Rep_04	Lithostathine 2 precursor	Q08731		3.8	0.07	19.4	5.89	169	7
C_Rep_05	Not identified			3.6	0.07				
C_Rep_06	Protein CDV3	Q4VAA2		3.5	0.04	29.7	5.84	124	6
C_Rep_07	Not identified			3.3	0.06				
C_Rep_08	Keratin, type II cytoskeletal 8	P11679		3.0	0.04	54.5	5.7	230	27
C_Rep_09	Not identified			2.8	0.03				
C_Rep_10	Not identified			2.7	0.02				
C_Rep_11	Not identified			2.4	0.05				
C_Rep_12	Cystathionine beta-synthase	Q91WT9		2.4	0.02	61.5	6.07	246	17

Lable[a]	Identification	Protein ID[b]	N-Term. sequence[g]	Fold change	p-value	MW[c]	pI[d]	Protein score[e]	Peptide count[f]
C_Rep_13	Glutathione S-transferase P 1	P19157		2.2	0.05	23.6	7.68	112	7
C_Rep_14	Golgin subfamily A member 2	Q921M4		2.2	0.04	101.3	4.83	180	24
C_Rep_15	Not identified			2.2	0.05				
C_Rep_16	Not identified			2.2	0.04				
C_Rep_17	Cystathionine beta-synthase	Q91WT9		2.2	0.00	61.5	6.07	588	29
C_Rep_18	Keratin, type I cytoskeletal 18	P05784		2.0	0.02	47.5	5.22	250	12
C_Rep_19	Cystathionine beta-synthase	Q91WT9		2.0	0.01	61.5	6.07	320	21
C_Rep_20	Vigilin	Q8VDJ3		2.0	0.02	141.7	6.43	80.3	23
C_Rep_21	Not identified			2.0	0.02				
C_Rep_22	Stress-70 protein, mitochondrial precursor	P38647		2.0	0.06	73.5	5.91	242	18
C_Rep_23	Not identified			2.0	0.03				
C_Rep_24	Keratin, type II cytoskeletal 8	P11679		1.9	0.03	54.5	5.7	255	23
C_Rep_25	Not identified			1.9	0.06				
C_Rep_26	Heat shock protein HSP 90-alpha	P07901		1.9	0.02	84.7	4.93	87.3	18
C_Rep_27	Splicing factor, arginine/serine-rich 1	Q6PDM2		1.9	0.01	27.7	10.4	169	12
C_Rep_28	Not identified			1.9	0.02				
C_Rep_29	Not identified			1.9	0.02				
C_Rep_30	Not identified			1.9	0.03				
C_Rep_31	Not identified			1.8	0.06				
C_Rep_32	Eukaryotic translation initiation factor 5A-1	P63242		1.8	0.04	16.8	5.08	157	10
C_Rep_33	Leucine-rich PPR motif-containing protein, mitochondrial precursor	Q6PB66		1.8	0.10	156.5	6.42	143	32
C_Rep_34	Not identified			1.8	0.05	0.0			

Lable[a]	Identification	Protein ID[b]	N-Term. sequence[g]	Fold change	p-value	MW[c]	pI[d]	Protein score[e]	Peptide count[f]
C_Rep_35	Eukaryotic translation initiation factor 3 subunit 1	Q66JS6		1.8	0.01	29.5	4.69	71.7	1
C_Rep_36	Not identified			1.8	0.02	0.0			
C_Rep_37	Lamin-B1	P14733		1.8	0.04	66.7	5.11	70.8	7
C_Rep_38	Not identified			1.8	0.04				
C_Rep_39	Not identified			1.8	0.04				
C_Rep_40	Not identified			1.7	0.03				
C_Rep_41	cAMP-dependent protein kinase type I-alpha regulatory subunit	Q9DBC7		1.7	0.03	43.2	5.27	314	18
C_Rep_42	Not identified			1.7	0.02				
C_Rep_43	Not identified			1.7	0.04				
C_Rep_44	T-complex protein 1 subunit epsilon	P80316		1.7	0.02	59.6	5.72	103	18
C_Rep_45	Not identified			1.7	0.01				
C_Rep_46	Not identified			1.7	0.08				
C_Rep_47	40S ribosomal protein S12	P63323		1.6	0.01	14.5	6.82	217	5
C_Rep_48	Not identified			1.6	0.05				
C_Rep_49	Not identified			1.6	0.02				
C_Rep_50	Not identified			1.6	0.02				
C_Rep_51	Seryl-tRNA synthetase, cytoplasmic	P26638		1.6	0.02	58.4	5.95	90.2	17
C_Rep_52	Phenylalanine-4-hydroxylase	P16331		1.6	0.04	51.9	6.01	174	16
C_Rep_53	Not identified			1.6	0.02				
C_Rep_54	Not identified			1.6	0.01				
C_Rep_55	Not identified			1.6	0.03				
C_Rep_56	Not identified			1.6	0.01				
C_Rep_57	Not identified			1.6	0.02				

Lable[a]	Identification	Protein ID[b]	N-Term. sequence[g]	Fold change	p-value	MW[c]	pI[d]	Protein score[e]	Peptide count[f]
C_Rep_58	Not identified			1.6	0.02				
C_Rep_59	Asparagine synthetase [glutamine-hydrolyzing]	Q61024		1.6	0.03	64.2	6.12	202	14
C_Rep_60	Asparagine synthetase [glutamine-hydrolyzing]	Q61024		1.6	0.01	64.2	6.12	210	11
C_Rep_61	Elongation factor 1-gamma	Q9D8N0		1.6	0.02	50.0	6.31	238	15
C_Rep_62	Fibrinogen gamma chain precursor	Q8VCM7		1.6	0.05	49.4	5.54	212	8
C_Rep_63	Not identified			1.6	0.03				
C_Rep_64	Not identified			1.5	0.03				
C_Rep_65	Not identified			1.5	0.02				
C_Rep_66	Heat shock cognate 71 kDa protein	P63017		1.5	0.03	70.8	5.37	184	18
C_Rep_67	Serine/threonine-protein phosphatase PP1-beta catalytic subunit	P62141		1.5	0.04	37.2	5.84	428	22
C_Rep_68	Not identified			1.5	0.02				
C_Rep_69	Collagen alpha-1(VI) chain precursor	Q04857		1.5	0.02	108.4	5.2	243	29
C_Rep_70	Collagen alpha-1(VI) chain precursor	Q04857		1.5	0.01	108.4	5.2	254	30
C_Rep_71	26S proteasome non-ATPase regulatory subunit 4	O35226		1.5	0.01	40.7	4.67	224	14
C_Rep_72	Endonuclease VIII-like 1	Q8K4Q6		1.5	0.01	43.6	9.86	78.4	13
C_Rep_73	Not identified			1.5	0.01				

[a]Label: Spot identification number; [b]Protein ID: Swissprot entry name;
[c]MW: Molecular weight calculated from amino acid sequence (in kDa);
[d]pI: isoelectric point calculated from amino acid sequence; [e]Peptide count: number of matched peptides

[f]Protein score: significance of protein identification
[g] N-Term.sequence: Theroretical N-terminal sequence after removing signal peptides (given only for spots with increased intensities; **Bold sequences**- follow N-end rule)

To assess to which degree differences also occurred prior to induction of pancreatitis by treatment with caerulin, we also included two controls groups of wild type and UBR1 knockout animals that were solely treated with saline in parallel to the two groups treated with caerulein. After saline treatment 33 protein spots were present at higher intensities and 22 protein spots were found to be reduced in intensities in this saline treated animals when UBR1 wild type mice were compared to UBR1 knockout mice. These proteins were labeled with numbers prefixing "N" indicating NaCl (Saline) treatment condition and "Ind" for induced and "Rep" for repressed spots intensities in UBR1 knockout condition (Fig. 33).

These differentially expressed proteins were excised from preparative gels and identified by MALDI ToF-ToF mass spectrometric as described in materials and methods section. The list of the identified proteins is presented in Table 8.
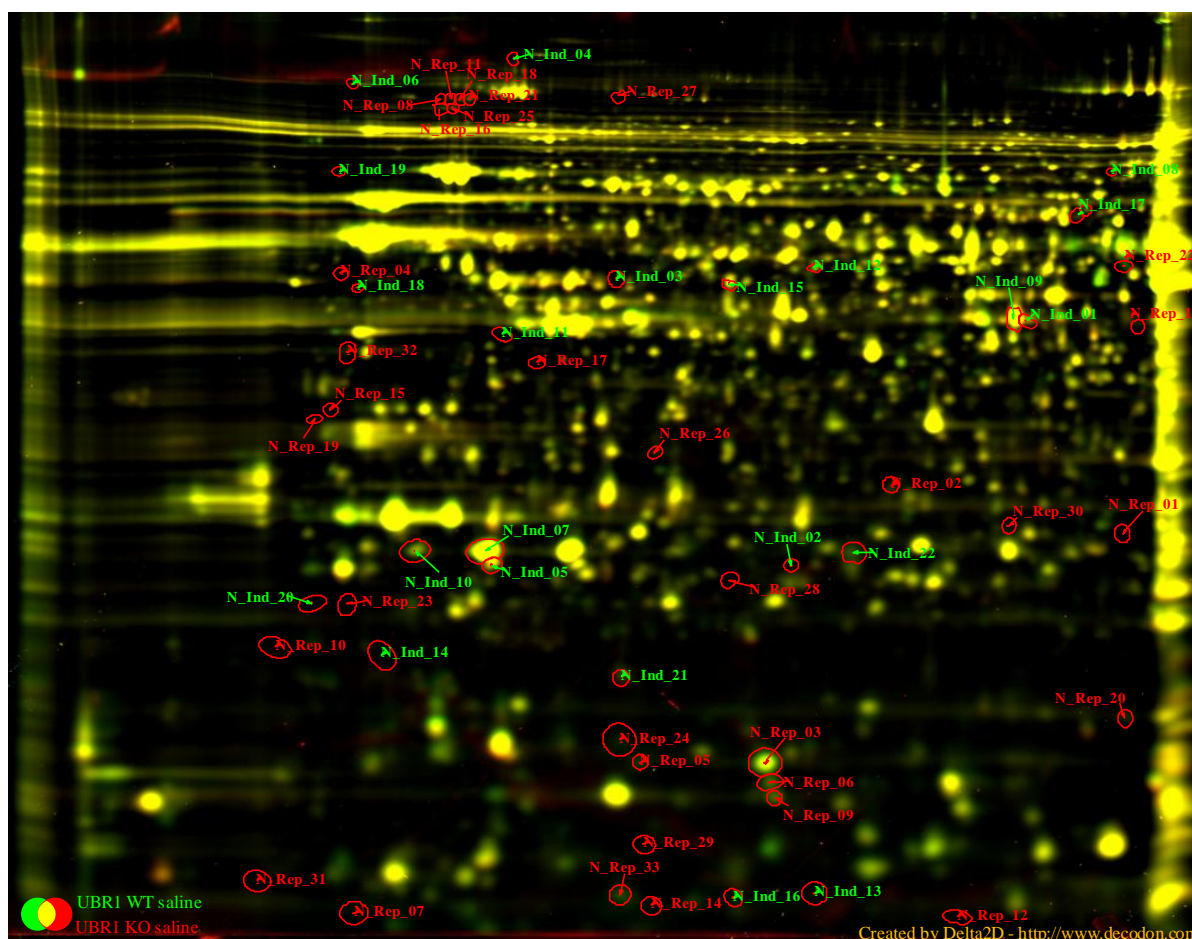
Fig. 33 Representative overlay of 2D-DIGE images showing differentially expressed proteins in saline treated pancreas of UBR1 knockout mice vs. UBR1 wildtype mice. Representative 2D-DIGE images of the saline treated pancreas of UBR1 wild type mice and of UBR1 knockout mice were false colored in green and red, respectively, and then overlaid. Yellow spots indicate no difference in intensity between the two conditions where as red spots are displaying higher and green spots lower intensity in saline induced pancreas of UBR1 knockout compared to wild type mice. Spots displaying differential intensties and fulfilling the criteria of

minimum fold change 1.5 and p-value below 0.05 were labeled with numbers prefixing "N" indicating NaCl (saline) treatment condition and "Ind" for induced and "Rep" for repressed spot intensities in the UBR1 knockout mice, respectively.

Table 8: Identification of differentially expressed proteins between UBR1 knockout and wild type mice treated with saline

Lable[a]	Identification	Protein ID.[b]	Fold change	p-value	MW[c]	pI[d]	Protein score[e]	Peptide count[f]
N_Ind_01	Adenosylhomocysteinase	P50247	1.5	0.03	47.7	6.08	235	2
N_Ind_02	Thioredoxin-dependent peroxide reductase, mitochondrial precursor	P20108	1.5	0.05	28.1	5.73	203	2
N_Ind_03	Heterogeneous nuclear ribonucleoprotein F	Q9Z2X1	1.5	0.04	45.7	5.31	473	5
N_Ind_04	Eukaryotic translation initiation factor 3 subunit A	P23116	1.6	0.05	161.9	6.39	136	2
N_Ind_05	Not identified		1.6	0.03				
N_Ind_06	Vigilin	Q8VDJ3	1.6	0.02	141.7	6.43	251	3
N_Ind_07	Not identified		1.6	0.03				
N_Ind_08	SAM domain and HD domain-containing protein 1	Q60710	1.6	0.02	72.6	8.17	225	3
N_Ind_09	Adenosylhomocysteinase	P50247	1.6	0.01	47.7	6.08	352	3
N_Ind_10	Anionic trypsin-2 precursor	P07146	1.7	0.03	26.2	4.57	84	2
N_Ind_11	40S ribosomal protein SA	P14206	1.7	0.00	32.8	4.8	149	2
N_Ind_12	Phenylalanine-4-hydroxylase	P16331	1.7	0.03	51.9	6.02	408	3
N_Ind_13	Not identified		1.7	0.00				
N_Ind_14	Not identified		1.7	0.00				
N_Ind_15	S-adenosylmethionine synthetase isoform type-1	Q91X83	1.9	0.03	43.5	5.51	611	5
N_Ind_16	Not identified		2.0	0.02				
N_Ind_17	Asparagine synthetase [glutamine-hydrolyzing]	Q61024	2.1	0.02	64.2	6.12	544	5
N_Ind_18	Elongation factor 1-gamma	Q9D8N0	2.2	0.00	50.0	6.33	279	3
N_Ind_19	78 kDa glucose-regulated protein precursor	P20029	2.3	0.05	72.4	5.01	141	4
N_Ind_20	Not identified		2.4	0.05				
N_Ind_21	Not identified		2.8	0.05				
N_Ind_22	Peroxiredoxin-6	O08709	3.0	0.00	24.9	5.72	636	4

Lable[a]	Identification	Protein ID.[b]	Fold change	p-value	MW[c]	pI[d]	Protein score[e]	Peptide count[f]
N_Rep_01	Ribosyldihydronicotinamide dehydrogenase [quinone]	Q9JI75	4.6	0.05	26.2	6.6	312	3
N_Rep_02	XTP3-transactivated gene B protein homolog precursor	Q8VEH8	3.0	0.02	54.9	5.98	64	2
N_Rep_03	Lithostathine 2 precursor	Q08731	2.8	0.02	19.4	5.91	418	3
N_Rep_04	Protein disulfide-isomerase precursor	P09103	2.8	0.00	57.1	4.75	115	2
N_Rep_05	Lithostathine 2 precursor	Q08731	2.8	0.02	19.4	5.91	339	3
N_Rep_06	Lithostathine 2 precursor	Q08731	2.7	0.01	19.4	5.91	224	3
N_Rep_07	Not identified		2.6	0.00				
N_Rep_08	Valyl-tRNA synthetase	Q9Z1Q9	2.3	0.01	140.1	7.9	100	2
N_Rep_09	Lithostathine 1 precursor	P43137	2.3	0.01	18.5	5.65	141	2
N_Rep_10	Not identified		2.3	0.00				
N_Rep_11	Hypoxia up-regulated protein 1 precursor	Q9JKR6	2.3	0.02	111.1	5.06	200	2
N_Rep_12	Not identified		2.2	0.00				
N_Rep_13	Kynurenine--oxoglutarate transaminase 1	Q8BTY1	2.2	0.02	47.5	6.46	288	4
N_Rep_14	Not identified		2.2	0.00				
N_Rep_15	Protein disulfide-isomerase A6 precursor	Q922R8	2.2	0.02	48.1	4.95	327	4
N_Rep_16	Hypoxia up-regulated protein 1 precursor	Q9JKR6	2.1	0.02	111.1	5.06	172	2
N_Rep_17	Transcriptional activator protein Pur-beta	O35295	2.1	0.00	33.9	5.35	284	3
N_Rep_18	Hypoxia up-regulated protein 1 precursor	Q9JKR6	2.1	0.01	111.1	5.06	290	3
N_Rep_19	40S ribosomal protein SA	P14206	2.0	0.00	32.8	4.8	567	5
N_Rep_20			2.0	0.00				
N_Rep_21	Hypoxia up-regulated protein 1 precursor	Q9JKR6	1.8	0.02	111.1	5.06	403	3
N_Rep_22	Pancreatic alpha-amylase precursor	P00688	1.8	0.00	57.4	6.95	323	2
N_Rep_23	Not identified		1.7	0.02				
N_Rep_24	Not identified		1.7	0.02				

Lable[a]	Identification	Protein ID.[b]	Fold change	p-value	MW[c]	pI[d]	Protein score[e]	Peptide count[f]
N_Rep_25	ATP synthase subunit beta, mitochondrial precursor	P56480	1.6	0.03	56.3	4.99	604	4
N_Rep_26	Apolipoprotein E precursor	P08226	1.6	0.01	35.8	5.46	466	5
N_Rep_27	Valyl-tRNA synthetase	Q9Z1Q9	1.6	0.03	140.1	7.9	155	3
N_Rep_28	Actin, cytoplasmic 1	P60710	1.6	0.03	41.7	5.29	170	2
N_Rep_29	Not identified		1.6	0.00				
N_Rep_30	ETHE1 protein, mitochondrial precursor	Q9DCM0	1.6	0.00	27.7	6.21	160	2
N_Rep_31	Not identified		1.5	0.00				
N_Rep_32	Protein SET	Q9EQU5	1.5	0.02	33.4	4.22	188	3
N_Rep_33	Not identified		1.5	0.04				

[a]Label: Spot identification number; [b]Protein ID: SwissProt Entry name;
[c]MW: Molecular weight calculated from amino acid sequence (in kDa);
[d]pI: isoelectric point calculated from amino acid sequence;
[e]Peptide count: number of matched peptides;
[f]Protein score: significance of protein identification

Gene spring analysis was performed to analyze the protein patterns in each condition and comparing them to the other conditions. The graphical display of this analysis revealed that in caerulein treated mice many more differences were observed then after saline treatment and that the proteins which displayed different levels in UBR1 wild type vs. knockout mice only partially overlapped (Fig. 34A and B). The Pie diagram depicted in Fig. 34C shows that 141 proteins out of 168 being present at different levels in caerulein treated UBR1 knockout vs. wild type were only recognized after caerulein treatment and only 27 proteins being changed in intensity also in saline treated animals. Of the 55 proteins displaying UBR1 knockout associated changes in intensity 27 were (close to 50 %) also noted after caerulein treatment (Fig. 34C).
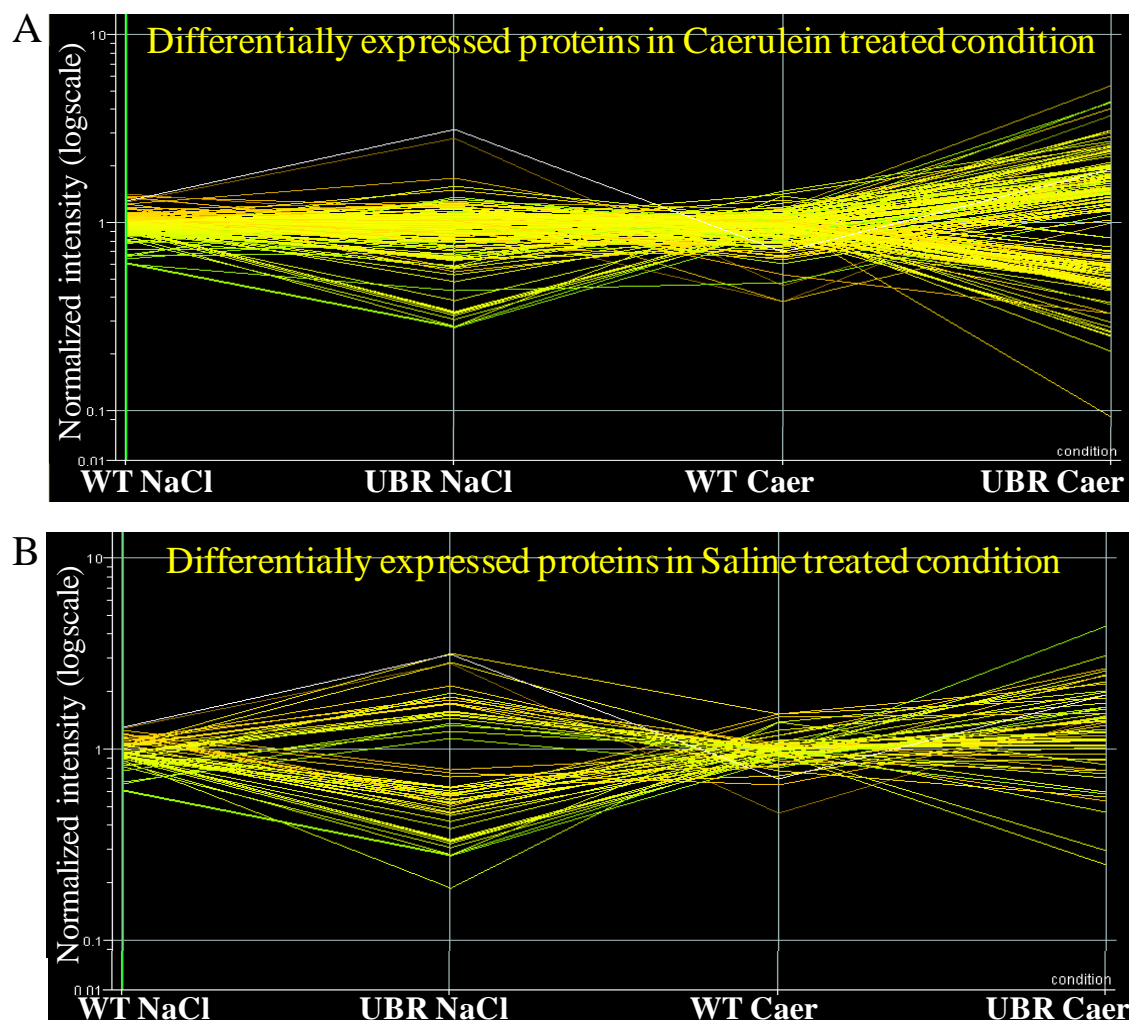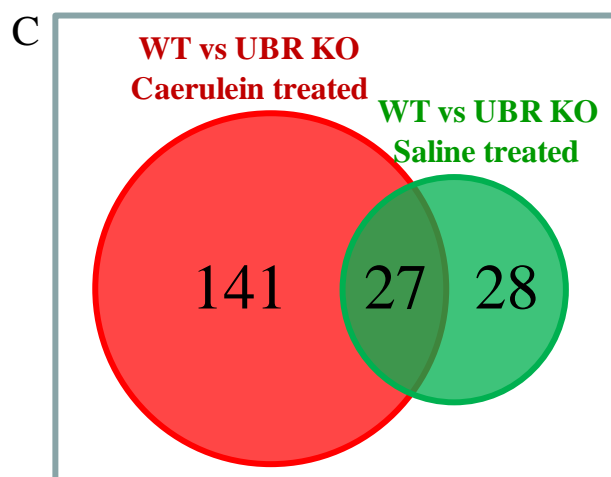
Fig. 34: Graphical presentation of the expression levels of differentially expressed proteins. A) after caerulein treatment and B) after treatment with saline. C) Pie diagram showing the number proteins which were differentially expressed in each condition and overlap with minimum 1.5 fold change and p value less than 0.05. The overlap between two conditions was 50 % of the saline affected proteins spots. The graph illustrates that the effects of knocking out UBR1 are much more pronounced after caerulein treatment than in saline treated controls.

5.2.2.2. Time-resolved analysis of the effects of caerulein induced pancreatitis

The murine knockout of UBR1 showed retarded growth, suffered from pancreatic exocrine insufficiency due to an impaired CCK receptor stimulus secretion coupling and displayed higher susceptibility for pancreatitis combined with a more severe systemic inflammatory response. We did observe upregulation of inflammation related proteins and some proteases in the 2D-DIGE experiment (Table 7) which could point to these proteases as specific substrates of UBR1. To understand the time dependency of the previously reported higher susceptibility to pancreatic damage in UBR1 knockout mice, we performed a time-resolved analysis of caerulein-induced pancreatitis comparing UBR1 knockout mice and wild type littermates. For the experiment samples were taken and analyzed immediately before (0 h) and 1 h, 4 h, 8 h, 24 h, 36 h and 48 h after treatment (Fig. 35).
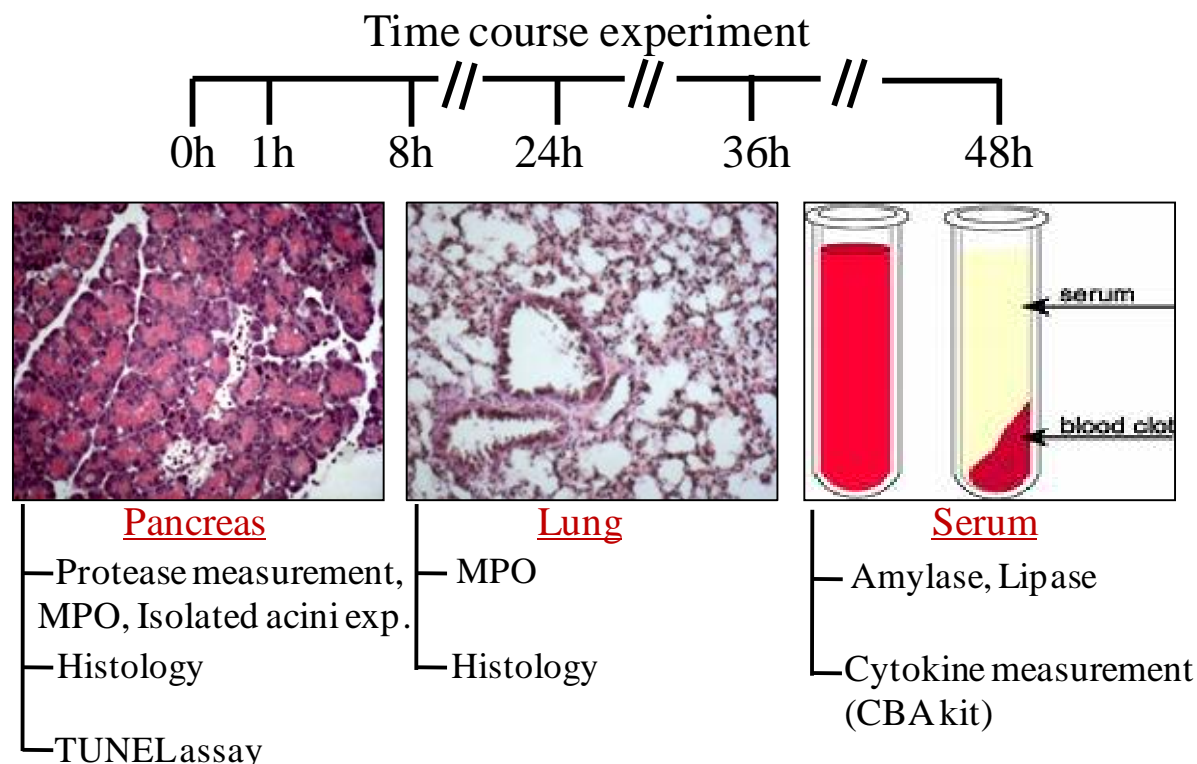
Fig. 35: Schematic presentation of the time course experiment showing the time points and types of tissues taken from mice for the experiment. Under each tissue name the list of the studies done is given. For every time point 5 UBR1 wild type and 5 UBR1 knockout mice were sacrificed and pancreas, lung and serum were collected. With pancreas homogenate protease and MPO activities were measured apart from histology and TUNEL assay. With lung homogenate MPO activity was measured apart from histology. Serum was prepared from the blood drawn from every mouse and amylase and lipase activities were measured. Cytokine production was measured using a CBA kit in serum.

For every time point 5 UBR1 wild type and 5 UBR1 knockout mice were sacrificed and pancreas, lung, blood were stored for further analysis. In the pancreatic homogenate protease and MPO activities were determined in addition to histology (HE staining) and TUNEL assay as described in the methods section. In lung homogenate MPO activity was measured apart from histology (HE staining). Serum was prepared and amylase and lipase activities were measured. Cytokine production in serum was detected using CBA kit as described in methods.

5.2.2.3. Measurement of protease activity

Protease activity measurements were done according to the protocols given in the method section. Elevated levels of amylase and lipase activities were observed in UBR1 knockout mice compare to UBR1 wild type mice and are shown in Fig. 36. Both amylase and lipase levels were significantly higher in UBR1 knockout mice compared to wild type mice at

8 h and 24 h time points indicating a more severe form of pancreatitis in UBR1 knockout mice.
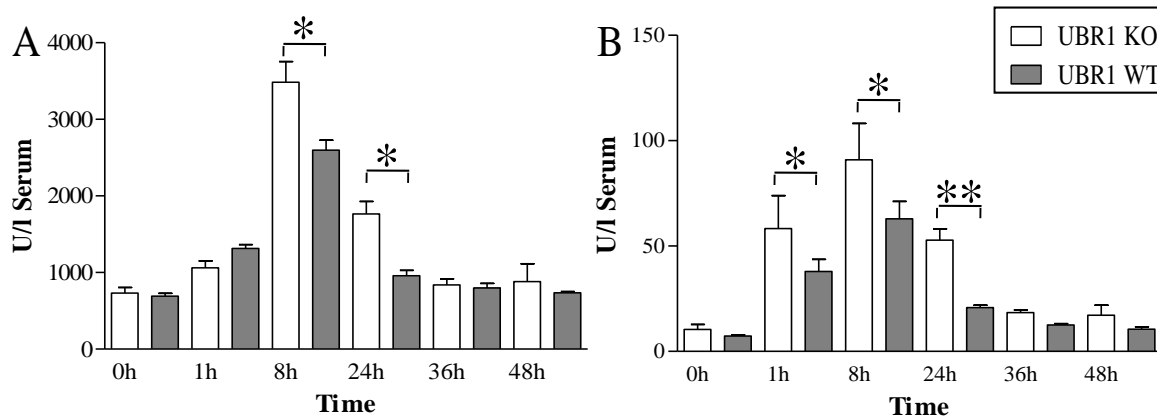
Fig. 36: Measurement of amylase (A) and lipase (B) activities at different time points in serum. Statistically significant differences were marked with an asterisk on top of the time point which passed the non-parametric Mann-Whitney t test with a p value of less than 0.05. One asterisk represents a p value of less than 0.05 and two asterisks represent p value of less than 0.01. Data for UBR1 knockout and wild type mice are displayed with white and grey bars, respectively.

Increased myeloperoxidase (MPO) activity in the pancreas homogenates was observed at 8 h and 24 h after treatment, whereas in lung homogenates at 8 h, 36 h and 48 h after treatment with caerulein higher MPO activities were observed in UBR1 knockout mice compared to wild type mice. (Fig. 37)
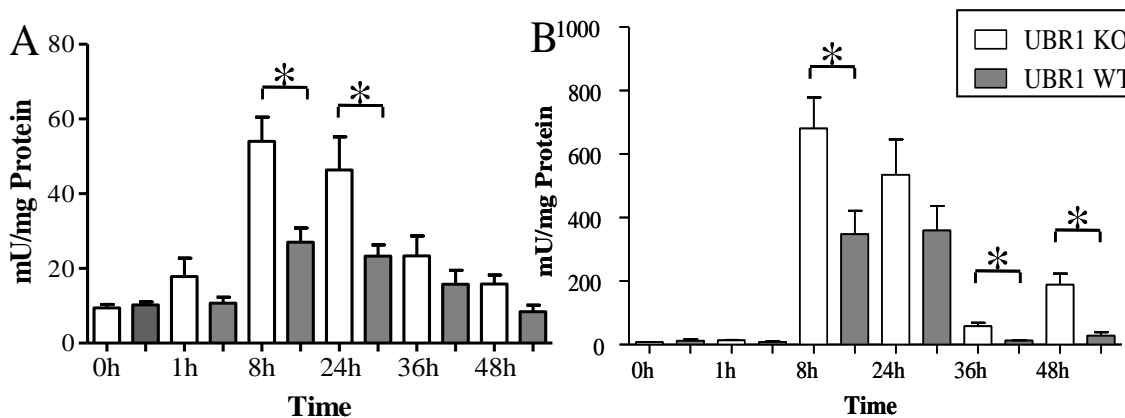
Fig. 37: Measurement of myeloperoxidase (MPO) activity at different time points in pancreatic (A) and lung homogenates (B). Statistically significant differences were marked with asterisk on top of the time point which passed the non-parametric Mann-Whitney t test with a p value of less than 0.05. Data for UBR1 knockout and wild type mice are displayed with white and grey bars, respectively.

Measurement of trypsin activity in pancreas homogenates revealed that higher trypsin activation occurred in UBR1 knockout mice compared to wild type mice at 8 h, 24 h, 36 h, and 48 h after caerulein treatment (Fig. 38). Enterokinase was used to convert all trypsinogen (inactive proform) to active trypsin to evaluate whether there are any differences at basal expression level changes of trypsinogen in UBR1 knockout mice compared to wild type mice. This particular control demonstrated that there were almost identical levels of trypsinogen present in UBR1 knockout and wild type mice after enterokinase treatment.
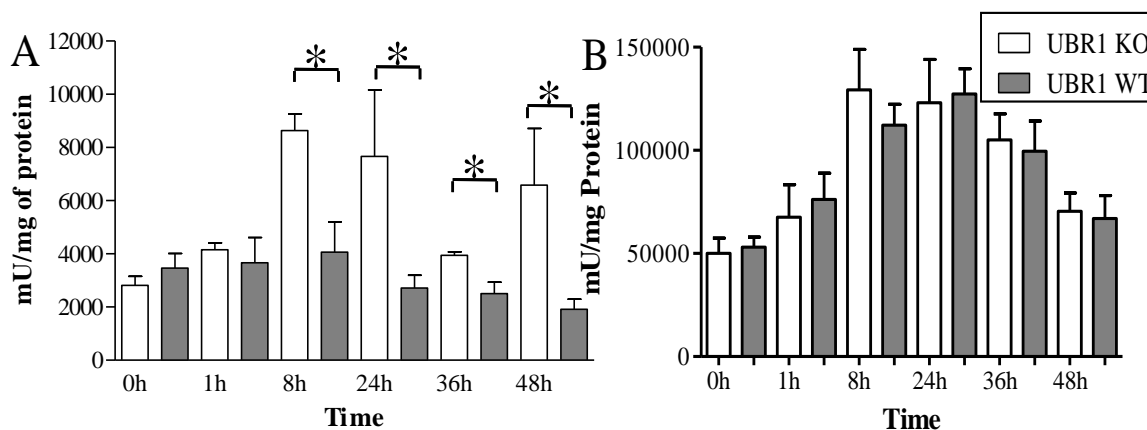
Fig. 38: Measurement of trypsin (A) and EK activated trypsin (B) activity in pancreatic homogenates at different time points after stimulation with caerulein. Statistically significant differences were marked with an asterisk on top of the time point which passed the non-parametric Mann-Whitney t test with a p value of less than 0.05 Data for UBR1 knockout and wild type mice are displayed with white and grey bars, respectively.

Measurement of *in vivo* active elastase activities as well as enterokinase activated elastase activities in pancreatic homogenates are given in Fig. 39. Higher *in vivo* elastase activities were observed at 1 h, 8 h, 36 h and 48 h after treatment in UBR1 knockout mice compared to wild type mice. However, there was no difference in enterokinase (EK) activated elastase activity levels implying that there was no change in basal expression between wild type and knockout animals. Higher levels of activated protease levels such as elastase and trypsin could be responsible for a more severe type of pancreatitis in UBR1 knockout mice compared to wild type mice.
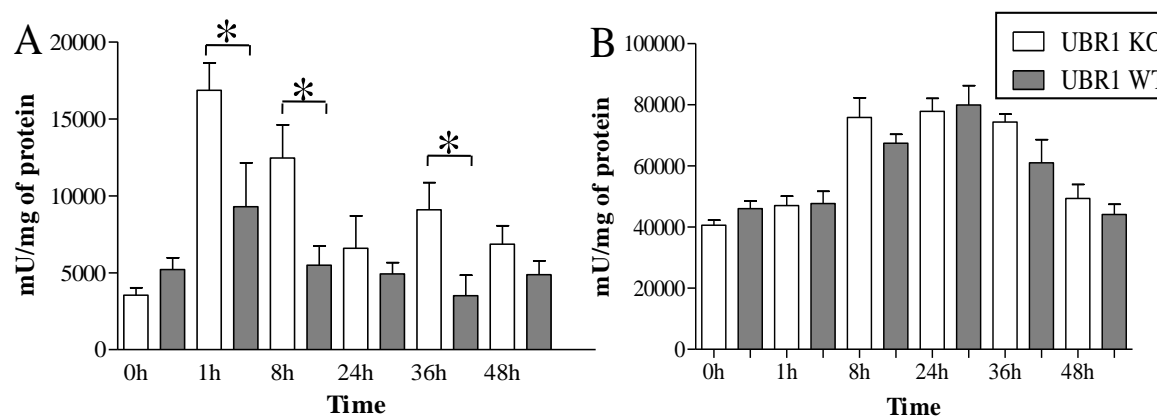
Fig. 39: Measurement of elastase (A) and enterokinase (EK) activated elastase (B) activities in pancreatic homogenates at different time points after treatment with caerulein. Statistically significant differences were marked with an asterisk on top of the time point which passed the non-parametric Mann-Whitney t test with a p value of less than 0.05. Data for UBR1 knockout and wild type mice are displayed with white and grey bars, respectively.

5.2.2.4. Cytokines measurement

Cytokine (IL6, IL10, IL12, TNF α, IFN, MCP-1) production in serum was measured using a CBA kit. Levels of IL6 and TNF α were significantly higher in UBR1 knockout mice compared to wild type mice 8 h after treatment might be leading to higher infiltration in UBR1 knockout mice, which was also seen by HE staining (Fig. 40A and B). MCP-1 levels were observed to be present at higher in UBR1 knockout mice compared to wild type mice at later time points (24 h and 48 h) in the course of experimental pancreatitis (Fig. 40C).
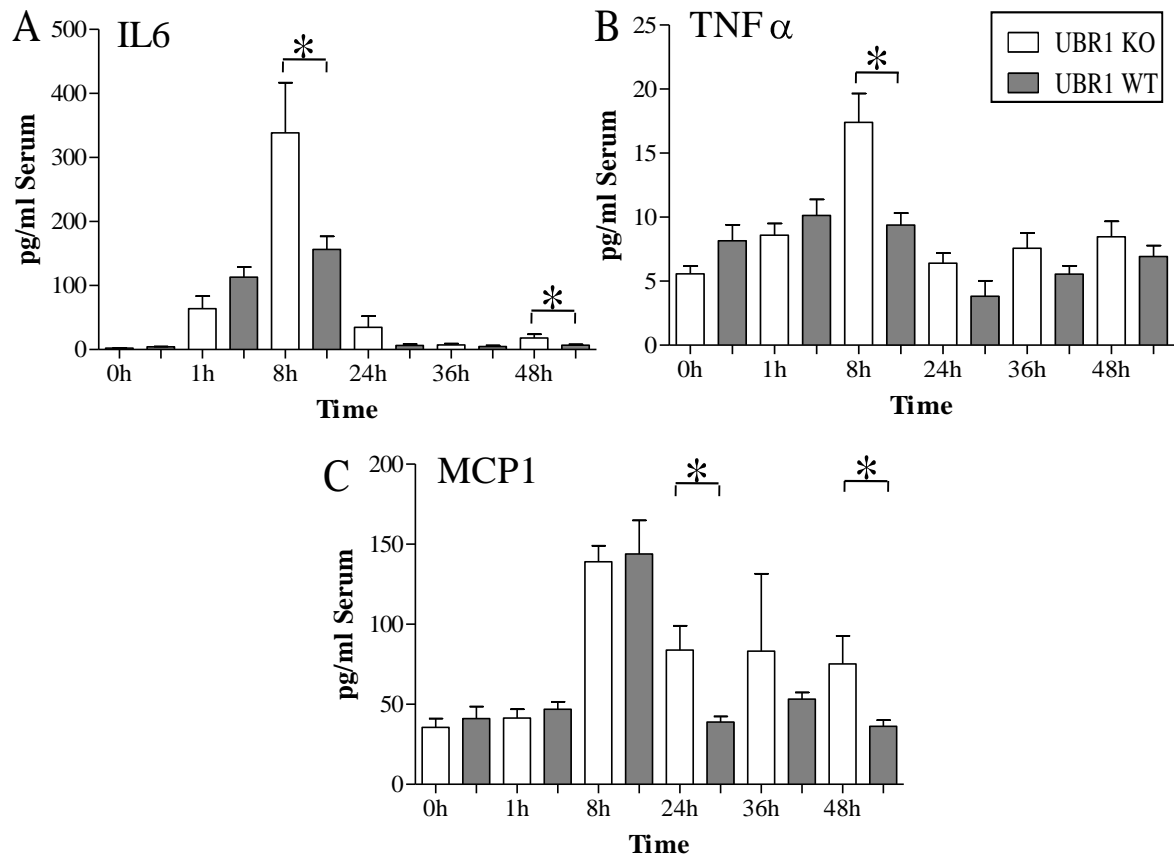
Fig. 40: Measurement of IL6 (A), TNF α (B) and MCP1 (C) using the CBA kit at different time points after treatment in serum. Statistically significant differences were marked with asterisk on top of the time point which passed the non-parametric Mann-Whitney t test with a p value of less than 0.05. One asterisk represents a p value of less than 0.05 and two asterisks represent p value of less than 0.01. Data for UBR1 knockout and wild type mice are displayed with white and grey bars, respectively.

5.2.2.5. Measurement of intracellular elastase activity and necrosis rate in isolated acini

Preparation of pancreatic acini was done according to the protocol given in the method section. Stimulation of isolated acini from UBR1 knockout and wild type mice were performed with supramaximal concentrations of CCK (10^{-6}M) leading to premature intracellular protease activation and cell necrosis. We measured elastase activity levels and rate of necrosis upon stimulation in freshly isolated pancreatic acini with supramaximal concentration of CCK to study the differences in the magnitude of the response *in vivo* between UBR1 knockout and wild type mice.
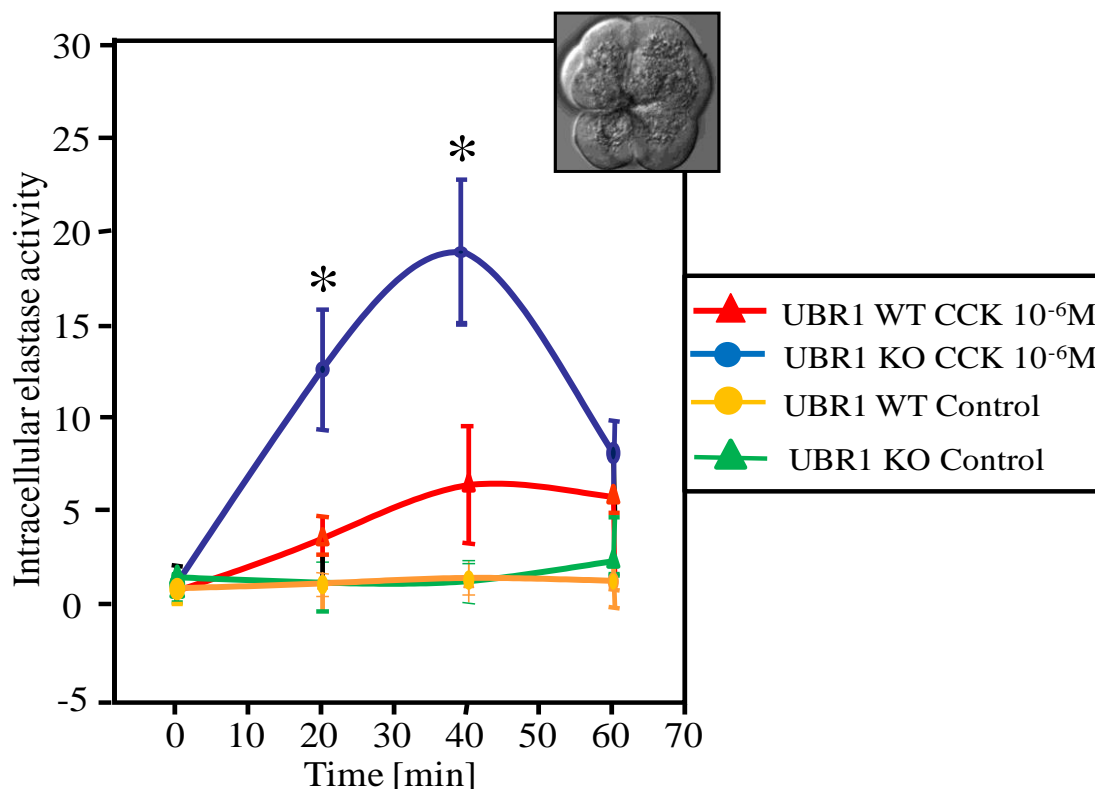
Fig. 41: Measurement of intracellular elastase activity in freshly isolated acini from pancreas. Higher intracellular elastase activities were observed in acini of UBR1 knockout mice treated with CCK compared to CCK treated acini of wild type mice. Statistically significant differences were marked with asterisk on top of the time point which passed the non-parametric Mann-Whitney t test with a P value of less than 0.05. The legend for different conditions is presented in a box at the right hand corner of the graph. n=4

Statistically significant higher levels of intracellular elastase activity (Fig. 41) and rate of necrosis (Fig. 42) were observed in UBR1 knockout mice compared to wild type mice upon stimulation with supramaximal concentrations of CCK stimulation.
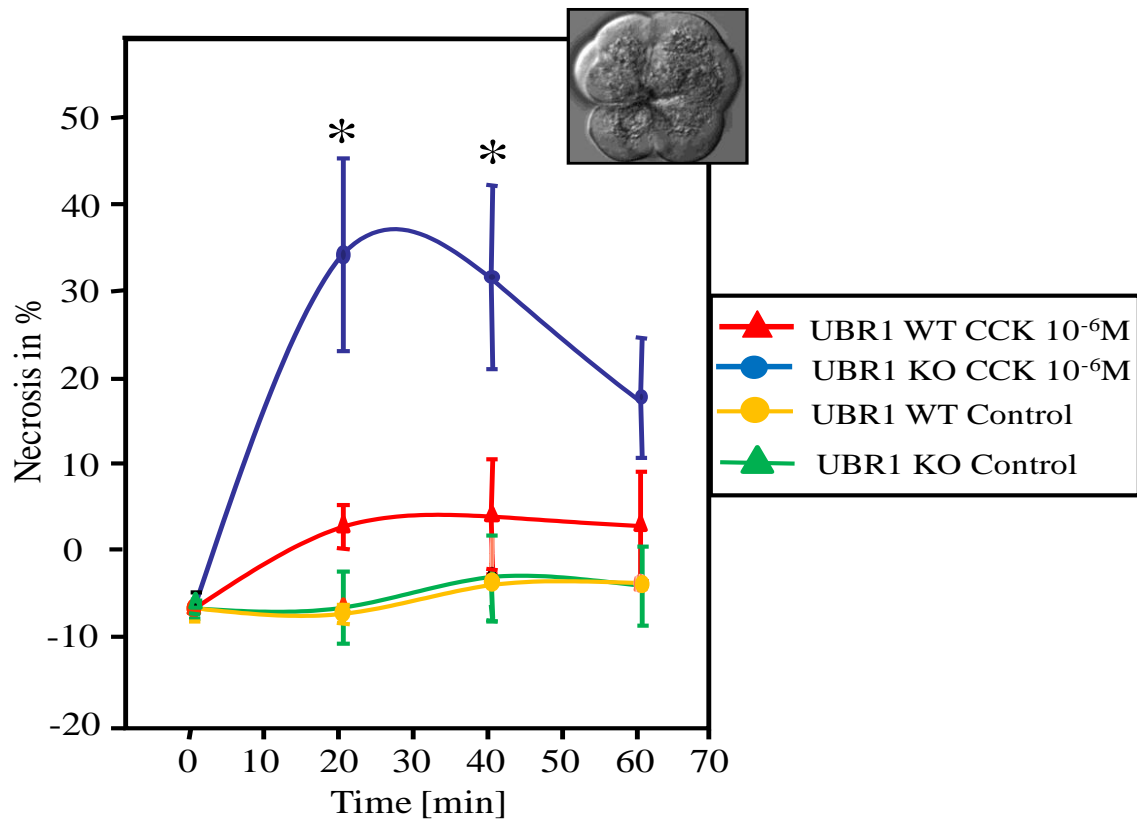
Fig. 42: Measurment of necrosis rate in freshly isolated acini from pancreas. Higher necrosis rates were observed in acini of UBR1 knockout mice treated with CCK compared to CCK treated acini of wild type mice. Statistically significant differences were marked with asterisk on top of the time point which passed the non-parametric Mann-Whitney t test with a p-value of less than 0.05. The legend for different conditions is presented in a box at the right hand corner of the graph . n=4

5.2.2.6. Histology/ HE staining

HE staining of Lung sections:

HE staining was done for all lung sections at different time points. There was more local damage and stronger neutrophil infiltration was observed in UBR1 knockout mice compared to wild type mice at 8 h and 24 h after treatment with caerulein. The differences were more pronounced at 8 h as illustrated in the HE stained section given in Fig. 43. This is in accordance with the observed higher myeloperoxidase (MPO) activity in lungs of UBR1 knockout mice compared to wild type mice at 8 h as MPO is most abundantly present in infiltrating neutrophils.
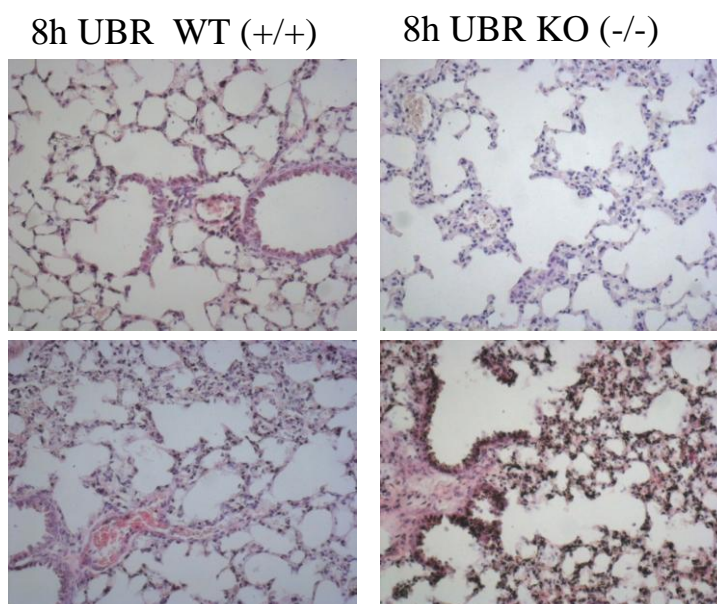
8h UBR WT (+/+)   8h UBR KO (-/-)

Fig. 43: HE stained lung sections. There was higher local damage and stronger neutrophil infiltration was observed in UBR1 knockout mice compared to wild type mice.

Histological score of pancreas sections

Pancreas sections at different time points after treatment with caerulein were stained with Haematoxylin and Eosin (HE) according to the protocol given in the methods section. We observed a statistically higher rate of inflammatory cells infiltrating the pancreas associated with a higher rate of tissue necrosis in UBR1 knockout mice compared to wild type mice in HE stained pancreatic tissue sections at time point 8 h (Fig. 44). The histological score was done according to the guidelines given by Claus Niederau et.al. and described in the methods section. The score was given based on extent of 1) necrosis 2) vacuolization and 3) inflammation/ infiltration. Though there was higher infiltration and necrosis at the time point 24 h but this finding did not reach statistical significance. This higher histological score at 8 h in the course of pancreatitis can be well explained with the earlier described observations of increased proteases activation, MPO activity and cytokine production in UBR1 knockout mice compared to wild type mice.
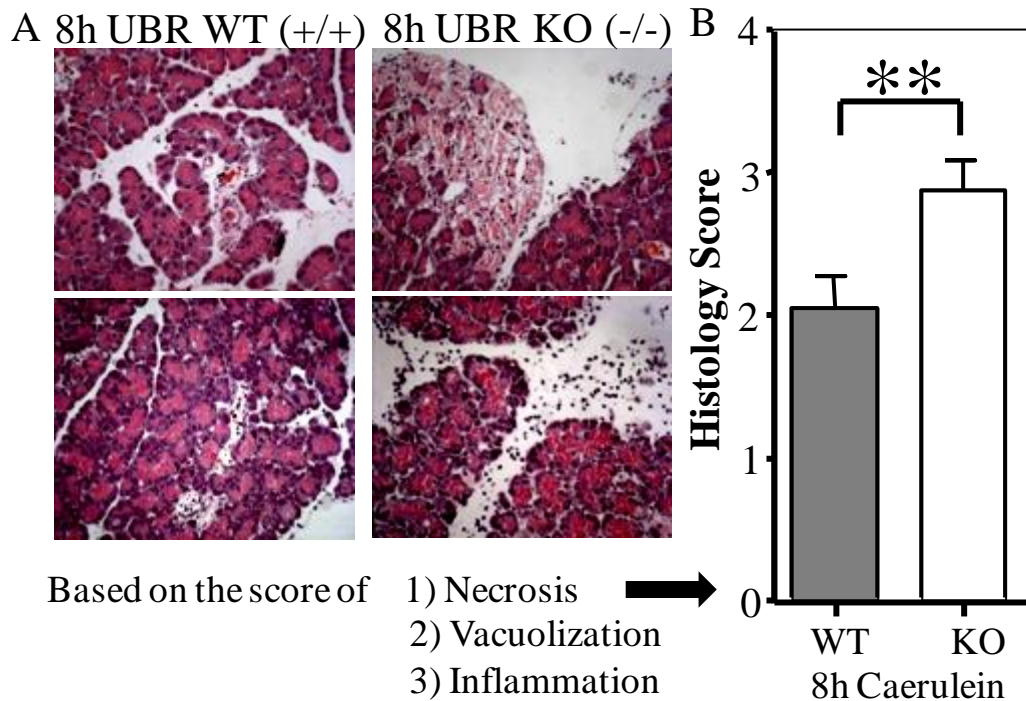
Fig. 44: Histological scoring of pancreas sections. Total histological scoring was done using the severity scores of necrosis, vacuolization and inflammation. A) HE stained pancreas sections of UBR1 knockout and wild type mice at 8 h of pancreatitis (treatment with caerulein). B) Graph showing statistically significant difference in the histological score between UBR1 knockout and wild type mice. Double asterisks show the significant difference by the non-parametric Mann-Whitney t test with a p value of less than 0.01.

5.2.2.7. TUNEL assay

TUNEL assay was performed to study the extent of apoptotic cell death in pancreatic sections. Necrosis was quantified in HE stainings. The TUNEL reaction was performed using *in situ* cell death detection kit according to the manufacturer's protocol. Nuclei were counterstained with DAPI to count the number of cells and to visualise the nucleus. Cell explorer software was used to count the percentage of apoptosis by taking 3 sections per mouse and 5 pictures per section. Treatment groups consisted of 4 mice. As time points we chose 0h and 8 h after the induction of caerulein induced pancreatitis. Neither in UBR1 knockout mice nor wild type littermates did we observe a significant rate of apoptosis at 0h. 8 h after the induction of caerulein pancreatitis we detected a significantly lower rate of apoptosis in UBR1 knockout animals in agreement with an increased rate of necrosis in these animals (Fig. 45).
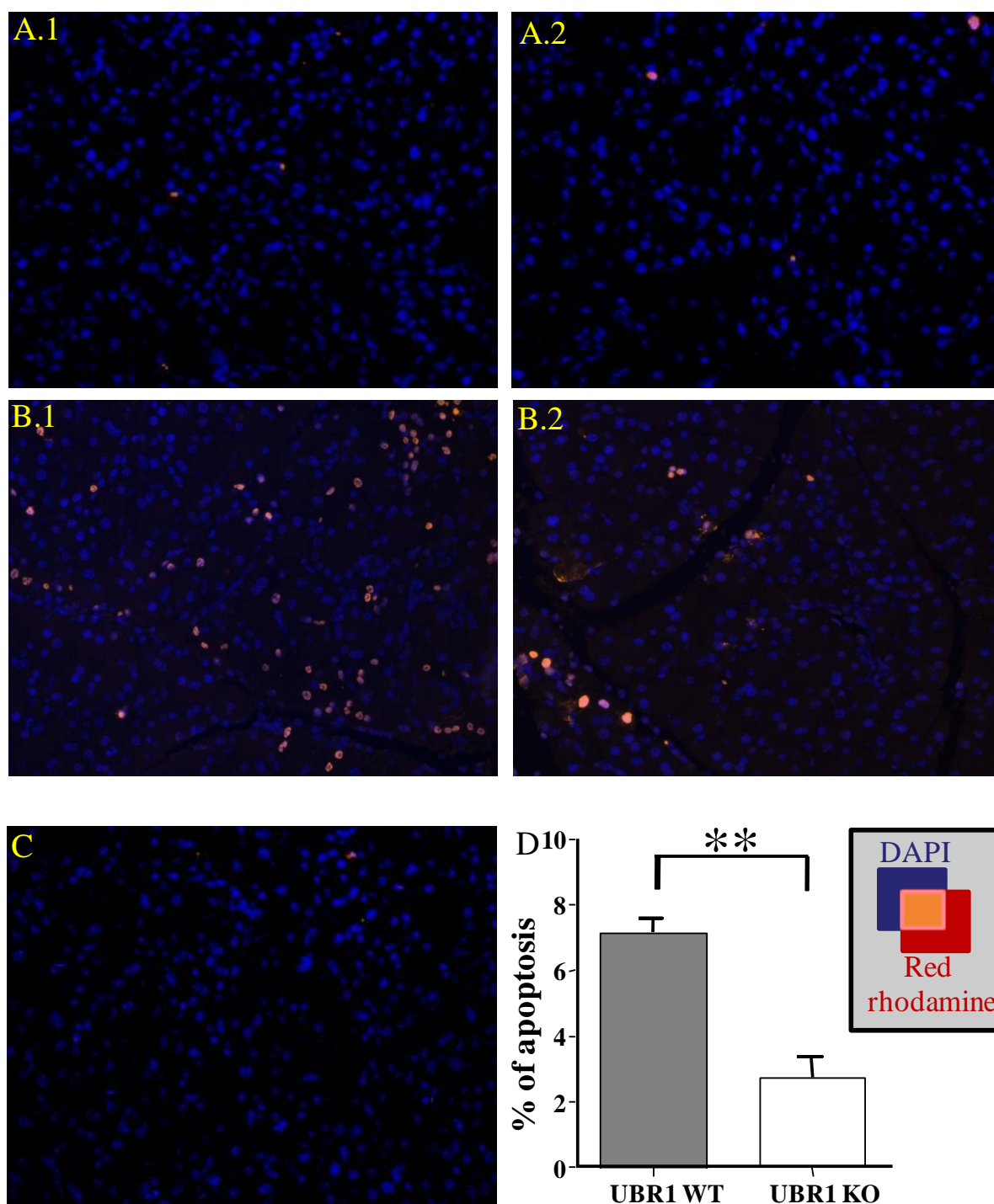
Fig. 45: Apoptotic measurement by TUNEL assay. Representative fluorescent microscopy pictures of the TUNEL assay in pancreas sections of UBR1 wild type mice 0h (A.1), UBR1 knockout mice 0h (A.2), UBR1 wild type mice 8 h (B.1), UBR1 knockout mice 8 h (B.2) and the negative control (C). D) Graph showing statistically significant higher percentage of apoptosis in UBR1 wild type mice compared to knockout mice at 8 h treatment with caerulein. Double asterisks show the significant difference by the non-parametric Mann-Whitney t test with a p value of less than 0.01. The inset is showing the colour legend for the DAPI and red rhodamine and the overlap to give the TUNEL assay positive signal was kept at the right hand top side of the graph. Negative control without using the fluorescent substrate was done to check the specificity of the signal.
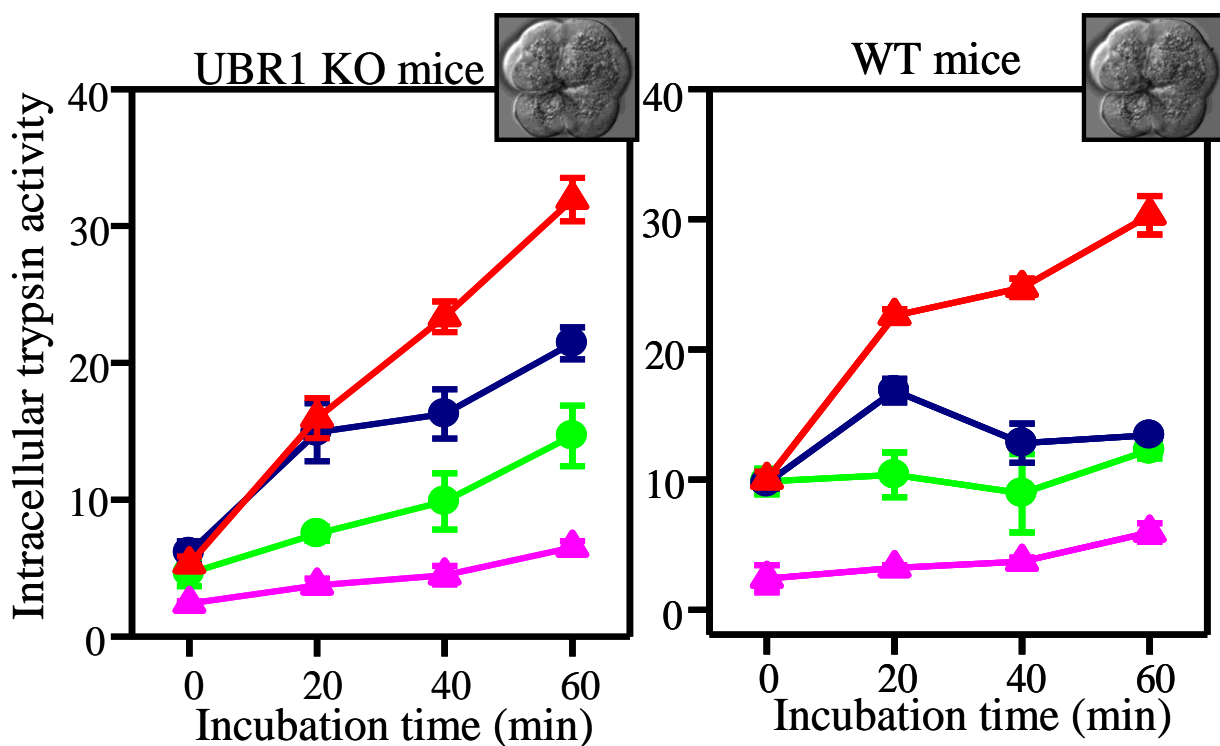
5.2.2.8. Identification and targeting of probable UBR1 substrates responsible for UBR1 knockout phenotype

So far we have observed the differences between the phenotype of UBR1 knockout mice and its wild type counterpart in terms of proteome and some cellular events. Apart from observing and understanding the differences between UBR1 knockout mice to wild type mice we attempted to target the most relevant probable direct UBR1 substrates which could explain the severe form of pancreatitis in UBR1 knockout mice and perhaps reverse the UBR1 knockout phenotype by inhibiting them. 2D-DIGE experiment showed up- regulation of some of the important proteases, inflammation related proteins and ER stress related proteins in UBR1 knockout mice (Table 7), which might be the result of their stabilization due to the absence of UBR1. From these results it was hypothesized that perturbation of direct UBR1 substrates levels could lead to the observed severe form of pancreatitis in UBR1 knockout mice. It is well known that premature or prolonged activation of proteases may lead to this severe form of pancreatitis. From the list of upregulated proteins (Table 7), which might be probable UBR1 substrates, trypsin, which is a key protease in the course of pancreatitis seems to be an attractive and relevant target as there might be reduced degradation of the activated form of trypsin resulting in a more severe form of pancreatitis in the absence of UBR1. Interestingly, from the sequence of trypsin we concluded that activated trypsin follows the rule of N-end-rule pathway with an Isoleucine (I) residue at its N-terminus, which is regarded as a type-2 destabilizing amino acids. Hence we tried to rescue the UBR1 knockout mice phenotype using the specific and reversible trypsin inhibitor S-124.

5.2.2.9. Impaired trypsin degradation and hereby prolonged activation of protease activity does not influence the phenotype

A century ago acute pancreatitis has been considered to be an autodigestive disorder, in which the parenchymal tissue of the organ is destroyed by its own digestive proteases (Chiari H Zeitschrift fur Heilhunde 1896). However there has been an extensive research and debate on where and by which the process of the premature zymogen activation is initiated. It was confirmed that highly purified trypsin not only auto-activates its inactive trypsinogen form to an active trypsin form but also activates other serine proteases (Kunitz and Northrop 1935, Northrop and Kunitz 1931). However, at least in rodents intrapancreatic trypsinogen activation depends significantly on the presence of cathepsin B in the pancreas (Halangk et al 2000, Saluja et al 1997) and autoactivation is not the cause of pancreatitis. Using the

reversible trypsin inhibitor S-124 Halangk W et al (Halangk et al 2002) showed that degradation of activated trypsin (autodegradation) can occur independent of trypsin. Moreover, they suspected an unidentified mechanism underlying the degradation of trypsin. Hence, we presumed that impaired degradation of the active form of trypsin and thereby prolonged activation of proteases could be the main cause of the severe form of pancreatitis in UBR1 knockout mice, where the UBR1 dependent proteasomal degradation mechanism is hampered because of the absence of UBR1. Since the active form of trypsin follows the N-end-rule pathway (from sequence) we targeted trypsin using the highly specific and reversible inhibitor S-124. Intra cellular trypsin activity was measured in the presence of the trypsin specific and reversible inhibitor S-124 using isolated acini from UBR1 knockout mice and wild type mice. S-124 can reversibly bind to the active site of trypsin and can be washed away with measuring buffer. In dissension with our hypothesis it was observed that low trypsin activity in acini of control and S124 without wash together with caerulein and high trypsin activity in acini treated with caerulein and S-124 with wash together with caerulein in both UBR1 knockout and wild type mice (Fig. 46). There was not much difference seen between knockout and wild type mice acini. It was observed that treatment with caerulein and S-124 wash before the measurement resulted in higher trypsin activation than treatment with caerulein alone (Fig. 46).

—●— Control   —●— Caerulein (10nM)

—▲— S 124 (10μM; without wash during measurement) + Caerulein (10nM)

—▲— S124 (10μM; washed before the measurement) + Caerulein (10nM)
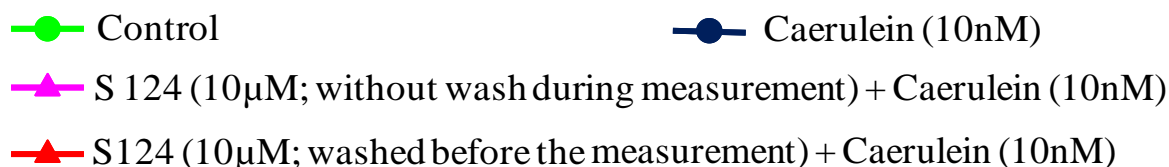
Fig. 46: Intracellular trypsin activity measurement in freshly isolated acini from UBR1 knockout mice and wild type mice in presence and absence of the reversible trypsin inhibitor S-124. Acini were isolated from UBR1 KO and WT mice pancreas. Intact living acini were incubated with supramaximal concentration of caerulein (10nM) and the trypsin reversible inhibitor S124 and trypsin activity was measured using a specific fluorogenic substrate over 60 min. In control acini without prior caerulein incubation, only small amounts of trypsin activity were generated. The same result was obtained when the acini were stimulated with caerulein but S124 was present throughout the experiment. Caerulein alone induced a rapid increase in trypsin activity followed by moderate decline after 40 min. When caerulein stimulation was done in the presence of S124 but subsequent measurement without S124, trypsin activity showed a more rapid and higher increase than after caerulein alone and did not decline over 60 min. There were no differences observed in UBR1 KO and WT mice acini in all conditions. The legend for different conditions is given below the graphs.

5.2.2.10. Identification of RGS4 as a direct substrate of UBR1

The experiment mentioned above ruled out a defect in trypsin degradation caused by loss of UBR1. Hence, we explored the upstream signalling events of protease activation which could lead to sustained activation of proteases thereby causing a severe form of pancreatitis in UBR1 knockout mice. From the list of few known N-end-rule pathway substrates (see introduction), Regulator of G protein Signalling (RGS) proteins seemed to be more interesting, particularly in the context of signalling pathways associated with pancreatitis,. Using ATE (Arg- transferase) knockout mice it was previously shown that RGS4 and RGS5 are *in vivo* mammalian N-end-rule pathway substrates (Lee et al 2005). However, the N-end-rule pathway involves several UBR (ubiquitin ligase) proteins such as UBR1, UBR2, UBR4, UBR5 etc. Hence, it was tested whether RGS proteins are direct substrates of UBR1. If they are direct substrates of UBR1 a UBR1 knockout would result in accumulation of RGS proteins in pancreas homogenates. Thus, using RGS4 and RGS5 (Abcam, UK) specific primary antibodies RGS4 and RGS5 levels were comparatively analzed in UBR1 knockout and wild type mice. These Western blot experiments revealed that RGS4 was accumulated in UBR1 knockout mice, where as the expression level of RGS5 in UBR1 knockout mice compared to wild type mice was unchanged implying that RGS4 might be a specific substrate of UBR1 (Fig. 47A).

5.2.2.11. Influence of loss of UBR1 on calcium signalling

RGS4 belongs to the R4 RGS proteins family, which act as negative regulators of G-protein coupled receptor mediated signalling pathway by their virtue of their GTPase activating capacity. Caerulein is a decapeptide and CCK analogue, which can induce pancreatitis through CCK receptors. CCK is known as 'brain-gut neuropeptide' due to its multiple anatomical locations in the gastrointestinal (GI) tract and central nervous system (CNS) (Buffa et al 1976, Liddle 1994). Two subtypes of CCK receptors have been identified: CCK1 and CCK2, which were initially classified on the basis of the affinity for the endogenous peptides CCK and gastrin (Noble et al 1999). Both receptors belong to a single family of G protein coupled receptors (GPCRs): CCK1 is predominantly located in the GI tract, whereas the CCK2 receptor is widely distributed in the CNS.

GPCRs have a conserved structure composed of seven transmembrane helices consisting of three subunits called alpha, beta and gamma (Bockaert and Pin 1999). On the basis of sequence similarities in their Galpha-subunits, G proteins have been grouped into four subfamilies: $G\alpha_s$, $G\alpha_{i/o}$, $G\alpha_q$ and $G\alpha_{12}$. It was shown that the RGS4 protein exerts its GAP activity towards the $G\alpha_{i/o}$ and $G\alpha_q$ classes of $G\alpha$ subunit (Berman et al 1996a, Berman et al 1996b, Xu et al 1999). G proteins of the $G\alpha_q$ class transduce Ca^{+2} signalling through PLCβ (Hepler and Gilman 1992).

Kruger et al (Kruger et al 2000) showed that protease activation is highly dependent on the spatial and temporal distribution of the corresponding Ca^{+2} release in pancreatic acinar cells. Hence, calcium signalling was studied in detail in isolated acini of UBR1 knockout and wild type mice. After isolation of pancreatic acini, caerulein stimulation was performed using supramaximal concentrations (10 nM) and calcium signalling oscillation frequency was measured using the calcium specific Fura-2 fluorochrome. Upon caerulein stimulation a lower number of calcium signalling spikes per minute were observed in UBR1 knockout mice compared to wild type mice (Fig. 47B and C). The number of spikes per 15 minutes was lower in UBR1 knockout mice but duration of the signal was prolonged in UBR1 knockout mice. In parallel to calcium signal measurement protease activities were measured, which showed higher protease activation in UBR1 knockout mice compare to wild type mice (Fig. 47D.1).
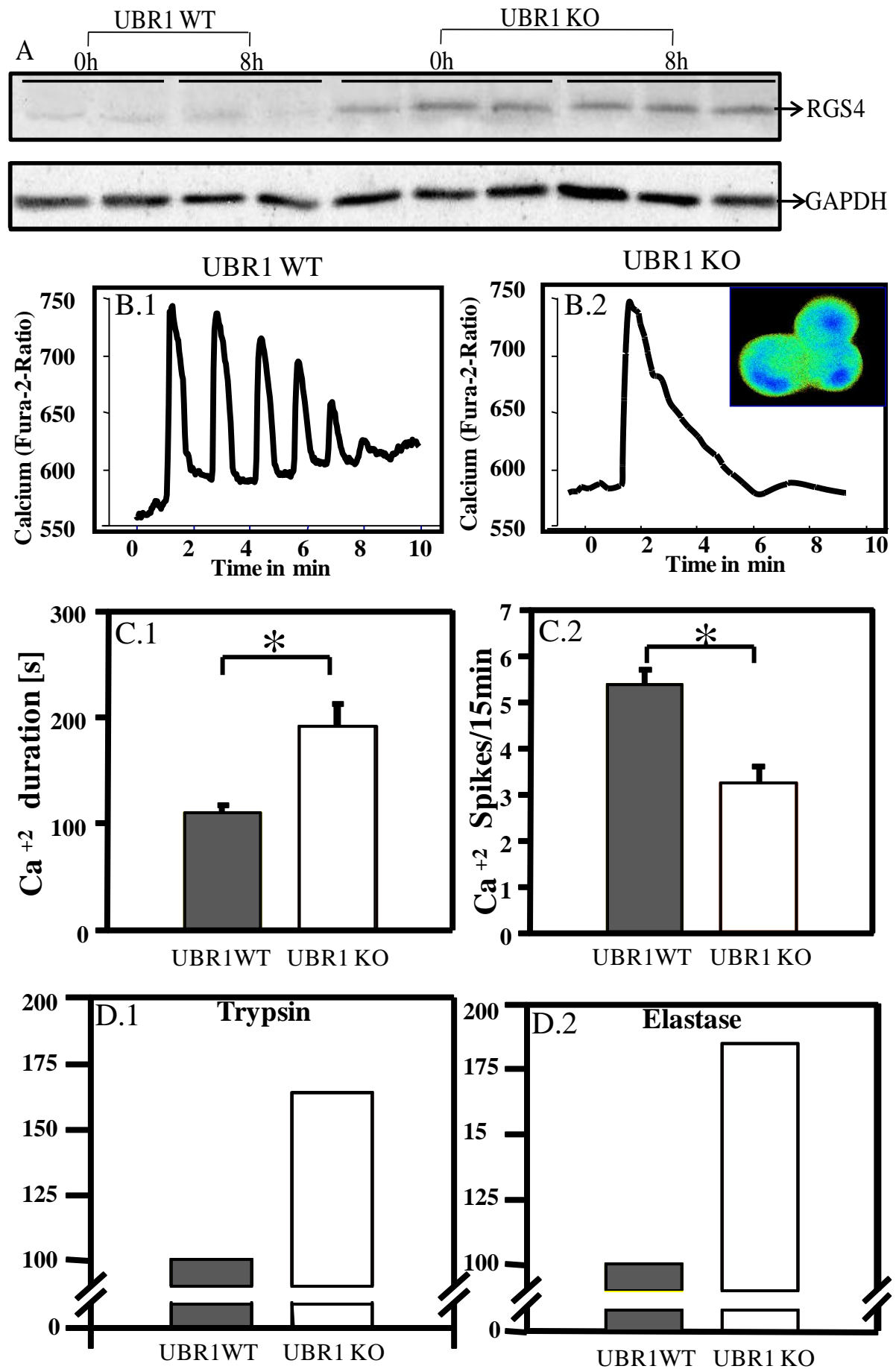
Fig. 47: Analysis of the influence of loss of UBR1 on RGS4 levels, calcium signalling and protease activity. A) Western blot analysis of RGS4 levels in UBR1 knockout and wild type mice. Equal amount of protein extracts of UBR1 knockout and wild type mice pancreas were loaded on 1D gel and blotted onto a PVDF membrane and RGS4 levels were checked using RGS4 specific primary antibodies. Equal loading was further verified by GAPDH antibodies. B) Analysis of calcium signalling in acini. Acini were freshly isolated from pancreas of UBR1 KO and wild type mice and stimulated using supramaximal concentrations of caerulein (10 nM) and calcium signalling was measured using the Ca^{+2} sensitive fluorogenic substrate fura-2. The fluorogenic fura-2 signal in acini of UBR1 knockout mice is exemplarily shown in the inset at the top of the right panel. Calcium signals in wild type mice (B.1) and UBR1 knockout mice (B.2). C) Quantification of Calcium signalling. The duration of the calcium signal (C.1) and the number of calcium signal spikes per 15 minutes (C.2) are displayed. D) Measurement of protease activity in acini. Trypsin activity (D.1) and Elastase activity (D.2) are shown. Statistically significant differences were marked with asterisks on top of the time point which passed the non-parametric Mann-Whitney t test with a p value of less than 0.05. n=5

5.2.2.12. Inhibition of RGS4 rescues the pancreatic phenotype of UBR1 knockout mice

The experiments outlined in the previous section suggested that a protein activity involved in calcium signalling of pancreatic acini and direct UBR1 substrate such as RGS4 could be the culprit of increased pancreatitis severity in UBR1 knockout mice. Hence, apart from trypsin we chose to target RGS4 to revert the severe UBR1 knockout phenotype, which is a key regulator of GPCRs mediated Ca^{+2} signalling and thereby protease activation in pancreatic acini. Using a Luminex 96-well plate bead analyzer and a novel flow-cytometric protein interaction assay to assess Gα-RGS interactions in a high-throughput screen it was found that RGS4/Gα binding can be specifically inhibited by 1, methyl N-[(4-chlorophenyl) sulfonyl]-4-nitrobenzenesulfinimidoate (CCG-4986) with an EC50 value of 5 μM *in vitro* (Roman et al 2007). Using highly purified trypsin from porcine (SERVA Electrophoresis GmbH, Heidelberg, Germany) it was revealed that CCG-4986 did not influence trypsin activity itself (Fig. 48A). After excluding a direct interaction of those two compounds we used CCG-4986 for *in vivo* trypsin activity measurements using UBR1 knockout mice pancreatic acini. We could show that CCG-4986 (10 μM) can be used *in vivo* and that it is cell permeable at least in pancreatic acini. With this set of experiments it was possible to reveal that the RGS4 specific inhibitor CCG-4986 reduced the trypsin activation to the level of observed in acini of UBR1 knockout mice which were not treated with caerulein (Fig. 48B). Thus, CCG-4986 can prevent the acinar cell specific phenotype of UBR1 knockout mice treated with caerulein.
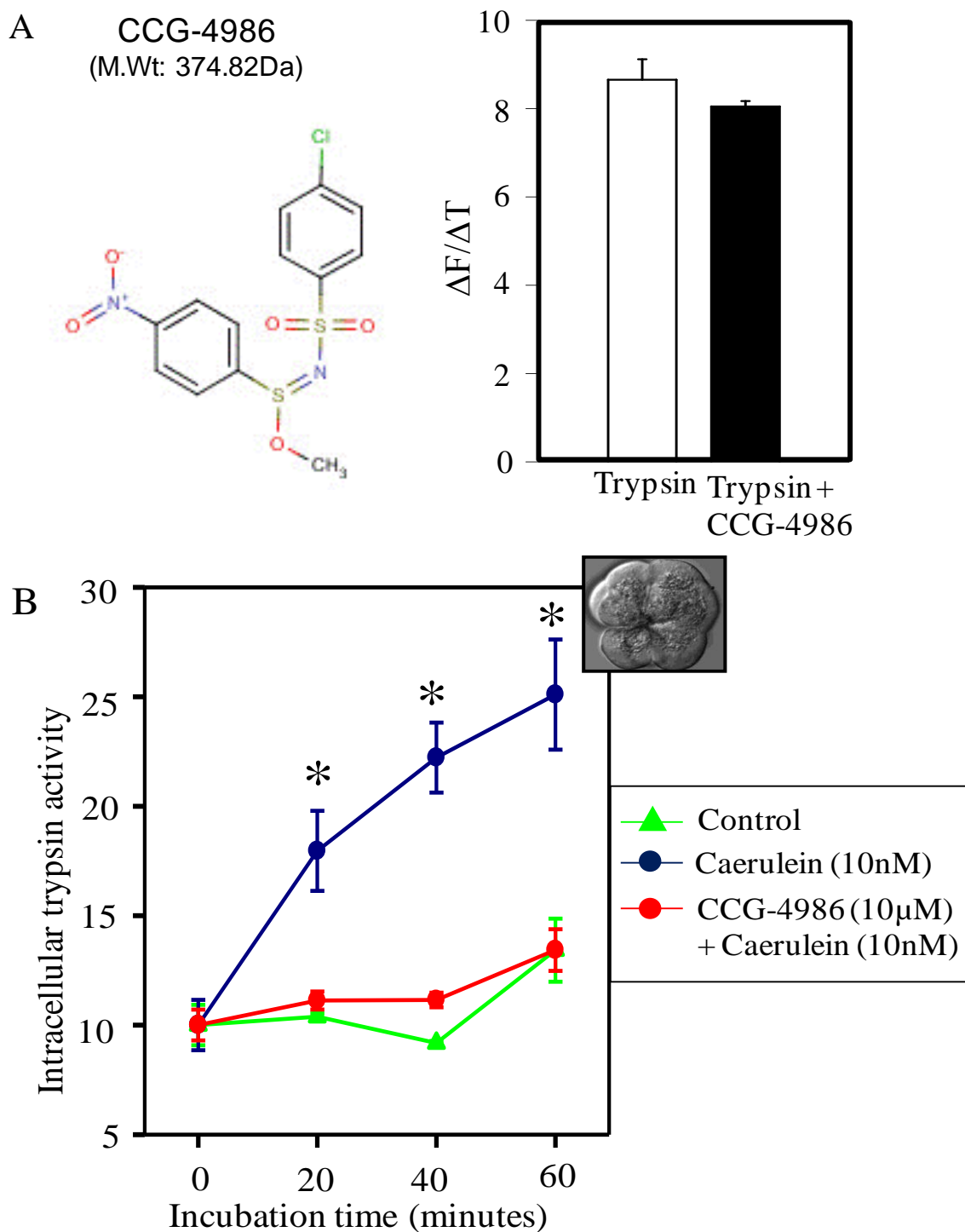
A CCG-4986
(M.Wt: 374.82Da)

Fig. 48: Assessment of the effect of the RGS4 inhibitor CCG-4986 on intracellular trypsin activity in freshly isolated acini from UBR1 knockout mice. A) Molecular structure of the RGS4 specific inhibitor CCG-4986. The effect of CCG-4986 (10 μM) on trypsin was measured using commercially available porcine purified trypsin (10 pM). B) Measurement of intracellular trypsin activity in presence or absence of CCG-4986. In control acini caerulein was not added, hence small amounts of trypsin activity were measured. Incubation of freshly isolated acini with supramaximal concentration of caerulein (10 nM) induced high trypsin activity where as supramaximal concentration of caerulein together with 10μM RGS4 specific inhibitor CCG-4986 showed

significantly reduced trypsin activity, implying a role for RGS4 in generating increased trypsin activity in UBR1 KO mice compare to WT mice upon stimulation with caerulein. Statistically significant differences were marked with asterisk on top of the time point which passed the non-parametric Mann-Whitney t test with a p value of less than 0.05. The legend for different conditions is given in a box at the right hand corner of the graph.

6. Discussion

6.1.   Characterization of the role of BCL11b in Human T cell lymphomas

Recent studies established Bcl11b as a general transcription repressor, (Cismasiu et al 2008) removal of which leads to DNA replication stress and damage (Kamimura et al 2007a), and finally apoptosis (Grabarczyk et al 2007) in T cells. However, the mechanism underlying the cell death is not completely understood. This prompted us to use a proteomic approach to investigate the effects of *BCL11B* knockdown in human T cells (Fig. 10). The majority of changes in the proteome in Jurkat and huT78 T cell lines observed following *BCL11B* knockdown were consistent in both cell lines (Fig. 11 and 12).

In the current study, we provide direct evidence for the activation of the intrinsic apoptotic pathway showing loss of mitochondrial membrane potential (Fig. 19). In our earlier report, we recognized suppression of the anti-apoptotic protein Bcl-xL, as a potential factor contributing to cell death in Bcl11b-deficient cells (Grabarczyk et al 2007). The critical role of Bcl-xL was proven by silencing of *BCL11B* expression in Bcl-xL over-expressing cells, which did not trigger any increase of apoptosis. In the current study, loss of mitochondrial outer membrane potential (MOMP) (Fig. 19) and increased apoptosis (Fig. 10) were not observed in Jurkat cells overexpressing Bcl-xL following Bcl11b-knockdown. Therefore, we exploited this system wherein Bcl11b dependent primary events which occur upstream of loss of MOMP take place but not apoptosis associated secondary effects. Interestingly, the activation of the extrinsic death-receptor mediated pathway, executed by TRAIL over-expression upon *BCL11B* knockdown, was not able to overcome the block of apoptosis in these cells (Grabarczyk et al 2007). This suggests that the full-blown effect requires the simultaneous activation of both apoptotic pathways. In addition, the results indicate that both cell lines used in our studies represent the type-2 response to death receptor stimulation which requires the augmentation of the mitochondrial loop to induce the caspase 3 executor (Rudner et al 2005).

In addition to the evidence for activation of mitochondrial and death-receptor apoptotic pathways upon *BCL11B* knockdown, we could identify cleaved caspase targets including spectrin, vimentin and myosin-9 (Fig.13). The initially noted aberrant migration properties on 2-DE were verified by detailed assignment of peptides by LC-MS/MS analysis. Spectrin was shown to be cleaved during Fas induced apoptosis in Jurkat cells (Martin et al 1996). Cleavage of vimentin into fragments of different lengths was reported in TNF alpha and Fas treated Hela and Jurkat cells. Moreover, it was shown that proteolysis of vimentin

promotes apoptosis by dismantling intermediate filaments, thereby amplifying the cell death signal (Byun et al 2001). Myosin heavy chain A (myosin-9) was also discovered as a caspase substrate in Jurkat cells treated with Fas (Kato et al 2005) (Fig. 13). The caspases activation, evidenced by identification of their cleaved substrates confirms previous findings and it was demonstrated that a significant protection against Bcl11b-knockdown induced apoptosis in cells treated with Caspase-8 and Caspase-9-specific inhibitors (Grabarczyk et al 2007).

Ezrin, Radixin, and Moesin (ERM) were found among the proteins induced upon Bcl11b depletion in Jurkat and huT78 cells (Table 3). ERM proteins belong to the 4.1 band protein family which connects the plasma membrane and the cortical actin cytoskeleton (Arpin et al 1994, Tsukita et al 1994). Activation of ERM proteins is triggered by phosphorylation of the conserved C-terminal threonine residue (T567 in ezrin, T564 in radixin, and T558 in moesin) triggering conformational changes which then unmask binding sites. Apart from cross-linking function, ERM act as signal transducer in various signal transduction pathways such as Rho GTPase (Ivetic and Ridley 2004), PKC/MAPK (Koss et al 2006), FAS (Hebert et al 2008), PI3K-PKB (Rasmussen et al 2008) and Ras signalling (Orian-Rousseau et al 2007) pathways. Collectively, these data suggest that ERM proteins represent an important node in the signaling network. Besides increases in ERM levels we also demonstrated enhanced phosphorylation of ERM proteins following Bcl11b suppression (Fig. 18). Together with the increase in level the enhanced phosphorylation of ERM proteins leading to their activation could play the crucial role in initiation and regulation of apoptosis as proven in death-receptor mediated FAS-induced cell death in Jurkat cells (Hebert et al 2008). Moreover, the increased levels of total and phospho-ERM observed in *BCL-xL* over-expressing cells, which do not undergo apoptosis followed *BCL11B* knockdown, suggest that the effect on ERM might represent an upstream event in the apoptotic cascade. It is worth noting that we observed reductions in level and phosphorylation of ERM proteins in Jurkat cells forced to over-express *BCL11B* (Fig. 22). These opposite effects of *BCL11B*-depletion and over-expression on ERM proteins probably indicate that ERM might be involved in the *BCL11B*- mediated control of cell survival.

Besides ERM increased levels of PDCD5 might also be related to the observed increased apoptosis because PDCD5 was identified as an enhancer or key regulator of apoptotic programmed cell death (Liu et al 1999) (Fig. 21). Decreased PDCD5 expression has been reported in various human tumors, e.g. breast cancer (Hedenfalk et al 2001) and chronic melogenous leukaemia (Ruan et al 2006). Interestingly it was shown recently that PDCD5, in cooperation with Tip60, plays a key role in DNA damage induced apoptosis: PDCD5

increased Tip60-dependent K120 acetylation of p53 and participated in the p53-dependent expression of apoptosis-related genes such as Bax upon DNA damage (Xu et al 2009).

The first evidence for the involvement of *BCL11B* in the control of cell death was provided by investigations of a knockout mouse model (Wakabayashi et al 2003b). These studies showed the necessity of *BCL11B* expression for normal development of a T cell lineage which otherwise was inhibited at the very early stages. The developmental block resulted from massive apoptosis accompanied by significant suppression of the Bcl-xL anti-apoptotic protein. Having found inactivating genomic alterations in the *BCL11B* locus in γ-irradiation-induced mouse lymphomas (Wakabayashi et al 2003a), which is the opposite of what would be predicted from the knockout model, the authors concluded that *BCL11B* might represent a tumor suppressor having both positive and negative effects on cell growth. According to this hypothesis the inactivation of the *BCL11B* tumor suppressor in thymocytes would lead to apoptosis preceded by improper activation and unscheduled cell cycle entry. In fact, similar effects were described earlier in cellular systems harboring activated oncogenes, like c-myc (Evan et al 1992) or inactivated tumor suppressors, like Rb (Almasan et al 1995, Knudsen et al 2000). However, so far there is no evidence that *BCL11B* acts the same way. The proteome data presented here seem to support the conclusion that apoptosis following *BCL11B* loss could be initiated by improper activation and proliferation. An induction of several proteins directly participating in cell cycle progression was observed in both T cell lines upon *BCL11B* suppression by RNA interference (Table 3). These include one of the key factors responsible for cell cycle entry: cyclin-dependent kinase 6 (CDK6) representing an important part of the cyclin D/CDK4/CDK6 complex, a major regulator of G1 to S phase transition of cell cycle. Further evidence for the over-activated proliferation was provided by discovering elevated levels of the human homolog of the minichromosome maintenance proteins 4 and 6 in the proteome study (MCM4 and MCM6, Table 3.). Together with four other members of the gene family (MCM 2, 3, 5 and 7) MCM4 and 6 are responsible for the formation of the so-called pre-replicative complex in G1, which is a key step in establishing replication competence (Labib et al 2000). The expression of MCM proteins is restricted to proliferating cells or cells with proliferation potential while in quiescent and terminally differentiated cells MCMs are undetectable (Stoeber et al 2001). MCMs play an important role not only in replication licensing but also in execution of the replication checkpoint upon genotoxic stress. The inhibition of MCMs after checkpoint induction(Ishimi et al 2003, Ishimi et al 2004, Labib et al 2001) seems to be particularly interesting since the defect of checkpoint control in *BCL11B*-deficient Jurkat cells have been reported (Kamimura et al 2007a).

The crucial requirement of *BCL11B* for cell survival and its postulated role in limiting proliferation and genomic integrity prompted us to screen our proteome data for further candidate proteins which could confirm the capacity of *BCL11B* to prevent apoptosis by controlling cell cycle entry and DNA damage. One of the proteins, which was induced in *BCL11B*-deficient cells and fulfilled these criteria, was desoxyuridine triphosphate nucleotidehydrolase (dUTPase, DUT, Table 3). The enzyme hydrolyses dUTP to dUDP and pyrophosphate and is absolutely essential for the viability of cells (McIntosh et al 1992). Its major function is limiting the intracellular pool of dUTP that otherwise gets incorporated into DNA during replication and repair replacing dTTP. The level of the nuclear isoform identified in our studies, DUT-N, strictly correlates with the proliferation status. Non-dividing cells, like resting peripheral blood lymphocytes strongly induce *DUT-N* upon mitogenic stimulation (Ladner et al 2000). In other non-malignant tissues, like colonic mucosa, the nuclear isoform of DUT is restricted to regions with residing mitotic activity (Grasser et al 2001). For the reasons mentioned above, inhibition of DUT leads to apoptosis (Deutsch 1995, Nation et al 1989). Interestingly, contrary to our observations, induction of apoptosis in Raji cells was accompanied by dramatic loss of DUT (Brockstedt et al 1998). In summary, DUT-N expression is growth dependent, resembling the pattern of genes engaged in DNA metabolism and replication. A common feature of these genes is the regulation mechanism involving activation of E2F transcription factor. In agreement with this, an E2F consensus binding site has been found in the promoter region upstream of DUT-N coding sequence (Ladner and Caradonna 1997). Apart from E2F1, a binding site for Sp1 basal transcription factor was identified in DUT-N promoter region. Of note, the suppression of Sp1 activity by *BCL11B* has been demonstrated before in the context of HIV latency (Marban et al 2007). Supporting the protein accumulation reported here, Piotr Grabarczyk et al (unpublished data) have shown that the level of DUT-N mRNA also increased following *BCL11B* knockdown. This suggests the possible involvement of *BCL11B* in transcriptional regulation of DUT-N. In sum, the elevated level of DUT-N in *BCL11B*-depleted cells is additional evidence supporting the aberrantly activated cell cycle entry and proliferation-driven apoptosis hypothesis (Fig. 20B).

Having found accumulation of the central enzyme in the uracil-misincorporation pathway, we decided to inspect the level of uracil in genomic DNA (gDNA) of *BCL11B*-deficient Jurkat and huT78 cells. The test for gDNA integrity by agarose gel electrophoresis showed massive DNA damage in *BCL11B*-depleted cells upon recombinant uracil N glycosylase (rUNG) treatment (Fig. 20C). This is most likely due to apoptosis-related endonucleases activity, since non-apoptotic Jurkat cells over-expressing Bcl-xL retained high

molecular weight gDNA regardless of *BCL11B* status. In contrast, the genetic material of control cells remained relatively unaffected by rUNG which indicated increased levels of genomic uracil upon *BCL11B* suppression (Fig. 20C). Of note, the degradation following rUNG treatment was also found in apoptosis resistant Jurkat Bcl-xL cells upon *BCL11B*-depletion, which suggests that the uracil misincorporation could represent one of the upstream events of apoptosis leading to cell death. Although it is troublesome to rationalize, the enhanced proliferation which is most likely responsible for DUT-N activation could be the reason for the elevated incorporation of its substrate dUTP. The studies employing mice deficient for the major dUMP-removing enzyme uracil-DNA glycosylase (Ung2) revealed a clear correlation between the DNA uracil level and cell proliferation (Andersen et al 2005). This data further indicate that the cell proliferation rate is the major determinant for the genomic uracil burden.

Besides dUTPase UCK2 is also implicated in DNA damage and exerts cytotoxicity and anti tumor activity. Increased levels of Uridine-cytidine kinase 2 (UCK2) are also compatible with a higher proliferation rate because this enzyme catalyzes the rate limiting step in pyrimidine biosynthesis, the phosphorylation of uridine and cytidine to UMP and CMP (Fig. 21). Several studies suggest that UCK activity may increase in tumor cells compared with normal tissues.

Apart from increased levels of CDK6, MCM4, MCM6 and dUTPase discussed before the increased levels of MAT1 also argues for Bcl11b mediated effects on cell cycle entry and progression (Fig. 21). Being a part of the CDK-activating kinase complex (CAK) MAT1 is responsible for the complex assembly and determines its specificity. The targets of CAK include CDK1, CDK2 and CDK4 (Fesquet et al 1993, Poon et al 1993), which play an essential role in cell cycle control. In agreement with this, MAT1 was found to be involved in G1 to S phase transition of cell cycle (Wu et al 1999) and DNA repair (Chalut et al 1994). In neuroblastoma, knockdown of MAT1 led to growth inhibition and directed the cells towards differentiation while its overexpression caused the opposite effect (Zhang et al 2004). Furthermore, the activation of the all-trans-retinoic acid triggered proteasomal degradation pathway led to fragmentation of MAT1 in HL60 cells which caused hypophosphorylation of Rb1 and retinoic acid receptor alpha (RARα) and as a consequence G1 arrest accompanied by activated differentiation.(Wang et al 2002) Summarizing this part, accumulation of proliferation-promoting factors in BCL11b-depleted cells support the enhanced replication stress which was formerly postulated by others.

Conclusions:

Collectively, the proteome analysis of *BCL11B*-depleted T cell lines revealed several previously unidentified mechanisms which could significantly contribute to cell death following *BCL11B* knockdown. By identifying the cleavage products we convincingly confirm the involvement of caspases in this process. In addition, the induction and hyperphosphorylation of the ERM signaling proteins did not only validate the previously observed activation of death-receptor pathway but also unmasked the potential downstream events in this apoptotic pathway. Furthermore, the overrepresentation of proteins committed to cell cycle entry strengthened the hypothesis of uncontrolled proliferation as a primary reason of cell death upon *BCL11B* suppression. Finally, the discovery of abnormal uracil-DNA metabolism unraveled the plausible mechanisms of *BCL11B*-mediated protection of genome integrity.

6.2. Elucidation of the mechanism of pathophysiology of Johanson Blizzard Syndrome (JBS) using UBR1 knockout mice and JBS patients' lymphoblasts cell lines

6.2.1. JBS-desease mechanisms and development of a diagnostic proteomic signature

Johanson-Blizzard syndrome (OMIM 243800) is an autosomal recessive disorder that includes congenital exocrine pancreatic insufficiency, multiple malformations such as nasal wing aplasia and frequent mental retardation (Johanson and Blizzard 1971). Previously, the disease associated locus was mapped to chromosome 15q14-21.1 and mutations, mostly truncating ones, in the gene UBR1 in 12 unrelated families with JBS were identified. UBR1 encodes one of at least 4 functionally overlapping E3 ubiquitin ligases in the N-end-rule pathway, a conserved proteolytic system whose substrates include proteins with destabilizing N-terminal residues (Bachmair et al 1986, Kwon et al 2002, Tasaki et al 2005, Varshavsky 1996). In the pancreas of individuals with Johanson-Blizzard syndrome, UBR1 is not expressed and thus patients suffer from intrauterine onset of destructive pancreatitis. In addition it was found that UBR1$^{-/-}$ mice, whose previously reported phenotypes include reduced weight and behavioral abnormalities (Kwon et al 2001, Kwon et al 2003) suffered from exocrine insufficiency with impaired stimulus secretion coupling and increased susceptibility to pancreatic injury (Zenker et al 2005). These findings indicated that deficiency of UBR1 perturbs pancreatic acinar cells and other organs, presumably owing to metabolic

stabilization of specific substrates of the N-end rule pathway. However, these observations were largely dependent on data from the UBR1$^{-/-}$ mice and did not reveal any specific candidates downstream of UBR1 explaining the phenotype. We therefore prospectively recruited 14 families with JBS from 2005 onwards, characterized their clinical phenotype and generated lymphoblastoid cell lines for further analysis (Table 1). As UBR1 regulates the intracellular protein turnover and acts as a catalytically active enzyme we opted for proteome analysis to identify downstream candidates perturbed by the lack of UBR1 and possibly explaining the pathophysiology of the syndrome. Even if by the setup of our experiments we could only expect descriptive data as the human material was too sparse to manipulate. However, we were able to retrieve valuable insight into 3 different signalling pathways closely linked to the UBR1 phenotype, which now have to be tested in appropriate knock-out models and which might offer prospective treatment options and will be briefly outlined below.

In mammalian cells, complex networks of signalling pathways tightly regulate cellular processes such as proliferation and differentiation. Recent studies indicate that annexin A6, one molecule significantly downregulated in JBS patients acts as a target protein for p120GAP which in turn inactivates Ras at the plasma membrane (Fig. 29). Annexin A6 functions as a tumor-suppressor and continous downregulation would render the JBS organism more prone to cancer development. However, data from knock-out models suggest that annexin A2 and A7 could compensate for the loss of function of A6 explaining why JBS patients do not seem to be at an increased cancer risk (Grewal and Enrich 2006).

Interferon-induced-GTP-binding protein was found to be consistently decreased in lymphoblastoids from JBS patients with a severe phenotype (Fig. 29). The family of IRG proteins is known to confer resistance to viral infections as well as intracellular bacteria such as *Listeria monocytogenes* and *Toxoplasma gondii* (Howard 2008). Even if JBS patients have a normal life expectancy the rate of prenatal abort is significantly increased. One could speculate whether lack of UBR1 function renders the fetal organism more susceptible to an intrauterine, possibly fatal infection, with *Toxoplasma gondii* or *Listeria monocytogenes*? However, both diseases could be easily prevented or treated if an increased risk during pregnancy would be established.

The endoplasmatic reticulum is involved in a variety of essential and interconnected processes in human cells, including protein biogenesis, signal transduction and calcium homeostasis. Our proteome approach in lymphoblastoid cells identified two crucial players involved in ER processing of proteins, the FK506 binding protein 4 (FKBP) (Davies and

Sanchez 2005) as well as GRP78 (BiP) (Dudek et al 2009) (Fig. 29). BiP and FKBP act as molecular chaperones regulating the unfolded protein response (UPR) induced by misfolded or accumulated proteins. A perturbed expression of those two key players is therefore not surprising as a loss of function of the E3 ligase UBR1 should result in accumulation of proteins. Moreover, BiP has been previously described as a direct substrate of the N-end-rule pathway (Hu et al 2006). Our own data investigating ER stress in UBR1$^{-/-}$ mice show a significant contribution of UPR to pancreatic cellular damage, which will be discussed in detail later. Most recently it was suggested that the BiP induced stress response in pancreatic acinar cells can be reversed by ursodesoxycholic acid a simple and non toxic medication which could be offered to JBS patient to maintain exocrine function (Kubisch and Logsdon 2008). Mutations in the SIL2 gene, a nucleotide exchange factor for BiP, results in a rare autosomal recessive neurodegenerative disorder called Marinesco-Sjögren syndrome resembling some hallmarks of JBS. In conclusion, we are fully aware that the above mentioned discussion is mere speculation at this point of time and that the hypotheses postulated, need now be tested in the respective genetically engineered models to learn about their physiological relevance. However, the results justify our experimental approach.

Sequence analysis was able to give a diagnosis in the patient cohort recruited for this study, but it did not give any insight into the phenotype of the disease (Table 1). Zenker and co-workers detected several splicing mutations (IVS16+14C>G, IVS26+5G>A, IVS9-13A>G, IVS4-13G>A, IVS20+2T>C, IVS35-1G>C, IVS1+5G>A) introducing a new splice site but keeping the original splice sites. How the different splice products behave is difficult to predict, but at least for the splice mutations IVS16+14C>G, IVS26+5G>A the prediction from mRNA analysis that there might be residual protein expression was proven wrong by Western blot analysis (Fig. 26). The generated mRNA was found to be instable and remained untranslated. This highlights that in a diseases were the phenotype depends on production and enzymatic function of a protein sequence analysis is not sufficient to understand the disease phenotype. A proteome-based approach identifying surrogate markers for protein function might therefore be helpful to predict disease severity or even to intervene at a stage where the full phenotype has yet to be developed e.g. in early childhood. With this aim we developed a protein based diagnostic assay to detect subclinical JBS which was mainly characterized by exocrine pancreatic insufficiency a common feature of a variety of diseases. With our proteomic signature consisting of 5 proteins we were able to identify in the patient cohort 4 patients with residual UBR1 levels (Fig. 26). In a population based cohort the prevalence of exocrine pancreatic insufficiency was determined with 11.5% (Rothenbacher et al 2005) and

one wonders about the number of subclinical JBS patients hidden in this cohort which at least would be in need of genetic counseling.

Reproducibility is a key point in genomics and proteomics (Mercier et al 2009) and was addressed in this study (Fi.g 23). Experiments were performed in biological duplicates and technical triplicates. Moreover, PCA analysis as well as a mixed-model of ANOVA for measurement of reproducibility of the proteome data was applied (Fig. 25). Obvious limitations of our study are the lack of prospective evaluation of the surrogate marker panel identified and this can be further verified in an appropriate mice models and cell lines.

Conclusions:

In summary, guided by the diversity of the genotype and the variety of the phenotype of Johanson-Blizzards syndrome we have in a proteome-based approach not only identified three different signalling pathways closely connected to the pathophysiology of JBS but established a protein panel of surrogate markers for residual UBR1 activity enabling us to detect milder variants of JBS without the need of time taking gene sequencing.

6.2.2. Characterization of mechanisms of pancreatic insufficiency in a murine model

To understand the underlying mechanism of exocrine pancreatic insufficiency, which is the most consistent symptom in JBS syndrome we explored experimental pancreatitis in UBR1 knockout mice in detail primarily using proteomics technology and later on, validated the findings using classical cell biology techniques. UBR1 knockout mice are viable but have defects including pancreatic insufficiency, fatty acid metabolism and behavior abnormality (Kwon et al 2001). UBR2 knockout mice exhibited gender and strain specific lethality, meaning that male UBR2 knockout mice were viable but infertile but their female counter parts died as embryos (Kwon et al 2003). Though UBR1 and UBR2 single knockout mice are viable, UBR1 and UBR2 double knockout mice are embryonically lethal at midgestation with defects in both neurogenesis and cardiovascular development (An et al 2006). From this it is clear that though UBR1 and UBR2 share strong sequence similarity (Varshavsky 2004) and similar patterns of binding to destabilizing N-terminal residues (Kwon et al 2003), both UBR1 and UBR2 have unique but also overlapping substrates for ubiquitin ligation and thereby degradation and thus UBR1 or UBR2 deletions alone were not severely lethal. However, severe lethality was observed in UBR1 and UBR2 double knockout mice due to the fact that in these animals substrate modification and thus degradation is completely abolished. This underlines the necessity of understanding the collections of specific substrates of either UBR1

or UBR2 in specific cell type or tissue (An et al 2006). Our hypothesis was that deletion of UBR1 leads to metabolic stabilization of its direct substrates in pancreas, which can give rise to the several defects in JBS patients and UBR1 knockout mice as well. Till now few substrates were reported as N-end-rule pathway substrates (see introduction) but there is not a single report about unique and direct substrates of any specific E3 Ub ligases (e.g. UBR1, UBR2 etc.,). Hence we studied the UBR1 dependent changes in the proteome using 2D-DIGE, expecting upregulation of the proteins which are stabilized in the absence of UBR1.

In the DIGE experiment in the murine model of experimental pancreatitis we comparatively profiled wild type and UBR1 knockout mice after treatment with caerulein inducing pacreatitis and control groups treated with saline (Fig. 31). These comparisons revealed that after induction of pancreatitis much more differences were observed between UBR1 knockout and wild type mice than in the controls treated with saline only. However, of the 55 proteins spots differing in intensity between wild type mice and UBR1 knockout mice (Table 8) after saline treatment almost 50% (27 spots) were also revealing differences in intensity after treatment with caerulein (Fig. 34). MS identification of the proteins displaying differential intensities and uniquely displaying differences after caerulein treatment revealed proteins which are involved in severe form of pancreatitis (proteases), ER stress (chaperons), inflammation and Ca^{+2} regulated pathways (Table 7). Almost 70% (68 out of 95) of the proteins which were up regulated in caerulein treated condition in UBR1 knockout mice pancreas follow the N-end-rule i.e. these proteins contain destabilizing amino acid at their N terminus (Table 7). This supports our notion and experimental strategy that UBR1 substrates, which are stabilized due to UBR1 deletion should display increased levels and might thus be contributing to the more severe form of pancreatitis observed in UBR1 knockout mice compared to wild type mice. For example proteases like chymotrypsin, anionic trypsin and other enzymes like alpha-amylase, lipase, were present at higher levels in the pancreas of UBR1 knockout mice compared to UBR1 wild type mice when treated with caerulein. For these proteases and enzymes, increased activity was confirmed by enzymatic assays using pancreatic homogenates and serum. It was confirmed that lipase and amylase levels were significantly higher in UBR1 knockout mice serum (Fig. 36) and this holds true for trypsin and elastase activities as well in pancreatic homogenates (Fig. 38). Using enterokinase to activate all pre-existing non-active forms of the proteases we could show that there is no difference in basal level of expression of trypsinogen and pro-elastase which are precursors of active forms of trypsin and elastase, respectively, between the UBR1 knockout and wild type mice (Fig. 39). hinting there is higher magnitude of response in UBR1 knockout mice to the

secretagogue, probably due to fact that active forms of these enzymes are stabilized because of lack of degradation in absence of UBR1.

Apart from proteases, proteins related to ER stress such as GRP78, PDI (Protein Disulfide Isomerase), HSC 71, hypoxia upregulated protein 1, ERp27, endoplasmin were present at higher levels in the UBR1 knockout and for Glutathione S-transferase P1, HSP90 reduced amounts compared to the wild type were observed (Table 7). The adaptive responses to ER stress provide protection from cell death in part by inducing the over expression of GRP78 or PDI (Liu et al 1997, Tanaka et al 2000). HSP70 and HSP27 were shown to exert a protective role and are normally increased after induction of pancreatitis (Bhagat et al 2000, Ethridge et al 2000, Frossard et al 2002). The endoplasmic reticulum (ER) is a central organelle of each eukaryotic cell as the place of lipid synthesis, protein folding and protein maturation. Normally proteins fold into their tertiary and quaternary structures in the ER. It can be assumed that deletion of UBR1, which is very important component of proteolytic system, will lead to accumulation of its direct substrates being rescued from degradation and thereby inducing a heavy load on ER and resulting in unfolded protein response or ER stress. It was reported that early activation of ER stress is associated with arginine induced acute pancreatitis (Kubisch et al 2006). The pancreas has one of the highest rates of protein synthesis in the body and possesses a particularly abundant ER. Furthermore, insults including oxidative stress and excessive Ca^{+2} release from ER stores, which are known to activate ER stress (Paschen and Doutheil 1999), are also associated with acute pancreatitis (Schulz et al 1999, Sutton et al 2003). There are three different and key ER stress transducers localized on the ER membrane which are constitutively expressed in all cells and activated during ER stress. They are-

1) PKR like endoplasmic reticulum kinase (PERK) activation of which involves autophosphorylation and leads to the subsequent phosphorylation of eukaryotic initiation factor (eIF2α) and decrease in translation initiation (Harding et al 1999, Liu et al 2000).

2) Activating transcription factor 6 (ATF6) activation of which leads to increased transcription of ER chaperones including GRP78 and protein folding enzymes which alleviate ER stress (Shen et al 2002, Ye et al 2000). Release of GRP78 from the N terminus of ATF6 frees ATF6 to translocate to the nucleus eventually and regulate gene expression.

3) Inositol required enzyme 1(IRE1) activation of which causes splicing and activation
of the transcription factor XBP1 that is also involved in regulation of expression of
different chaperones (Calfon et al 2002).

It is worth noting that ER stress indications like enlargement of ER at electron microscopic
level was observed in pancreas samples of JBS patients also (Mayerle J et al., unpublished
data). However, being aware of the fact that we didn't perform any experiments to prove this
thesis, one can envision using chemical chaperones to reduce ER stress thereby reducing the
severity of disease in case of JBS like it was shown in diabetes mouse model (Ozcan et al
2006).

Besides ER stress, among the proteins showing significantly different levels in
caerulein-treated UBR1 knockout mice compared to wild type mice inflammation related
proteins like leukocyte elastae inhibitor A and Toll-interacting protein were upregulated and
lithostathine 2 was downregulated (Table 7). Toll-interacting protein which is also known as
TOLLIP binds to IL-1RI (Interleukin 1 receptor type I) complex as well as TLR2 (Toll like
receptor 2) and TLR4 (Toll like receptor 4) complexes, which are key components of innate
immunity system to elicit inflammation reactions (Bulut et al 2001, Zhang and Ghosh 2002).
TOLLIP was shown to control the magnitude of the inflammatory cytokine production (IL-6
and TNF-α) in response to minimal dosage of IL-1β and LPS (Didierlaurent et al 2006). In
accordance with these previous findings in experimental pancreatitis model studied in this
thesis UBR1 knockout mice displayed higher levels of TOLLIP, which might be involved in
stronger inflammatory response and cytokines production.

CBA kit analysis of serum samples was done to explore which cytokines were
released at higher levels in UBR1 knockout mice compared to the wild type. CBA kit analysis
revealed that TNF-a, IL-6 and MCP-1 were released in significantly higher amounts in UBR1
knockout mice compared to wild type mice (Fig. 40). It was reported that oxidative stress and
pro-inflammatory cytokines trigger common signal transduction pathways that lead to
amplification of the inflammatory cascade (Pereda et al 2006). Moreover, we could observe
stronger neutrophil infiltration after induction of pancreatitis, which can be interpreted as
direct evidence at the histological level of more inflammation in the pancreas of UBR1 wild
type mice compared to knockout mice. To assess the severity of the UBR1 knockout
phenotype at the tissue level we stained the pancreas and lung sections with Haematoxylin
and Eosin (HE). Lung HE stained sections revealed that there was more local damage and
neutrophil infiltration in UBR1 wild type mice compared to knockout mice (Fig. 43). With
pancreatic tissue sections it was observed that there was more necrosis and infiltration in

UBR1 wild type mice compared to knockout mice after induction of pancreatitis with caerulein. The histological scoring of pancreas sections provided supporting evidence that the severity of pancreatitis was significantly stronger in UBR1 knockout mice based on the 1) necrosis 2) vacuolization and 3) inflammation/infiltration (Fig. 44). The observed stronger infiltration by neutrophils into lung and pancreas sections was in accordance with the observed higher myeloperoxidase (MPO) activities in both lung and pancreas homogenates of UBR1 wild type mice compared to knockout mice (Fig. 37). *In vivo* studies using isolated acinar cells also supported the notion that the necrosis rate is much more pronounced in UBR1 wild type mice compared to knockout mice (Fig. 42). TUNEL assay showed that there was more apoptosis in wild type compared to UBR1 knockout mice (Fig. 45). In human and experimental pancreatitis acinar cells die through both necrosis and apoptosis (Frossard et al 2003, Gukovskaya et al 1996, He et al 2000, Kaiser et al 1996, Rau et al 2001, Walker 1987). Apoptosis occurs not only in acinar cells stimulated with supraphysiological doses of CCK-8 but also *in vivo* in caerulein induced pancreatitis (Gukovsky et al 2003). While apoptosis often provides beneficial effects to the organism, necrosis is almost always detrimental and can be fatal. In UBR1 knockout mice severe pancreatitis is associated with more necrosis and less apoptosis as shown in results, which might be resemble the JBS patients' pathological status. Though we did not analyse the cell death pathway mechanism responsible for death of acinar cells in detail, the apoptosis and necrosis balance could be targeted for alleviation of severity of exocrine pancreatic insufficiency in JBS patients and improved outcome.

So far we described the differences between UBR1 knockout and wild type phenotypes at the proteome, histology and protease activation level. After having clarified that UBR1 knockout mice display a more severe form of pancreatitis compared to wild type mice we tried to elucidate the mechanism responsible for this severe phenotype by rescue experiments. From our 2D-DIGE and enzymatic assay results we suspected that impaired degradation of the active form of trypsin in the absence of UBR1could be the main reason for increased protease activation in UBR1 knockout mice (Table 6). It is well known that acute pancreatitis is an autolytic process, where activated pancreatic enzymes are found within (Hofbauer et al 1998, Leach et al 1991, Mithofer et al 1998) and subsequently around acinar cells, precipitated by ductal hypertension, bile salts, ethanol, ischaemia, hypercalcaemia, hyperlipidaemia, viral infections, drugs or toxins (Neoptolemos et al 1998, Ward et al 1995). So far it is evident that initial changes during pancreatitis which consist of apical enzyme activation, cytoskeletal disruption, loss of secretory polarity, vacuolization, co-localisation of zymogen granules and lysosomes and expression of pro-inflammatory cytokines take place

intracellulary (Gorelick and Matovcik 1995, Gukovskaya et al 1997, Niederau et al 1990, O'Konski and Pandol 1990, Ward et al 1996). It is still not known which of the many pro-enzymes of acinar cells can initiate acute pancreatitis. There is substantial evidence in favor of trypsinogen as the critical mediator (Neoptolemos et al 2000, Pfutzer et al 2000, Sahin-Toth 2001, Whitcomb et al 1996) and it was firmly established that highly purified trypsin cannot only activate other serine protease precursors, but also can convert itself from the inactive trypsinogen form to active trypsin (Kunitz and Northrop 1935, Northrop and Kunitz 1931). However, at least in rodents intrapancreatic trypsinogen activation depends significantly on the presence of cathepsin B in the pancreas (Halangk et al 2000, Saluja et al 1997) and auto-activation is not the cause of pancreatitis. Using a cell permeable, reversible and specific trypsin inhibitor S-124 Halangk W et al. showed that trypsin activity is not involved in premature, intrapancreatic trypsinogen activation (Halangk et al 2002) and suspected that there could be an unidentified mechanism for the rapid degradation of activated trypsin other than serine proteases which can be inhibited by S-124. We tested the hypothesis that this activated trypsin is degraded by a UBR1 dependent proteolytic system. It is interesting to note that the active form of trypsin which is overrepresented in UBR1 knockout mice consists of 224 amino acids (for both anionic and cationic forms) and starts with isoleucine (I), which is a type-2 bulky hydrophobic destabilizing amino acids category according to N-end-rule pathway. It was found in acinar cells that in the presence of S-124, trypsin can be inhibited but removal of S-124 leads to even higher levels of trypsin activation in UBR1 knockout mice aswell as wild type mice in presence of supramaximal concentrations of CCK-8 (10 nM) (Fig. 46). If trypsin would be a direct substrate of UBR1 we should have seen much more activation of trypsin in UBR1 knockout mice after removal of S-124 due to impaired degradation. Thus, it was concluded that trypsin even if it bears a targetable N-degron does not cause the observed phenotypic effects by being a direct substrate of UBR1.

After ruling out trypsin as a functionally important direct substrate of UBR1, we focused on the upstream signalling cascade leading to protease activation to explain the severe UBR1 knockout phenotype. From the list of known N-end rule pathway substrates (Table 2) Regulators of G protein signalling (RGS) proteins RGS4 and RGS5 seems to be promising targets as they serve as upstream negative regulators of protease activation by regulating Ca^{+2} signalling pathways in response to secretagogue (CCK-8, caerulein) stimulation through CCK receptors, which belongs to the family of G protein coupled receptors (GPCR). G proteins of the $G\alpha_q$ class transduce Ca^{+2} signalling through PLCβ (Hepler and Gilman 1992). Stimulation of acinar cells with a physiological concentration of cholecystokinin (up to 10^-

^{10}M) elicits repetitive cytosolic calcium spikes, primarily due to release of calcium from intracellular stores (Berridge et al 2000, Berridge et al 2003, Williams 2001). Such calcium spikes evoke normal secretion, but not premature trypsinogen activation. On the other hand, cholecystokinin stimulation at supramaximal concentration (10^{-6} M) evokes a sustained elevation of the cytosolic calcium level that induces trypsinogen activation (Kruger et al 2000, Raraty et al 2000) *in vivo*. Cholecystokinin hyper stimulation has been found to induce acute pancreatitis in all species that have been examined (Sutton et al 2003). Prolonged elevations of cytosolic calcium can activate degradative calcium-dependent enzymes, leading to necrosis or apoptosis (Nicotera et al 1992). Ca^{+2} signalling in pancreatic acini triggers the exocytic release of digestive enzymes from granules adjacent to the secretory membrane (Muallem and Lee 1997). Being aware of the published data on the role of calcium signalling in protease activation during pancreatitis we studied calcium signalling in detail using the calcium sensitive Fura-2 fluorescent dye in freshly isolated pancreatic acini from UBR1 knockout and wild type mice. It was very clear from the calcium signalling results that there was sustained release of Ca^{+2} and more trypsin and elastase activity in acinar cells of UBR1 knockout mice, whereas in wild type mice acinar cells systematic oscillations of calcium release peaks was observed (Fig. 47). Earlier Kruger et al. (Kruger et al 2000) showed that protease activation is highly dependent on the spatial and temporal distribution of the corresponding Ca^{+2} release in pancreatic acinar cells. Hence, this sustained Ca^{+2} release and higher levels of protease activities could be the main factor behind the observed severe pancreatitis in UBR1 knockout mice compared to the respective wild type. Though there are experimental data that patho-physiological calcium signalling is a trigger of acute pancreatitis (Frick et al 1997, Kruger et al 2000, Raraty et al 2000, Saluja et al 1999) in accordance of our results, so far there is no obvious target that could be manipulated therapeutically.

Hence we tried to target RGS proteins, which are known negative regulators of CCK receptors (GPCR) in calcium signalling to counteract the severe phenotype observed upon loss of UBR1. Western blot experiments revealed that RGS4 might be a specific substrate of UBR1 as RGS4 is accumulated in UBR1 knockout mice irrespective of caerulein treatment but not in wild type mice (Fig. 47A). This effect was specific for RGS4 because RGS5 levels wer not influenced by loss of UBR1 (data not shown). To the best of our knowledge this is the first report about specific substrates for a specific UBR-ligase, since so far N-end rule pathway substrates have been reported (Table 2) without specifying the type of UBR ligase involved in the degradation. GPCR signal transduction mediated by heterotrimeric G proteins (Gαβγ) elicit responses in every organ system by nucleotide-driven conformational changes

and evoke such diverse outcomes as neurotransmission, immunity, cardiovascular function and hormone secretion (Gilman 1987, Kaziro et al 1991, Neer 1995, Saluja et al 2007, Xu et al 1999). Almost 60% of all pharmaceutical agents in current use target GPCRs, making detailed understanding of their intracellular signalling routes critical for the treatment of human disease (Pierce et al 2002). Regulators of G protein signalling (RGS) proteins bind to activated G α subunits and accelerate their intrinsic GTPase activity (GAP) (Blumer 2004, He et al 1998). As RGS proteins GAP activity hastens G protein deactivation, RGS proteins would be predicted to reduce signalling output elicited by GPCR activation. Later on many reports established that RGS proteins were negative regulators of G-protein mediated signalling in part due to their GAP activity mostly for the Gi or Gq classes of G proteins (De Vries et al 2000, Huang et al 1997, Ross and Wilkie 2000, Willars 2006, Yan et al 1997). So far more than 30 types of RGS proteins were found in mammalian cells and subdivided into subfamilies based on their primary sequence homology and presence of additional domains (Abramow-Newerly et al 2006a, Abramow-Newerly et al 2006b). Due to their unique capacity to modulate G protein signalling combined with their highly differential expression in different organs, RGS proteins have been eyed as important new drug targets (Neubig and Siderovski 2002, Zhong and Neubig 2001). On the basis of sequence similarities in their Galpha-subunits, G proteins have been grouped into four subfamilies: $G\alpha_s$, $G\alpha_{i/o}$, $G\alpha_q$ and $G\alpha_{12}$.

Among RGS proteins, RGS4 belongs to the R4/B subfamily of RGS proteins and acts as G protein specific GTPase activating protein (Neves et al 2002). In both humans and rodents RGS4 appears to be selectively enriched in the CNS and heart (Erdely et al 2004, Zhang et al 1998). Through human genetic studies RGS4 has emerged as a candidate susceptibility gene for schizophrenia (Chen et al 2004, Chowdari et al 2002, Morris et al 2004, Williams et al 2004) and has been reported to be downregulated in postmortem cortices of schizophrenic patients (Mirnics et al 2001). RGS4 appears to be up regulated in patients and animal models with heart dysfunction (Mittmann et al 2002, Owen et al 2001). RGS4 knockout mice were found to have normal neuronal development, are viable and fertile and didn't exhibit any substantial behavioral abnormalities (Grillet et al 2005). Transgenic mice over expressing RGS4 in postnatal ventricular myocardium displayed upon transverse aortic constriction left ventricular dilatation, depressed systolic function and higher postoperative mortality, and failed to induce βMHC expression (Rogers et al 1999). *In vitro* studies suggest that RGS4 protein exhibit GAP activity toward different $G\alpha_i$ and/or $G\alpha_q$ but not $G\alpha_s$ or $G\alpha_{12}$

class of Gα subunits (Berman et al 1996a, Berman et al 1996b, Huang et al 1997, Yan et al 1997). Gα_q of G proteins transduce Ca^{+2} signals by coupling heptahelical transmembrane receptors to the β isoforms of phospholipase C (PLC) (Hepler and Gilman 1992). Pancreatic acinar cells respond to acetylecholine, bombesin and cholecystokinin (CCK) by intense activation of PLC to generate IP3 and mobilize Ca^{+2} from internal stores. These three agonists activate the same G$_q$ regulated signalling pathway to mobilize the same Ca^{+2} pool and each agonist evokes a distinct pattern of Ca^{+2} wave propagation (Xu et al 1996). Xu X et al. showed that RGS are involved in exhibiting different pattern of Ca^{+2} response and RGS4 regulates Ca^{+2} signalling by GTPase catalytic activity mechanism through Gα_q of G protein receptor signalling (Xu et al 1999). We have tested whether higher levels of RGS4 in UBR1 knockout mice would be involved in a pathological Ca^{+2} signalling response leading to severe pancreatitis (Fig. 47). RGS4 can be selectively inhibited by 1, methyl N-[(4-chlorophenyl) sulfonyl]-4-nitrobenzenesulfinimidoate (CCG-4986) with high efficacy (IC50 < 10 μM) on μ-opioid receptor mediated signalling (Roman et al 2007) _in vitro_. Moreover CCG-4986 is selective for RGS4 compared to RGS8, the most closely related RGS family member (Neubig 2002). Thus, we used CCG-4986 to selectively inhibit RGS4 in freshly isolated pancreatic acini in UBR1 knockout mice and tested protease activation and Ca^{+2} signalling. Interestingly, CCG-4986 at 10 μM concentration could abolish trypsin activation almost completely (Fig. 48). We could successfully show for the first time that CCG-4986 can be used _in vivo_ and is cell permeable using freshly isolated pancreatic acini. Surprisingly, Xu X et al showed that RGS4 can inhibit Ca^{+2} signalling, but in UBR1 knockout mice presence of higher levels of RGS4 could not show any such inhibitory effect, in fact sustained elevation of Ca^{+2} signalling was observed in UBR1 knockout mice in pancreatic acinar cells when challenged with supramaximal concentration of CCK. It would be interesting to elucidate from Gq or Gi coupled receptors, what is rendering in sustained Ca^{+2} elevation signalling in UBR1 knockout mice. Interestingly, there was a recent report that a human RGS4^{S30C} mutant showed a gain of function (GOF) mutation _in vitro_ in _Schizosaccharomyces Pombe_ (Hill et al 2008) pointing to different action of RGS in different pathological scenarios. Gain of function mutations in the RGS4 gene could be a predisposing genetic factor for idiopathic chronic pancreatitis in humans. Thus, we are now screening patients' samples for possible RGS4 mutations as risk factor in acute pancreatitis. With the CCG-4986 inhibition assay we could convincingly show that RGS4 might be an attractive new therapeutic target for the treatment of pancreatitis lying upstream of premature zymogen activation.

Conclusions:

In summary, using UBR1 knockout mice in an experimental pancreatitis model we could show increased expression levels of proteases, disturbed expression of ER stress related and Ca^{+2} signalling related proteins as well as inflammation related proteins using a proteomics based approach. Furthermore, we confirmed our findings from proteomics experiments with an time course animal model of experimental pancreatitis using specific protease enzymatic assays. In isolated pancreatic acini of UBR1 knockout mice we found a significant increase in intracellular trypsin activation and rate of necrosis already upon physiological CCK-stimulation (CCK 0.1 nM). A lack of degradation of activated trypsin due to the UBR1 knockout was excluded by inhibition with the reversible trypsin inhibitor S124. Calcium analysis after physiological stimulation revealed an increase of pathological Ca^{+2} signalling events, i.e. significant decrease of spike number and significant increase of spike duration. Western blot analysis showed increased levels of RGS4 in UBR1 knockout animals compared to wild type animals. Pre-incubation of UBR1 knockout pancreatic acini with a specific RGS4 inhibitor (CCG-4986, 10 μM) normalized Ca^{+2} pattern and prevented premature trypsin activation. CCG-4986 did not affect trypsin activity itself. In acinar cells of UBR1 knockout mice pathophysiological signalling pathways were followed by acinar destruction, which could be abolished by RGS4 inhibition, suggesting a vital function of UBR1 and RGS4 in the defense against pathologic pancreatic damage and JBS as an inflammatory disorder due to an inadequate UBR1 defense.

7. References

Abramow-Newerly M, Ming H, Chidiac P (2006a). Modulation of subfamily B/R4 RGS protein function by 14-3-3 proteins. *Cellular signalling* **18:** 2209-2222.

Abramow-Newerly M, Roy AA, Nunn C, Chidiac P (2006b). RGS proteins have a signalling complex: interactions between RGS proteins and GPCRs, effectors, and auxiliary proteins. *Cellular signalling* **18:** 579-591.

Aebersold R (2003). A mass spectrometric journey into protein and proteome research. *Journal of the American Society for Mass Spectrometry* **14:** 685-695.

Ahram M, Emmert-Buck MR (2003). Approaches to proteomic analysis of human tumors. *Methods in molecular biology (Clifton, NJ* **222:** 375-384.

Al-Dosari MS, Al-Muhsen S, Al-Jazaeri A, Mayerle J, Zenker M, Alkuraya FS (2008). Johanson-Blizzard syndrome: report of a novel mutation and severe liver involvement. *Am J Med Genet A* **146A:** 1875-1879.

Alkhouri N, Kaplan B, Kay M, Shealy A, Crowe C, Bauhuber S *et al* (2008). Johanson-Blizzard syndrome with mild phenotypic features confirmed by UBR1 gene testing. *World J Gastroenterol* **14:** 6863-6866.

Almasan A, Yin Y, Kelly RE, Lee EY, Bradley A, Li W *et al* (1995). Deficiency of retinoblastoma protein leads to inappropriate S-phase entry, activation of E2F-responsive genes, and apoptosis. *Proc Natl Acad Sci U S A* **92:** 5436-5440.

An JY, Seo JW, Tasaki T, Lee MJ, Varshavsky A, Kwon YT (2006). Impaired neurogenesis and cardiovascular development in mice lacking the E3 ubiquitin ligases UBR1 and UBR2 of the N-end rule pathway. *Proceedings of the National Academy of Sciences of the United States of America* **103:** 6212-6217.

Andersen S, Heine T, Sneve R, Konig I, Krokan HE, Epe B *et al* (2005). Incorporation of dUMP into DNA is a major source of spontaneous DNA damage, while excision of uracil is not required for cytotoxicity of fluoropyrimidines in mouse embryonic fibroblasts. *Carcinogenesis* **26:** 547-555.

Anderson L, Seilhamer J (1997). A comparison of selected mRNA and protein abundances in human liver. *Electrophoresis* **18:** 533-537.

Arlotta P, Molyneaux BJ, Chen J, Inoue J, Kominami R, Macklis JD (2005). Neuronal subtype-specific genes that control corticospinal motor neuron development in vivo. *Neuron* **45:** 207-221.

Arpin M, Algrain M, Louvard D (1994). Membrane-actin microfilament connections: an increasing diversity of players related to band 4.1. *Curr Opin Cell Biol* **6:** 136-141.

Asara JM, Christofk HR, Freimark LM, Cantley LC (2008). A label-free quantification method by MS/MS TIC compared to SILAC and spectral counting in a proteomics screen. *Proteomics* **8:** 994-999.

Avram D, Fields A, Pretty On Top K, Nevrivy DJ, Ishmael JE, Leid M (2000a). Isolation of a novel family of C(2)H(2) zinc finger proteins implicated in transcriptional repression mediated by chicken ovalbumin upstream promoter transcription factor (COUP-TF) orphan nuclear receptors. *J Biol Chem* **275:** 10315-10322.

Avram D, Fields A, Pretty On Top K, Nevrivy DJ, Ishmael JE, Leid M (2000b). Isolation of a novel family of C(2)H(2) zinc finger proteins implicated in transcriptional repression mediated by chicken ovalbumin upstream promoter transcription factor (COUP-TF) orphan nuclear receptors. *Journal of Biological Chemistry* **275:** 10315-10322.

Avram D, Fields A, Senawong T, Topark-Ngarm A, Leid M (2002). COUP-TF (chicken ovalbumin upstream promoter transcription factor)-interacting protein 1 (CTIP1) is a sequence-specific DNA binding protein. *Biochemical Journal* **368:** 555-563.

Bachmair A, Finley D, Varshavsky A (1986). In vivo half-life of a protein is a function of its amino-terminal residue. *Science (New York, NY* **234:** 179-186.

Balogh SA, McDowell CS, Denenberg VH (2002). Behavioral characterization of mice lacking the ubiquitin ligase UBR1 of the N-end rule pathway. *Genes, brain, and behavior* **1:** 223-229.

Bantscheff M, Schirle M, Sweetman G, Rick J, Kuster B (2007). Quantitative mass spectrometry in proteomics: a critical review. *Analytical and bioanalytical chemistry* **389:** 1017-1031.

Berggren K, Chernokalskaya E, Steinberg TH, Kemper C, Lopez MF, Diwu Z *et al* (2000). Background-free, high sensitivity staining of proteins in one- and two-dimensional sodium dodecyl sulfate-polyacrylamide gels using a luminescent ruthenium complex. *Electrophoresis* **21:** 2509-2521.

Berman DM, Kozasa T, Gilman AG (1996a). The GTPase-activating protein RGS4 stabilizes the transition state for nucleotide hydrolysis. *The Journal of biological chemistry* **271:** 27209-27212.

Berman DM, Wilkie TM, Gilman AG (1996b). GAIP and RGS4 are GTPase-activating proteins for the Gi subfamily of G protein alpha subunits. *Cell* **86:** 445-452.

Berridge MJ, Lipp P, Bootman MD (2000). The versatility and universality of calcium signalling. *Nature reviews* **1:** 11-21.

Berridge MJ, Bootman MD, Roderick HL (2003). Calcium signalling: dynamics, homeostasis and remodelling. *Nature reviews* **4:** 517-529.

Bhagat L, Singh VP, Hietaranta AJ, Agrawal S, Steer ML, Saluja AK (2000). Heat shock protein 70 prevents secretagogue-induced cell injury in the pancreas by preventing intracellular trypsinogen activation. *The Journal of clinical investigation* **106:** 81-89.

Bjellquist B, Sachez JC, Pasquali C, Ravier F, Paquet N, Frutiger S *et al* (1993). Micropreparative two-dimensional electrophoresis allowing the separation of samples containing milligram amounts of proteins. *Electrophoresis* **14:** 1375-1378.

Bjellqvist B, Ek K, Righetti PG, Gianazza E, Gorg A, Westermeier R *et al* (1982). Isoelectric focusing in immobilized pH gradients: principle, methodology and some applications. *J Biochem Biophys Methods* **6:** 317-339.

Black DL (2003). Mechanisms of alternative pre-messenger RNA splicing. *Annual review of biochemistry* **72:** 291-336.

Blumer KJ (2004). Vision: the need for speed. *Nature* **427:** 20-21.

Bockaert J, Pin JP (1999). Molecular tinkering of G protein-coupled receptors: an evolutionary success. *EMBO J* **18:** 1723-1729.

Boehning D, Patterson RL, Sedaghat L, Glebova NO, Kurosaki T, Snyder SH (2003). Cytochrome c binds to inositol (1,4,5) trisphosphate receptors, amplifying calcium-dependent apoptosis. *Nature cell biology* **5**: 1051-1061.

Brockstedt E, Rickers A, Kostka S, Laubersheimer A, Dorken B, Wittmann-Liebold B *et al* (1998). Identification of apoptosis-associated proteins in a human Burkitt lymphoma cell line. Cleavage of heterogeneous nuclear ribonucleoprotein A1 by caspase 3. *J Biol Chem* **273:** 28057-28064.

Buckley AF, Kuo CT, Leiden JM (2001). Transcription factor LKLF is sufficient to program T cell quiescence via a c-Myc--dependent pathway. *Nat Immunol* **2:** 698-704.

Buffa R, Solcia E, Go VL (1976). Immunohistochemical identification of the cholecystokinin cell in the intestinal mucosa. *Gastroenterology* **70:** 528-532.

Bulut Y, Faure E, Thomas L, Equils O, Arditi M (2001). Cooperation of Toll-like receptor 2 and 6 for cellular activation by soluble tuberculosis factor and Borrelia burgdorferi outer

surface protein A lipoprotein: role of Toll-interacting protein and IL-1 receptor signaling molecules in Toll-like receptor 2 signaling. *J Immunol* **167:** 987-994.

Byrd C, Turner GC, Varshavsky A (1998). The N-end rule pathway controls the import of peptides through degradation of a transcriptional repressor. *The EMBO journal* **17:** 269-277.

Byun Y, Chen F, Chang R, Trivedi M, Green KJ, Cryns VL (2001). Caspase cleavage of vimentin disrupts intermediate filaments and promotes apoptosis. *Cell Death Differ* **8:** 443-450.

Calfon M, Zeng H, Urano F, Till JH, Hubbard SR, Harding HP *et al* (2002). IRE1 couples endoplasmic reticulum load to secretory capacity by processing the XBP-1 mRNA. *Nature* **415:** 92-96.

Chalut C, Moncollin V, Egly JM (1994). Transcription by RNA polymerase II: a process linked to DNA repair. *Bioessays* **16:** 651-655.

Chen X, Dunham C, Kendler S, Wang X, O'Neill FA, Walsh D *et al* (2004). Regulator of G-protein signaling 4 (RGS4) gene is associated with schizophrenia in Irish high density families. *Am J Med Genet B Neuropsychiatr Genet* **129B:** 23-26.

Cherrier T, Suzanne S, Redel L, Calao M, Marban C, Samah B *et al* (2009). p21(WAF1) gene promoter is epigenetically silenced by CTIP2 and SUV39H1. *Oncogene* **28:** 3380-3389.

Chowdari KV, Mirnics K, Semwal P, Wood J, Lawrence E, Bhatia T *et al* (2002). Association and linkage analyses of RGS4 polymorphisms in schizophrenia. *Human molecular genetics* **11:** 1373-1380.

Cismasiu VB, Adamo K, Gecewicz J, Duque J, Lin Q, Avram D (2005). *BCL11B* functionally associates with the NuRD complex in T lymphocytes to repress targeted promoter. *Oncogene* **24:** 6753-6764.

Cismasiu VB, Ghanta S, Duque J, Albu DI, Chen HM, Kasturi R *et al* (2006). *BCL11B* participates in the activation of IL2 gene expression in CD4+ T lymphocytes. *Blood* **108:** 2695-2702.

Cismasiu VB, Paskaleva E, Suman Daya S, Canki M, Duus K, Avram D (2008). *BCL11B* is a general transcriptional repressor of the HIV-1 long terminal repeat in T lymphocytes through recruitment of the NuRD complex. *Virology* **380:** 173-181.

Cismasiu VB, Duque J, Paskaleva E, Califano D, Ghanta S, Young HA *et al* (2009). *BCL11B* enhances TCR/CD28-triggered NF-kappaB activation through up-regulation of Cot kinase gene expression in T-lymphocytes. *Biochemical Journal* **417:** 457-466.

Cuschieri A (2002). Anorectal anomalies associated with or as part of other anomalies. *American journal of medical genetics* **110:** 122-130.

Daentl DL, Frias JL, Gilbert EF, Opitz JM (1979). The Johanson-Blizzard syndrome: case report and autopsy findings. *American journal of medical genetics* **3:** 129-135.

Davies TH, Sanchez ER (2005). Fkbp52. *The international journal of biochemistry & cell biology* **37:** 42-47.

Davydov IV, Varshavsky A (2000). RGS4 is arginylated and degraded by the N-end rule pathway in vitro. *The Journal of biological chemistry* **275:** 22931-22941.

de Groot RJ, Rumenapf T, Kuhn RJ, Strauss EG, Strauss JH (1991). Sindbis virus RNA polymerase is degraded by the N-end rule pathway. *Proceedings of the National Academy of Sciences of the United States of America* **88:** 8967-8971.

De Vries L, Zheng B, Fischer T, Elenko E, Farquhar MG (2000). The regulator of G protein signaling family. *Annual review of pharmacology and toxicology* **40:** 235-271.

Deutsch WA (1995). Why do pupating insects lack an activity for the repair of uracil-containing DNA? One explanation involves apoptosis. *Insect Mol Biol* **4:** 1-5.

Didierlaurent A, Brissoni B, Velin D, Aebi N, Tardivel A, Kaslin E *et al* (2006). Tollip regulates proinflammatory responses to interleukin-1 and lipopolysaccharide. *Molecular and cellular biology* **26:** 735-742.

Dudek J, Benedix J, Cappel S, Greiner M, Jalal C, Muller L *et al* (2009). Functions and pathologies of BiP and its interaction partners. *Cell Mol Life Sci* **66:** 1556-1569.

Durum SK (2003). Bcl11: sibling rivalry in lymphoid development. *Nat Immunol* **4:** 512-514.

Elting M, Kariminejad A, de Sonnaville ML, Ottenkamp J, Bauhuber S, Bozorgmehr B *et al* (2008). Johanson-Blizzard syndrome caused by identical UBR1 mutations in two unrelated girls, one with a cardiomyopathy. *Am J Med Genet A* **146A:** 3058-3061.

Eng JK, McCormack AL, Yates JR (1994). An approach to correlate tandem mass spectral data of peptides with amino acid sequences in a protein database. *J Am Soc Mass Spec* **5:** 976-989.

Erdely HA, Lahti RA, Lopez MB, Myers CS, Roberts RC, Tamminga CA *et al* (2004). Regional expression of RGS4 mRNA in human brain. *The European journal of neuroscience* **19:** 3125-3128.

Ethridge RT, Ehlers RA, Hellmich MR, Rajaraman S, Evers BM (2000). Acute pancreatitis results in induction of heat shock proteins 70 and 27 and heat shock factor-1. *Pancreas* **21:** 248-256.

Evan GI, Wyllie AH, Gilbert CS, Littlewood TD, Land H, Brooks M *et al* (1992). Induction of apoptosis in fibroblasts by c-myc protein. *Cell* **69:** 119-128.

Eymann C, Dreisbach A, Albrecht D, Bernhardt J, Becher D, Gentner S *et al* (2004). A comprehensive proteome map of growing *Bacillus subtilis* cells. *Proteomics* **4:** 2849-2876.

Fadeel B, Gleiss B, Hogstrand K, Chandra J, Wiedmer T, Sims PJ *et al* (1999). Phosphatidylserine exposure during apoptosis is a cell-type-specific event and does not correlate with plasma membrane phospholipid scramblase expression. *Biochemical and biophysical research communications* **266:** 504-511.

Fenn JB, Mann M, Meng CK, Wong SF, Whitehouse CM (1989). Electrospray ionization for mass spectrometry of large biomolecules. *Science (New York, NY* **246:** 64-71.

Fesquet D, Labbe JC, Derancourt J, Capony JP, Galas S, Girard F *et al* (1993). The MO15 gene encodes the catalytic subunit of a protein kinase that activates cdc2 and other cyclin-dependent kinases (CDKs) through phosphorylation of Thr161 and its homologues. *EMBO J* **12:** 3111-3121.

Frick TW, Fernandez-del Castillo C, Bimmler D, Warshaw AL (1997). Elevated calcium and activation of trypsinogen in rat pancreatic acini. *Gut* **41:** 339-343.

Frossard JL, Bhagat L, Lee HS, Hietaranta AJ, Singh VP, Song AM *et al* (2002). Both thermal and non-thermal stress protect against caerulein induced pancreatitis and prevent trypsinogen activation in the pancreas. *Gut* **50:** 78-83.

Frossard JL, Rubbia-Brandt L, Wallig MA, Benathan M, Ott T, Morel P *et al* (2003). Severe acute pancreatitis and reduced acinar cell apoptosis in the exocrine pancreas of mice deficient for the Cx32 gene. *Gastroenterology* **124:** 481-493.

Gafken PR, Lampe PD (2006). Methodologies for characterizing phosphoproteins by massspectrometry. *Cell Commun. Adhes* **13:** 249-262

Ganguli-Indra G, Wasylyk C, Liang X, Millon R, Leid M, Wasylyk B *et al* (2009). CTIP2 expression in human head and neck squamous cell carcinoma is linked to poorly differentiated tumor status. *PLoS One* **4:** e5367.

Ge Y, Rajkumar L, Guzman RC, Nandi S, Patton WF, Agnew BJ (2004). Multiplexed fluorescence detection of phosphorylation, glycosylation, and total protein in the proteomic analysis of breast cancer refractoriness. *Proteomics* **4:** 3464-3467.

Georgopoulos K (2002). Haematopoietic cell-fate decisions, chromatin regulation and ikaros. *Nat Rev Immunol* **2:** 162-174.

Gershoni-Baruch R, Lerner A, Braun J, Katzir Y, Iancu TC, Benderly A (1990). Johanson-Blizzard syndrome: clinical spectrum and further delineation of the syndrome. *American journal of medical genetics* **35:** 546-551.

Gharahdaghi F, Weinberg CR, Meagher DA, Imai BS, Mische SM (1999). Mass spectrometric identification of proteins from silver-stained polyacrylamide gel: a method for the removal of silver ions to enhance sensitivity. *Electrophoresis* **20:** 601-605.

Gilman AG (1987). G proteins: transducers of receptor-generated signals. *Annual review of biochemistry* **56:** 615-649.

Golonzhka O, Leid M, Indra G, Indra AK (2007). Expression of COUP-TF-interacting protein 2 (CTIP2) in mouse skin during development and in adulthood. *Gene Expr Patterns* **7:** 754-760.

Golonzhka O, Liang X, Messaddeq N, Bornert JM, Campbell AL, Metzger D *et al* (2009a). Dual role of COUP-TF-interacting protein 2 in epidermal homeostasis and permeability barrier formation. *Journal of Investigative Dermatology* **129:** 1459-1470.

Golonzhka O, Metzger D, Bornert JM, Bay BK, Gross MK, Kioussi C *et al* (2009b). Ctip2/Bcl11b controls ameloblast formation during mammalian odontogenesis. *Proc Natl Acad Sci U S A* **106:** 4278-4283.

Gonda DK, Bachmair A, Wunning I, Tobias JW, Lane WS, Varshavsky A (1989). Universality and structure of the N-end rule. *The Journal of biological chemistry* **264:** 16700-16712.

Gorczyca W, Gong J, Darzynkiewicz Z (1993). Detection of DNA strand breaks in individual apoptotic cells by the in situ terminal deoxynucleotidyl transferase and nick translation assays. *Cancer Res* **53:** 1945-1951.

Gorelick FS, Matovcik LM (1995). Lysosomal enzymes and pancreatitis. *Gastroenterology* **109:** 620-625.

Gorg A, Postel W, Domscheit A, Gunther S (1988a). Two-dimensional electrophoresis with immobilized pH gradients of leaf proteins from barley (Hordeum vulgare): method, reproducibility and genetic aspects. *Electrophoresis* **9:** 681-692.

Gorg A, Postel W, Gunther S (1988b). The current state of two-dimensional electrophoresis with immobilized pH gradients. *Electrophoresis* **9:** 531-546.

Gorg A, Postel W, Gunther S, Friedrich C (1988c). Horizontal two-dimensional electrophoresis with immobilized pH gradients using PhastSystem. *Electrophoresis* **9:** 57-59.

Grabarczyk P, Przybylski GK, Depke M, Völker U, Bahr J, Assmus K *et al* (2007). Inhibition of *BCL11B* expression leads to apoptosis of malignant but not normal mature T cells. *Oncogene* **26:** 3797-3810.

Grasser FA, Romeike BF, Niedobitek G, Nicholls J, Kremmer E (2001). dUTPase in human neoplastic cells as a potential target for therapeutic intervention. *Curr Protein Pept Sci* **2:** 349-360.

Grewal T, Enrich C (2006). Molecular mechanisms involved in Ras inactivation: the annexin A6-p120GAP complex. *Bioessays* **28:** 1211-1220.

Grillet N, Pattyn A, Contet C, Kieffer BL, Goridis C, Brunet JF (2005). Generation and characterization of Rgs4 mutant mice. *Molecular and cellular biology* **25:** 4221-4228.

Gukovskaya AS, Perkins P, Zaninovic V, Sandoval D, Rutherford R, Fitzsimmons T *et al* (1996). Mechanisms of cell death after pancreatic duct obstruction in the opossum and the rat. *Gastroenterology* **110:** 875-884.

Gukovskaya AS, Gukovsky I, Zaninovic V, Song M, Sandoval D, Gukovsky S *et al* (1997). Pancreatic acinar cells produce, release, and respond to tumor necrosis factor-alpha. Role in regulating cell death and pancreatitis. *The Journal of clinical investigation* **100:** 1853-1862.

Gukovskaya AS, Gukovsky I, Jung Y, Mouria M, Pandol SJ (2002). Cholecystokinin induces caspase activation and mitochondrial dysfunction in pancreatic acinar cells. Roles in cell injury processes of pancreatitis. *The Journal of biological chemistry* **277:** 22595-22604.

Gukovsky I, Reyes CN, Vaquero EC, Gukovskaya AS, Pandol SJ (2003). Curcumin ameliorates ethanol and nonethanol experimental pancreatitis. *American journal of physiology* **284:** G85-95.

Gygi SP, Rist B, Gerber SA, Turecek F, Gelb MH, Aebersold R (1999a). Quantitative analysis of complex protein mixtures using isotope-coded affinity tags. *Nature Biotechnology* **17:** 994-999.

Gygi SP, Rochon Y, Franza BR, Aebersold R (1999b). Correlation between protein and mRNA abundance in yeast. *Molecular and cellular biology* **19:** 1720-1730.

Halangk W, Lerch MM, Brandt-Nedelev B, Roth W, Ruthenbuerger M, Reinheckel T *et al* (2000). Role of cathepsin B in intracellular trypsinogen activation and the onset of acute pancreatitis. *The Journal of clinical investigation* **106:** 773-781.

Halangk W, Kruger B, Ruthenburger M, Sturzebecher J, Albrecht E, Lippert H *et al* (2002). Trypsin activity is not involved in premature, intrapancreatic trypsinogen activation. *American journal of physiology* **282:** G367-374.

Han KK, Martinage A (1992). Post-translational chemical modification(s) of proteins. *The International journal of biochemistry* **24:** 19-28.

Harding HP, Zhang Y, Ron D (1999). Protein translation and folding are coupled by an endoplasmic-reticulum-resident kinase. *Nature* **397:** 271-274.

He W, Cowan CW, Wensel TG (1998). RGS9, a GTPase accelerator for phototransduction. *Neuron* **20:** 95-102.

He ZJ, Podkletnova I, Alho H, Sand J, Nordback I (2000). Apoptosis in acute pancreatitis. *Annales chirurgiae et gynaecologiae* **89:** 65-67.

Hebert M, Potin S, Sebbagh M, Bertoglio J, Breard J, Hamelin J (2008). Rho-ROCK-dependent ezrin-radixin-moesin phosphorylation regulates Fas-mediated apoptosis in Jurkat cells. *J Immunol* **181:** 5963-5973.

Hedenfalk I, Duggan D, Chen Y, Radmacher M, Bittner M, Simon R *et al* (2001). Gene-expression profiles in hereditary breast cancer. *N Engl J Med* **344:** 539-548.

Henzel WJ, Billeci TM, Stults JT, Wong SC, Grimley C, Watanabe C (1993). Identifying proteins from two-dimensional gels by molecular mass searching of peptide fragments in protein sequence databases. *Proceedings of the National Academy of Sciences of the United States of America* **90:** 5011-5015.

Hepler JR, Gilman AG (1992). G proteins. *Trends in biochemical sciences* **17:** 383-387.

Hill C, Brownlie Z, Davey J, Milligan G, Ladds G (2008). Isolation and characterization of a novel human RGS mutant displaying gain-of-function activity. *Cellular signalling* **20:** 323-336.

Hofbauer B, Saluja AK, Lerch MM, Bhagat L, Bhatia M, Lee HS *et al* (1998). Intra-acinar cell activation of trypsinogen during caerulein-induced pancreatitis in rats. *The American journal of physiology* **275:** G352-362.

Howard J (2008). The IRG proteins: a function in search of a mechanism. *Immunobiology* **213:** 367-375.

Hu RG, Brower CS, Wang H, Davydov IV, Sheng J, Zhou J *et al* (2006). Arginyltransferase, its specificity, putative substrates, bidirectional promoter, and splicing-derived isoforms. *The Journal of biological chemistry* **281:** 32559-32573.

Huang C, Hepler JR, Gilman AG, Mumby SM (1997). Attenuation of Gi- and Gq-mediated signaling by expression of RGS4 or GAIP in mammalian cells. *Proceedings of the National Academy of Sciences of the United States of America* **94:** 6159-6163.

Hurst JA, Baraitser M (1989). Johanson-Blizzard syndrome. *Journal of medical genetics* **26:** 45-48.

Hwang CS, Shemorry A, Varshavsky A (2009). Two proteolytic pathways regulate DNA repair by cotargeting the Mgt1 alkylguanine transferase. *Proceedings of the National Academy of Sciences of the United States of America* **106:** 2142-2147.

Ishimi Y, Komamura-Kohno Y, Kwon HJ, Yamada K, Nakanishi M (2003). Identification of MCM4 as a target of the DNA replication block checkpoint system. *J Biol Chem* **278:** 24644-24650.

Ishimi Y, Komamura-Kohno Y, Karasawa-Shimizu K, Yamada K (2004). Levels of MCM4 phosphorylation and DNA synthesis in DNA replication block checkpoint control. *J Struct Biol* **146:** 234-241.

Ivetic A, Ridley AJ (2004). Ezrin/radixin/moesin proteins and Rho GTPase signalling in leucocytes. *Immunology* **112:** 165-176.

James P, Quadroni M, Carafoli E, Gonnet G (1994). Protein identification in DNA databases by peptide mass fingerprinting. *Protein Sci* **3:** 1347-1350.

James P (1997). Protein identification in the post-genome era: the rapid rise of proteomics. *Q Rev Biophys* **30:** 279-331.

Johanson A, Blizzard R (1971). A syndrome of congenital aplasia of the alae nasi, deafness, hypothyroidism, dwarfism, absent permanent teeth, and malabsorption. *The Journal of pediatrics* **79:** 982-987.

Kaczynski J, Cook T, Urrutia R (2003). Sp1- and Kruppel-like transcription factors. *Genome Biol* **4:** 206.

Kaiser AM, Saluja AK, Lu L, Yamanaka K, Yamaguchi Y, Steer ML (1996). Effects of cycloheximide on pancreatic endonuclease activity, apoptosis, and severity of acute pancreatitis. *The American journal of physiology* **271:** C982-993.

Kamimura K, Mishima Y, Obata M, Endo T, Aoyagi Y, Kominami R (2007a). Lack of Bcl11b tumor suppressor results in vulnerability to DNA replication stress and damages. *Oncogene* **26:** 5840-5850.

Kamimura K, Ohi H, Kubota T, Okazuka K, Yoshikai Y, Wakabayashi Y *et al* (2007b). Haploinsufficiency of Bcl11b for suppression of lymphomagenesis and thymocyte development. *Biochem Biophys Res Commun* **355:** 538-542.

Karas M, Hillenkamp F (1988). Laser desorption ionization of proteins with molecular masses exceeding 10,000 daltons. *Analytical chemistry* **60:** 2299-2301.

Karlsson A, Nordigarden A, Jonsson JI, Soderkvist P (2007). Bcl11b mutations identified in murine lymphomas increase the proliferation rate of hematopoietic progenitor cells. *BMC Cancer* **7:** 195.

Kato M, Fukuda H, Nonaka T, Imajoh-Ohmi S (2005). Cleavage of nonmuscle myosin heavy chain-A during apoptosis in human Jurkat T cells. *J Biochem* **137:** 157-166.

Kaziro Y, Itoh H, Kozasa T, Nakafuku M, Satoh T (1991). Structure and function of signal-transducing GTP-binding proteins. *Annual review of biochemistry* **60:** 349-400.

Klose J (1975). Protein mapping by combined isoelectric focusing and electrophoresis of mouse tissues. A novel approach to testing for induced point mutations in mammals. *Humangenetik* **26:** 231-243.

Knudsen KE, Booth D, Naderi S, Sever-Chroneos Z, Fribourg AF, Hunton IC *et al* (2000). RB-dependent S-phase response to DNA damage. *Mol Cell Biol* **20:** 7751-7763.

Koss M, Pfeiffer GR, 2nd, Wang Y, Thomas ST, Yerukhimovich M, Gaarde WA *et al* (2006). Ezrin/radixin/moesin proteins are phosphorylated by TNF-alpha and modulate permeability increases in human pulmonary microvascular endothelial cells. *J Immunol* **176:** 1218-1227.

Kruger B, Albrecht E, Lerch MM (2000). The role of intracellular calcium signaling in premature protease activation and the onset of pancreatitis. *The American journal of pathology* **157:** 43-50.

Kubisch CH, Sans MD, Arumugam T, Ernst SA, Williams JA, Logsdon CD (2006). Early activation of endoplasmic reticulum stress is associated with arginine-induced acute pancreatitis. *American journal of physiology* **291:** G238-245.

Kubisch CH, Logsdon CD (2008). Endoplasmic reticulum stress and the pancreatic acinar cell. *Expert review of gastroenterology & hepatology* **2:** 249-260.

Kunitz M, Northrop JH (1935). Crystalline Chymo-Trypsin and Chymo-Trypsinogen : I. Isolation, Crystallization, and General Properties of a New Proteolytic Enzyme and Its Precursor. *The Journal of general physiology* **18:** 433-458.

Kwon YT, Xia Z, Davydov IV, Lecker SH, Varshavsky A (2001). Construction and analysis of mouse strains lacking the ubiquitin ligase UBR1 (E3alpha) of the N-end rule pathway. *Molecular and cellular biology* **21:** 8007-8021.

Kwon YT, Kashina AS, Davydov IV, Hu RG, An JY, Seo JW *et al* (2002). An essential role of N-terminal arginylation in cardiovascular development. *Science (New York, NY* **297:** 96-99.

Kwon YT, Xia Z, An JY, Tasaki T, Davydov IV, Seo JW *et al* (2003). Female lethality and apoptosis of spermatocytes in mice lacking the UBR2 ubiquitin ligase of the N-end rule pathway. *Molecular and cellular biology* **23:** 8255-8271.

Labib K, Tercero JA, Diffley JF (2000). Uninterrupted MCM2-7 function required for DNA replication fork progression. *Science* **288:** 1643-1647.

Labib K, Kearsey SE, Diffley JF (2001). MCM2-7 proteins are essential components of prereplicative complexes that accumulate cooperatively in the nucleus during G1-phase and are required to establish, but not maintain, the S-phase checkpoint. *Mol Biol Cell* **12:** 3658-3667.

Ladner RD, Caradonna SJ (1997). The human dUTPase gene encodes both nuclear and mitochondrial isoforms. Differential expression of the isoforms and characterization of a cDNA encoding the mitochondrial species. *J Biol Chem* **272:** 19072-19080.

Ladner RD, Lynch FJ, Groshen S, Xiong YP, Sherrod A, Caradonna SJ *et al* (2000). dUTP nucleotidohydrolase isoform expression in normal and neoplastic tissues: association with survival and response to 5-fluorouracil in colorectal cancer. *Cancer Res* **60:** 3493-3503.

Lander ES, Linton LM, Birren B, Nusbaum C, Zody MC, Baldwin J *et al* (2001). Initial sequencing and analysis of the human genome. *Nature* **409:** 860-921.

Lawson TG, Gronros DL, Evans PE, Bastien MC, Michalewich KM, Clark JK *et al* (1999). Identification and characterization of a protein destruction signal in the encephalomyocarditis virus 3C protease. *The Journal of biological chemistry* **274:** 9871-9880.

Leach SD, Modlin IM, Scheele GA, Gorelick FS (1991). Intracellular activation of digestive zymogens in rat pancreatic acini. Stimulation by high doses of cholecystokinin. *The Journal of clinical investigation* **87:** 362-366.

Lee MJ, Tasaki T, Moroi K, An JY, Kimura S, Davydov IV *et al* (2005). RGS4 and RGS5 are in vivo substrates of the N-end rule pathway. *Proceedings of the National Academy of Sciences of the United States of America* **102:** 15030-15035.

Leid M, Ishmael JE, Avram D, Shepherd D, Fraulob V, Dolle P (2004). CTIP1 and CTIP2 are differentially expressed during mouse embryogenesis. *Gene Expr Patterns* **4:** 733-739.

Lerch MM, Zenker M, Turi S, Mayerle J (2006). Developmental and metabolic disorders of the pancreas. *Endocrinology and metabolism clinics of North America* **35:** 219-241, vii.

Liddle RA (1994). Regulation of cholecystokinin gene expression in rat intestine. *Ann N Y Acad Sci* **713:** 22-31.

Liotta LA, Ferrari M, Petricoin E (2003). Clinical proteomics: written in blood. *Nature* **425:** 905.

Liu CY, Schroder M, Kaufman RJ (2000). Ligand-independent dimerization activates the stress response kinases IRE1 and PERK in the lumen of the endoplasmic reticulum. *The Journal of biological chemistry* **275:** 24881-24885.

Liu H, Bowes RC, 3rd, van de Water B, Sillence C, Nagelkerke JF, Stevens JL (1997). Endoplasmic reticulum chaperones GRP78 and calreticulin prevent oxidative stress, Ca2+ disturbances, and cell death in renal epithelial cells. *The Journal of biological chemistry* **272:** 21751-21759.

Liu H, Wang Y, Zhang Y, Song Q, Di C, Chen G *et al* (1999). TFAR19, a novel apoptosis-related gene cloned from human leukemia cell line TF-1, could enhance apoptosis of some tumor cells induced by growth factor withdrawal. *Biochem Biophys Res Commun* **254:** 203-210.

Luthen R, Niederau C, Grendell JH (1995a). Intrapancreatic zymogen activation and levels of ATP and glutathione during caerulein pancreatitis in rats. *The American journal of physiology* **268:** G592-604.

Luthen RE, Niederau C, Ferrell LD, Grendell JH (1995b). Energy metabolism in mouse pancreas in response to different dosages of a CCK analogue. *Pancreas* **11:** 141-146.

Madura K, Varshavsky A (1994). Degradation of G alpha by the N-end rule pathway. *Science (New York, NY* 265: 1454-1458.

Mann M, Hojrup P, Roepstorff P (1993). Use of mass spectrometric molecular weight information to identify proteins in sequence databases. *Biological mass spectrometry* **22:** 338-345.

Marban C, Redel L, Suzanne S, Van Lint C, Lecestre D, Chasserot-Golaz S *et al* (2005). COUP-TF interacting protein 2 represses the initial phase of HIV-1 gene transcription in human microglial cells. *Nucleic Acids Res* **33:** 2318-2331.

Marban C, Suzanne S, Dequiedt F, de Walque S, Redel L, Van Lint C *et al* (2007). Recruitment of chromatin-modifying enzymes by CTIP2 promotes HIV-1 transcriptional silencing. *EMBO J* **26:** 412-423.

Marouga R, David S, Hawkins E (2005). The development of the DIGE system: 2D fluorescence difference gel analysis technology. *Analytical and bioanalytical chemistry* **382:** 669-678.

Martin SJ, Finucane DM, Amarante-Mendes GP, O'Brien GA, Green DR (1996). Phosphatidylserine externalization during CD95-induced apoptosis of cells and cytoplasts requires ICE/CED-3 protease activity. *J Biol Chem* **271:** 28753-28756.

McIntosh EM, Ager DD, Gadsden MH, Haynes RH (1992). Human dUTP pyrophosphatase: cDNA sequence and potential biological importance of the enzyme. *Proc Natl Acad Sci U S A* **89:** 8020-8024.

Mercier C, Truntzer C, Pecqueur D, Gimeno JP, Belz G, Roy P (2009). Mixed-model of ANOVA for measurement reproducibility in proteomics. *Journal of proteomics* **72:** 974-981.

Mirnics K, Middleton FA, Stanwood GD, Lewis DA, Levitt P (2001). Disease-specific changes in regulator of G-protein signaling 4 (RGS4) expression in schizophrenia. *Molecular psychiatry* **6:** 293-301.

Mithofer K, Fernandez-del Castillo C, Rattner D, Warshaw AL (1998). Subcellular kinetics of early trypsinogen activation in acute rodent pancreatitis. *The American journal of physiology* **274:** G71-79.

Mittmann C, Chung CH, Hoppner G, Michalek C, Nose M, Schuler C *et al* (2002). Expression of ten RGS proteins in human myocardium: functional characterization of an upregulation of RGS4 in heart failure. *Cardiovascular research* **55:** 778-786.

Moeschler JB, Lubinsky MS (1985). Johanson-Blizzard syndrome with normal intelligence. *American journal of medical genetics* **22:** 69-73.

Moeschler JB, Polak MJ, Jenkins JJ, 3rd, Amato RS (1987). The Johanson-Blizzard syndrome: a second report of full autopsy findings. *American journal of medical genetics* **26:** 133-138.

Mogk A, Schmidt R, Bukau B (2007). The N-end rule pathway for regulated proteolysis: prokaryotic and eukaryotic strategies. *Trends in cell biology* **17:** 165-172.

Molnar I, Horvath C (1976). Reverse-phase chromatography of polar biological substances: separation of catechol compounds by high-performance liquid chromatography. *Clinical chemistry* **22:** 1497-1502.

Morris DW, Rodgers A, McGhee KA, Schwaiger S, Scully P, Quinn J *et al* (2004). Confirming RGS4 as a susceptibility gene for schizophrenia. *Am J Med Genet B Neuropsychiatr Genet* **125B:** 50-53.

Muallem S, Lee MG (1997). High [Ca2+]i domains, secretory granules and exocytosis. *Cell calcium* **22:** 1-4.

Mulder LC, Muesing MA (2000). Degradation of HIV-1 integrase by the N-end rule pathway. *The Journal of biological chemistry* **275:** 29749-29753.

Nagel S, Kaufmann M, Drexler HG, MacLeod RA (2003). The cardiac homeobox gene NKX2-5 is deregulated by juxtaposition with *BCL11B* in pediatric T-ALL cell lines via a novel t(5;14)(q35.1;q32.2). *Cancer Res* **63:** 5329-5334.

Nation MD, Guzder SN, Giroir LE, Deutsch WA (1989). Control of Drosophila deoxyuridine triphosphatase. Existence of a developmentally expressed protein inhibitor. *Biochem J* **259:** 593-596.

Neer EJ (1995). Heterotrimeric G proteins: organizers of transmembrane signals. *Cell* **80:** 249-257.

Neoptolemos JP, Raraty M, Finch M, Sutton R (1998). Acute pancreatitis: the substantial human and financial costs. *Gut* **42:** 886-891.

Neoptolemos JP, Kemppainen EA, Mayer JM, Fitzpatrick JM, Raraty MG, Slavin J *et al* (2000). Early prediction of severity in acute pancreatitis by urinary trypsinogen activation peptide: a multicentre study. *Lancet* **355:** 1955-1960.

Neubig RR (2002). Regulators of G protein signaling (RGS proteins): novel central nervous system drug targets. *J Pept Res* **60:** 312-316.

Neubig RR, Siderovski DP (2002). Regulators of G-protein signalling as new central nervous system drug targets. *Nat Rev Drug Discov* **1:** 187-197.

Neves SR, Ram PT, Iyengar R (2002). G protein pathways. *Science (New York, NY* **296:** 1636-1639.

Nicotera P, Bellomo G, Orrenius S (1992). Calcium-mediated mechanisms in chemically induced cell death. *Annual review of pharmacology and toxicology* **32:** 449-470.

Niederau C, Ferrell LD, Grendell JH (1985). Caerulein-induced acute necrotizing pancreatitis in mice: protective effects of proglumide, benzotript, and secretin. *Gastroenterology* **88:** 1192-1204.

Niederau C, Niederau M, Luthen R, Strohmeyer G, Ferrell LD, Grendell JH (1990). Pancreatic exocrine secretion in acute experimental pancreatitis. *Gastroenterology* **99:** 1120-1127.

Ninnis RL, Spall SK, Talbo GH, Truscott KN, Dougan DA (2009). Modification of PATase by L/F-transferase generates a ClpS-dependent N-end rule substrate in Escherichia coli. *The EMBO journal* **28:** 1732-1744.

Noble F, Wank SA, Crawley JN, Bradwejn J, Seroogy KB, Hamon M *et al* (1999). International Union of Pharmacology. XXI. Structure, distribution, and functions of cholecystokinin receptors. *Pharmacol Rev* **51:** 745-781.

Northrop JH, Kunitz M (1931). Isolation of Protein Crystals Possessing Tryptic Activity. *Science (New York, NY* **73:** 262-263.

O'Konski MS, Pandol SJ (1990). Effects of caerulein on the apical cytoskeleton of the pancreatic acinar cell. *The Journal of clinical investigation* **86:** 1649-1657.

O´Farrell PH (1975). High resolution two-dimensional electrophoresis of proteins. *Journal of Biological Chemistry* **250:** 4007-4021.

Ong SE, Blagoev B, Kratchmarova I, Kristensen DB, Steen H, Pandey A *et al* (2002). Stable isotope labeling by amino acids in cell culture, SILAC, as a simple and accurate approach to expression proteomics. *Mol Cell Proteomics* **1:** 376-386.

Ong SE, Mann M (2006). A practical recipe for stable isotope labeling by amino acids in cell culture (SILAC). *Nature protocols* **1:** 2650-2660.

Orian-Rousseau V, Morrison H, Matzke A, Kastilan T, Pace G, Herrlich P *et al* (2007). Hepatocyte growth factor-induced Ras activation requires ERM proteins linked to both CD44v6 and F-actin. *Mol Biol Cell* **18:** 76-83.

Oshiro A, Tagawa H, Ohshima K, Karube K, Uike N, Tashiro Y *et al* (2006). Identification of subtype-specific genomic alterations in aggressive adult T-cell leukemia/lymphoma. *Blood* **107:** 4500-4507.

Owen VJ, Burton PB, Mullen AJ, Birks EJ, Barton P, Yacoub MH (2001). Expression of RGS3, RGS4 and Gi alpha 2 in acutely failing donor hearts and end-stage heart failure. *European heart journal* **22:** 1015-1020.

Ozcan U, Yilmaz E, Ozcan L, Furuhashi M, Vaillancourt E, Smith RO *et al* (2006). Chemical chaperones reduce ER stress and restore glucose homeostasis in a mouse model of type 2 diabetes. *Science (New York, NY* **313:** 1137-1140.

Paschen W, Doutheil J (1999). Disturbance of endoplasmic reticulum functions: a key mechanism underlying cell damage? *Acta neurochirurgica* **73:** 1-5.

Patterson SD, Aebersold RH (2003). Proteomics: the first decade and beyond. *Nature genetics* **33 Suppl:** 311-323.

Patton WF (2000). A thousand points of light: the application of fluorescence detection technologies to two-dimensional gel electrophoresis and proteomics. *Electrophoresis* **21:** 1123-1144.

Pereda J, Sabater L, Aparisi L, Escobar J, Sandoval J, Vina J *et al* (2006). Interaction between cytokines and oxidative stress in acute pancreatitis. *Current medicinal chemistry* **13:** 2775-2787.

Petit PX, Lecoeur H, Zorn E, Dauguet C, Mignotte B, Gougeon ML (1995). Alterations in mitochondrial structure and function are early events of dexamethasone-induced thymocyte apoptosis. *J Cell Biol* **130:** 157-167.

Pfutzer RH, Barmada MM, Brunskill AP, Finch R, Hart PS, Neoptolemos J *et al* (2000). SPINK1/PSTI polymorphisms act as disease modifiers in familial and idiopathic chronic pancreatitis. *Gastroenterology* **119:** 615-623.

Pierce KL, Premont RT, Lefkowitz RJ (2002). Seven-transmembrane receptors. *Nature reviews* **3:** 639-650.

Poon RY, Yamashita K, Adamczewski JP, Hunt T, Shuttleworth J (1993). The cdc2-related protein p40MO15 is the catalytic subunit of a protein kinase that can activate p33cdk2 and p34cdc2. *EMBO J* **12:** 3123-3132.

Przybylski GK, Dik WA, Wanzeck J, Grabarczyk P, Majunke S, Martin-Subero JI *et al* (2005). Disruption of the *BCL11B* gene through inv(14)(q11.2q32.31) results in the expression of *BCL11B*-TRDC fusion transcripts and is associated with the absence of wild-type *BCL11B* transcripts in T-ALL. *Leukemia* **19:** 201-208.

Rabilloud T, Valette C, Lawrence JJ (1994). Sample application by in-gel rehydration improves the resolution of two-dimensional electrophoresis with immobilized pH gradients in the first dimension. *Electrophoresis* **15:** 1552-1558.

Rabilloud T, Strub JM, Luche S, van Dorsselaer A, Lunardi J (2001). A comparison between Sypro Ruby and ruthenium II tris (bathophenanthroline disulfonate) as fluorescent stains for protein detection in gels. *Proteomics* **1:** 699-704.

Rao H, Uhlmann F, Nasmyth K, Varshavsky A (2001). Degradation of a cohesin subunit by the N-end rule pathway is essential for chromosome stability. *Nature* **410:** 955-959.

Raraty M, Ward J, Erdemli G, Vaillant C, Neoptolemos JP, Sutton R *et al* (2000). Calcium-dependent enzyme activation and vacuole formation in the apical granular region of pancreatic acinar cells. *Proceedings of the National Academy of Sciences of the United States of America* **97:** 13126-13131.

Rasmussen M, Alexander RT, Darborg BV, Mobjerg N, Hoffmann EK, Kapus A *et al* (2008). Osmotic cell shrinkage activates ezrin/radixin/moesin (ERM) proteins: activation mechanisms and physiological implications. *Am J Physiol Cell Physiol* **294:** C197-212.

Rau B, Paszkowski A, Lillich S, Baumgart K, Moller P, Beger HG (2001). Differential effects of caspase-1/interleukin-1beta-converting enzyme on acinar cell necrosis and apoptosis in severe acute experimental pancreatitis. *Laboratory investigation; a journal of technical methods and pathology* **81:** 1001-1013.

Reiss Y, Kaim D, Hershko A (1988). Specificity of binding of NH2-terminal residue of proteins to ubiquitin-protein ligase. Use of amino acid derivatives to characterize specific binding sites. *The Journal of biological chemistry* **263:** 2693-2698.

Richert S, Luche S, Chevallet M, Van Dorsselaer A, Leize-Wagner E, Rabilloud T (2004). About the mechanism of interference of silver staining with peptide mass spectrometry. *Proteomics* **4:** 909-916.

Rogers JH, Tamirisa P, Kovacs A, Weinheimer C, Courtois M, Blumer KJ *et al* (1999). RGS4 causes increased mortality and reduced cardiac hypertrophy in response to pressure overload. *The Journal of clinical investigation* **104:** 567-576.

Roman DL, Talbot JN, Roof RA, Sunahara RK, Traynor JR, Neubig RR (2007). Identification of small-molecule inhibitors of RGS4 using a high-throughput flow cytometry protein interaction assay. *Molecular pharmacology* **71:** 169-175.

Ross EM, Wilkie TM (2000). GTPase-activating proteins for heterotrimeric G proteins: regulators of G protein signaling (RGS) and RGS-like proteins. *Annual review of biochemistry* **69:** 795-827.

Rothenbacher D, Low M, Hardt PD, Klor HU, Ziegler H, Brenner H (2005). Prevalence and determinants of exocrine pancreatic insufficiency among older adults: results of a population-based study. *Scandinavian journal of gastroenterology* **40:** 697-704.

Ruan GR, Qin YZ, Chen SS, Li JL, Ma X, Chang Y *et al* (2006). Abnormal expression of the programmed cell death 5 gene in acute and chronic myeloid leukemia. *Leuk Res* **30:** 1159-1165.

Rudner J, Jendrossek V, Lauber K, Daniel PT, Wesselborg S, Belka C (2005). Type I and type II reactions in TRAIL-induced apoptosis -- results from dose-response studies. *Oncogene* **24:** 130-140.

Rudnik-Schoneborn S, Keller B, Beemer FA, Pistor K, Swanenburg de Veye HF, Zerres K (1991). [Johanson-Blizzard syndrome]. *Klinische Padiatrie* **203:** 33-38.

Sahin-Toth M (2001). The pathobiochemistry of hereditary pancreatitis: studies on recombinant human cationic trypsinogen. *Pancreatology* **1:** 461-465.

Saluja AK, Donovan EA, Yamanaka K, Yamaguchi Y, Hofbauer B, Steer ML (1997). Cerulein-induced in vitro activation of trypsinogen in rat pancreatic acini is mediated by cathepsin B. *Gastroenterology* **113:** 304-310.

Saluja AK, Bhagat L, Lee HS, Bhatia M, Frossard JL, Steer ML (1999). Secretagogue-induced digestive enzyme activation and cell injury in rat pancreatic acini. *The American journal of physiology* **276:** G835-842.

Saluja AK, Lerch MM, Phillips PA, Dudeja V (2007). Why does pancreatic overstimulation cause pancreatitis? *Annual review of physiology* **69:** 249-269.

Sasaki T, Kojima H, Kishimoto R, Ikeda A, Kunimoto H, Nakajima K (2006). Spatiotemporal regulation of c-Fos by ERK5 and the E3 ubiquitin ligase UBR1, and its biological role. *Molecular cell* **24:** 63-75.

Satterwhite E, Sonoki T, Willis TG, Harder L, Nowak R, Arriola EL *et al* (2001). The BCL11 gene family: involvement of BCL11A in lymphoid malignancies. *Blood* **98:** 3413-3420.

Schaub M, Keller W (2002). RNA editing by adenosine deaminases generates RNA and protein diversity. *Biochimie* **84:** 791-803.

Schauber C, Chen L, Tongaonkar P, Vega I, Madura K (1998). Sequence elements that contribute to the degradation of yeast G alpha. *Genes Cells* **3:** 307-319.

Schmutz J, Wheeler J, Grimwood J, Dickson M, Yang J, Caoile C *et al* (2004). Quality assessment of the human genome sequence. *Nature* **429:** 365-368.

Schulenberg B, Aggeler R, Beechem JM, Capaldi RA, Patton WF (2003). Analysis of steady-state protein phosphorylation in mitochondria using a novel fluorescent phosphosensor dye. *The Journal of biological chemistry* **278:** 27251-27255.

Schulenberg B, Goodman TN, Aggeler R, Capaldi RA, Patton WF (2004). Characterization of dynamic and steady-state protein phosphorylation using a fluorescent phosphoprotein gel stain and mass spectrometry. *Electrophoresis* **25:** 2526-2532.

Schulz HU, Niederau C, Klonowski-Stumpe H, Halangk W, Luthen R, Lippert H (1999). Oxidative stress in acute pancreatitis. *Hepato-gastroenterology* **46:** 2736-2750.

Schwanhausser B, Gossen M, Dittmar G, Selbach M (2009). Global analysis of cellular protein translation by pulsed SILAC. *Proteomics* **9:** 205-209.

Senawong T, Peterson VJ, Avram D, Shepherd DM, Frye RA, Minucci S *et al* (2003). Involvement of the histone deacetylase SIRT1 in chicken ovalbumin upstream promoter transcription factor (COUP-TF)-interacting protein 2-mediated transcriptional repression. *J Biol Chem* **278:** 43041-43050.

Shen J, Chen X, Hendershot L, Prywes R (2002). ER stress regulation of ATF6 localization by dissociation of BiP/GRP78 binding and unmasking of Golgi localization signals. *Developmental cell* **3:** 99-111.

Shinbo T, Matsuki A, Matsumoto Y, Kosugi S, Takahashi Y, Niwa O *et al* (1999). Allelic loss mapping and physical delineation of a region harboring a putative thymic lymphoma suppressor gene on mouse chromosome 12. *Oncogene* **18:** 4131-4136.

Sijts AJ, Pilip I, Pamer EG (1997). The Listeria monocytogenes-secreted p60 protein is an N-end rule substrate in the cytosol of infected cells. Implications for major histocompatibility complex class I antigen processing of bacterial proteins. *The Journal of biological chemistry* **272:** 19261-19268.

Sonnemann J, Gekeler V, Sagrauske A, Muller C, Hofmann HP, Beck JF (2004). Apoptotic responsiveness of PC-3 prostate cancer cells to tumor necrosis factor-related apoptosis-inducing ligand: evidence for differential effects of Bcl-xL and Bcl-2 down-regulation. *Int J Oncol* **25:** 1171-1181.

Steinbach WJ, Hintz RL (2000). Diabetes mellitus and profound insulin resistance in Johanson-Blizzard syndrome. *J Pediatr Endocrinol Metab* **13:** 1633-1636.

Steinberg TH, Haugland RP, Singer VL (1996a). Applications of SYPRO orange and SYPRO red protein gel stains. *Analytical biochemistry* **239:** 238-245.

Steinberg TH, Jones LJ, Haugland RP, Singer VL (1996b). SYPRO orange and SYPRO red protein gel stains: one-step fluorescent staining of denaturing gels for detection of nanogram levels of protein. *Analytical biochemistry* **239:** 223-237.

Steinberg TH, Chernokalskaya E, Berggren K, Lopez MF, Diwu Z, Haugland RP *et al* (2000). Ultrasensitive fluorescence protein detection in isoelectric focusing gels using a ruthenium metal chelate stain. *Electrophoresis* **21:** 486-496.

Steinberg TH, Pretty On Top K, Berggren KN, Kemper C, Jones L, Diwu Z *et al* (2001). Rapid and simple single nanogram detection of glycoproteins in polyacrylamide gels and on electroblots. *Proteomics* **1:** 841-855.

Steinberg TH, Agnew BJ, Gee KR, Leung WY, Goodman T, Schulenberg B *et al* (2003). Global quantitative phosphoprotein analysis using Multiplexed Proteomics technology. *Proteomics* **3:** 1128-1144.

Stoeber K, Tlsty TD, Happerfield L, Thomas GA, Romanov S, Bobrow L *et al* (2001). DNA replication licensing and human cell proliferation. *J Cell Sci* **114:** 2027-2041.

Sutton R, Criddle D, Raraty MG, Tepikin A, Neoptolemos JP, Petersen OH (2003). Signal transduction, calcium and acute pancreatitis. *Pancreatology* **3:** 497-505.

Switzer RC, 3rd, Merril CR, Shifrin S (1979). A highly sensitive silver stain for detecting proteins and peptides in polyacrylamide gels. *Analytical biochemistry* **98:** 231-237.

Takemoto D, Jones DA (2005). Membrane release and destabilization of Arabidopsis RIN4 following cleavage by Pseudomonas syringae AvrRpt2. *Mol Plant Microbe Interact* **18:** 1258-1268.

Tanaka S, Uehara T, Nomura Y (2000). Up-regulation of protein-disulfide isomerase in response to hypoxia/brain ischemia and its protective effect against apoptotic cell death. *The Journal of biological chemistry* **275:** 10388-10393.

Tasaki T, Mulder LC, Iwamatsu A, Lee MJ, Davydov IV, Varshavsky A *et al* (2005). A family of mammalian E3 ubiquitin ligases that contain the UBR box motif and recognize N-degrons. *Molecular and cellular biology* **25:** 7120-7136.

Thompson A, Schäfer J, Kuhn K, Kienle S, Schwarz J, Schmidt G *et al.* (2003). Tandem mass tags: a novel quantification strategy for comparative analysis of complex protein mixtures by MS/MS. *Anal. Chem.* **75:** 1895–1904.

Topark-Ngarm A, Golonzhka O, Peterson VJ, Barrett B, Jr., Martinez B, Crofoot K *et al* (2006). CTIP2 associates with the NuRD complex on the promoter of p57KIP2, a newly identified CTIP2 target gene. *J Biol Chem* **281:** 32272-32283.

Trellis DR, Clouse RE (1991). Johanson-Blizzard syndrome. Progression of pancreatic involvement in adulthood. *Digestive diseases and sciences* **36:** 365-369.

Tsukita S, Oishi K, Sato N, Sagara J, Kawai A (1994). ERM family members as molecular linkers between the cell surface glycoprotein CD44 and actin-based cytoskeletons. *J Cell Biol* **126:** 391-401.

Turner GC, Du F, Varshavsky A (2000). Peptides accelerate their uptake by activating a ubiquitin-dependent proteolytic pathway. *Nature* **405:** 579-583.

Unwin RD, Evans CA, Whetton AD (2006). Relative quantification in proteomics: new approaches for biochemistry. *Trends in biochemical sciences* **31:** 473-484

Vanlieferinghen P, Gallot D, Francannet C, Meyer F, Dechelotte P (2003). Prenatal ultrasonographic diagnosis of a recurrent case of Johanson-Blizzard syndrome. *Genetic counseling (Geneva, Switzerland)* **14:** 105-107.

Vanlieferinghen PH, Borderon C, Francannet CH, Gembara P, Dechelotte P (2001). Johanson-Blizzard syndrome. a new case with autopsy findings. *Genetic counseling (Geneva, Switzerland)* **12:** 245-250.

Varshavsky A (1996). The N-end rule: functions, mysteries, uses. *Proceedings of the National Academy of Sciences of the United States of America* **93:** 12142-12149.

Varshavsky A (2004). 'Spalog' and 'sequelog': neutral terms for spatial and sequence similarity. *Curr Biol* **14:** R181-183.

Venter JC, Adams MD, Myers EW, Li PW, Mural RJ, Sutton GG *et al* (2001). The sequence of the human genome. *Science (New York, NY* **291:** 1304-1351.

Wakabayashi Y, Inoue J, Takahashi Y, Matsuki A, Kosugi-Okano H, Shinbo T *et al* (2003a). Homozygous deletions and point mutations of the Rit1/Bcl11b gene in gamma-ray induced mouse thymic lymphomas. *Biochem Biophys Res Commun* **301:** 598-603.

Wakabayashi Y, Watanabe H, Inoue J, Takeda N, Sakata J, Mishima Y *et al* (2003b). Bcl11b is required for differentiation and survival of alphabeta T lymphocytes. *Nat Immunol* **4:** 533-539.

Walker NI (1987). Ultrastructure of the rat pancreas after experimental duct ligation. I. The role of apoptosis and intraepithelial macrophages in acinar cell deletion. *The American journal of pathology* **126:** 439-451.

Wang J, Barsky LW, Shum CH, Jong A, Weinberg KI, Collins SJ *et al* (2002). Retinoid-induced G1 arrest and differentiation activation are associated with a switch to cyclin-dependent kinase-activating kinase hypophosphorylation of retinoic acid receptor alpha. *J Biol Chem* **277:** 43369-43376.

Ward JB, Petersen OH, Jenkins SA, Sutton R (1995). Is an elevated concentration of acinar cytosolic free ionised calcium the trigger for acute pancreatitis? *Lancet* **346:** 1016-1019.

Ward JB, Sutton R, Jenkins SA, Petersen OH (1996). Progressive disruption of acinar cell calcium signaling is an early feature of cerulein-induced pancreatitis in mice. *Gastroenterology* **111:** 481-491.

Weiss FU, Simon P, Mayerle J, Kraft M, Lerch MM (2006). Germline mutations and gene polymorphism associated with human pancreatitis. *Endocrinology and metabolism clinics of North America* **35:** 289-302, viii-ix.

Whitcomb DC, Gorry MC, Preston RA, Furey W, Sossenheimer MJ, Ulrich CD *et al* (1996). Hereditary pancreatitis is caused by a mutation in the cationic trypsinogen gene. *Nature genetics* **14:** 141-145.

Wickliffe KE, Leppla SH, Moayeri M (2008). Killing of macrophages by anthrax lethal toxin: involvement of the N-end rule pathway. *Cellular microbiology* **10:** 1352-1362.

Wilkins MR, Sanchez JC, Gooley AA, Appel RD, Humphery-Smith I, Hochstrasser DF *et al* (1996). Progress with proteome projects: why all proteins expressed by a genome should be identified and how to do it. *Biotechnology & genetic engineering reviews* **13:** 19-50.

Willars GB (2006). Mammalian RGS proteins: multifunctional regulators of cellular signalling. *Seminars in cell & developmental biology* **17:** 363-376.

Williams JA (2001). Intracellular signaling mechanisms activated by cholecystokinin-regulating synthesis and secretion of digestive enzymes in pancreatic acinar cells. *Annual review of physiology* **63:** 77-97.

Williams NM, Preece A, Spurlock G, Norton N, Williams HJ, McCreadie RG *et al* (2004). Support for RGS4 as a susceptibility gene for schizophrenia. *Biological psychiatry* **55:** 192-195.

Wolfe SA, Nekludova L, Pabo CO (2000). DNA recognition by Cys2His2 zinc finger proteins. *Annu Rev Biophys Biomol Struct* **29:** 183-212.

Wu L, Chen P, Hwang JJ, Barsky LW, Weinberg KI, Jong A *et al* (1999). RNA antisense abrogation of MAT1 induces G1 phase arrest and triggers apoptosis in aortic smooth muscle cells. *J Biol Chem* **274:** 5564-5572.

Xu L, Chen Y, Song Q, Xu D, Wang Y, Ma D (2009). PDCD5 interacts with Tip60 and functions as a cooperator in acetyltransferase activity and DNA damage-induced apoptosis. *Neoplasia* **11:** 345-354.

Xu X, Zeng W, Diaz J, Muallem S (1996). Spacial compartmentalization of Ca2+ signaling complexes in pancreatic acini. *The Journal of biological chemistry* **271:** 24684-24690.

Xu X, Zeng W, Popov S, Berman DM, Davignon I, Yu K *et al* (1999). RGS proteins determine signaling specificity of Gq-coupled receptors. *The Journal of biological chemistry* **274:** 3549-3556.

Yan JX, Wait R, Berkelman T, Harry RA, Westbrook JA, Wheeler CH *et al* (2000). A modified silver staining protocol for visualization of proteins compatible with matrix-assisted laser desorption/ionization and electrospray ionization-mass spectrometry. *Electrophoresis* **21:** 3666-3672.

Yan Y, Chi PP, Bourne HR (1997). RGS4 inhibits Gq-mediated activation of mitogen-activated protein kinase and phosphoinositide synthesis. *The Journal of biological chemistry* **272:** 11924-11927.

Yates JR, 3rd, Speicher S, Griffin PR, Hunkapiller T (1993). Peptide mass maps: a highly informative approach to protein identification. *Analytical biochemistry* **214:** 397-408.

Ye J, Rawson RB, Komuro R, Chen X, Dave UP, Prywes R *et al* (2000). ER stress induces cleavage of membrane-bound ATF6 by the same proteases that process SREBPs. *Molecular cell* **6:** 1355-1364.

Zenker M, Mayerle J, Lerch MM, Tagariello A, Zerres K, Durie PR *et al* (2005). Deficiency of UBR1, a ubiquitin ligase of the N-end rule pathway, causes pancreatic dysfunction, malformations and mental retardation (Johanson-Blizzard syndrome). *Nature genetics* **37:** 1345-1350.

Zenker M, Mayerle J, Reis A, Lerch MM (2006). Genetic basis and pancreatic biology of Johanson-Blizzard syndrome. *Endocrinology and metabolism clinics of North America* **35:** 243-253, vii-viii.

Zhang G, Ghosh S (2002). Negative regulation of toll-like receptor-mediated signaling by Tollip. *The Journal of biological chemistry* **277:** 7059-7065.

Zhang S, Watson N, Zahner J, Rottman JN, Blumer KJ, Muslin AJ (1998). RGS3 and RGS4 are GTPase activating proteins in the heart. *Journal of molecular and cellular cardiology* **30:** 269-276.

Zhang S, He Q, Peng H, Tedeschi-Blok N, Triche TJ, Wu L (2004). MAT1-modulated cyclin-dependent kinase-activating kinase activity cross-regulates neuroblastoma cell G1 arrest and neurite outgrowth. *Cancer Res* **64:** 2977-2983.

Zhong H, Neubig RR (2001). Regulator of G protein signaling proteins: novel multifunctional drug targets. *The Journal of pharmacology and experimental therapeutics* **297:** 837-845.

Zieske LR (2006). A perspective on the use of iTRAQ reagent technology for protein complex and profiling studies. *Journal of experimental botany* **57:** 1501-1508.

Zuo X, Echan L, Hembach P, Tang HY, Speicher KD, Santoli D *et al* (2001). Towards global analysis of mammalian proteomes using sample prefractionation prior to narrow pH range two-dimensional gels and using one-dimensional gels for insoluble and large proteins. *Electrophoresis* **22:** 1603-1615.

EIDESSTAATLICHE ERKLÄRUNG

Hiermit erkläre ich, daß diese Arbeit bisher von mir weder an der Mathematisch-Naturwissenschaftlichen Fakultät der Ernst-Moritz-Arndt-Universität Greifswald noch einer anderen wissenschaftlichen Einrichtung zum Zwecke der Promotion eingereicht wurde.

Ferner erkläre ich, daß ich diese Arbeit selbständig verfaßt und keine anderen als die darin angegebenen Hilfsmittel benutzt habe.

Unterschrift des Promovenden

Curriculum Vitae

Personal Information

Name	**: NARASIMHA KUMAR. KARANAM**
Date of Birth	: 16-07-1979
Father's Name	: Narasimha Rao. Karanam
Gender	: Male
Marital status	: Married
Perm. Address	: S/O K.Narasimha Rao,
	H.No- 1/6, Teachers colony,Shadnagar,
	Andhra Pradesh, India.
Nationality	: Indian
Languages	: English, Hindi, Telugu

Education and work experience

1984-1994	: Primary and Secondary school, Andhrapradesh, India
1994-1996	: Board of Intermediate Education, Andhrapradesh, India
1996-1999	: Bachelor of Science (Biology), Sri Krishnadevaraya University, Anantapur. India
1999-2001	: Bachelor of Education (Biology), Osmania University, Hyderabad. India
2001-2003	: Masters of Science (Biochemistry), University of Hyderabad, Hyderabad. India
2003-2005	: Research fellow at Centre for Cellular and Molecular Biology (CCMB), Hyderabad. Inida
2005-2010	: Ph.D. student of the Interfakultary Institute for Functional Genomics, Ernst-Moritz-Arndt University Of Greifswald, Greifswald. Germany.

Scientific Contributions

Publications:

1) **Karanam NK**, Grabarczyk P, Hammer E, Scharf C, Venz S, Gesell-Salazar M, Barthlen W, Przybylski GK, Schmidt CA, Volker U (2010). Proteome Analysis Reveals New Mechanisms of Bcl11b-loss Driven Apoptosis. *J Proteome Res* **9:** 3799-3811.

2) Rameshwaram NR, **Karanam NK**, Scharf C, Volker U, Nadimpalli SK (2009). Complete primary structure of a newly characterized galactose-specific lectin from the seeds of Dolichos lablab. *Glycoconj J* **26:** 161-72.

3) Chumbalkar VC, Subhashini C, Dhople VM, Sundaram CS, Jagannadham MV, **Kumar KN**, Srinivas PN, Mythili R, Rao MK, Kulkarni MJ, Hegde S, Hegde AS, Samual C, Santosh V, Singh L, Sirdeshmukh R (2005). Differential protein expression in human gliomas and molecular insights. *Proteomics* **5:** 1167-77.

4) **Karanam NK,** Zenker M, Bauhuber S, Weiss FU, Steil L, Hammer E, Völker U, Lerch MM, Mayerle J. Development of a protein based assay to detect subclinical Johanson-Blizzard-Syndrome (Ready for sumbmission)

Published abstracts:

1) Mayerle J, **Karanam NK**, Zenker M, Bauhuber S, Hammer E, Weiss FU, Krüger B, Völker U, Lerch MM (2009). Johanson-Blizzard-Syndrome - UBR1 Target Identification by Proteome Analysis and Pathophysiological Relevance. *Gastroenterology* **136:** 914.

2) **Karanam NK,** Zenker M, Matejas V, Kwon YT, Hammer E, Weiss FU, Völker U, Lerch MM, Mayerle J (2008). Johanson-Blizzard-Syndrome, an inherited disorder with pancreatic insufficiency - UBR-1 dependent target identification by proteome analysis in UBR1 deficient mice. *Pancreatology* **8:** A 312

3) Chumbalkar VC, Subhashini C, **Kumar KN**, Dhople VM, Sundaram CS, Jagannadham MV, Srinivas PN, Mythili R, Rao MK, Kulkarni MJ, Hegde S, Hegde AS, Samual C, Santosh V, Singh L, Sirdeshmukh R(2004). Human Gliomas: Differential Protein Expression and Understanding of Glial Tumor Pathology *Molecular and Cellular Proteomics* **3:** S47

Oral presentations:

1) Johanson Blizzard Syndrome,an inherited disorder with pancreatic insufficiency- UBR1 dependent target identification by proteome analysis in UBR1 deficient mice.

Karanam NK, Zenker M, Matejas V, Kwon YT, Hammer E, Weiss FU, Völker U, Lerch MM, Mayerle J. Joint EPC/IAP Meeting in Łódź,Poland, June 25-28th 2008. (awarded European Pancreatic Club travel scholarship)

Poster presentations:

1) Analysis of UBR1 targets in patients with Johanson-Blizzard-Syndrome and a murine model. **Karanam NK**, Zenker M, Varshavsky A, Scharf C, Hammer E, Steil L, Lerch MM, Völker U, Mayerle J. HUPO 7th World congress. Amsterdam, Netherlands. August 16-20th , 2008.

2) A combined proteomics and cell biology approach to elucidate the function of BCL11B in T cell lymphoma cell lines. **Karanam NK**, Grabarczyk P, Depke M, Schöbel F, Scharf C, Schmidt CA, Völker U. AACR-NCI-EORTC International conference "Molecular targets and Cancer therapeutics". San Francisco, CA, USA. October 22-26th, 2007.

3) Proteome analysis of Johanson-Blizzard syndrome patients and UBR1 deficient mice.

Karanam NK, Mayerle J, Zenker M, Scharf C, Weiss FU, Völker U, Lerch MM

Deutsche Pancreatic Club (DPC). Dresden, Germany. November 22-24th, 2007.

Acknowledgements

First and foremost I sincerely express my gratitude to my mentor **Prof. Dr. Uwe Völker** for providing an endless support during my PhD tenure. Thank you so much for providing a stimulating and encouraging environment in which I learnt a lot and became more mature scientifically. I dared to ask questions in our lab seminars only because of your encouragement and fruitful discussions. You have given me lot of freedom in science and made constructive criticisms which made me complete my PhD successfully. I specially thank you for allowing me to work more in our collaborators' labs and letting me acquaint different fields of science. All the my life, I can't forget the moment you attended my marriage and blessed us personally by flying all the way from Germany to India. Thank you so much. The best quality among many others I personally like in you is to keep your promise at any cost, ever if you commit, I will try my best to aquire it. I hope and pray god to give me strength and wisdom to follow your suggestions and achieve some of your success in my life.

I extend sincere thanks to my second gigantic (physically and professionally) supervisor **Prof. Dr. Markus M. Lerch**. Thank you for allowing me to work in your group. My special thanks to you for conducting our lab seminars in english so that we can learn from discussions. I definitely learnt much more than what I knew about Pancreas and how to construct questions from your discussions. I can't forget your cheerful smile and wish when you enter seminar room.

Thank you very much **Prof. Dr. Julia Mayerle** for your valuable time, endless support and discussions. I was totally unaware that I will be introduced into pancreatic field until you came to our lab in Biotechnikum on one fine evening. I could learn different techniques and improve my analytical skills with your encouragement and useful discussions. I specially thank for correcting my thesis and shaping it nicely with your suggestions. You make us feel very comfortable at our group meetings with your friendly nature and outings on nice sunny evenings. Thanks a lot.

I would like to thank **Prof. Dr. Christian Schmidt** for your collaboration and fruitful discussions. Not only as our collaborator but also as a chair of our graduate school you used to encourage me alot. Thanks for that and the meetings you arranged for us to improve our knowledge.

I thank **Dr. Piotr Grabarczyk** for your timely help and very useful discussions. I learnt more about BCL11b and other techniques with your help. My heartful thanks for all your efforts to make our BCL11b story published. I will remember our informal discussions during sample preparation for long.

Dr. Elke Hammer, Thank you for your kind support in lab and correcting first draft of my thesis. I cant for get the day when you cancelled other appointment and gave immense support when I was totally depressed. I could have lost that time without your kind words.

My special thanks to **Dr. Leif Steil**, for his introduction to D2D and Genespring softwares and formatting my thesis at the end. I thank my other colleagues **Dr. Christian Scharf , Dr. Simone Venz** and **Dr. Manuella Gessel Salazar** for making MALDI results ready in quick time and for their personal helps whenever I go to visa office.

I express my heartful thanks to **Prof. Dr. Martin Zenker** for his collaboration and giving rare JBS patients samples for my work. My special thanks for your nice treat in Indian restaurant when I visited Erlangen on our work.

I also express my gratitude to **Dr. Burkhard Kruger** for his useful calcium measurement experiments in my thesis.

I am indebted to our all lab technicians **Katrin Schoknecht, Ulrike Lissner, Katrin Darm, Bea Badorrek, Karsta Barnekow, Manya Moller** for their help in lab right from casting gels to entertainment, and care they have provided.

I also express my heartfelt thanks to **Sudu, Anne, Mathias** for teaching me animal experiments and **Kathrin** for CBA kit analysis and for their friendship and help whenever I was in need.

I am grateful to our lab secretaries **Kathrin Passow** (former) and **Nicholas Ehlers** (present) for their understanding and all administrative help at office.

I am also thankful to **all my freinds** in Greifswald for their support during my work.

I can not forget to mention my thanks to *Alfried-Krupp von Bohlen und Halbach Stiftung, Graduiertenkolleg Tumorbiologie* for the financial support of my stay as well as research in Greifswald.

Most importantly, I wish to thank **my parents**. They bore me, raised me, supported me, taught me, and loved me. To them I dedicate this thesis.

Last but not the least, I want to express my special thanks to my wife **Lakshmi** for her support. She was very supportive and understanding whenever I go home late with work.

Thanks to all and my sincere apology if I missed anyone who deserved to be mentioned.